COOPERATION

CANADA- NOVA SCOTIA COOPERATION AGREEMENT ON MINERAL DEVELOPMENT

ENTENTE DE COOPÉRATION CANADA-NOUVELLE-ÉCOSSE SUR L'EXPLOITATION MINÉRALE

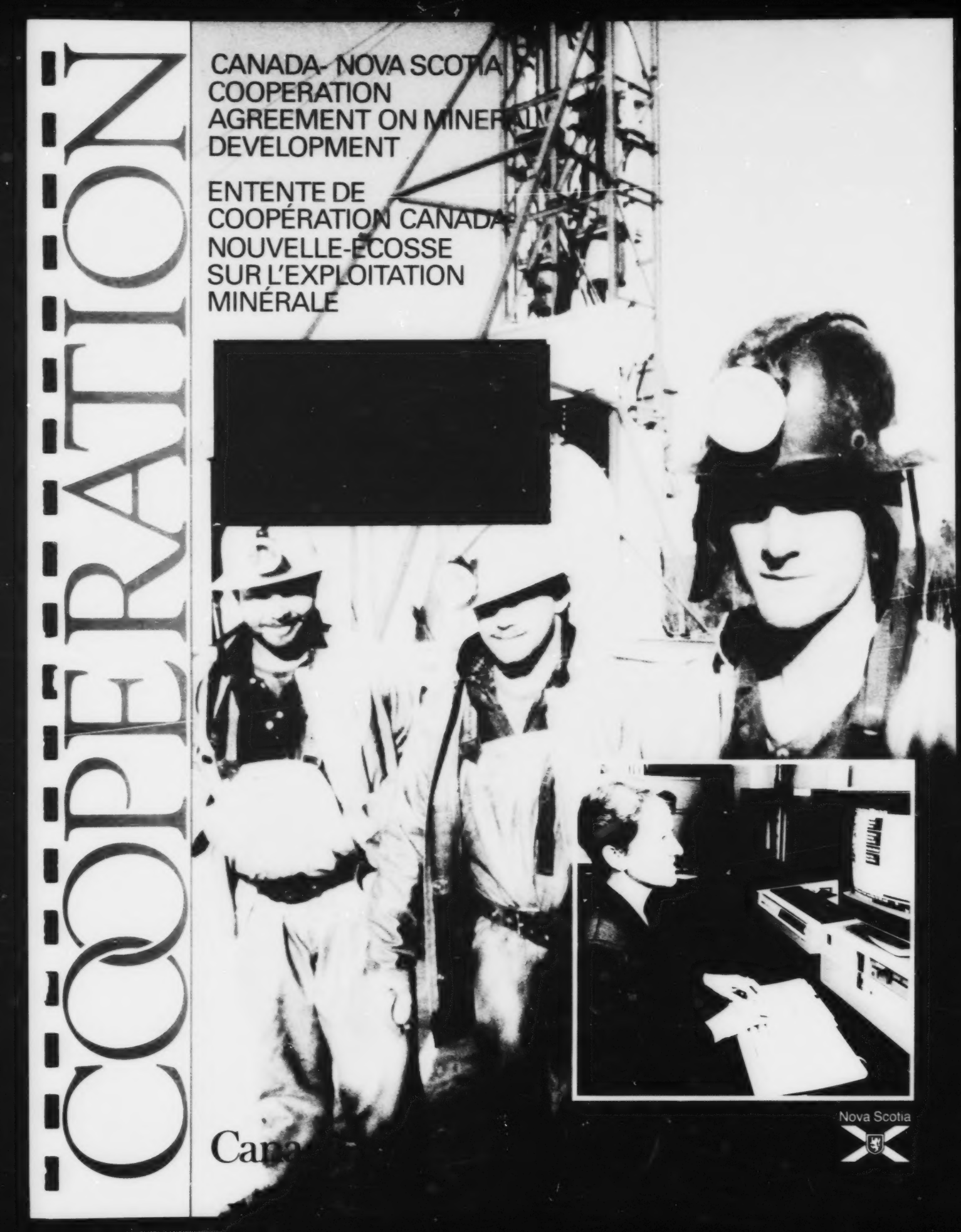

Nova Scotia

OPEN FILE REPORT 92-014

A Preliminary Report on Geological, Geochemical, Fluid Inclusion and Isotopic Studies of the Gays River Zn-Pb Deposit, Nova Scotia

D. J. Kontak

Nova Scotia Department of Natural Resources

Honourable John G. Leefe, Minister

Halifax, Nova Scotia
1992

COOPERATION
COOPERATION AGREEMENT ON MINERAL DEVELOPMENT
ENTENTE DE COOPERATION SUR LE DEVELOPPEMENT DES MINERAUX
Canada and Nova Scotia, Working for a Stronger Mineral Industry
Canada
Nova Scotia

93-00816/

TABLE OF CONTENTS

ABSTRACT.....1

CHAPTER 1: INTRODUCTION TO THE GAYS RIVER DEPOSIT AND SCOPE OF PRESENT INVESTIGATION

1.0 Introduction.....3

1.1 Exploration History.....5

1.2 Previous Geological Investigations of the Gays River Deposit.....6

1.3 General Overview of Mississippi Valley Type Pb-Zn Deposits.....8

CHAPTER 2: REGIONAL AND LOCAL GEOLOGY AND STRATIGRAPHY

2.0 Regional Geological Setting.....14

2.1 Local Geology.....15

2.2 Mine Geology.....17
- 2.2.1 Meguma Group.....19
- 2.2.2 Basal Breccia Unit.....27
- 2.2.3 Carbonate Rocks.....32
- 2.2.4 Evaporites.....34
- 2.2.5 Trench Sediments.....35

CHAPTER 3: MINERALIZATION AT GAYS RIVER

3.0 Introduction.....89

3.1 Definition of Ore Zones.....89

3.2 Nature, Extent and Description of Mineralization on the Deposit Scale
- 3.2.1 Generalizations Inferred from the Composite Vertical Sections.....93
- 3.2.2 Detailed Examination of some Composite Vertical Sections.....99

3.2.3 Evidence for Elemental Zonation in the Deposit....100

3.3 Macroscopic and Microscopic Features of the Mineralization
3.3.1 Macroscopic Features and Types of Ore....100
3.3.2 Microscopic Features of the Ore....103

3.4 Mineral Paragenesis and Timing of Mineralization at Gays River....110

CHAPTER 4: GEOCHEMICAL STUDIES

4.0 Introduction....131

4.1 Analytical Procedures....131

4.2 Analytical Results
4.2.1 Geochemistry of High-Grade Ore Samples....133
4.2.2 Geochemistry of Dolostone....135
4.2.3 Geochemistry of Carbonate Cement....139
4.2.4 Geochemistry of Ore Minerals....147

4.3 Discussion....150

CHAPTER 5: FLUID INCLUSION STUDIES

5.0 Introduction....164

5.1 Fluid Inclusion Petrography....165
5.1.1 Sphalerite....165
5.1.2 Calcite....168
5.1.3 Fluorite....170
5.1.4 Quartz Grains in Meguma Group Clasts....171

5.2 Thermometric Data....171
5.2.1 Heating Data....172
5.2.2 Freezing Data....176

5.3 Discussion of Fluid Inclusion Data....178

CHAPTER 6: ISOTOPIC STUDIES

6.0 Introduction....202

6.1 Sulphur Isotopic Analyses....202
6.1.1 Previous Sulphur Isotopic Analyses....202
6.1.2 New Sulphur Isotopic Analyses....204

6.2 Carbon and Oxygen Isotopes....206

6.3 Strontium Isotopes....207

6.4 Lead Isotopes....208

CHAPTER 7: GENERAL DISCUSSION OF THE GAYS RIVER DEPOSIT IN LIGHT OF RECENT GEOLOGICAL, GEOCHEMICAL AND FLUID INCLUSION STUDIES

7.0 Introduction....212

7.1 Summary of Present Investigation....212

7.2 Future Work Planned....215

ACKNOWLEDGEMENTS....217

REFERENCES....218

ABSTRACT

The Gays River Zn-Pb deposit is hosted by a Lower Carboniferous (Viséan) carbonate buildup (reef structure) of the marine Windsor Group, southern Nova Scotia. The deposit was discovered in the 1975's (Gays River Lead Mines) and briefly mined in the early 1980's (Esso Minerals Ltd.) and more recently from 1989-1991 (Westminer Canada Ltd.). Previous workers have interpreted the geological setting (shallow marine environment), syndiagenetic dolomitization and style of mineralization (cementation of primary porosity and replacement) in the context of Mississippi Valley Type (MVT) deposits. Results of the present investigation generally concurs with this idea, although some observations pertaining to the disposition of the ore zones, nature of fluid inclusions and geochemistry of the deposit are presented which are at odds with previous data and may, therefore, require rethinking of some aspects of the deposit.

The local stratigraphy consists of: (1) Meguma Group basement; (2) a overlying basal breccia; (3) the carbonate buildup; (4) evaporites; and (5) Cretaceous sediments. Units 2, 3 and 4 form part of the basal Windsor Group. Prior to mineralization the carbonate was pervasively dolomitized with primary features preserved (i.e., constant volume replacement). The ore is defined herein (after work of Westminer Canada Ltd.) as material grading $\geq$ 7% Zn equivalent 1% Pb = 0.8% Zn) over a 2 metre interval and such material outlines a corrugated sheet of ca. 4 km lateral extent (unfolded) located at the contact between the fore reef (i.e., leg of the reef) and the overlying evaporite unit; the ore has a very narrow vertical extent (i.e., 85% of ore in 60 m). Elemental zonation is such that the Pb:Zn ratio increases down dip towards the basin. In much of the deposit the hanging wall is now represented by partially consolidated sediments of Cretaceous to recent age infilling a sinuous trench preferentially localized to this contact. The ore consists of massive and disseminated types; the former occurs as >80-90% galena and sphalerite in various proportions replacing precursor dolostone. The sphalerite is Fe-poor (<0.5 wt. % Fe), yellow to beige colour and fine (<10-20μ, massive ore) to medium (<3-4 mm; disseminated ore) grained, while galena is consistently coarser (2-5 mm) grained and often euhedral. Lower-grade mineralization (<2-3% metal with Zn>>Pb) in the saddle part of the reef forms a halo where solutions migrated up slope into this area and infilled primary porosity.

Geochemical studies indicate that: (1) sphalerite of various textures and paragenesis is similar chemically (Fe, Ge, Cd, As); (2) galena is free of impurities (e.g., Ag); (3) calcite cements of uniform major element chemistry have contrasting REE signatures (ΣREE, La/Lu_N, but $Eu/Eu^* << 1$) indicating multiple source reservoirs and oxidizing fluids; (4) the massive ore contains only traces of elements other than Pb and Zn (i.e., Cd, Ge, Cu); and (5) the chondrite-normalized REE pattern for a sample of massive ore is similar to that of the dolostone host, thereby consistent with a replacement origin.

Fluid inclusion studies indicate several inclusion types exist, including L+V, V- and L monophase types, L+V+H (or other solids) and H_2O-CO_2 (rare), but their relationship remains ambiguous. Homogenization data (sphalerite, calcite and fluorite) have a large range (90°C to >250°C) and freezing experiments indicate fluids of high salinities (23-35 wt. % equiv. NaCl)

with variable Na:Ca ratios. The homogenization data either reflect initial high temperatures of formation or subsequent complexities (e.g., reheating) and future work will address this.

CHAPTER 1

INTRODUCTION TO THE GAYS RIVER DEPOSIT AND SCOPE OF PRESENT INVESTIGATION

1.0 INTRODUCTION AND SCOPE

The Gays River Zn-Pb deposit (reserves 2.4 million tonnes at 8.63% Zn, 6.33% Pb; Western Mining Co. Annual Report 1991-1992) is located in southern Nova Scotia about 65 km northeast of Halifax and 10 km east of the town of Shubenacadie (Lat. 45°02'N, Long. 63°22'W; Fig. 1.1). The deposit site is easily accessible via paved highway from Halifax (Route 102) and Shubenacadie (Route 224).

The deposit is hosted by dolomitized limestone rock that formed as part of an ancient reef complex during Lower Carboniferous (i.e., Visean) time when Nova Scotia was situated within 10° paleolatitude of the equator (Roy and Robertson, 1968). Subsequently low temperature (i.e., $\leq$ 200°C), mineralizing fluids migrated to the site and deposited the Pb and Zn now observed. Initial geological studies conducted as exploration of the deposit commenced (MacEachern and Hannon, 1974; MacLeod, 1975a) indicated that the Gays River mineralization shared many common features with the richly mineraled Pb-Zn-F districts of the Continental U.S.A. which are referred to as Mississippi Valley-type (MVT) deposits (for review see Anderson, 1982). Thus, the Gays River site has traditionally been considered to represent MVT mineralization, although many of the initial conclusions regarding the nature of the ore-forming fluids and the controls on mineralization have changed subsequently as a result of more detailed studies (see below).

The purpose of the present investigation is to re-examine the the Gays River deposit

because of renewed interest in this locality specifically, but also to extend the results to the basal Windsor Group stratigraphy of Nova Scotia on a broader scale. The project was designed to examine in detail specific features that would provide the most useful information in terms of evaluating the origin of the deposit. In the present investigation the main topics studied were as follows:

1. examination of previous drill hole data and construction of composite cross-sections to determine geometrical relationships between various stratigraphic units and mineralization. As an additional benefit of this work, the elemental zonation of Pb and Zn were also examined;

2. detailed petrographic study of the host rock and ore material;

3. detailed study of fluid inclusions in order to determine the physical and chemical characteristics of the fluid(s) involved in the mineralizing process;

4. geochemical study of the ore and host rock to evaluate the primary geochemical signature of the ore and to commence compilation of a data base for comparative purposes;

5. chemcial study (specifically REE signature) of syn- and post-ore calcite to assess the nature of the fluids involved at the deposit site;

6. S isotopic study of the massive ore zone to compare to the lower-grade disseminated ore and a C, O, Sr isotope study of the carbonates within the host rock and ore.

Whereas most of this work has been completed, parts of 4 and 6 are still in progress and only partial results are reported herein.

The data base upon which the preliminary findings of this study are based include:

1. use of about 400 surface diamond drill hole logs;

2. collection of approximately 200 drill core samples from surface and underground drilling; this

was complimented with sampling of ore piles from mine workings and underground workings;

3. preparation of about 50 fluid inclusion sections and 100 polished sections;

4. 6 massive ore samples for multi-element analyses;

5. 30-40 whole rock sample for routine major and trace element analyses (still in progress at time of writing), 8 whole rock samples for REE analyses and 20 calcites for trace element and REE analyses;

6. sulphur isotope anlayses of the massive and breccia ores;

7. electron microprobe analyses of ore minerals and carbonates.

Additional work is planned and the results will be reported at a later data as they become available. These studies include: (1) gas analyses of the fluid inclusions, (2) geochronology ($^{40}Ar/^{39}Ar$, Rb/Sr), (3) laser ablation spot analyses using ICP-MS technology for trace element chemistry of carbonates and sphalerite, (4) fluid inclusion studies of regional samples outside the deposit area, and (5) stable (C, O) and radiogenic (Sr) isotopic studies of carbonate material.

1.1 EXPLORATION HISTORY

Occurrences of Pb-Zn mineralization date back to 1824 according to early records, but the first attempt to systematically explore for Pb and Zn mineralization in the Gays River area was in the early 1950's by Gays River Lead Mines. A deposit of 1.0 million tonnes grading 1.1-3.3 % combined Pb and Zn was outlined from diamond drilling (MacEachern and Hannon, 1974). Intermittent work was carried out from the 1950's to 1970, but it was the discovery of mineralized boulders south of the old showings by staff of Cuvier Mines Ltd. that prompted a re-evaluation of the deposit area. According to MacEachern and Hannon (1974), the area was

delimited as having potential for MVT mineralization and Imperial Oil Ltd. began extensive exploration for the source of the high-grade float recently discovered. As a result of extensive diamond drilling in this extensively glaciated area, Imperial Oil Ltd. outlined a deposit (4 km by 0.6 km) with drill-indicated reserves of 12 million tonnes of 7% metal (Pb+Zn) using as a cut off 2.4% metal over 2.5 metres. In 1977 Imperial Oil Ltd. bought out Cuvier Mines Ltd. interest and turned over operations to Esso Minerals Canada Ltd.. Development began in 1978 by Canada Wide Mines (subsidiary of Esso Minerals) and terminated in 1982 after production of about 550,00 tonnes grading 3.3% combined metal. The property was acquired by Seabright Resources Ltd. in the 1980's and the mill converted to recover gold. Subsequent purchase of Seabright by Westminer Canada Ltd. transferred ownership of the property. As a result of re-examination of the deposit, the geological staff of Westminer Canada Ltd. reclassified the ore and calculated a total inferred tonnage of 2.4 million tonnes at 8.63% Zn and 6.33% Pb.

1.2 PREVIOUS GEOLOGICAL INVESTIGATIONS OF THE GAYS RIVER DEPOSIT

The first study of the Gays River area was that of MacEachern and Hannon (1974) who based their interpretations on the results of diamond drilling. These authors recognized the presence of a complex carbonate build up and based on their observations constructed a cross section illustrating the distribution of lithofacies (Fig. 1.2). They also recognized that the mineralization was akin to that of the carbonate-hosted Mississippi Valley-Type deposits. Following this work, McLeod (1975a, 1975b), based on detailed studies of three diamond drill holes, suggested that the mineralization was a result of early, low temperature, diagenetic processes with later reconcentration during karsting to form the high-grade ore zones. Detailed

studies of the carbonate host rocks were done by Hartling (1977) and Osborne (1977) in order to interpret the paleoenvironment, while Hatt (1978), Hatt and Schenk (1977), and Schenk and Hatt (1984) present the most detailed account of carbonate petrography and interpretation of the depositional environment. Giles et al. (1979) included the Gays River carbonate bank in their regional examination and interpretation of similar buildups througout the Gays River Formation.

The most detailed and comprehensive account of the Gays River deposit area is found in the Ph.D. thesis of Akande (1982; see also Akande and Zentilli 1983, 1984). Akande examined the distribution of ore and host rock based on extensive underground mapping and logging of diamond drill core, and supplemented this with an exhaustive program including isotopic (C, O, S), fluid inclusion and petrographic study. The most significant aspects of his work include: (1) recognition of distinct high-grade and low-grade ore types and a possible inter-relationship (Fig. 1.3); (2) high temperatures for mineralization (i.e., >200°C, but see later for discussion); (3) isotopic data suggesting marine water or evaporite source for S; and (4) a non-diagenetic (i.e., early cement) origin for the mineralization. In their 1984 paper, Akande and Zentilli advocated a basin dewatering model and realized the potential significance of intergrating the local geological features with regional scale evolution of the Upper Paleozoic basins. Ravenhurst and co-workers (Ravenhurst, 1987; Ravenhurst and Zentilli, 1989; Ravenhurst et al., 1986, 1987, 1989) developed this model further based on additional studies at Gays River [K-Ar and zircon fission track geochronology, fluid inclusions, isotopes (C, O, Sr, Pb)] and other carbonate-hosted deposits of similar age. They developed a model, summarized in Figure 1.4, which relates all Pb-Zn-Ba mineralization in the basal Carboniferous stratigraphy to large-scale basin dewatering related to overpressured pore fluids. Where metal-bearing solutions were able to escape to sites

of low pressure (i.e., physio-chemical traps), ore deposit formation resulted (e.g., Gays River, Jubilee, Walton). Recently, Arne et al. (1990) have obtained apatite fission track ages within and around the deposit area, while Boehner et al. (1989) reviewed the history of work at Gays River in the context of the regional extent of the host Gays River Formation.

The aforementioned authors have established the following features for the Gays River deposit area, namely: (1) the carbonate reef complex formed during the Visean; (2) mineralization is post 330 Ma (age of host rock) and post-cooling of the Meguma Group to 110°C (blocking temperature of apatite fission tracks); (3) mineralization consists of both low- and high-grade ore; (4) mineralization was from moderately high temperature (ca. 200°C), highly saline brines; (5) S is derived from a marine reservoir (evaporites), but C and O have multiple reservoirs, including the host carbonates; and (6) the deposit formed as a result of regional-scale basin evolution (i.e., expulsion of overpressured waters).

1.3 GENERAL OVERVIEW OF MISSISSIPPI VALLEY TYPE PB-ZN DEPOSITS

Mississippi Valley-Type deposits refer broadly to a set of deposits that are hosted by carbonate rocks and characterized by the element association Pb-Zn-Ag-F-Ba-Cu and are formed from low- to moderate temperature (<150°C), highly saline (ca. 20-30 wt. % equivalent NaCl) fluids. The fluids are generally considered analagous in terms of their physical and chemical features to basinal brines and, consequently, most genetic models for these deposits integrate them with basin evolution.

Anderson (1982) provides an overview of this deposit class and emphasizes the following points or features:

1. most deposits occur within carbonate rocks or their dolomitized equivalents and are located at the edges of basins or along arches;

2. mineralization occurred at shallow depth and the deposits have rarely been buried very deeply;

3. ore mineralogy is simple with galena and sphalerite dominant with low Ag and Fe contents, respectively. Associated mineralization includes Ba, F and Cu, but is highly variable among deposit areas;

4. fluid inclusion studies indicate that the mineralizing fluids were of 80-200°C and highly saline (Na-Ca-Cl brines 5-10 x sea water salinity);

5. an association with organic materials in the form of kerogen or bitumen in the host rocks and/or petroleum in the fluid inclusions is commonly observed.

As will be apparent in the following section, many of the features listed by Anderson (1982) are found at Gays River. However, there are also important differences and these will be stressed in the concluding chapter where a discussion of the orign of the Gays River deposit is presented.

Fig. 1.1. General location map of the Gays River deposit area in southern Nova Scotia.

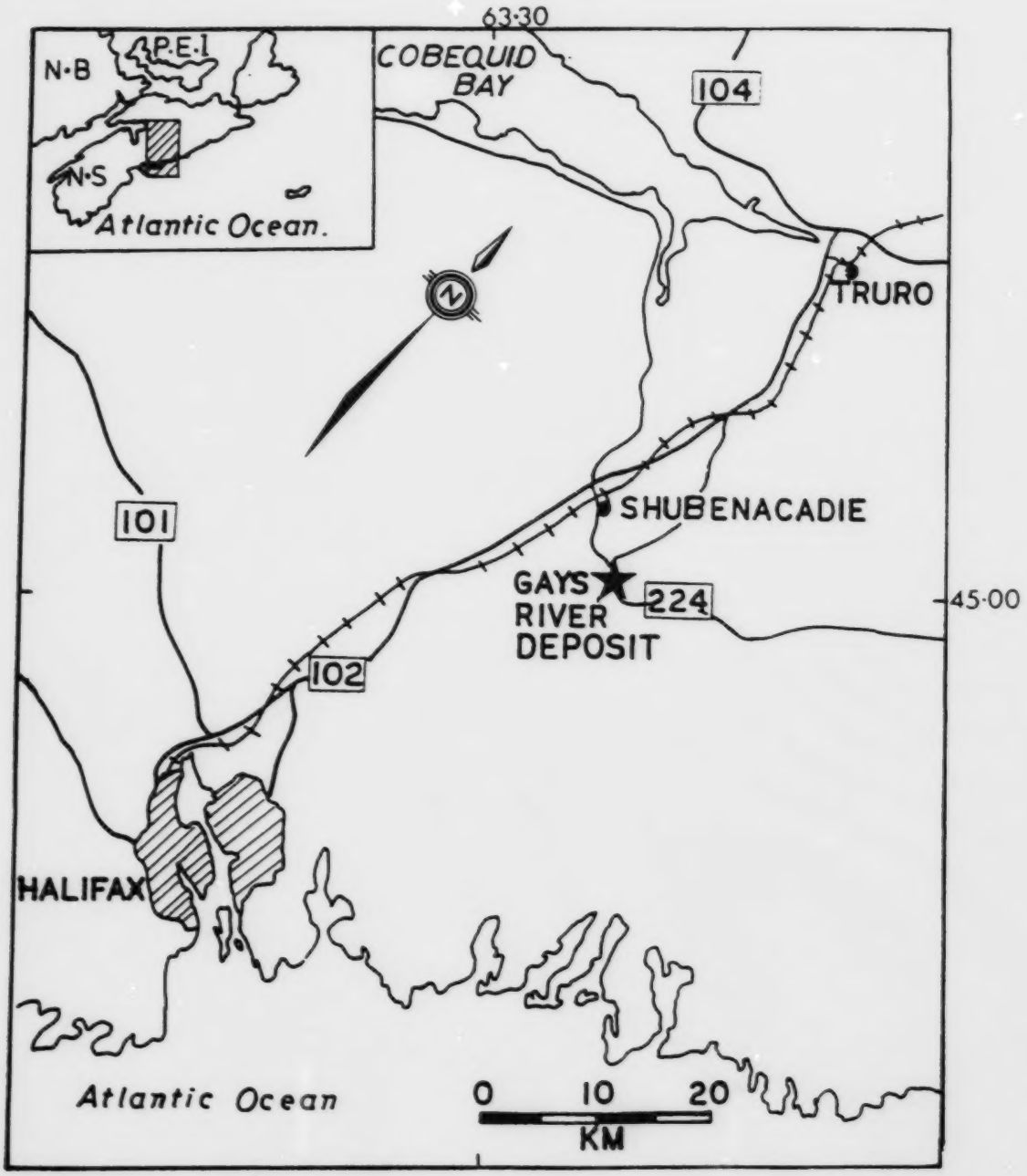

Fig. 1.2. Schematic cross section of the Gays River bank and deposit area showing the distribution of carbonate facies (after MacEachern and Hannon, 1974). Diagram is based in interpretation from diamond drill data.

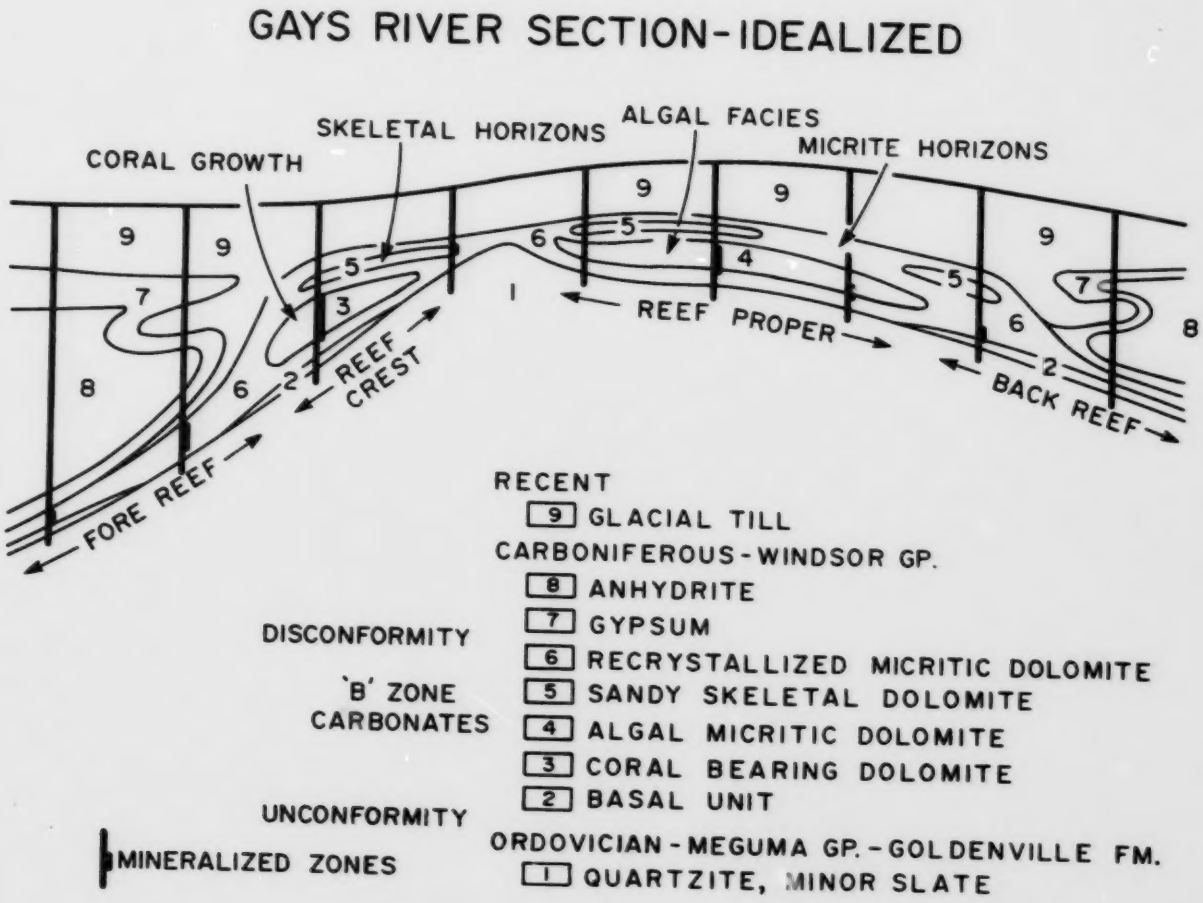

Fig. 1.3. Schematic cross section of the Gays River bank and mineralization proposed by Akande and Zentilli (1984). This section is approximately the same as section 13 presented as part of Figure 2.6 in Chapter 2.

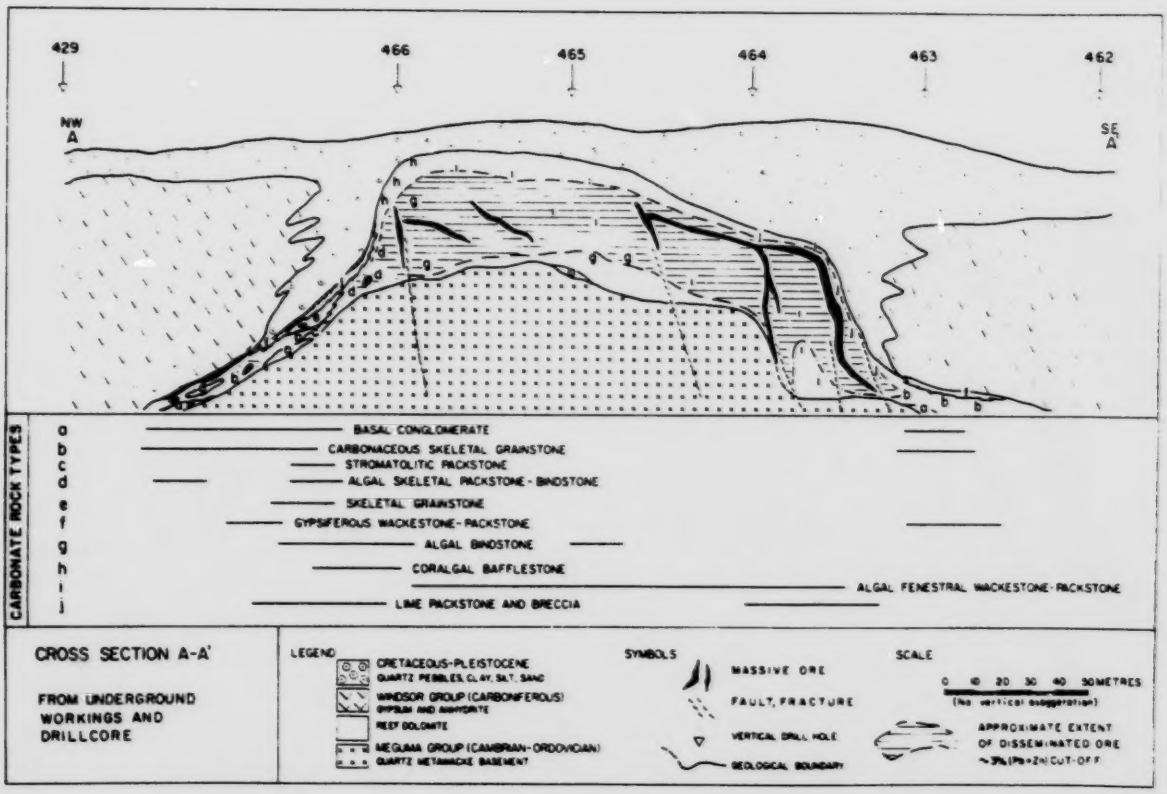

Fig. 1.4. The basin dewatering model of Ravenhurst and Zentilli (1989) which proposes that Pb-Zn-Ba mineralization in the Maritimes Basin resulted from overpressured fluids that originated in the deeper parts of the basin and migrated laterally under an evaporite seal.

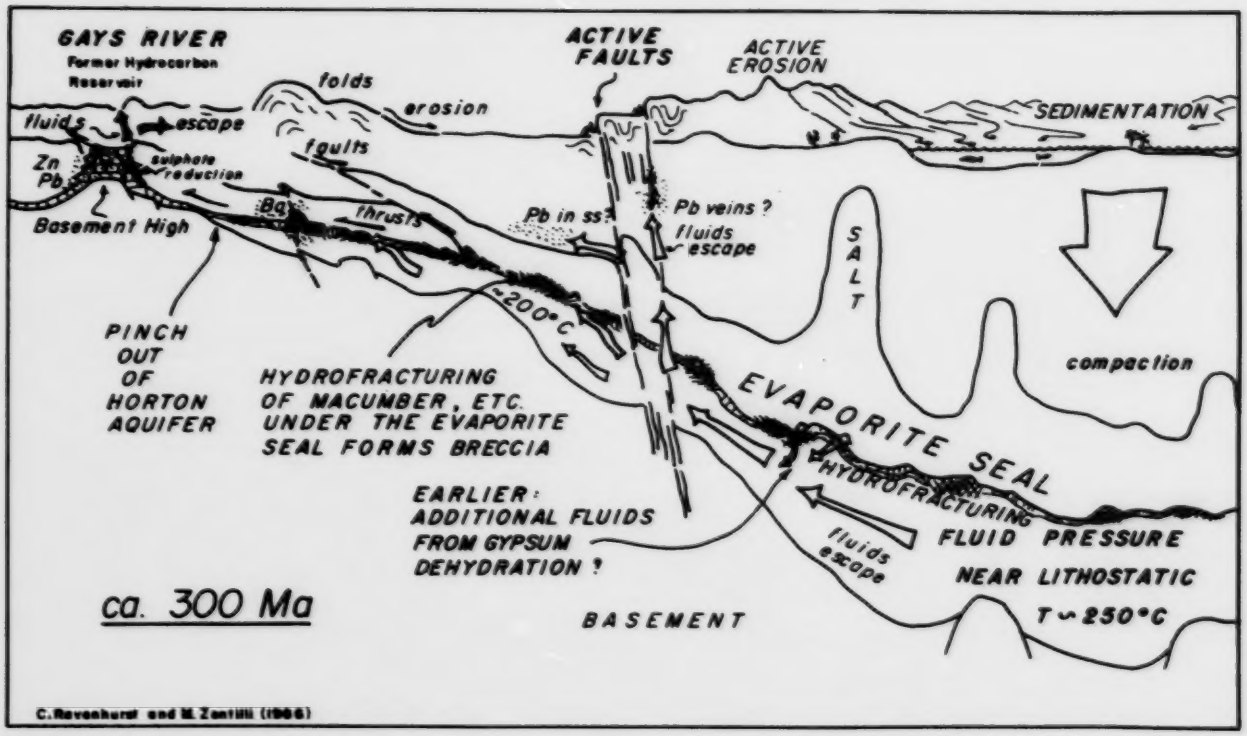

CHAPTER 2

REGIONAL AND LOCAL GEOLOGY AND STRATIGRAPHY

2.0 REGIONAL GEOLOGICAL SETTING

The Gays River area is located along the boundary between two sub-basins, the Subenacadie and Musquodoboit (Fig. 2.1), which are part of the large (>250,000 km^2), deep (8 km) Maritime or Fundy Basin which dominates Upper Paleozoic stratigraphy of Eastern Canada (Fig. 2.2). As is obvious from Figure 2.1, there are many occurrences of Pb-Zn-Ba-F mineralization in the basal Windsor Group of southern Nova Scotia in addition to the Gays River deposit. The Carboniferous basin formed upon deformed and metamorphosed Meguma Group basement rocks in southern Nova Scotia which was folded into northeast-trending, upright structures and metamorphosed to greenschist-amphibolite facies (Keppie, 1982; Keppie and Muekce, 1979) during the mid-Devonian Acadian Orogeny (ca. 400 $\pm$ 10 Ma; Reynolds and Muecke, 1978; Muecke et al., 1988; Keppie and Dallmeyer, 1987). Following this deformation, Maritime Canada was dominated by dextral wrench faulting along E-W and NE-SW faults (Webb, 1969) with subsequent formation of pull apart basins (Fralick and Schenk, 1981; Bradley, 1982) which were infilled with up to 12 km (prior to erosion) of terrestial and shallow marine sediments of Late Devonian to Permian age (Belt, 1968; Sheridan and Drake, 1968; Howie and Barss, 1975; Fralick and Schenk, 1981). These basins occupied a large, northeast-trending trough with platforms on the southeast (Meguma platform) and northwest (New Brunswick platform).

The stratigraphic columns of the two sub-basins relevant to this study are presented in Figure 2.3. The basal unit, represented by the coarse detritus of the Late Devonian Horton

Group, is noted to be present in the Shubenacadie Basin but absent in the Musquodoboit Basin (Giles et al., 1979). This unit represents the flysch eroded from the uplands following the Acadian Orogeny and facies transitions vary rapidly through fanglomerate, fluviatile and lacustrine. The Lower Carboniferous Windsor Group post-dates the Horton Group and rests unconformably on these terrestial sediments or Meguma Group basement after a significant erosional and depositional hiatus in the early Viséan (Geldsetzer, 1978). The Windsor Group rocks onlapped the pre-existing stratigraphy and formed laterally extensive deposits throughout the Martimes Basin. The formations of the stratigraphically important Windsor Group are fully described by Giles and Boehner (1982) and it is only important to note here that it represents a series of marine transgressions and regressions (Giles, 1981) with lateral variation reflecting facies transitions (e.g., Macumber and Gays River Formations).

The most important geological unit in a regional context is the Gays River Formation since it is the host rock for mineralization at Gays River. This formation consists of carbonate reef buildups that are located throughout the Shubenacdie and Musquodoboit Basins, particularly on the southern flank of the latter basin (Fig. 2.2; Boehner et al., 1989).

2.1 LOCAL GEOLOGY

A simplified version of the surface geology of the Gays River deposit area stripped of overburden, which can locally be several metres thick, is shown in Figure 2.4. The oldest rocks are represented by paleotopographic highs of Meguma Group stratigraphy which occur as windows within the younger units. Akande (1982) and Akande and Zentilli (1984) noted that these rocks are cut by joints of dominantly N-S, E-W and N 60° W orientation and that many

of them contained fault gouge and slickensides. These structures were important in controlling the Carboniferous paleotopography that consisted of prominent NW and NE trending ridges which controlled the location of the Gays River carbonate bank and ultimately the location of the ore zones (see below). The carbonate host rocks of the Gays River Formation overlie the Meguma Group unconformably and form a NE-trending ridge of maximum thickness of about 30-40 metres which thins to the NW and SE as one goes into the bordering basins. The carbonate rocks are overlain by evaporites (anhydrite, gypsum) of the Carrolls Corner Formation which form a sharp contact with the carbonates where observed. However, within a large part of the mine area this contact has been preferentially replaced by what is referred to as the trench sediments. This structure is a long, sinuous, NE-trending karstic ditch which was infilled with variably consolidated, and at present water-saturated, material of clay to gravel size with some lignite. Dating of spores and pollen by Davies et al. (1984) suggest an Albian (i.e., Early Cretaceous) age for the material analysed.

The carbonate rocks of the Gays River bank have been studied in detail and described in several theses at Dalhousie University (MacLeod, 1975a; Osborne, 1977; Hartling, 1977; Hatt, 1978; Hancock, 1982, Akande, 1982), and additional work (Schenk and Hatt, 1984). These carbonate rocks are also incorporated in more regional studies of the basal Windsor Group stratigraphy by Ryan (1976), Giles (1981), Giles et al. (1979) and Giles and Boehner (1982). Most recently Boehner et al. (1989) have summarized the information on Gays River in the context of the regional buildups. The carbonate bank consists of a wide variety of lithologies representing both allochthonous and autochthonous members of Dunham's (1962) classification and the distribution of the carbonate facies reflects their depositional environment and proximity

to basement ridges (Akande, 1982). However, the most important aspect of these rocks in the context of the present investigation is that they have been thoroughly dolomitized post-deposition and pre-mineralization via a mechanism of constant volume such that delicate, primary textures (e.g., fossil remains) are preserved. In the present study the nature of the carbonate has not been investigated in detail and is treated only as the host rock, thus, the dolomitized carbonate is described simply as dolostone.

2.2 MINE GEOLOGY

The geology of the mine area specifically has been examined from studying drill core and constructing vertical sections of the deposit area using both the previous and more recent results of diamond drilling as compiled by geologists of Westminer Canada Ltd. In this data base the following information is noted: (1) elevation, location and number of the diamond drill holes in each section; (2) lithologies and elevations of contacts between lithologies; and (3) assays for Pb and Zn over various intervals depending on the nature of mineralization (i.e., continuity and grade). Only a few select lithogeochemical profiles for Pb and Zn are shown for each section, but the same information (i.e., grades and metres intervals) are summarized for all the holes where available. With respect to the vertical sections it is emphasized that soem of the holes used may lie outside the plane of the section as indicated in Figure 2.5 and this may influence the geology to an unknown extent.

In Figure 2.5 the locations of the 36 vertical sections for the main deposit area (29 sections) and the adjoining Getty deposit (7 sections) are shown which were prepared using data from 358 surface drill holes. In these composite cross sections (Fig. 2.6) the following points

are to be noted: (1) the geological continuity is inferred between drill holes and in some cases the geology has been projected onto the plane of the section. From underground observations and discussions with the mine geologists, it is apparent that the geology can quickly change in a lateral dimension; and (2) the actual extent of the trench is only approximate and in most cases has been inferred from the general configuration of the depression formed in the underlying carbonate-evaporite lithologies. With the limitations of the data in mind, the following points concerning the mine geology are noted.

1. The carbonate reef varies in thickness (note this is minimum thickness since unknown amounts of erosion have occurred) as inferred from the maximum intersections in drill core along the trend of the bank (Fig. 2.7). The greatest thickness is attained in the southwest with 30-40 m of carbonate forming the saddle part of the structure and this thins to about 10 m in the northeast. In going from the main deposit area to the Getty deposit there is a rapid thinning of the reef, presumably reflecting a paleotopographic low, before again thickening to >30 m. Note also that in the central part of the main deposit the carbonate is very thin (few metres) on the promontory which protrudes into the basin (sections 26, 27, 28, 29) and in section 25 the carbonate is only a few metres thick, but is continuous down into the basin to the north. It is important to note that the inferred thickness for the carbonate at each location is a minimum thickness since the possible affects of erosion and location of drill holes remains unknown.

2. The carbonate bank is located between two sub-basins such that the width of the carbonate bank is at the most only about 500 m (e.g., section 15). To both the northwest and southeast the carbonate is overlain by evaporite deposits.

3. The basal breccia unit is highly irregular in nature. This unit may: (1) form in paleo-

depressions (section 1) or (2) occur as talus around prominent highs (sections 4, 13). In addition, this unit may form a continous unit (sections B, D), be of considerable thickness (sections 9, C), or be absent in parts of sections (section 1).

4. The trench sediments occur at the contact between the evaporite unit and carbonate on the northwest side of the reef only and is present in all sections except 9, 23, 24, 25 and D. The trench sediments generally define an inverted cone structure with a maximum vertical dimension of about 100 m and a width of over 100 m at the top.

Section 13 presented here is the same section shown as Figure 1.3 which is from Akande (1982) and Akande and Zentilli (1984). In general the two sections are similar with respect to the host rock geology except for the southeast part of the section. This discrepancy reflects the additional information provided by more detailed infill drilling which indicated that the paleotopography in this area was complex. This section (#13) also serves to illustrate how quickly the geology can change laterally over a few metres.

Although the distribution of Pb and Zn grades are shown on these sections, this information will be discussed in a later section (see below).

2.2.1 Meguma Group

The Lower Paleozoic Meguma Group forms the basement rocks in the mine stratigraphy and consists of massive psammites and lesser pelite which typically characterize the Goldenville Formation. They are only weakly deformed and even the pelitic interbeds have only a weakly defined fabric. Akande (1982) reports measurements of the main structural elements in these rocks and found that prominent joint sets occur at 330/70°W and 085/50°N with faults of N-S,

E-W and N60°W oreintation.

A total of 6 samples of massive, fine grained psammite from just below the basal breccia or carbonate were examined in polished section. The rocks are very similar and therefore the following description, although generalized, is adequate for all the samples. The rocks are dominated by anhedral to subhedral quartz and feldspar (80-85 modal %) with lesser biotite, muscovite, chlorite, calcite, tourmaline, zircon and opaques (includes sphalerite, galena). The generally poorly-developed fabric is defined by fine grained biotite and muscovite, but in places the fabric may be well developed and in such cases is defined by biotite. The following features characterize the mineralogy: (1) Biotite is generally greenish in colour although brown biotite is also present. In general it appears that the green biotite occurs in rocks that have more calcite and chlorite and, therefore, formation of green biotite is a secondary process. Biotite is variably altered to chlorite and may be intergrown with calcite. In rare instances sphalerite and/or pyrite may be associated with altered biotite. (2) Plagioclase is either free of inclusions or inundated with very fine mineral and fluid inclusions which are preferentially concentrated in the core areas with clear epitaxial (?) overgrowths. This feature occurs most frequently in mineralized samples. Many of the plagioclase (10-20%) grains are characterized by chessboard albite texture, but most are clear, fresh grains of albitic composition. (3) Calcite is late and occurs as irregular disseminations, along fine fractures or completely replacing large areas of the matrix. Where there may be considerable replacement of the sedimentary rock by calcite, the matix material is preferentially replaced, then the coarse feldspar grains and finally quartz. Sulphides (mostly sphalerite), chlorite and biotite are sometimes associated with the calcite. (4) Muscovite occurs in two morphologies, either coarse euhedral grains or finely disseminated grains. The coarse

grains are fresh, inlcusion free and generally coarser than other mineral phases and are randomly oriented (i.e., perpendicular to the fabric). Thus, a late-stage growth of this muscovite is suggested based on the aforementioned features. In contrast, the fine grained muscovite defines the weak to moderate fabric, rims quartz and feldspar and grows along fractures. (5) Chlorite occurs as a replacement of biotite and its texture is, therefore, dependent upon the degree of replacement. Chlorite is most abundant where carbonate is present. Sphalerite and/or pyrite may be associated with the chlorite, where the sphalerite occurs as fine grained aggregates about the margins of the chlorite. (6) Quartz is anhedral, of variable shape and has variably embayed and sutured margins, presumably from pressure solution processes, and generally is free of undulatory extinction. In areas of mineralization, especially where good mineralization is noted, the texture of quartz changes noticeably with increase in the degree of sutured margins, decrease in undulatory extinction (i.e., subgrain development) and the presence of abundant fluid inclusions. These inclusions are (1) generally negative shaped, (2) consist of 2 and 3 phases (L+V$\pm$Halite) with the L+V types the most common (V-rich rare); and (3) occur along healed fractures or random clusters and are interpreted to be of secondary origin. Thermometric data have been obtained for these fluid inclusions and the data are presented in a later section (see Chapter 5). (7) Sulphide phases include pyrite, sphalerite and galena. Pyrite occurs as (1) euhedral to subhedral equant grains, (2) as sinuous, irregular grains and (3) circular framboidal-type grains with a concentric internal structure. While the first two types are common, the third type is rare. The framboidal-type pyrite is often found in and around styolitic material. Sphalerite occurs as isolated, single grains or aggregates of similar size grains and is found in areas of calcite and chlorite formation. Galena is rarely found in the sediments, only a single observation being made

except for very rich mineralization in one sample. In the latter case galena occurs as coarse euhedra infilling fracture planes that truncate the psammite host in an irregular manner.

In summary, there is clear evidence of textural modification of the host Meguma Group psammites where mineralization is present and this is reflected in textural and mineralogical changes. Most important is that where secondary carbonate is present there is chlorite after biotite, the biotite is greenish-brown and sphalerite $\pm$ galena mineralization occurs. The mineralization is spatially and paragenetically related to the presence of carbonate $\pm$ coarse muscovite. In addition, the presence of abundant fluid inclusions (see Chapter 5 for more details) and altered cores of plagioclase grains are features prevalent near mineralization. All these features noted are not typical of Meguma Group rocks in general suggesting, therefore, a possible causitive relationship to the mineralization at Gays River.

Microanalyses of biotite, chlorite, muscovite, plagioclase and carbonate have been obtained using a JEOL 733 Superprobe at Dalhousie University (see Chapter 5 for details). Biotite (Table 2.1; Figs. 2.8, 2.9) chemistry is typical of that found in the Meguma Group metasedimentary rocks (S. Douma data base, pers. commun., 1990). There is a progression in chemistry from fresh biotite towards biotite with lower contents of Ti, tetrahedral Al, K and Fe/(Fe+Mg) values as chloritic alteration occurs. The deviation of the biotite data from the phologopite/annite - siderophyllite/eastonite tie line in the Al-Si-M^{2+} plot (Fig. 2.9) also reflects the chloritic alteration of the biotite and subsequent relative increase in Al content.

Chlorite (Table 2.1) is repidolitic in composition with a narrow range of chemistry, again this is typical of what is found in the Meguma Group (S. Douma, pers. commun., 1990) and also in auriferous and barren quartz veins cutting the Meguma Group (Kontak and Smith, 1988, in

TABLE 2.1. Mica Analyses (EMPA), Gays River.

Sample	GR91-71	GR91-71	GR91-25	GR91-10	GR91-71	GR91-71	GR91-25	GG91-25	GR91-25	GR91-25
Point	11	4	59	76	12	8	39	41	42	43
Mineral	chl	chl	chl	chl	chl/biot	chl/biot	musc	musc	musc	musc
SiO2	24.33	24.43	24.84	24.58	29.85	34.69	49.17	49.48	51.01	48.42
TiO2	0.13	0.11	0.12	1.01	1.27	1.27	0.22	0.42	0.3	0.73
Al2O3	20.3	19.13	20.93	10.87	14.81	16.26	32.64	30.96	29.62	35.98
FeO	29.54	29.05	29.78	12.88	21.96	17.32	2.82	3.27	2.41	1.1
MnO	0.68	0.7	0.41	0.09	0.17	0.2	0	0.09	0	0
MgO	10.88	11.01	11.01	5.59	7.61	7.72	1.68	2	1.78	0.93
CaO	0.05	0	0	0.06	0.37	0.13	0.1	0	0.24	0
Na2O	0.33	0.19	0.24	0.12	2.88	0.35	0.25	0.27	0.23	0.6
K2O	0	0.06	0	5.37	3.29	6.18	8.75	8.35	7.13	8.17
BaO	0	0	0	0	0	0	0.16	0.17	0.26	0.23
total	86.24	84.68	87.33	60.57	82.21	84.12	95.79	95.01	92.98	96.16
	28	OXYGEN					22	OXYGEN		
Si	5.376	5.488	5.404	7.42	6.804	7.448	6.468	6.38	6.82	6.27
Aliv	2.624	2.512	2.596	0.58	1.196	0.552	1.532	1.62	1.18	1.73
Alvi	2.668	2.556	2.78	3.284	2.78	3.564	3.528	3.22	3.484	3.77
Ti	0.028	0.028	0.028	0.224	0.224	0.196	0.022	0.044	0.022	0.066
Fe	5.46	5.46	5.404	3.248	4.172	3.108	0.308	0.374	0.264	0.11
Mn	0.14	0.14	0.084	0.028	0.028	0.028	0	0.022	0	0
Mg	3.584	3.696	3.556	2.52	2.576	2.464	0.33	0.396	0.352	0.176
Ca	0	0	0	0.028	0.084	0.028	0.022	0	0.044	0
Na	0.14	0.084	0.112	0.084	1.26	0.14	0.066	0.066	0.066	0.154
K	0	0.028	0	2.072	0.952	1.68	1.474	1.408	1.21	1.342
Ba	0	0	0	0	0	0	0	0	0.022	0.022
Fe/ (Fe+Mg)	0.60	0.60	0.60	0.56	0.62	0.56	0.48	0.49	0.43	0.38

TABLE 2.1. Mica Analyses, Continued.

Sample	GR91-25	GR91-25	GR91-25	GR91-25	GR91-25	GR91-25	GR91-25	GR91-25	GR91-25	GR91-25
Point	44	46	47	48	49	50	51	52	53	54
Mineral	musc	musc	musc	musc	musc	musc	musc	musc	musc	musc
SiO2	48.02	47.85	48.17	48.59	47.65	48.32	47.42	50.2	47.76	48.11
TiO2	0.59	0.78	0.81	0.51	0.68	0.51	0.67	0.25	0.15	0.232
Al2O3	36.31	32.66	32.44	36.2	35.18	35.42	35.7	32.27	31.61	31.66
FeO	1.15	3.13	3.12	1.02	1.47	1.5	1.04	2.17	4.19	5.01
MnO	0	0	0	0	0	0	0	0.11	0	0.078
MgO	0.95	1.44	1.51	0.89	1.02	0.83	0.69	1.49	2.59	2.81
CaO	0	0	0	0	0.05	0	0	0	0.11	0.14
Na2O	0.73	0.16	0.22	0.46	0.48	0.5	0.33	0.15	0.15	0.18
K2O	8.45	8.97	8.93	7.9	8.37	8.48	9.16	8.82	8.46	7.83
BaO	0.31	0.18	0.33	0.4	0	0.2	0.27	0.35	0.19	0.16
total	96.51	95.17	95.53	95.97	94.9	95.76	95.28	95.81	95.21	96.21
	22	OXYGEN								
Si	6.226	6.358	6.38	6.292	6.27	6.314	6.248	6.512	6.38	6.358
Aliv	1.774	1.642	1.62	1.708	1.73	1.686	1.752	1.488	1.62	1.642
Alvi	3.77	3.484	3.462	3.814	3.726	3.77	3.792	3.594	3.352	3.286
Ti	0.066	0.088	0.088	0.044	0.066	0.044	0.066	0.022	0.022	0.022
Fe	0.132	0.352	0.352	0.11	0.154	0.154	0.11	0.242	0.462	0.55
Mn	0	0	0	0	0	0	0	0.022	0	0
Mg	0.176	0.286	0.308	0.176	0.198	0.154	0.132	0.286	0.528	0.55
Ca	0	0	0	0	0	0	0	0	0.022	0.022
Na	0.176	0.044	0.066	0.11	0.132	0.132	0.088	0.044	0.044	0.044
K	1.408	1.518	1.518	1.298	1.408	1.408	1.54	1.452	1.452	1.32
Ba	0.022	0	0.022	0.022	0	0	0.022	0.022	0	0
Fe/ (Fe+Mg)	0.43	0.55	0.53	0.38	0.44	0.50	0.45	0.46	0.47	0.50

chl=chlorite, musc=muscovite, biot=biotite

TABLE 2.1. Mica Analyses, Continued.

Sample	GR91-25	GR91-25	GR91-25	GR91-25	GR91-10	GR91-10	GR91-10	GR91-10	GR91-10	GR91-10
Point	55	56	57	58	62	63	73	74	78	79
Mineral	musc	musc	musc	musc	musc	musc	musc	musc	musc	musc
SiO2	47.91	46.93	47.4	48.05	47.13	47.23	52.19	50.88	53.39	51.57
TiO2	0.67	0.49	0.31	0.5	0.39	0.388	0	0.17	0.36	0.36
Al2O3	32.99	34.91	34.65	33.55	32.7	32.19	29.74	31.98	29.46	28.17
FeO	3.7	3.15	3.15	2.87	4.58	4.13	2.61	2.72	1.64	3.15
MnO	0	0	0.1	0	0	0.08	0	0	0	0
MgO	1.24	0.82	0.83	1.08	0.92	0.96	2.44	1.98	3.42	3.86
CaO	0	0.08	0	0.05	0.08	0	0	0	0	0
Na2O	0.45	0.66	0.74	0.51	0.25	0.37	0.18	0.16	0.39	0.2
K2O	8.53	8.09	8.02	7.88	9.2	10.01	8.34	8.81	8.13	7.92
BaO	0.38	0.31	0.44	0.27	0	0	0.38	0.44	0.37	0.37
total	95.87	95.44	95.64	94.76	95.25	95.358	95.88	97.14	97.16	95.6
		22	OXYGEN							
Si	6.336	6.16	6.27	6.38	6.314	6.358	6.82	6.6	6.842	6.776
Aliv	1.664	1.84	1.73	1.62	1.686	1.642	1.18	1.4	1.158	1.224
Alvi	3.484	3.616	3.66	3.616	3.484	3.462	3.396	3.484	3.286	3.132
Ti	0.066	0.044	0.022	0.044	0.044	0.044	0	0.022	0.044	0.044
Fe	0.418	0.352	0.352	0.308	0.506	0.462	0.286	0.286	0.176	0.352
Mn	0	0	0.022	0	0	0	0	0	0	0
Mg	0.242	0.154	0.154	0.22	0.176	0.198	0.484	0.374	0.66	0.748
Ca	0	0.022	0	0	0.022	0	0	0	0	0
Na	0.11	0.176	0.198	0.132	0.066	0.088	0.044	0.044	0.088	0.044
K	1.452	1.364	1.342	1.342	1.584	1.716	1.386	1.452	1.32	1.32
Ba	0.022	0.022	0.022	0.022	0	0	0.022	0.022	0.022	0.022
Fe/ (Fe+Mg)	0.63	0.70	0.70	0.58	0.74	0.70	0.37	0.43	0.21	0.32

chl=chlorite, musc=muscovite, biot=biotite

TABLE 2.1. Mica Analyses, Continued.

Sample	GR91-10	GR91-10	GR91-71	GR91-71	GR91-71	GR91-71	GR91-71	GR91-71	GR91-71	GR91-25
Point	80	71	13	14	15	16	2	9	10	60
Mineral	biot	biot	biot	biot	biot	biot	biot	biot	biot	biot
SiO2	37.63	35.63	36.3	38.89	36.04	34.74	35.59	35.61	34.06	35.58
TiO2	1.36	1.55	1.61	1.5	1.53	1.54	1.71	1.47	1.5	0.18
Al2O3	18.39	17.51	17.29	18.4	17.24	16.64	16.92	16.97	16.86	24.77
FeO	19.11	21.97	22.77	19.73	22.38	22.16	22.42	22.74	22.37	17.2
MnO	0.12	0.23	0.17	0.2	0.36	0.32	0.21	0.22	0.33	0.44
MgO	8.49	9.79	8.49	7.62	8.32	8.47	8.7	8.05	8.57	8.12
CaO	0.11	0.14	0.08	0.08	0.13	0.17	0.11	0.05	0.12	0.38
Na2O	0.32	0.34	0.31	0.14	0.37	0.2	0.31	0.18	1.48	0.39
K2O	8.04	7.23	8.89	8.22	7.92	7.99	7.9	8.4	6.71	3.1
BaO	0	0.15	0	0	0	0	0	0.16	0	0.12
total	93.57	94.54	95.91	94.78	94.29	92.23	93.87	93.85	92	90.28
	22	OXYGEN								
Si	5.742	5.478	5.566	5.852	5.588	5.522	5.544	5.588	5.434	5.39
Aliv	2.258	2.522	2.434	2.148	2.412	2.478	2.456	2.412	2.566	2.61
Alvi	1.042	0.646	0.69	1.108	0.734	0.646	0.646	0.734	0.602	1.812
Ti	0.154	0.176	0.176	0.176	0.176	0.176	0.198	0.176	0.176	0.022
Fe	2.442	2.838	2.926	2.486	2.904	2.948	2.926	2.926	2.992	2.178
Mn	0.022	0.022	0.022	0.022	0.044	0.044	0.022	0.022	0.044	0.066
Mg	1.936	2.244	1.936	1.716	1.914	2.002	2.046	1.892	2.046	1.848
Ca	0.022	0.022	0.022	0.022	0.022	0.022	0.022	0	0.022	0.066
Na	0.088	0.11	0.088	0.044	0.11	0.066	0.088	0.066	0.462	0.11
K	1.562	1.43	1.738	1.584	1.562	1.628	1.584	1.694	1.364	0.594
Ba	0	0	0	0	0	0	0	0	0	0
Fe/ (Fe+Mg)	0.56	0.56	0.60	0.59	0.60	0.60	0.59	0.61	0.59	0.54

chl=chlorite, musc=muscovite, biot=biotite

prep).

The coarse muscovite grains analyzed (i.e., versus fine grained white mica) are characterized by high FeO (to 5 wt. %), MgO (to 4 wt. %) and TiO_2 (to 0.9 wt. %) and are, therefore, not of pure end-member composition, but contain a substantial celadonitic component (Figs. 2.9, 2.10). The chemistry is again similar to that found in the quartz veins of gold deposits, although the trend of decreasing TiO_2 with increasing MgO is in contrast to that observed in the veins. In the Al-Si-M^{2+} ternary plot the muscovite data overlap the field for hydrothermal muscovites from Meguma gold veins and broadly coincide with the range observed for muscovite from metasedimentary rocks of the Meguma Group. The BaO content of muscovite ranges from 0 to 0.45 wt. % (Fig. 2.11) and, although this is considerbly higher that Ba contents noted in muscovites from granitic rocks of the Meguma Terrane (Ham and Kontak, 1988; Kontak et al., 1991), there is no data base for comparison to the Meguma Group. These data are consistent with the presence of barite at Gays River, albeit in trace amounts, and the general geochemical affinity of Ba with Pb-Zn mineralization in the basal Windsor Group.

Plagioclase (Table 2.2) is of near end-member albite composition for both clear and inclusion-rich varieties of this phase; note that elevated K and Ca probably reflect fine grained sericitic and carbonate alteration of the feldspar, respectively.

The carbonate is near pure calcite in composition and is discussed in more detail in Chapter 5 where it is compared with a variety of carbonate types at Gays River.

2.2.2 Basal Breccia Unit

The basal breccia unit is of sedimentary origin and consists of clasts of Meguma Group

TABLE 2.2. Plagioclase Feldspar Analyses (EMPA), Gays River.

Sample	GR91-71	GR91-71	GR91-71	GR91-71	GR91-71	GR91-25	GR91-25	GR91-10	GR91-10	GR91-10	GR91-10
Point	1	5	17	18	19	45	61	72	75	81	82
Mineral	plag	plag	plag	plag	plag	plag	plag	plag	plag	plag	plag
SiO2	69.8	69.67	69.97	66.46	69.53	62.53	70.22	70.73	71.62	70.95	70.27
Al2O3	19.48	19.71	19.9	20.3	19.58	17.11	19.88	20.35	20.64	19.75	19.95
FeO	0	0.3	0	0.82	0	0	0	0.16	0.13	0.17	0
CaO	0.14	0.08	0.25	0.16	0.15	0.082	0.32	0.28	0.47	0.09	0.4
Na2O	10.05	10.14	9.61	8.72	8.17	8.88	9.94	8.68	10.36	10.18	10.47
K2O	0.04	0.08	0.12	0.9	0.87	0.11	0.04	0.24	0.11	0	0
BaO	0	0	0	0	0	0.2	0	0	0	0.11	0
total	99.51	99.98	99.85	97.36	98.3	88.912	100.4	100.44	103.33	101.25	101.09
				8 OXYGEN							
Si	3.032	3.024	3.032	2.96	3.048	3.048	3.024	3.032	3.008	3.032	3.016
Al	1	1.008	1.016	1.064	1.016	0.984	1.008	1.032	1.024	1	1.008
Fe	0	0.008	0	0.032	0	0	0	0.008	0.008	0.008	0
Ca	0.008	0	0.008	0.008	0.008	0.008	0.016	0.016	0.024	0.008	0.016
Na	0.848	0.856	0.808	0.752	0.696	0.84	0.832	0.72	0.848	0.848	0.872
K	0	0.008	0.008	0.048	0.048	0.008	0	0.016	0.008	0	0
Ba	0	0	0	0	0	0	0	0	0	0	0
				END MEMBER							
An	0.93	0.00	0.97	0.99	1.06	0.93	1.89	2.13	2.73	0.93	1.80
Ab	99.07	99.07	98.06	93.07	92.55	98.13	98.11	95.74	96.36	99.07	98.20
Or	0.00	0.93	0.97	5.94	6.38	0.93	0.00	2.13	0.91	0.00	0.00

Sample	GR91-71	GR91-71	GR91-71	GR91-71	GR91-71	GR91-25	GR91-25	GR91-10	GR91-10	GR91-10	GR91-10
Point	1	5	17	18	19	45	61	72	75	81	82
Mineral	plag	plag	plag	plag	plag	plag	plag	plag	plag	plag	plag
SiO2	69.8	69.67	69.97	66.46	69.53	62.53	70.22	70.73	71.62	70.95	70.27
Al2O3	19.48	19.71	19.9	20.3	19.58	17.11	19.88	20.35	20.64	19.75	19.95
FeO	0	0.3	0	0.82	0	0	0	0.16	0.13	0.17	0
CaO	0.14	0.08	0.25	0.16	0.15	0.082	0.32	0.28	0.47	0.09	0.4
Na2O	10.05	10.14	9.61	8.72	8.17	8.88	9.94	8.68	10.36	10.18	10.47
K2O	0.04	0.08	0.12	0.9	0.87	0.11	0.04	0.24	0.11	0	0
BaO	0	0	0	0	0	0.2	0	0	0	0.11	0
total	99.51	99.98	99.85	97.36	98.3	88.912	100.4	100.44	103.33	101.25	101.09
				8 OXYGEN							
Si	3.032	3.024	3.032	2.96	3.048	3.048	3.024	3.032	3.008	3.032	3.016
Al	1	1.008	1.016	1.064	1.016	0.984	1.008	1.032	1.024	1	1.008
Fe	0	0.008	0	0.032	0	0	0	0.008	0.008	0.008	0
Ca	0.008	0	0.008	0.008	0.008	0.008	0.016	0.016	0.024	0.008	0.016
Na	0.848	0.856	0.808	0.752	0.696	0.84	0.832	0.72	0.848	0.848	0.872
K	0	0.008	0.008	0.048	0.048	0.008	0	0.016	0.008	0	0
Ba	0	0	0	0	0	0	0	0	0	0	0
				END MEMBER							
An	0.93	0.00	0.97	0.99	1.06	0.93	1.89	2.13	2.73	0.93	1.80
Ab	99.07	99.07	98.06	93.07	92.55	98.13	98.11	95.74	96.36	99.07	98.20
Or	0.00	0.93	0.97	5.94	6.38	0.93	0.00	2.13	0.91	0.00	0.00

TABLE 2.2. Plagioclase Feldspar Analyses (EMPA), Gays River.

Sample	GR91-71	GR91-71	GR91-71	GR91-71	GR91-71	GR91-25	GR91-25	GR91-10	GR91-10	GR91-10	GR91-10
Point	1	5	17	18	19	45	61	72	75	81	82
Mineral	plag	plag	plag	plag	plag	plag	plag	plag	plag	plag	plag
SiO2	69.8	69.67	69.97	66.46	69.53	62.53	70.22	70.73	71.62	70.95	70.27
Al2O3	19.48	19.71	19.9	20.3	19.58	17.11	19.88	20.35	20.64	19.75	19.95
FeO	0	0.3	0	0.82	0	0	0	0.16	0.13	0.17	0
CaO	0.14	0.08	0.25	0.16	0.15	0.082	0.32	0.28	0.47	0.09	0.4
Na2O	10.05	10.14	9.61	8.72	8.17	8.88	9.94	8.68	10.36	10.18	10.47
K2O	0.04	0.08	0.12	0.9	0.87	0.11	0.04	0.24	0.11	0	0
BaO	0	0	0	0	0	0.2	0	0	0	0.11	0
total	99.51	99.98	99.85	97.36	98.3	88.912	100.4	100.44	103.33	101.25	101.09
				8 OXYGEN							
Si	3.032	3.024	3.032	2.96	3.048	3.048	3.024	3.032	3.008	3.032	3.016
Al	1	1.008	1.016	1.064	1.016	0.984	1.008	1.032	1.024	1	1.008
Fe	0	0.008	0	0.032	0	0	0	0.008	0.008	0.008	0
Ca	0.008	0	0.008	0.008	0.008	0.008	0.016	0.016	0.024	0.008	0.016
Na	0.848	0.856	0.808	0.752	0.696	0.84	0.832	0.72	0.848	0.848	0.872
K	0	0.008	0.008	0.048	0.048	0.008	0	0.016	0.008	0	0
Ba	0	0	0	0	0	0	0	0	0	0	0
				END MEMBER							
An	0.93	0.00	0.97	0.99	1.06	0.93	1.89	2.13	2.73	0.93	1.80
Ab	99.07	99.07	98.06	93.07	92.55	98.13	98.11	95.74	96.36	99.07	98.20
Or	0.00	0.93	0.97	5.94	6.38	0.93	0.00	2.13	0.91	0.00	0.00

lithologies in a dolomitic matrix. The thickness of this unit varies considerably (see sections above), presumeably reflecting paleotopography, and the large variation in size (mm to metre scale; Fig. 2.12a) and shape (angular to subrounded) of the Meguma Group clasts is probably also a reflection of paleotopography. Mineralization occurs within the breccia unit, but it is highly irregular in nature and varies from trace amounts to high-grade ore with both Pb- and Zn-rich varieties, although the former is more common based on the authors observations. Carbonate veins, either barren or mineralized, occur within the breccia and may also cut across clasts of Meguma Group (Fig. 2.12f). The veins are up to several cm wide, but because they have been mainly observed within drill core their full extent is unknown.

Examination of the breccia unit in polished section reveals the following features. The fragments are composed of equal amounts of psammitic and pelitic material, with the former coarser and the latter being differentiated on the abundance of micaceous material and finer grain size. The fragments are of variable shape and their margins have been modified to different degrees due to a combination of (1) pressure solution and (2) carbonate alteration (Fig. 2.12d). In the former case, it is common to observe fragments penetrating into adjacent fragments reflecting post-depositional modification (Fig. 2.12b, c). Many of the frag..ents also indicate weak development of a new fabric which crenulates earlier fabrics in the clasts, truncates fragment boundaries and rarely deforms matrix calcite and mineralization. The fragments have a mineralogy similar to that described for the Meguma Group, although the pelitic clasts are richer in muscovite and biotite. It is very common for the fragments to be enveloped by a thin rind of reddish-brown material (Fe or Mn oxide?) and corrosion of the fragments is very common (Fig. 2.12c, d).

The matrix is composed of very fine fragmental material or single quartz and feldspar grains, although it is mostly fine to medium grained dolomite and calcite. The quartz grains show highly irregular shapes (Fig. 2.12e) suggesting fracturing of grains during transport. The fracturing predated lithification and mineralization since the grains are subsequently coated by fine grained sphalerite, as are fragments of the Meguma Group lithologies (Fig. 2.12g, h). The dolomite is light to dark brownish and the medium-grained material has a granular texture which locally coarsens and gives way to calcite. Textures suggest that the calcite has replaced the dolomite, but there is also textural evidence of open space infilling of vugs (i.e., cementation).

Mineralization consists of variable amounts of galena and sphalerite, with traces of pyrite and chalcopyrite, and occurs within matrix carbonate, calcite veins and the metasedimentary fragments; matrix type mineralization is by far the most abundant. Mineralization within fragments is most common in pelitic material as disseminations and more rarely as lenses parallel to schistosity (Fig. 2.12g). Matrix mineralization is either of replacive type or occurs as euhedral grains outlining cavities within the dolomite which are then infilled with calcite (Fig. 2.12c, e, g, h). Sphalerite is commonly of the replacive type with fine grained aggregates or disseminations occurring. The coarse grained sphalerite is multi-faceted and yellowish to orange. Galena occurs as coarser grains of either anhedral or euhedral shape, occurring within the dolomite, as part of irregular-shaped calcite patches or within the calcite veins. Galena is more abundant as a cementation-type mineralization and may exceed the calcite in terms of modal proportion (Fig. 2.12h), while sphalerite is more common within the matrix dolomite. The few occurrences of pyrite include euhedral aggregates in the dolomite and calcite, and also anhedral grains within the dolomite and fragments.

2.2.3 Carbonate Rocks

The carbonate buildup, bank or mound which occurs at Gays River consists of numerous rock types (e.g., Fig. 2.13) and have been fully described by a number of authors (MacLeod, 1975; Hartling, 1977; Osborne, 1977; Hatt, 1978; Akande, 1982; Schenk and Hatt, 1984; Boehner et al., 1989). In the present study the author was not particularly concerned with the nature and origin (i.e., environment of deposition) of the carbonate rocks, but instead the features which were related to mineralization. The most important observation based on drill core examined from the central and western parts of the carbonate bank is that the most abundant carbonate type is a massive, fine grained, buff to brown colored, variably porous carbonate (Fig. 2.13a, b, c). The carbonates were completely dolomitized during diagenesis and now consist of microdolostone (see Table 5.4 for analyses) with minor amounts of dedolomitized limestone (see Akande (1982) for discussion of this lithology). The dolomitization was a constant volume, mole for mole replacement and consequently delicated textures have been preserved, such as fossils (Figs. 2.13d, 2.14c, d). There is a complete gradation in rock type depending on the proportion of fine-grained micritic type material and fossil remains. However, for the most part the dolomitization process has produced a homogeneous rock with a fine-grained, medium to dark brown, granular texture. There is a large range in the amount of porosity present and the degree of fill of the pore space varies from almost nil to complete cementation (Figs. 2.13c, 2.14) . The pores are of mm to cm size (rarely to 10-20 cm). The porosity is variably cemented in the following sequence (Fig. 2.14): (1) euhedral dolomite, (2) fine grained yellow to orange sphalerite, (3) sparry calcite, and (4) galena euhedra. In some cases stages 2 and 4 may be absent or only one present. The sphalerite may also occur as fine grained disseminations within

the massive dolostone and, more rarely, galena may have the same texture. Aspects of the mineralization are discussed in more detail in Chapter 3.

The dolostone contains, in addition to carbonate, detritus from varibly comminuted or disaggregated Meguma Group rocks which occurs within the basal part of the carbonate stratigraphy (i.e., few metres; Fig. 2.13e). The detritus consists of both small rock fragments and also single mineral grains of quartz, albitic feldspar, mica and tourmaline. Quite frequently this comminuted material is concentrated where styolitic textures are developed (Fig. 2.13f), although styolites may develop without this association. There are areas of the dolostone where coarsening occurs as an abrupt phenomenon such that fine grained material gives way to much coarser grained, equigranular material (Fig. 2.13g). This coarsening is sometimes associated with a distinct lightening of the dark brownish dolostone along a network of microfractures with the growth of calcite as either a replacement or void infill phenonmenon (Fig. 2.13h). In some cases this transformation may result in a coarse, polygonal textured dolostone.

The dolostone is also cut by veinlets infilled with calcite (Fig. 2.14e, f) which appears to be syn-calcite cementation of the primary porosity.

2.2.4 Evaporites

The evaporite sequence within the mine area has not been examined to date and has only been observed in two locations underground. The material observed was massive, whitish to grey gypsum and was not deformed, but locally recrystallization and distortion of the beds occurs (J. Campbell, personal communication, 1992).

2.2.5 Trench Sediments

The term trench was used by the mine geologists at Gays River to described a long, narrow, sinuous, sediment-filled ditch (karst ?) or depression at the carbonate-evaporite contact. The sections illustrated in Figure 2.6 indicate that the depression has an inverted cone shape and pinches out at depth with a maximum vertical extent approaching 100 metres. The infill consists of semi-consolidated material of gravel to clay size which is water saturated and causes problems with respect to mining since it forms the hanging wall within most of the deposit; minor amounts of coaly material are also present. Underground observations by J. Campbell (personal communication, 1992) suggest that reworking of previously deposited material continues within the trench and, therefore, that this is a very dynamic environment. In fact, Campbell considers that the trench has remained an active site of fluid flow for its entire history from its initial time of formation to present.

The age of the trech infill is constrained by the following geological relationships: (1) it is of post Viséan age based on stratigraphic relationships; (2) it is unmineralized and, therefore, post-dates the Zn-Pb mineralization (post Lower Carbonaifierous ?); and (3) it is overlain by glacial deposits of Pleistocene age. In an attempt to directly date the sediments Davies et al. (1984) extracted six samples from the western end of the deposit for palynologicaly study. Pollen and spores from these samples are of Aptian to Early Albian age (Cretaceous). This age is consistent with the presence of additional Cretacous deposits nearby (Giles and Boehner, 1982). Coaly material in the trech sediments was analyzed for vitrinite reflectance and results (R_o=0.44) suggest a rank of lignite (Davies et al., 1984). If the reflectance values are real and have not been modified due to the water-rich environment and effects of oxidation, then burial

to a depth of 1-2 km would be required to account for the rank of lignite (Akande, 1982). An alternative interpretation is that the coaly material has been transported into the trench and that the reflectance values record an earlier, pre-transport thermal history. In this case the trench represent an erosional feature that was likely not buried since the Cretaceous, except by glaciers, to any appreciable depth.

Fig. 2.1. General geology of the area aroung the Shubenacadie and Musquodoboit basins showing the location of basal Windsor Group carbonate-hosted Pb-Zn-Ba-F mineralization. Gays

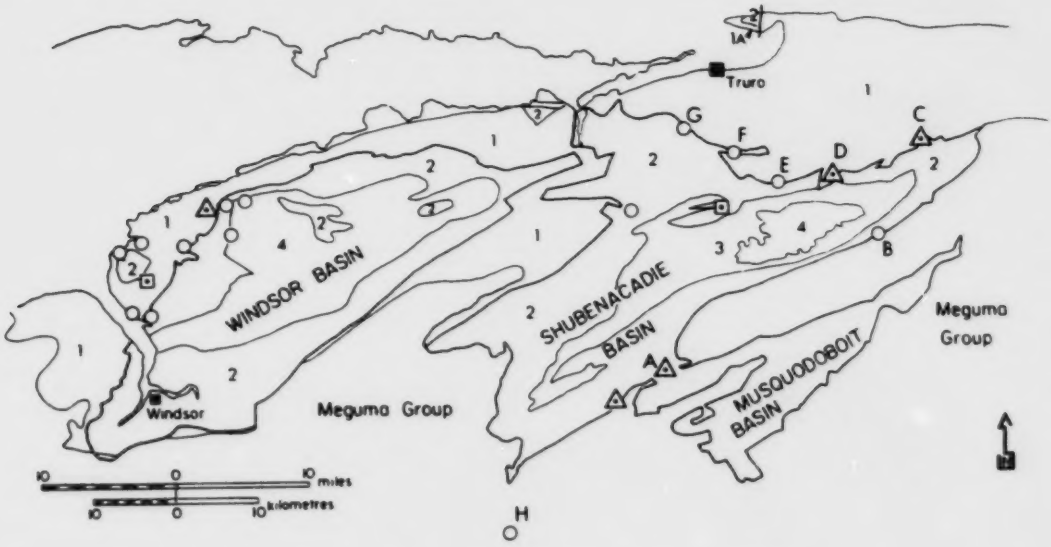

UPPER CARBONIFEROUS

PICTOU GROUP

4 Sandstone, siltstone, shale, coal

CANSO GROUP

3 Sandstone, siltstone, shale

LOWER CARBONIFEROUS

WINDSOR GROUP

2 Sandstone, siltstone, carbonates, evaporites

HORTON GROUP

1 Sandstone, siltstone shale, conglomerate, dolostone, coal

Symbols

△ Carbonate-hosted Pb-Zn occurrence

○ Barite occurrence

⊡ Fluorite occurrence

Fig. 2.2. Geological outline of the Shubenacadie and Musquodoboit basins showing the locations of carbonate banks of the Gays River Formation. Inset map shows the distribution of the Lower Carboniferous Windsor Group and the extent of the Fundy Basin (part of the larger Maritimes Basin). Diagram from Akande and Zentilli (1984).

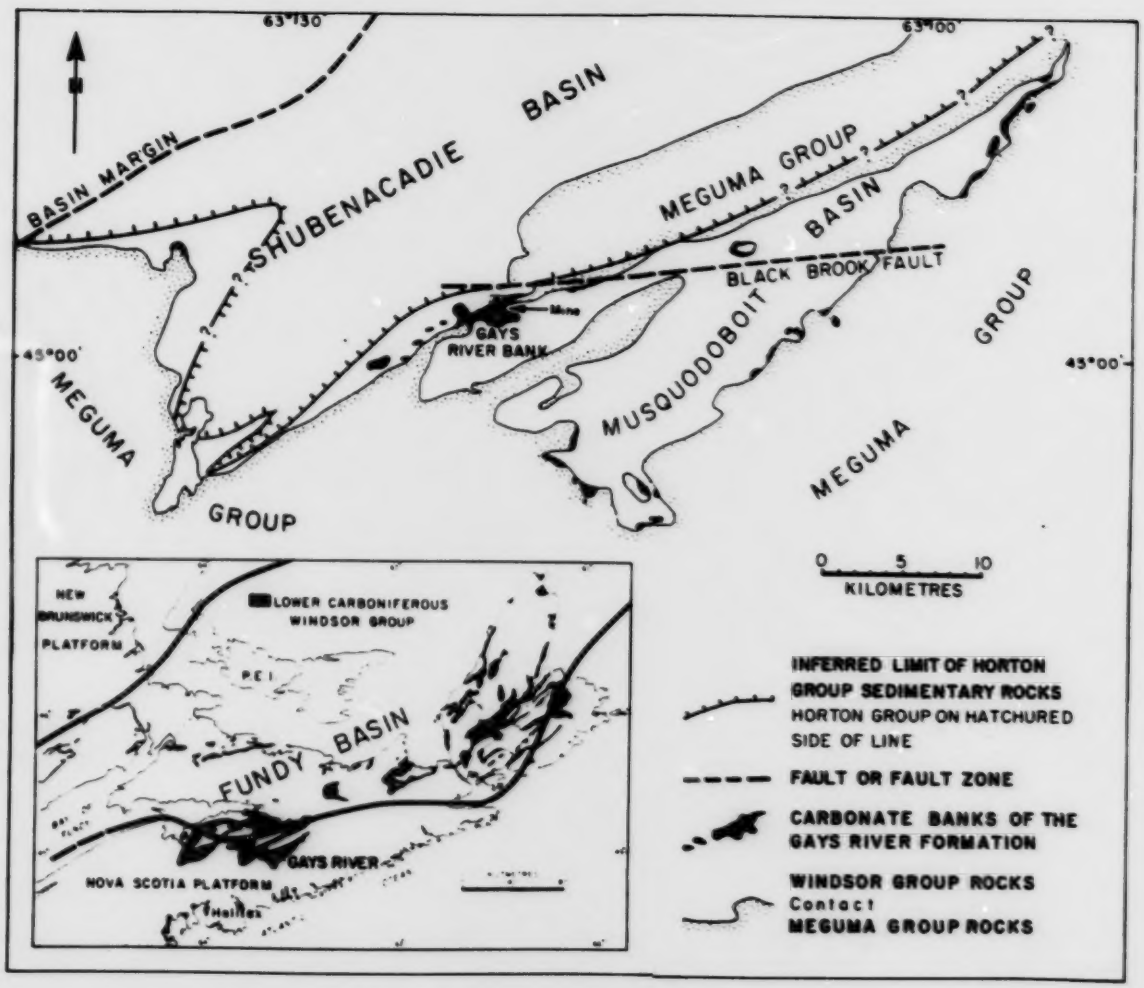

Fig. 2.3. Stratigraphy of the Shubenacadie and Musquodoboit basins (after Giles and Boehner, 1979).

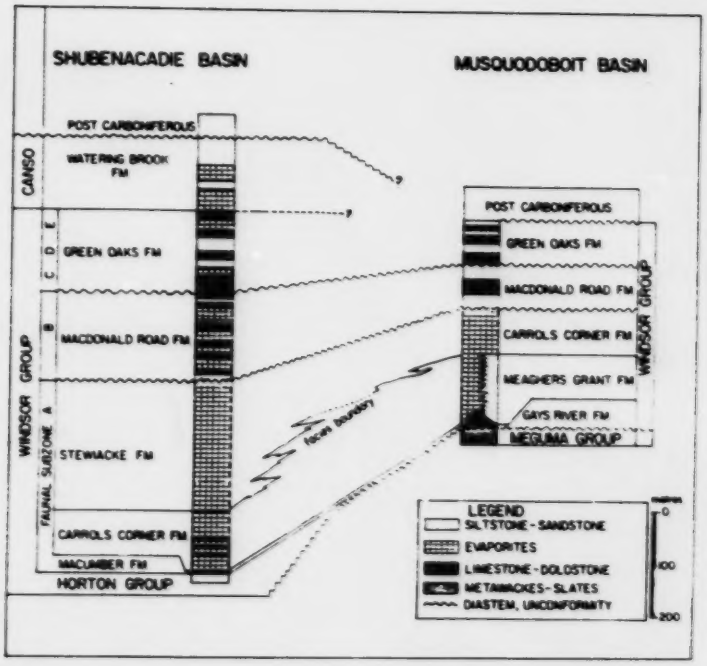

Fig. 2.4. Simplified plan map of the Gays River deposit area (from Akande and Zentilli, 1984) showing the outline of the Main Deposit area and the Getty Deposit. Note the coincidence of the orebody and the evaporite-carbonate contact. Line A-B represents the geological section presented in Figure 1.3.

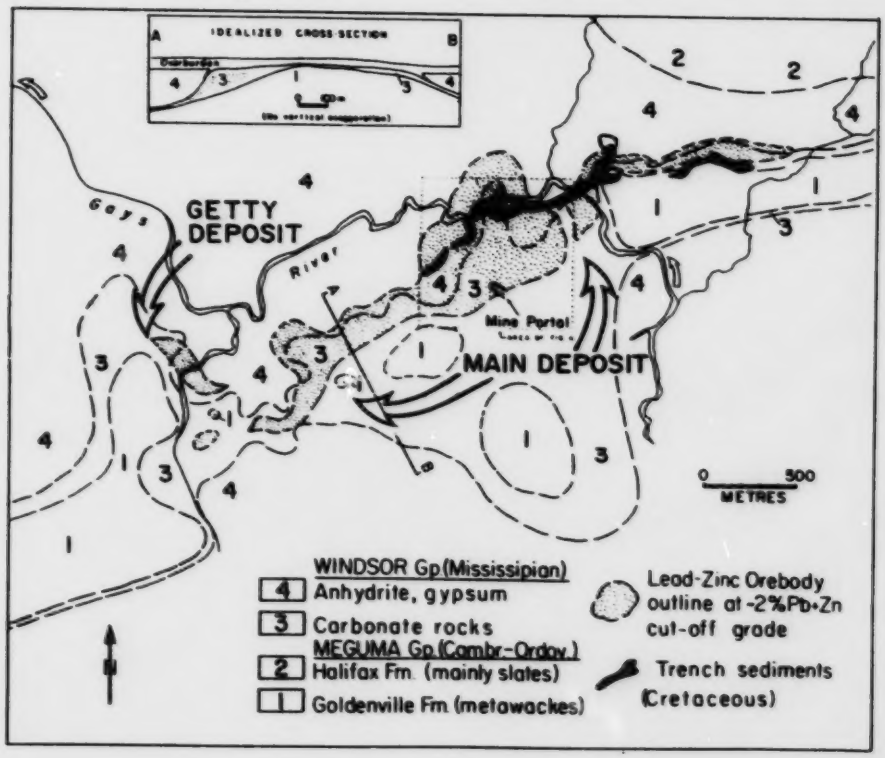

Fig. 2.5. Plan map of the Gays River deposit showing the outline of ore zones and 10 m level contours (thin black lines) as delineated by diamond drilling. Note that the ore zones dip off towards the basin (i.e., northwest as indicated by broad arrows) and that there is a prominent orientation of the ore zones along generally N-S and E-W trends which coincides with main fracture trends in the Meguma Group basement. The lines indicated are the locations of the vertical sections shown in Figure 2.6 (1-29 Main Deposit and AA'-GG' Getty Deposit). The grid system is that of Westminer Canada Ltd. for the deposit area. Diagram modified after Westminer Canada Ltd.

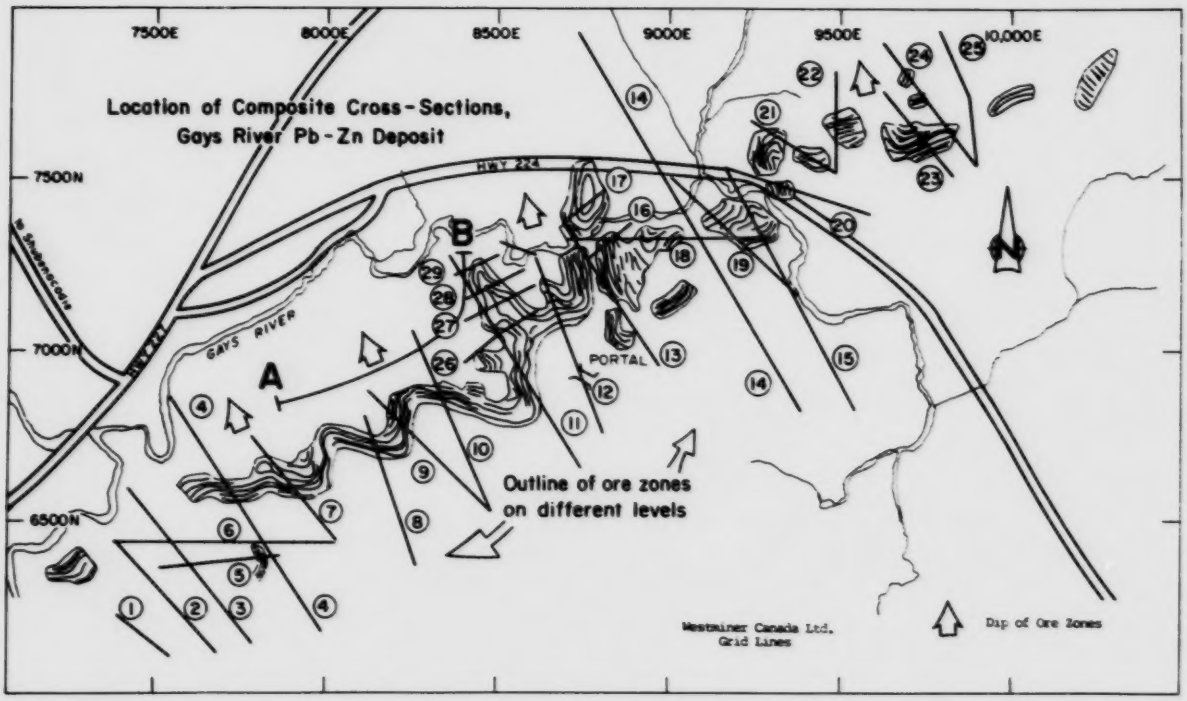

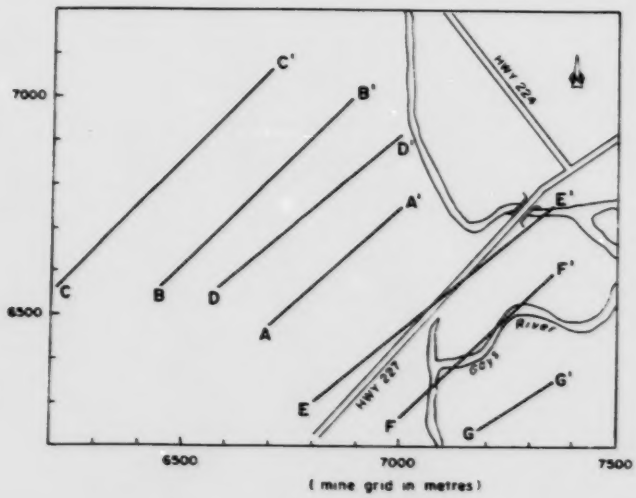

Fig. 2.6. Composite vertical sections through the Main deposit area (see Figure 2.5 for the location of the sections). Sections have been constructed using information for the various diamond drill holes indicated as compiled by geologists of Westminer Canada Ltd.. The legend shown is for all the sections. For all the sections note the following: (1) the vertical scale refers to elevation in metres using the mine levels as reference and does not reflect the local topography; (2) the horizontal scale varies in each diagram and the length of the sections can be obtained from Figure 2.5; and (3) there is a variable vertical exaggeration in all the sections.

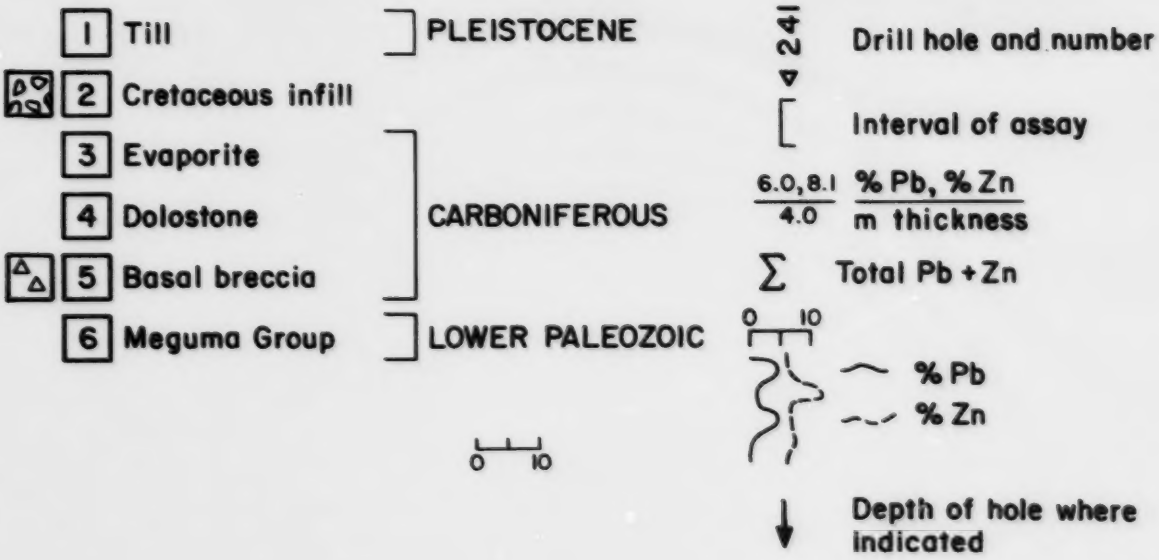

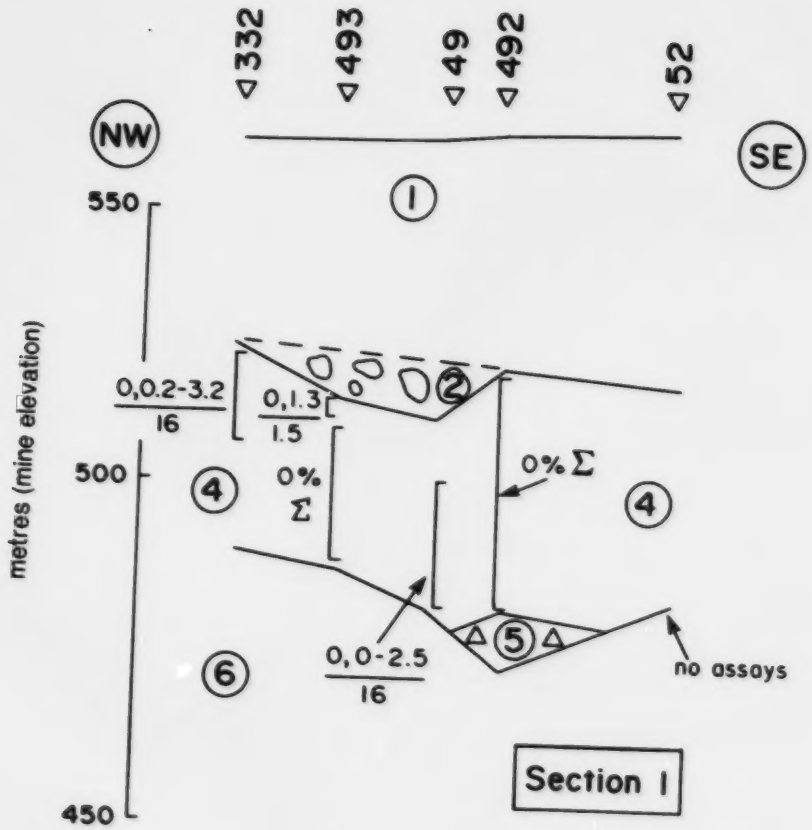
332
493
49
492
52
NW
SE
1
550
500
450
metres (mine elevation)
0,0.2-3.2
16
0,1.3
1.5
2
0% Σ
4
0% Σ
4
5
6
0,0-2.5
16
no assays
Section 1

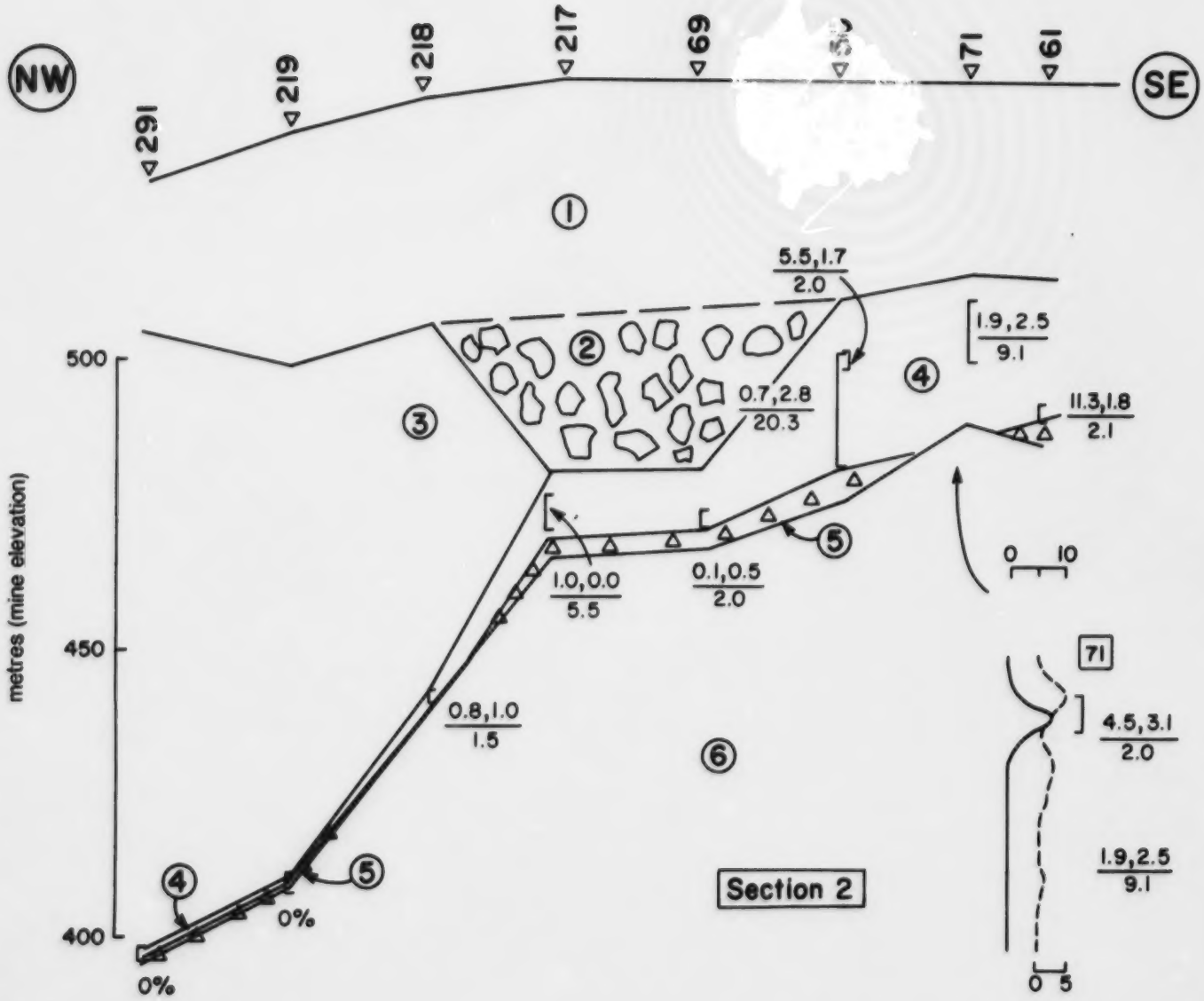
NW
SE
291
219
218
217
69
71
61
1
2
3
4
5
6
5.5,1.7
2.0
0.7,2.8
20.3
1.9,2.5
9.1
11.3,1.8
2.1
1.0,0.0
5.5
0.1,0.5
2.0
0.8,1.0
1.5
0
10
71
4.5,3.1
2.0
1.9,2.5
9.1
0
5
0%
0%
500
450
400
metres (mine elevation)
Section 2

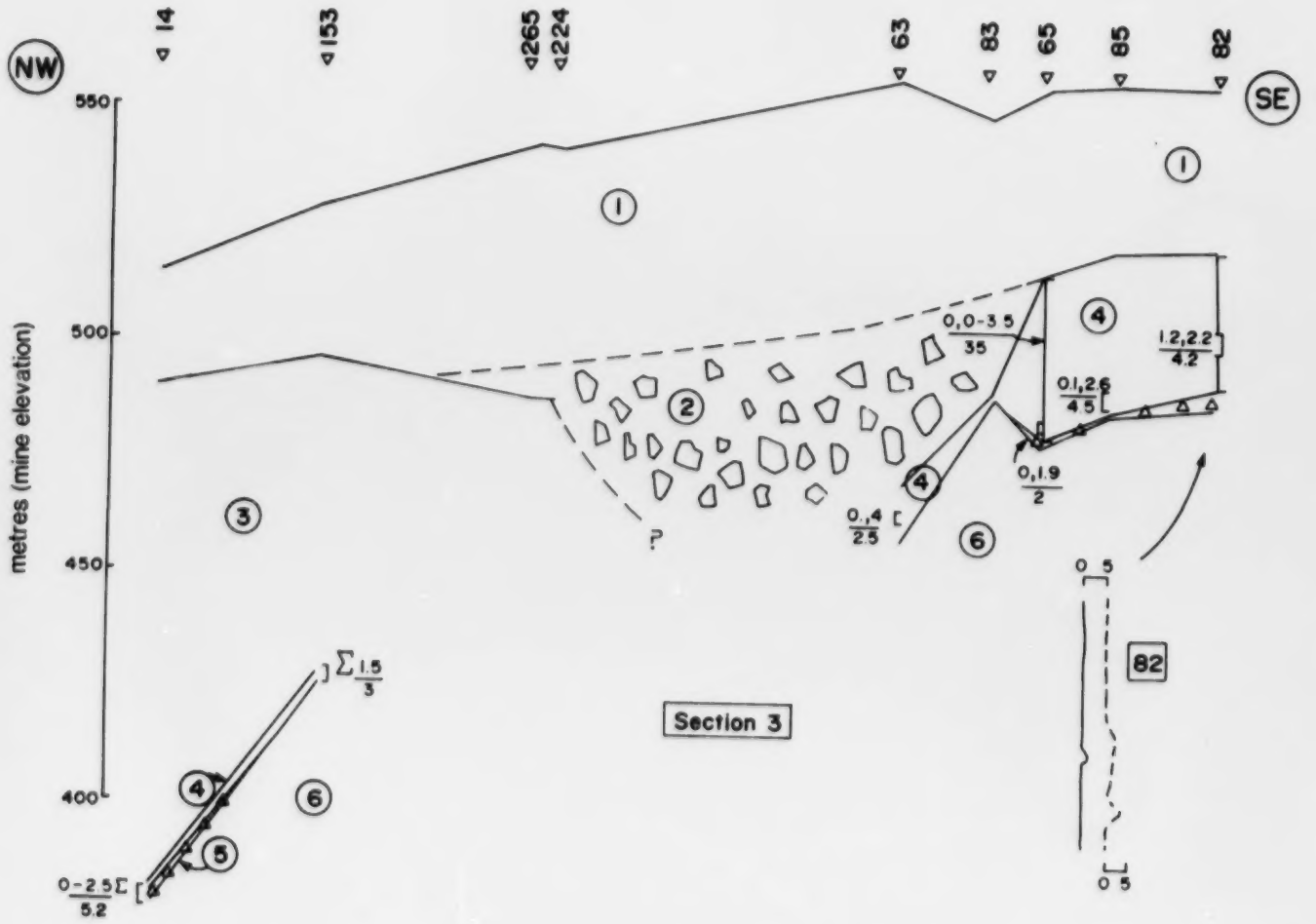
NW
SE
14
153
265
224
63
83
65
85
82
550
500
450
400
metres (mine elevation)
1
2
3
4
5
6
0,0-3.5
35
12,22
4.2
0,12.6
4.5
0,1.9
2
0,4
2.5
?
Σ 1.5
3
0-2.5 Σ
5.2
0.5
0.5
82
Section 3

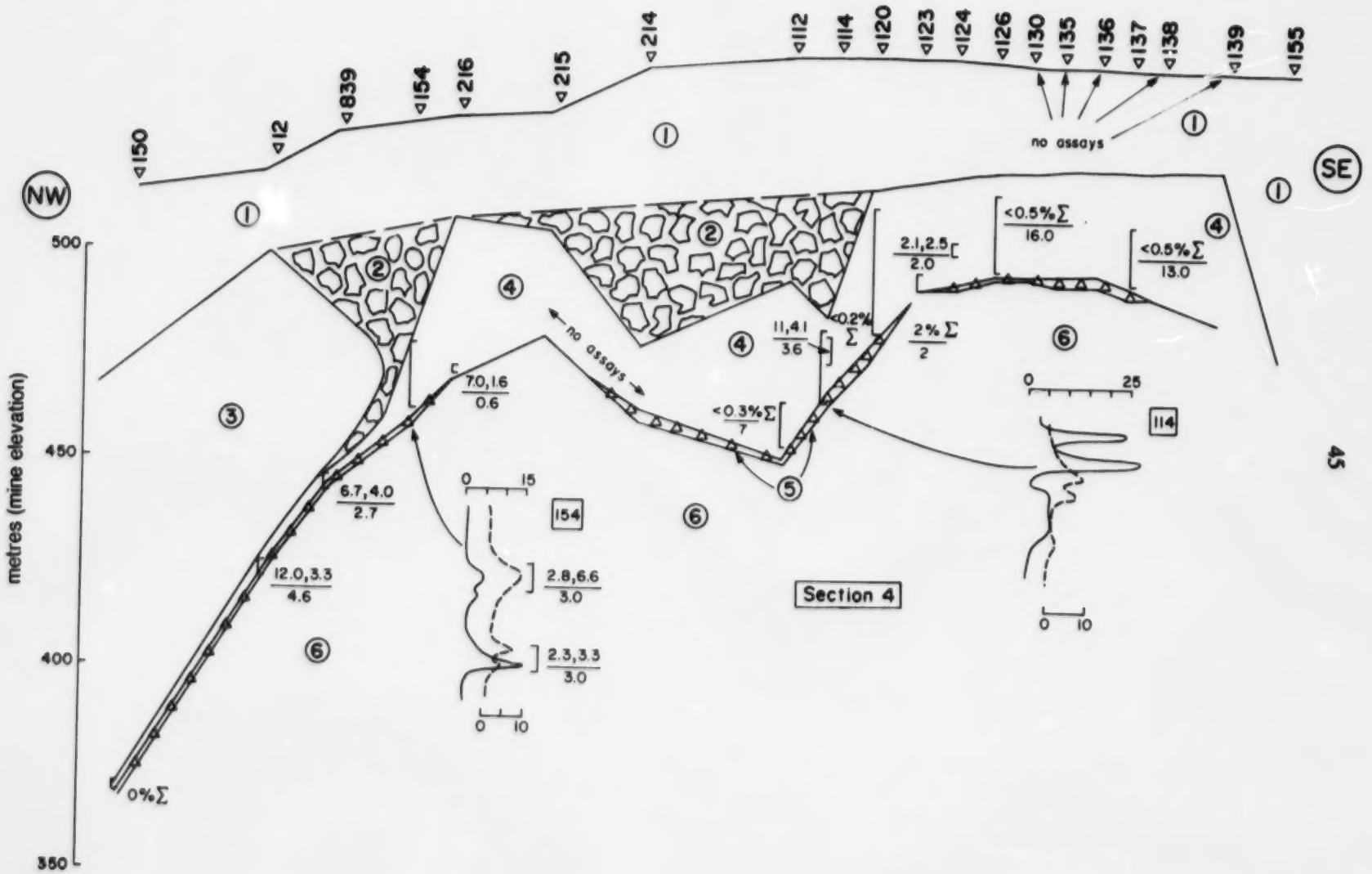
150
12
839
154
216
215
214
112
114
120
123
124
126
130
135
136
137
138
139
155
no assays
NW
SE
metres (mine elevation)
500
450
400
350
no assays
7.0, 1.6
0.6
6.7, 4.0
2.7
12.0, 3.3
4.6
0%Σ
0 15
154
2.8, 6.6
3.0
2.3, 3.3
3.0
0 10
11, 41
36
<0.2%Σ
<0.3%Σ
7
2.1, 2.5
2.0
<0.5%Σ
16.0
<0.5%Σ
13.0
2%Σ
2
0 25
114
0 10
Section 4

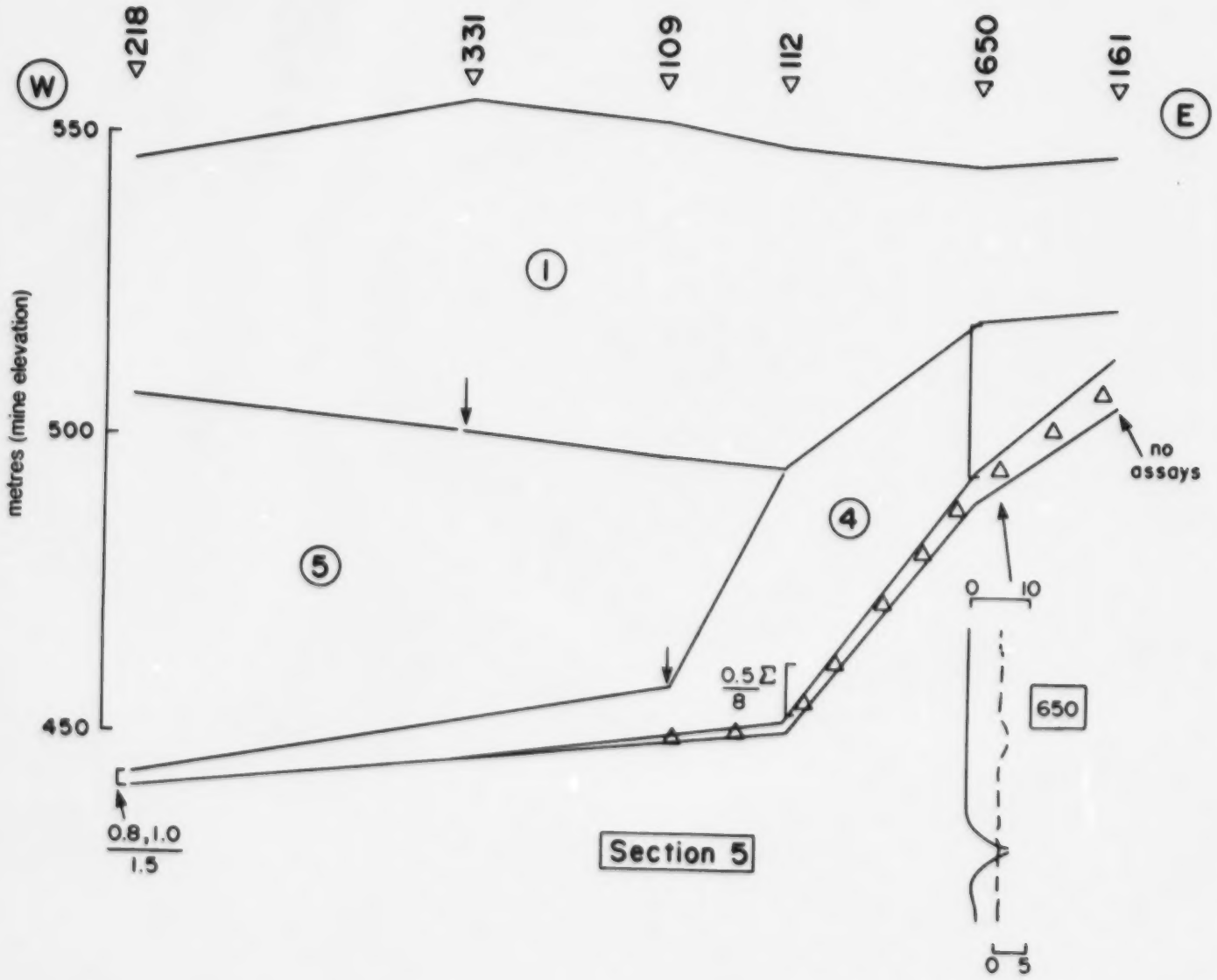
W
E
218
331
109
112
650
161
550
500
450
metres (mine elevation)
1
4
5
no assays
0 10
0.5Σ / 8
650
0.8, 1.0 / 1.5
Section 5
0 5

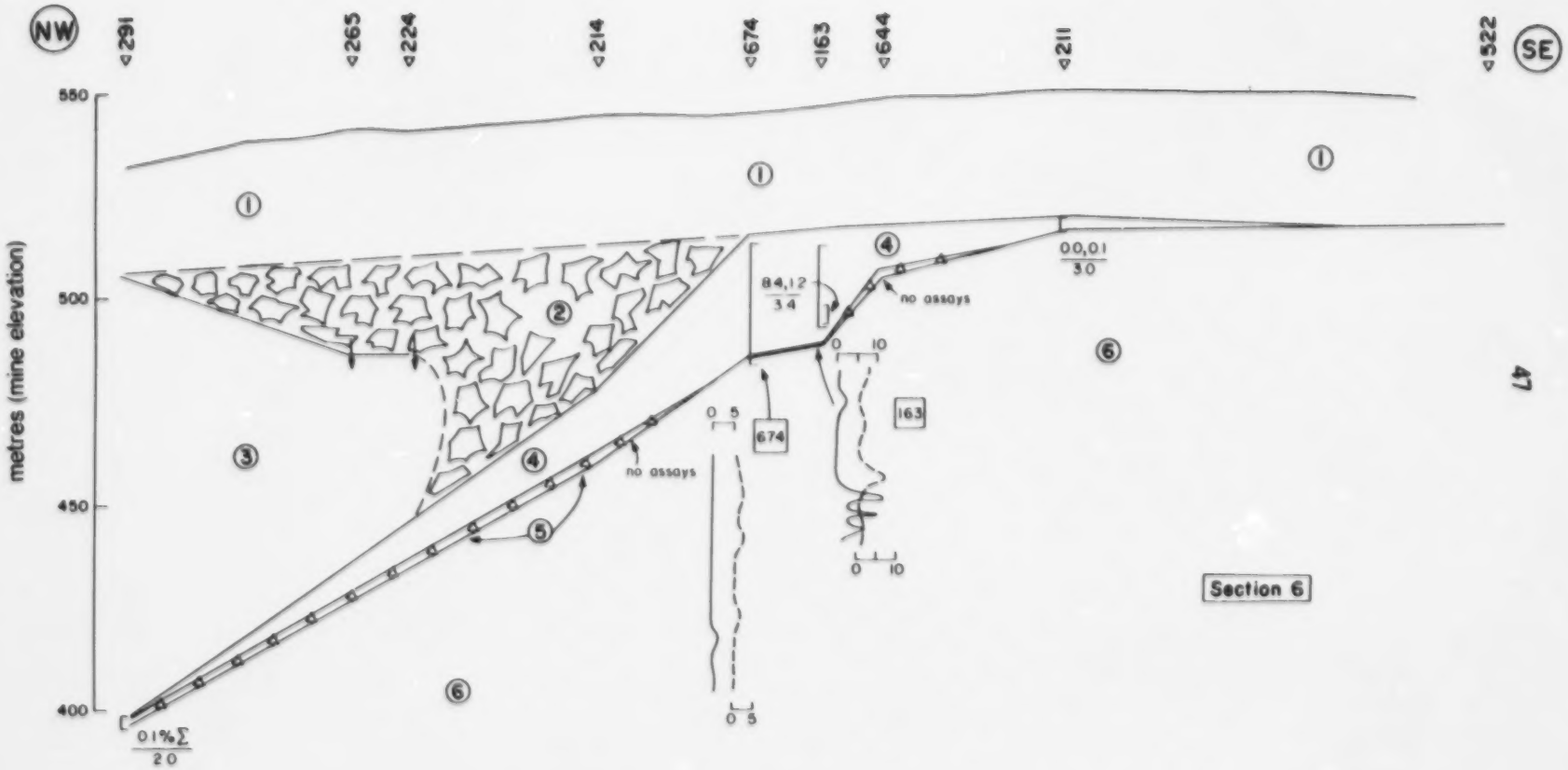
NW
291
265
224
214
674
163
644
211
522
SE
550
500
450
400
metres (mine elevation)
①
②
③
④
⑤
⑥
84,12
34
00,01
30
no assays
0 10
0 5
674
163
0 10
0 5
no assays
01%Σ
20
Section 6

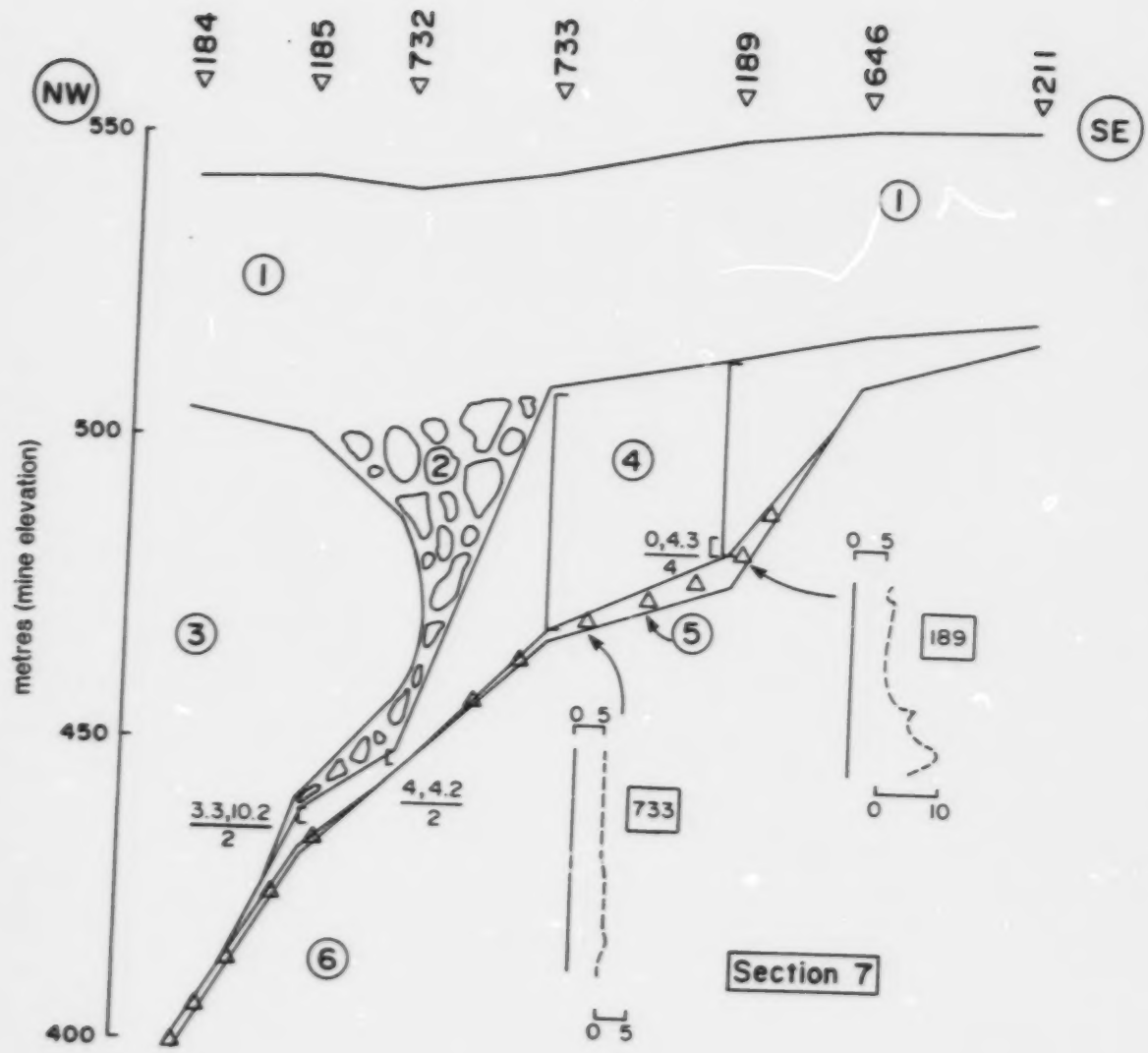
NW
SE
184
185
732
733
189
646
211
550
500
450
400
metres (mine elevation)
1
2
3
4
5
6
3,3,10.2
2
4,4.2
2
0,4.3
4
0 5
733
0 5
189
0 10
0 5
Section 7

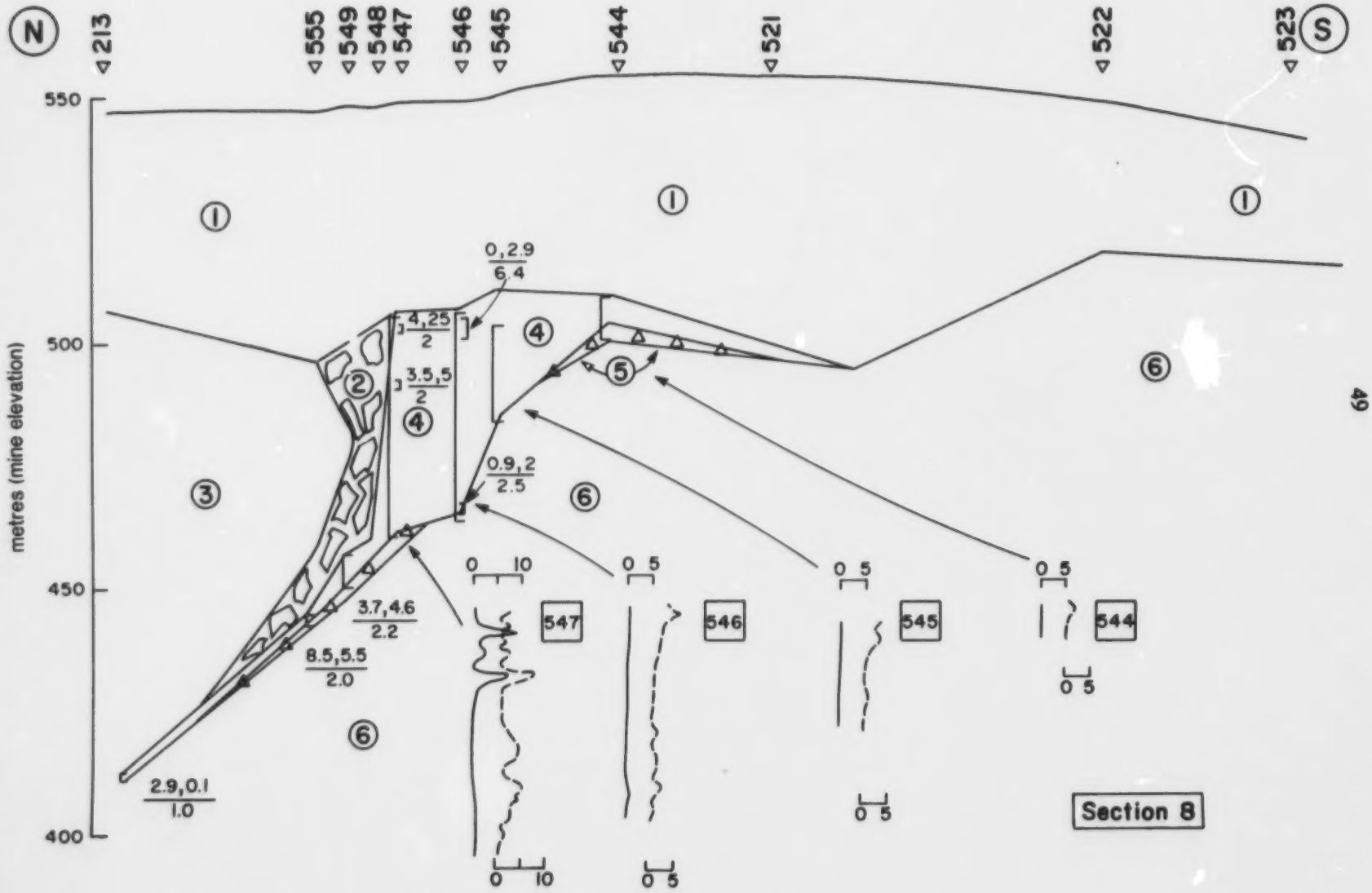
N
213
555
549
548
547
546
545
544
521
522
523
S
550
500
450
400
metres (mine elevation)
0,2.9
6.4
4,25
2
3.5,5
2
0.9,2
2.5
3.7,4.6
2.2
8.5,5.5
2.0
2.9,0.1
1.0
0 10
0 5
547
546
545
544
Section 8

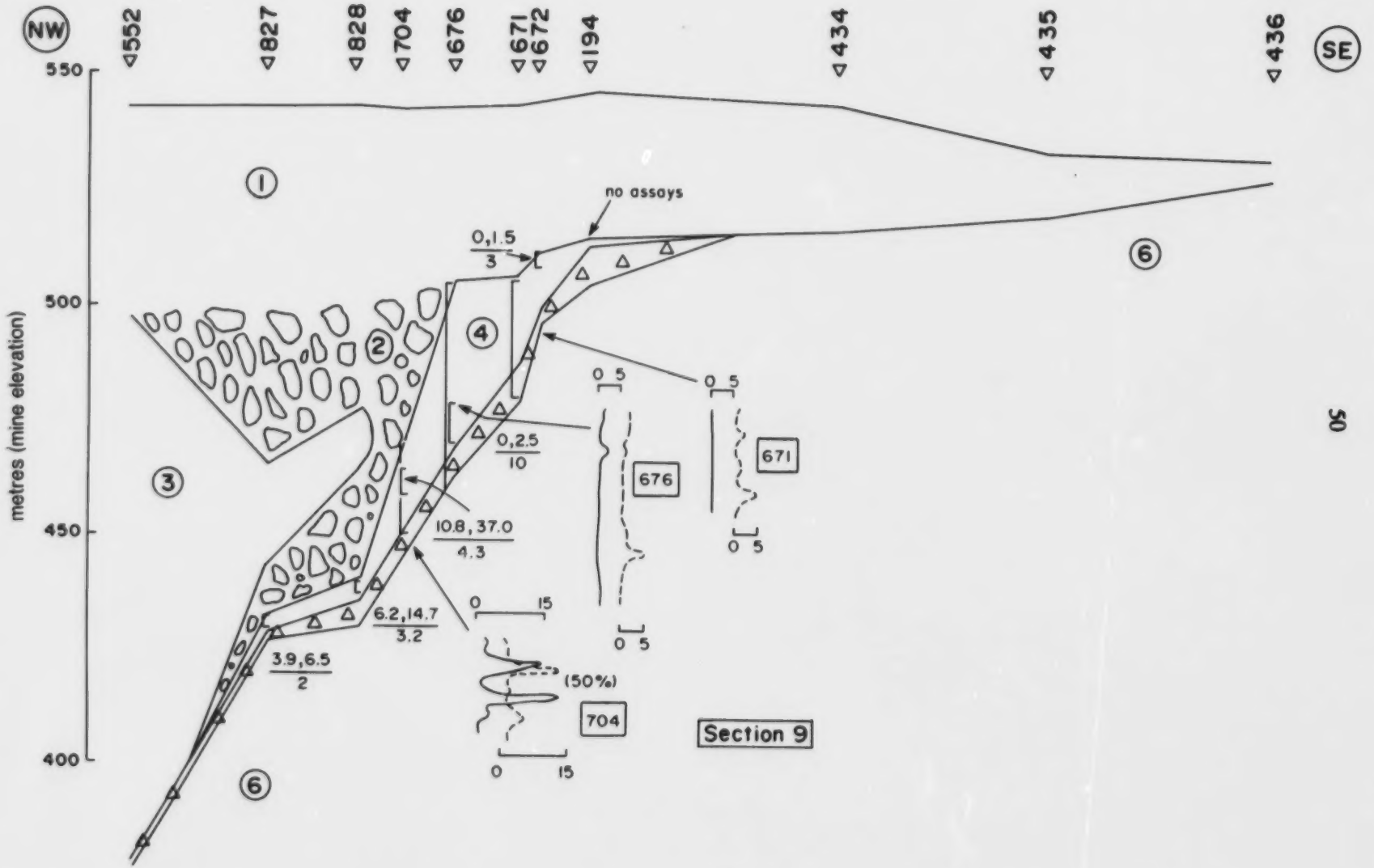
NW
SE
552
827
828
704
676
671
672
194
434
435
436
550
500
450
400
metres (mine elevation)
1
2
3
4
6
no assays
0,1.5
3
0,2.5
10
10.8, 37.0
4.3
6.2,14.7
3.2
3.9,6.5
2
0 5
0 5
676
671
0 5
0 15
(50%)
704
0 15
Section 9
50

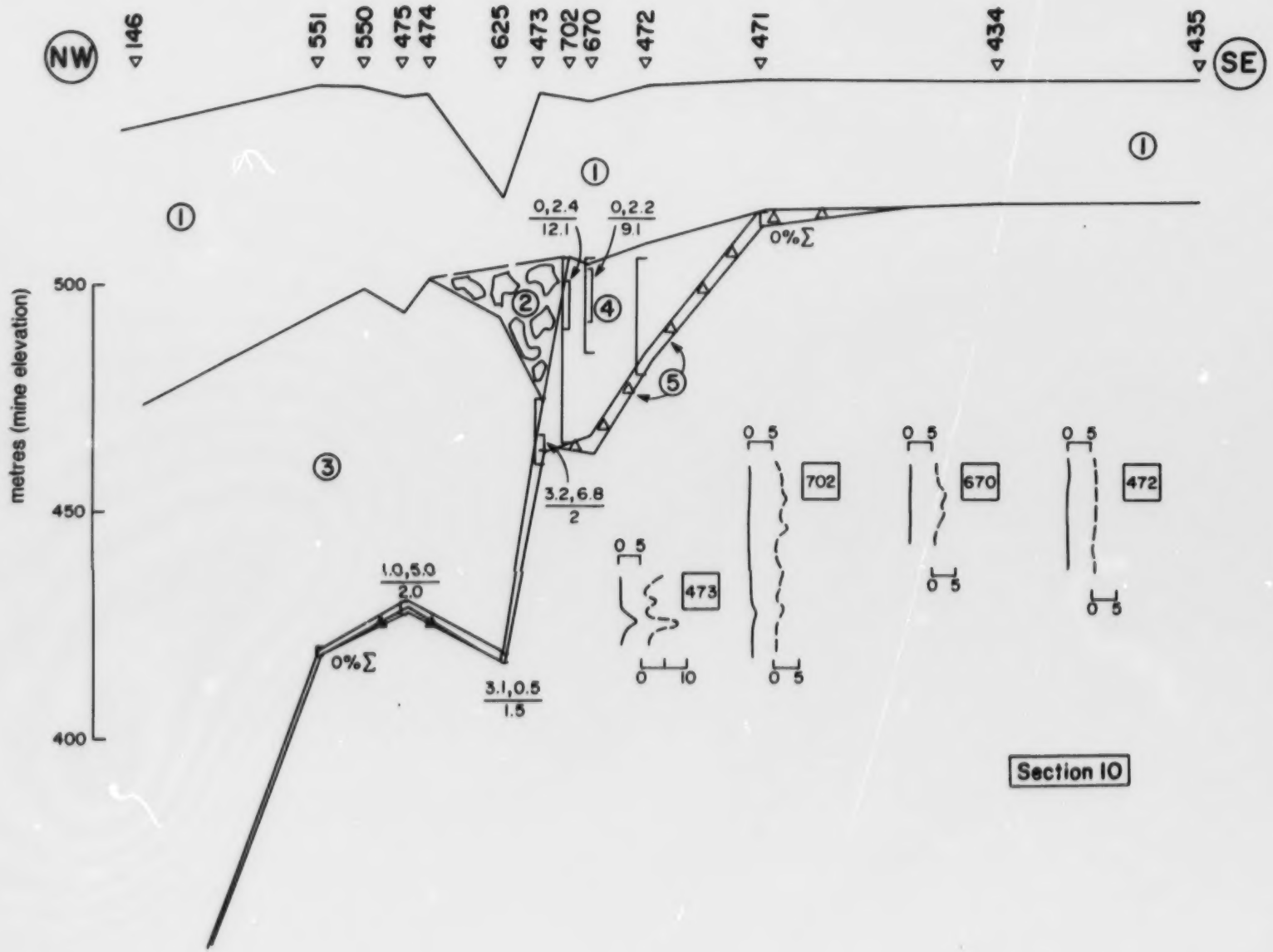
NW
SE
146
551
550
475
474
625
473
702
670
472
471
434
435
metres (mine elevation)
500
450
400
0,2.4
12.1
0,2.2
9.1
0%Σ
3.2,6.8
2
1.0,5.0
2.0
0%Σ
3.1,0.5
1.5
0 5
473
0 10
0 5
702
0 5
670
0 5
0 5
472
0 5
Section 10

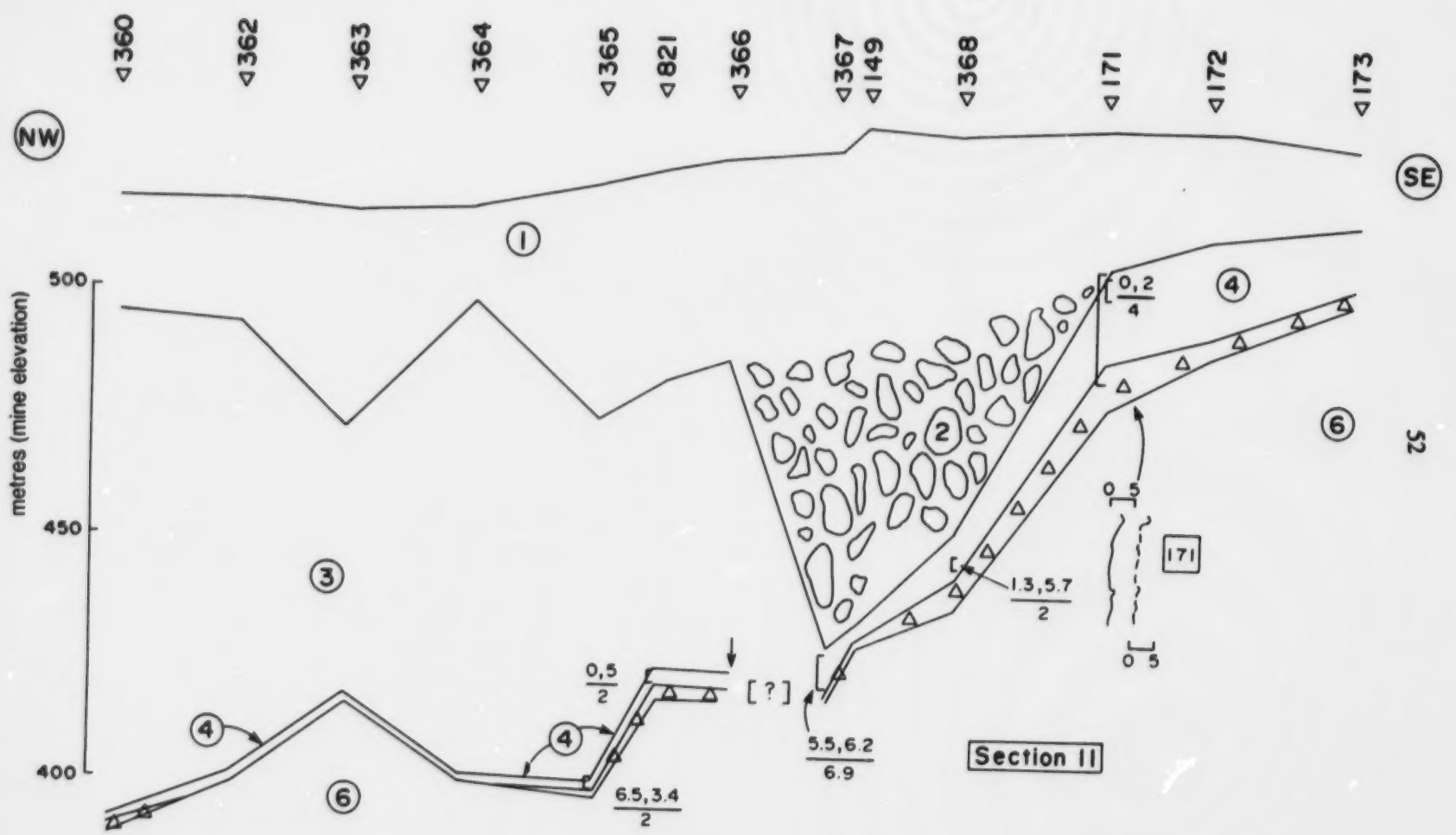
360
362
363
364
365
821
366
367
149
368
171
172
173
NW
SE
metres (mine elevation)
500
450
400
1
2
3
4
6
0,2
4
1.3,5.7
2
0,5
2
[?]
5.5,6.2
6.9
6.5,3.4
2
0
5
171
Section 11
52

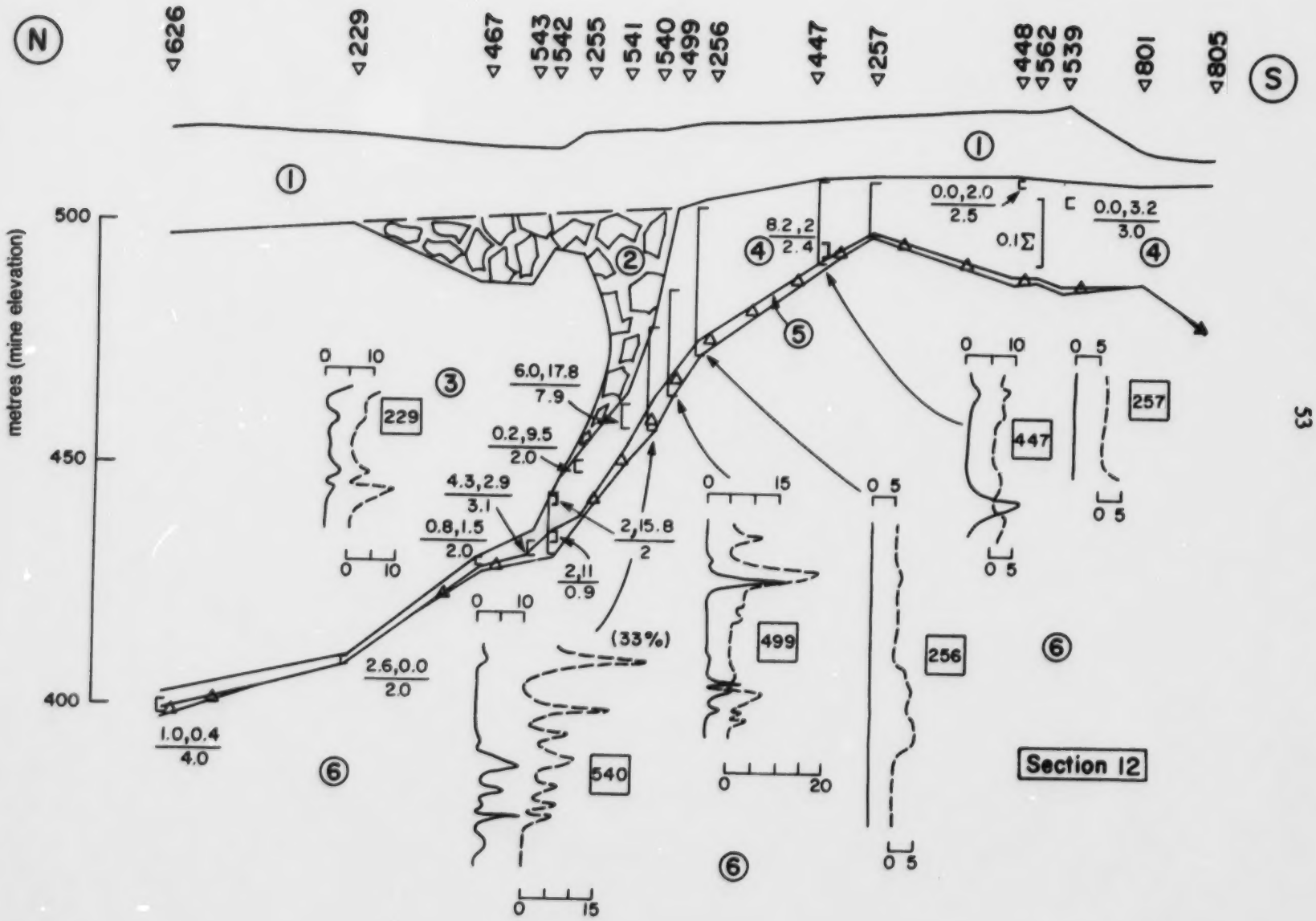
N
626
229
467
543
542
255
541
540
499
256
447
257
448
562
539
801
805
S
metres (mine elevation)
500
450
400
1
2
3
4
5
6
8.2, 2
2.4
0.0, 2.0
2.5
0.0, 3.2
3.0
0.1Σ
6.0, 17.8
7.9
0.2, 9.5
2.0
4.3, 2.9
3.1
0.8, 1.5
2.0
2, 15.8
2
2, 11
0.9
2.6, 0.0
2.0
1.0, 0.4
4.0
(33%)
229
447
257
499
256
540
0 10
0 15
0 5
0 20
Section 12

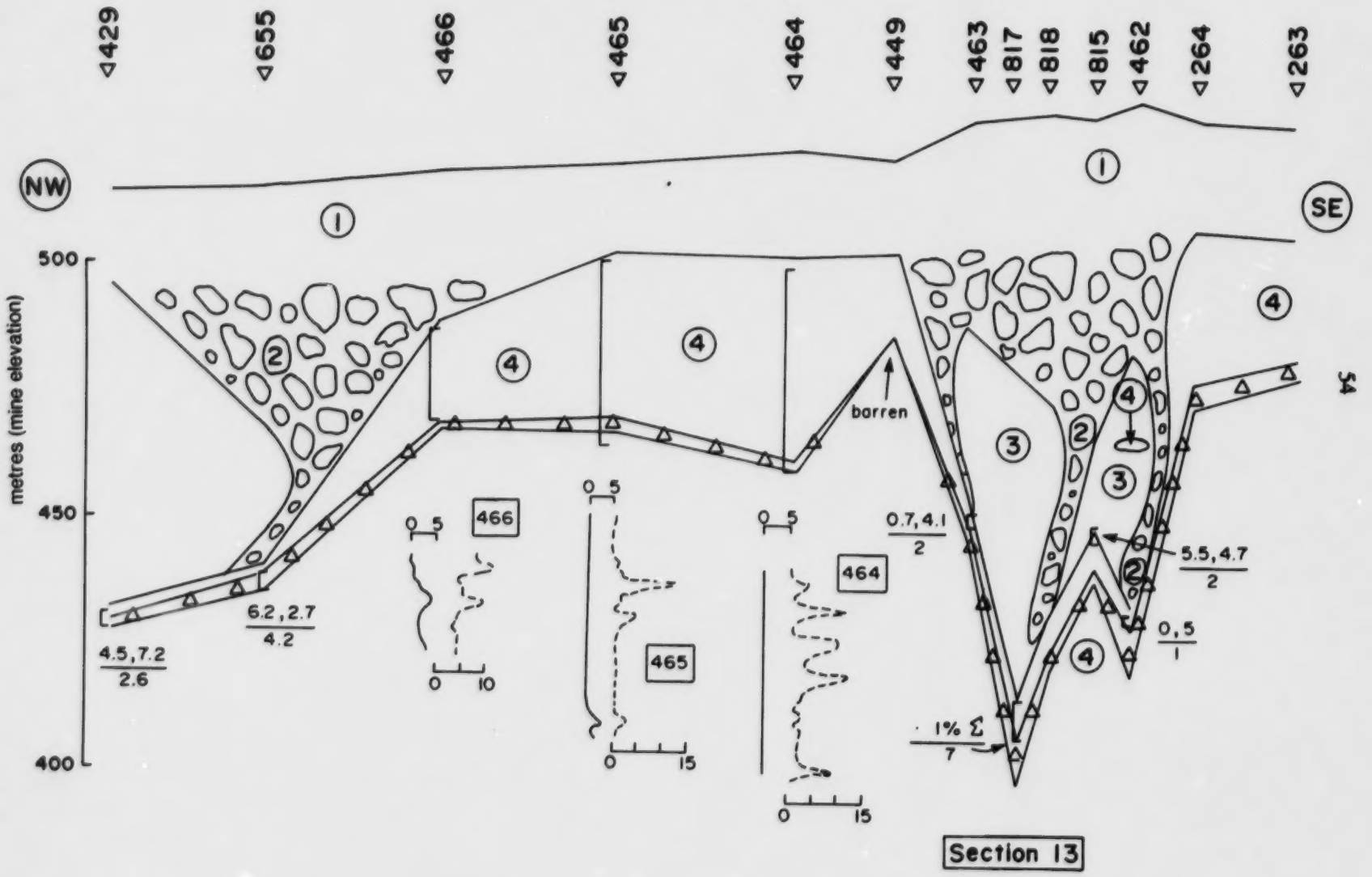
429
655
466
465
464
449
463
817
818
815
462
264
263
NW
SE
1
2
3
4
500
450
400
metres (mine elevation)
barren
6.2, 2.7
4.2
4.5, 7.2
2.6
0.7, 4.1
2
5.5, 4.7
2
0, 5
1
1% Σ
7
466
465
464
0 5
0 10
0 15
0 15
Section 13

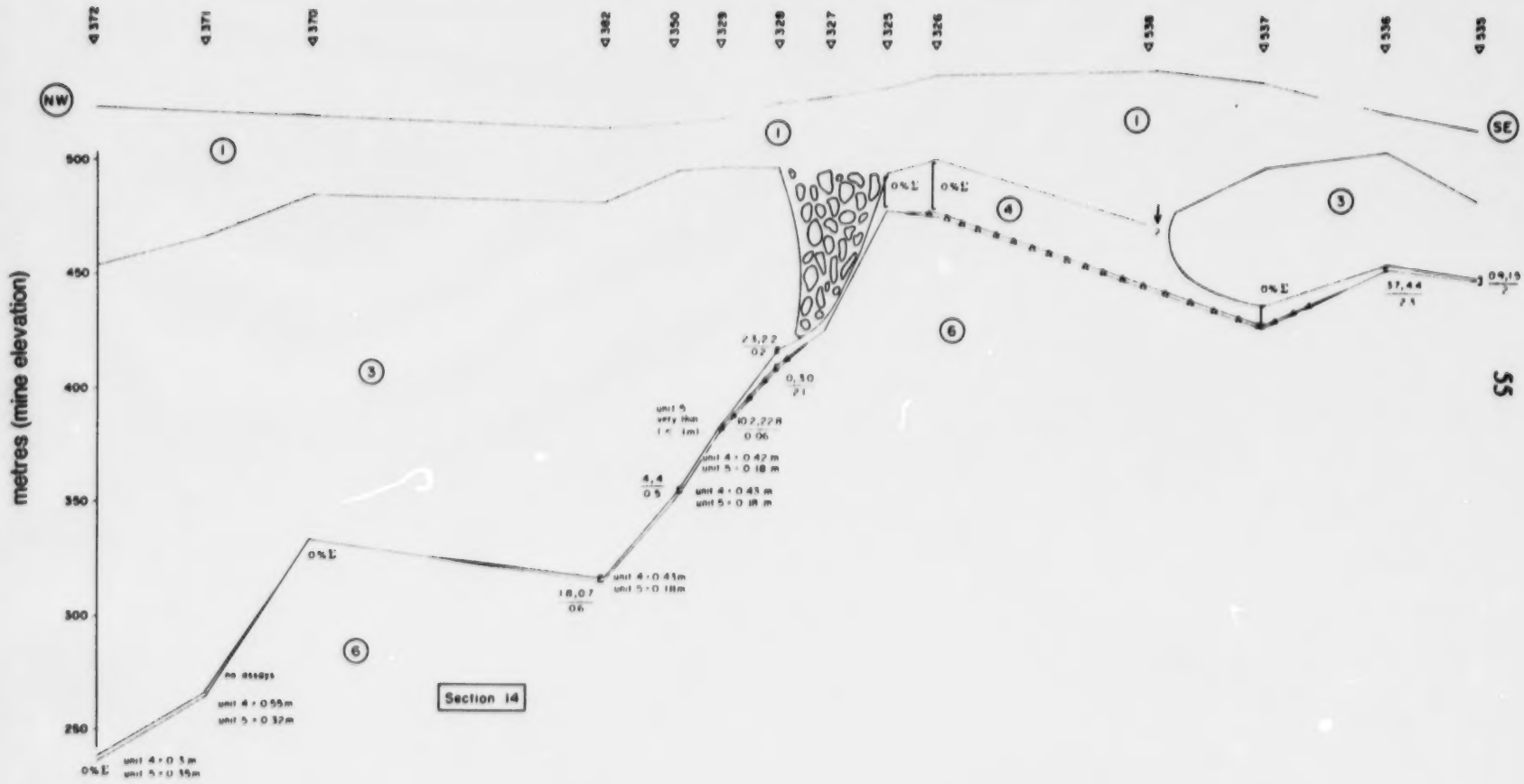
4372
4371
4370
4362
4350
4329
4328
4327
4325
4326
4338
4337
4336
4335
NW
SE
500
450
400
350
300
250
metres (mine elevation)
0%E
no assays
unit 4 : 0.55m
unit 5 : 0.32m
unit 4 : 0.3 m
unit 5 : 0.35m
18,07
06
unit 4 : 0.43m
unit 5 : 0.18m
4,4
05
unit 4 : 0.43 m
unit 5 : 0.18 m
unit 5
very thin
(< 1m)
2,22,8
0.06
23,22
02
0,30
21
Section 14
37,44
21
55

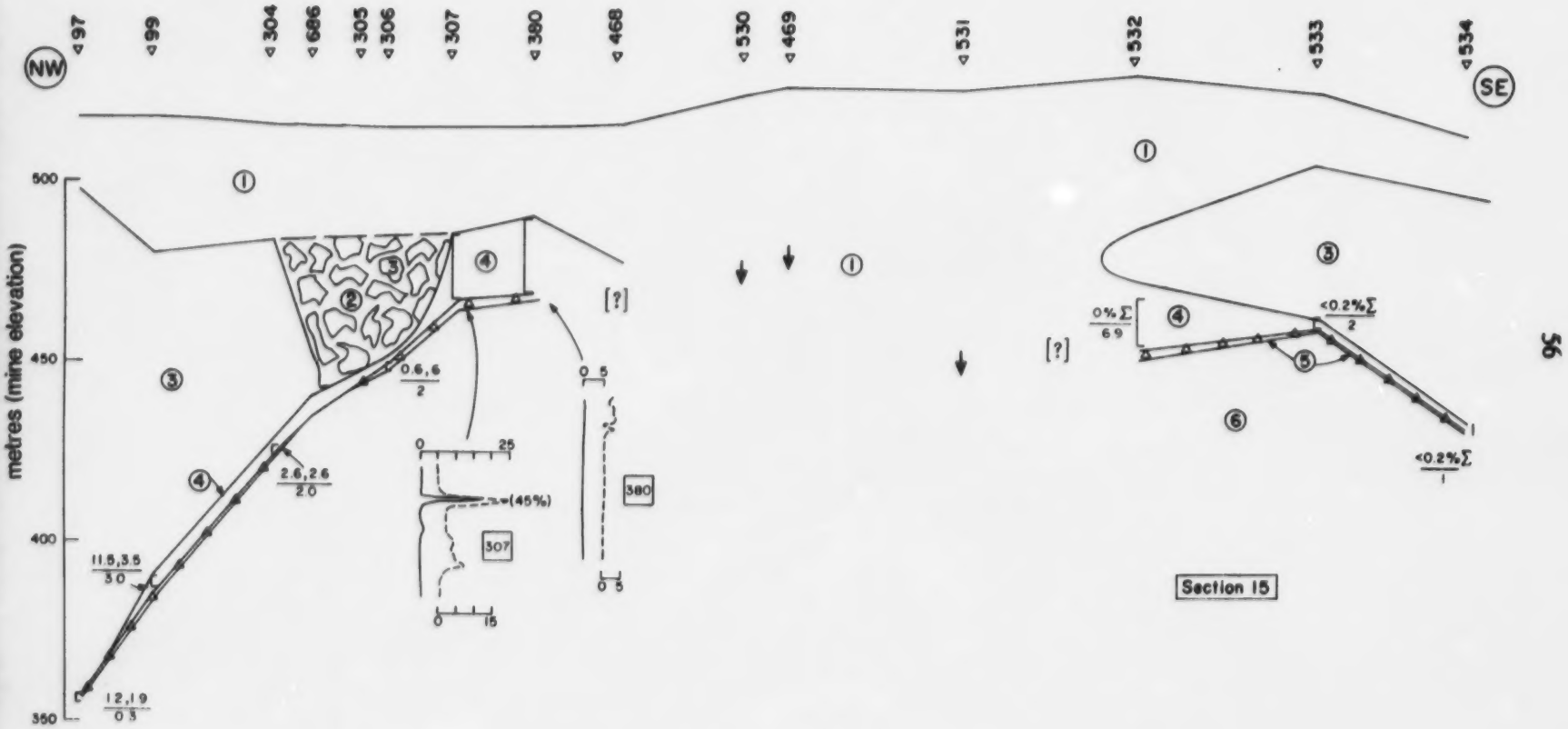
NW
SE
97
99
304
686
305
306
307
390
468
530
469
531
532
533
534
metres (mine elevation)
500
450
400
350
[?]
0.6,6
2
0 5
0 25
(45%)
380
307
0 5
0 15
2.6,2.6
2.0
11.5,3.5
3.0
12,1.9
0.5
0%Σ
6.9
<0.2%Σ
2
<0.2%Σ
1
Section 15

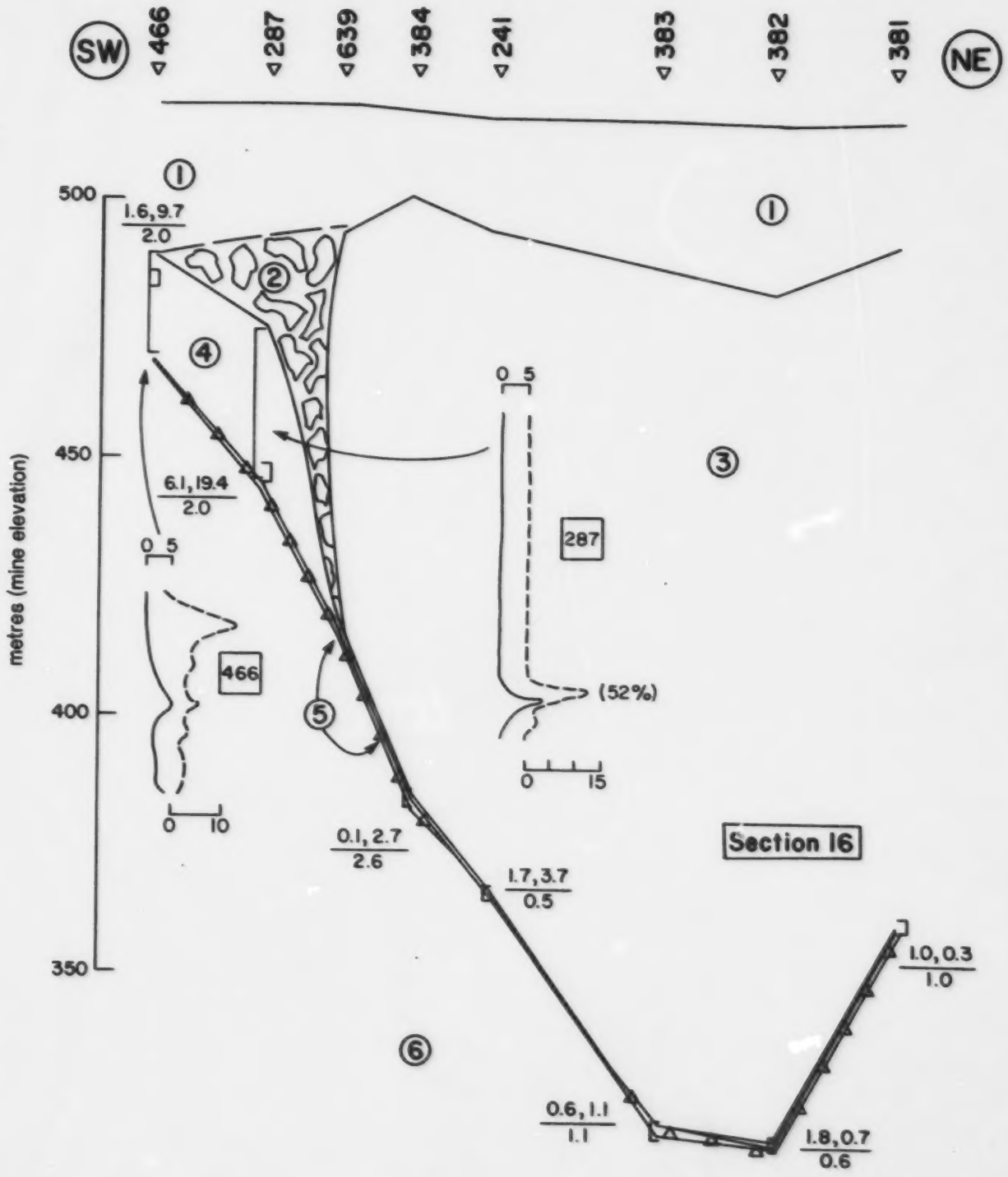
SW
NE
466
287
639
384
241
383
382
381
500
450
400
350
metres (mine elevation)
1
2
3
4
5
6
1.6, 9.7
2.0
6.1, 19.4
2.0
0 5
0 10
0 5
0 15
(52%)
287
466
0.1, 2.7
2.6
1.7, 3.7
0.5
0.6, 1.1
1.1
1.8, 0.7
0.6
1.0, 0.3
1.0
Section 16

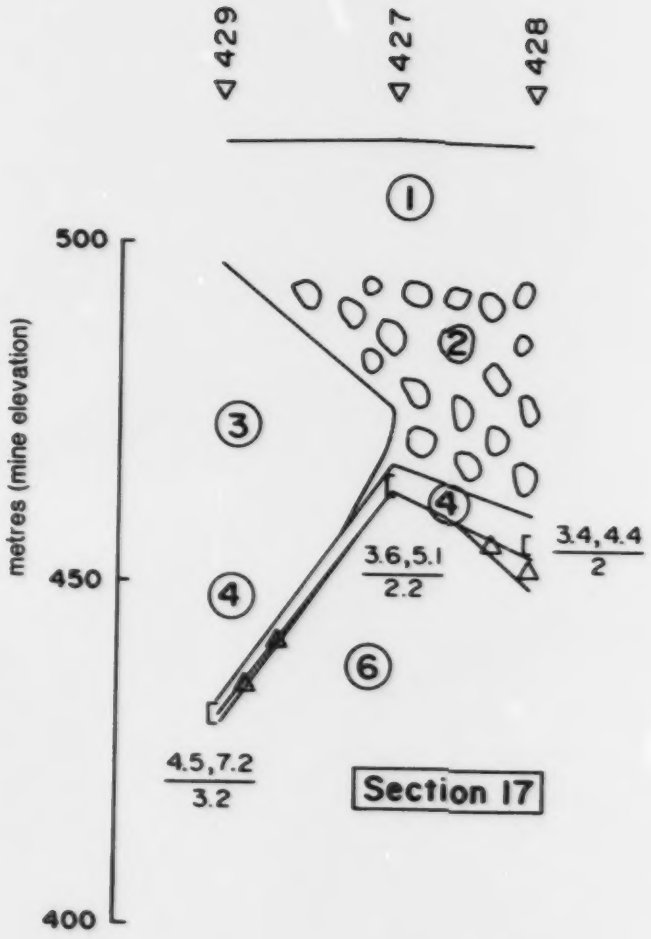
429
427
428
1
500
2
3
4
3.4, 4.4
2
3.6, 5.1
2.2
4
6
metres (mine elevation)
450
4.5, 7.2
3.2
400
Section 17

Section 18
W
E
285
465
288
628
386
299
238
621
358
623
327
665
663
658
356
360
[?]
meters (mine elevation)
500
450
400

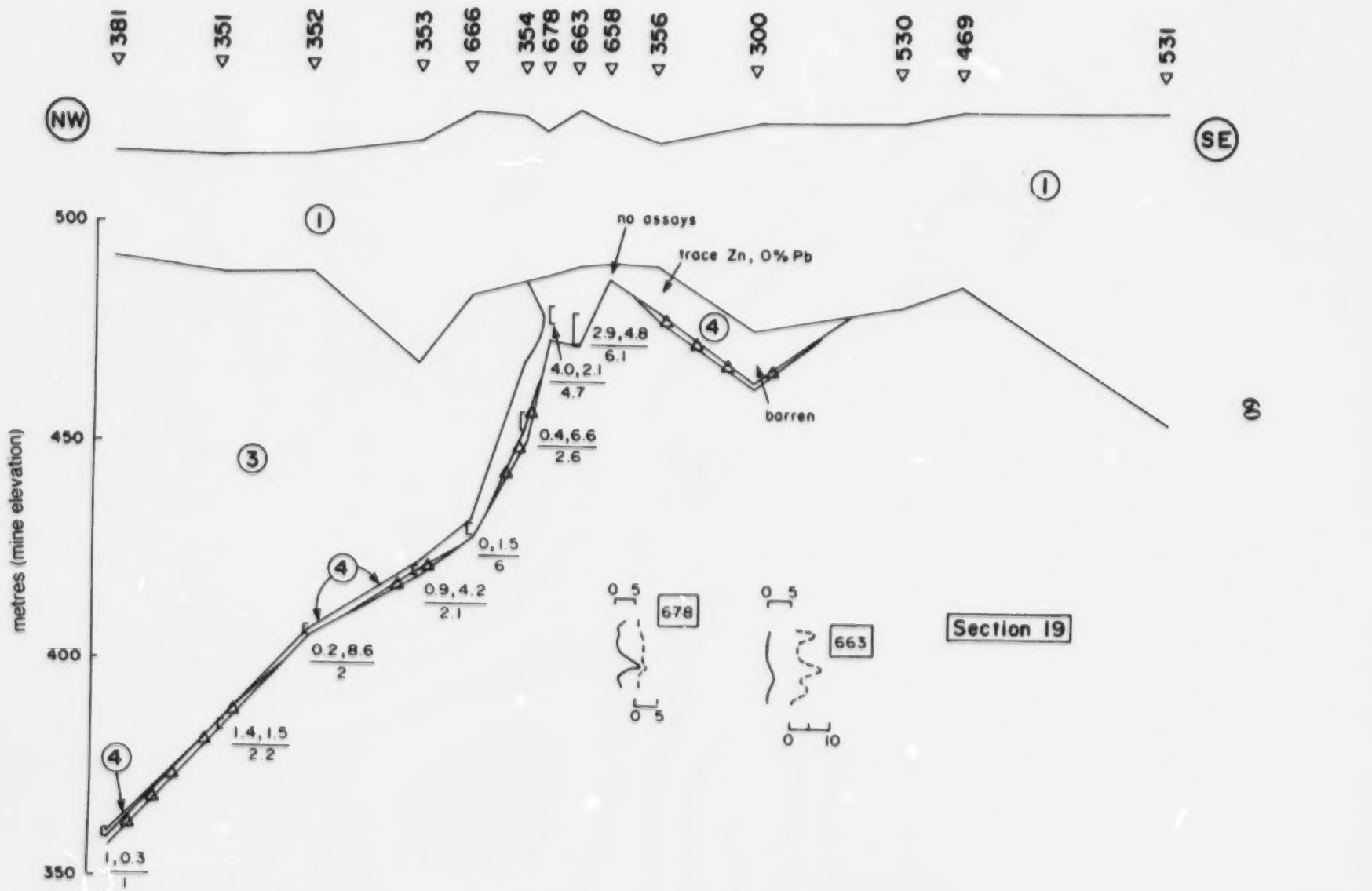
381
351
352
353
666
354
678
663
658
356
300
530
469
531
NW
SE
500
450
400
350
metres (mine elevation)
1
3
4
no assays
trace Zn, 0% Pb
barren
2.9, 4.8 / 6.1
4.0, 2.1 / 4.7
0.4, 6.6 / 2.6
0, 1.5 / 6
0.9, 4.2 / 2.1
0.2, 8.6 / 2
1.4, 1.5 / 2.2
1, 0.3 / 1
678
663
0 5
0 10
Section 19

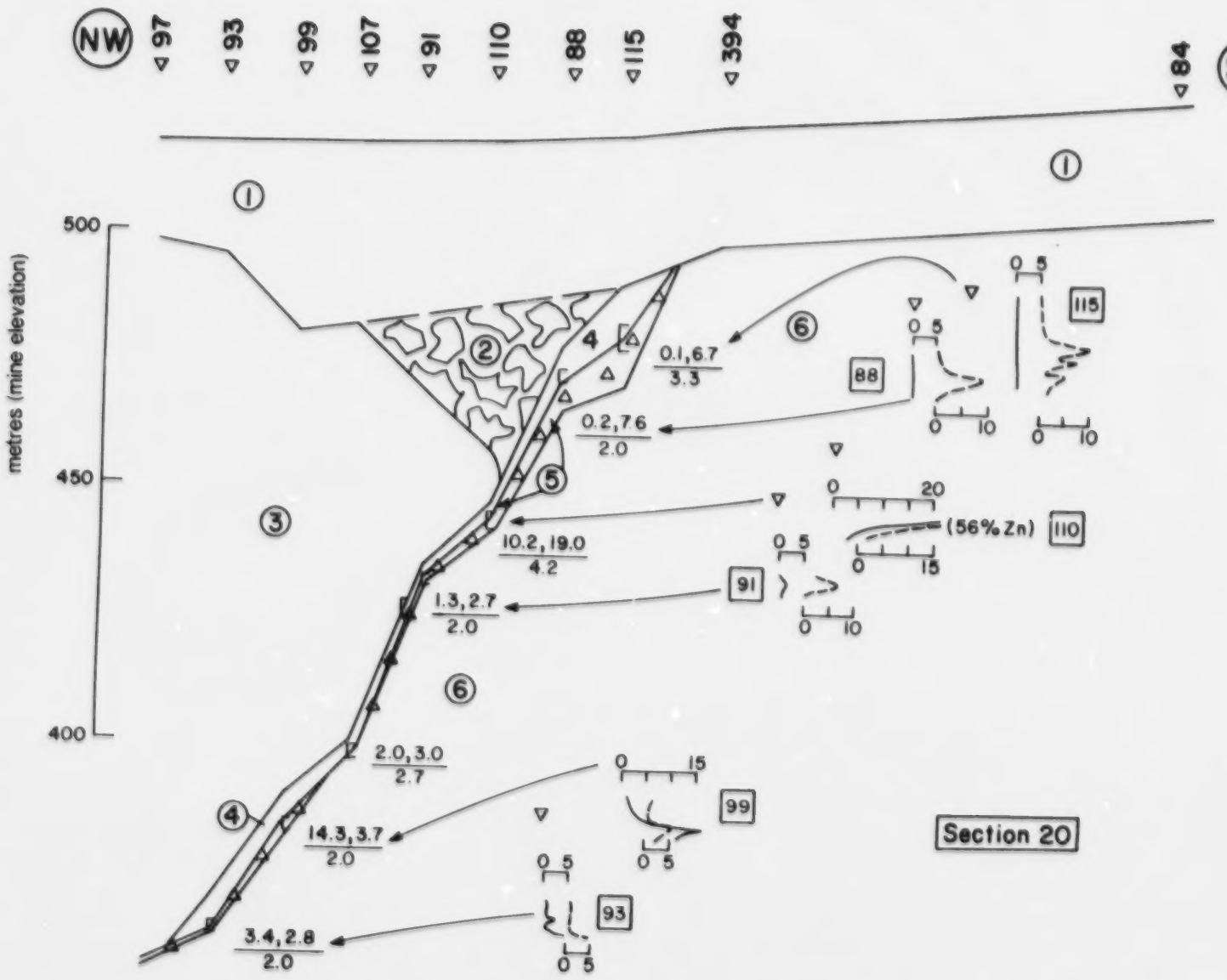
NW
SE
97
93
99
107
91
110
88
115
394
84
500
450
400
metres (mine elevation)
1
2
3
4
5
6
0.1, 6.7
3.3
0.2, 7.6
2.0
10.2, 19.0
4.2
1.3, 2.7
2.0
2.0, 3.0
2.7
14.3, 3.7
2.0
3.4, 2.8
2.0
115
88
110
(56% Zn)
91
99
93
Section 20

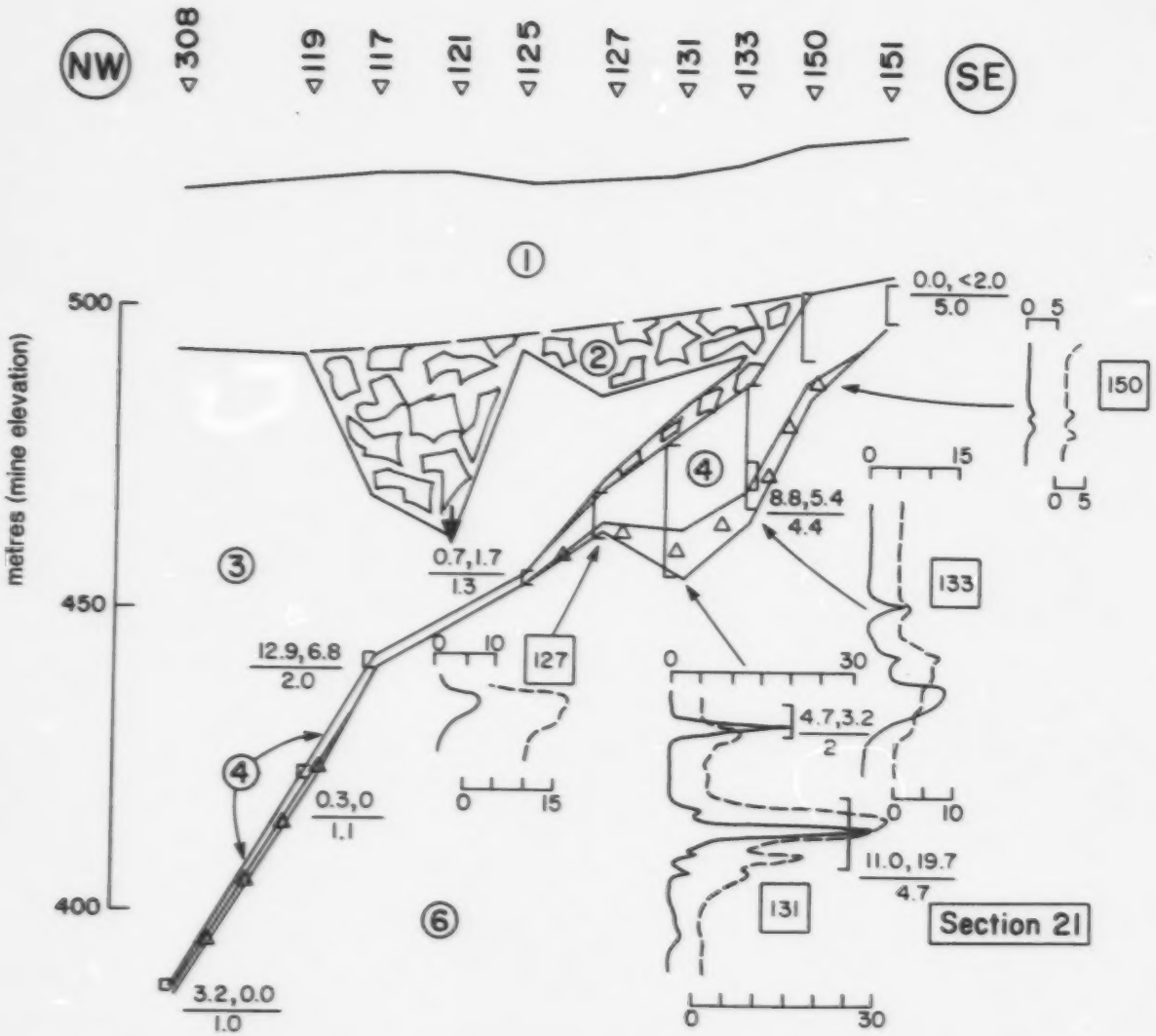
NW
SE
308
119
117
121
125
127
131
133
150
151
metres (mine elevation)
500
450
400
1
2
3
4
5
6
0.0, <2.0
5.0
150
0 5
0 5
0 15
8.8, 5.4
4.4
133
0.7, 1.7
1.3
12.9, 6.8
2.0
0 10
127
0 15
0.3, 0
1.1
0 30
4.7, 3.2
2
0 10
11.0, 19.7
4.7
131
0 30
3.2, 0.0
1.0
Section 21

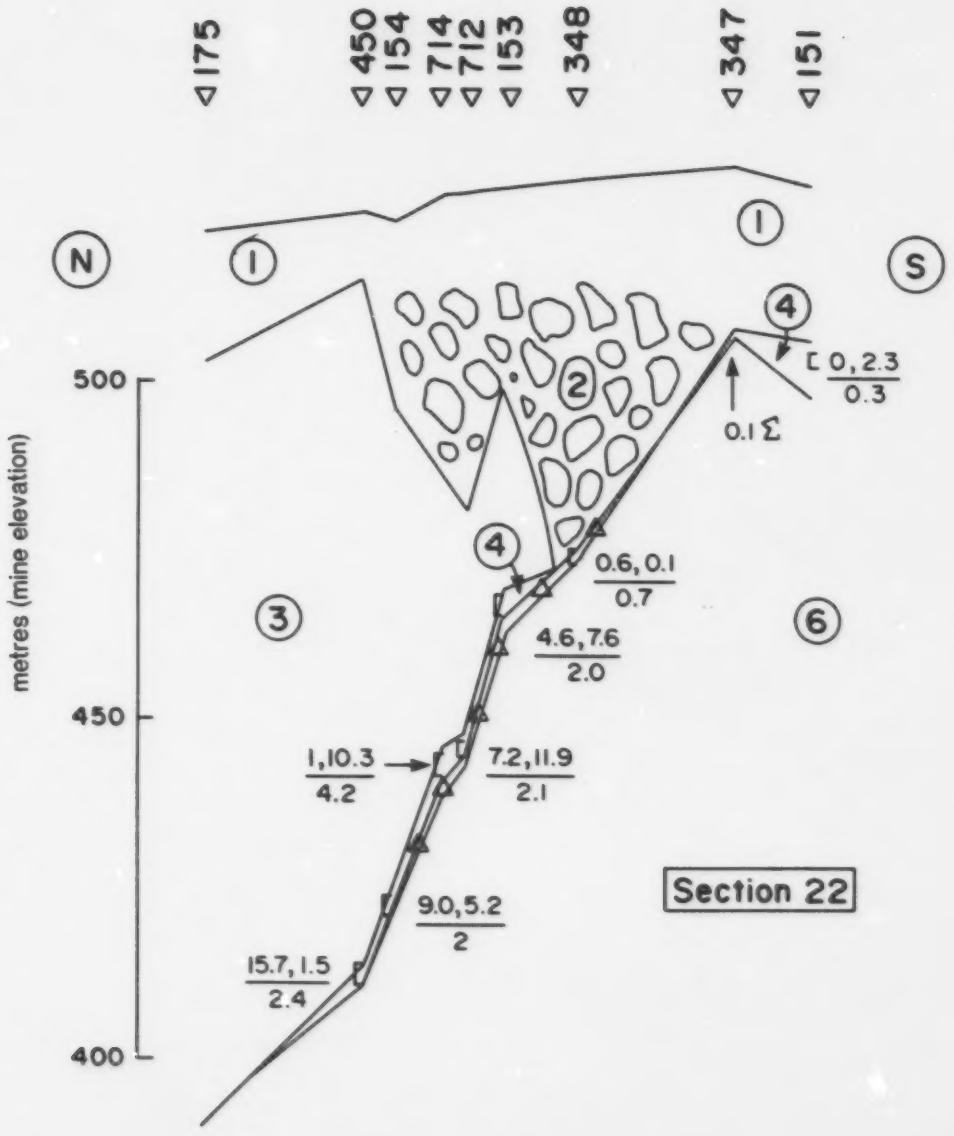
175
450
154
714
712
153
348
347
151
N
S
1
2
3
4
6
500
450
400
metres (mine elevation)
0, 2.3
0.3
0.1 Σ
0.6, 0.1
0.7
4.6, 7.6
2.0
1, 10.3
4.2
7.2, 11.9
2.1
9.0, 5.2
2
15.7, 1.5
2.4
Section 22

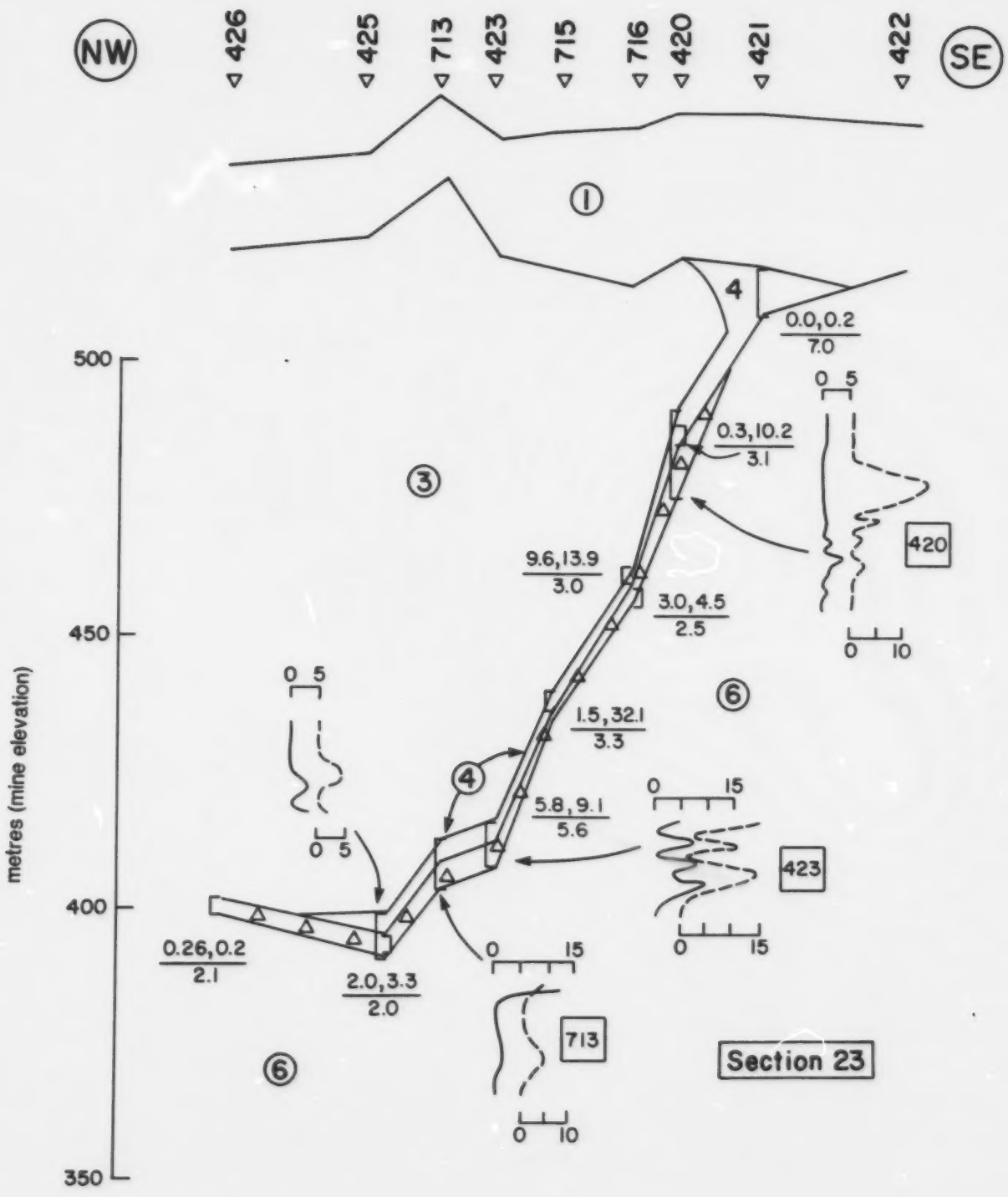
NW
SE
426
425
713
423
715
716
420
421
422
1
3
4
6
0.0,0.2
7.0
0.3,10.2
3.1
9.6,13.9
3.0
3.0,4.5
2.5
1.5,32.1
3.3
5.8,9.1
5.6
0.26,0.2
2.1
2.0,3.3
2.0
420
423
713
0 5
0 10
0 15
500
450
400
350
metres (mine elevation)
Section 23

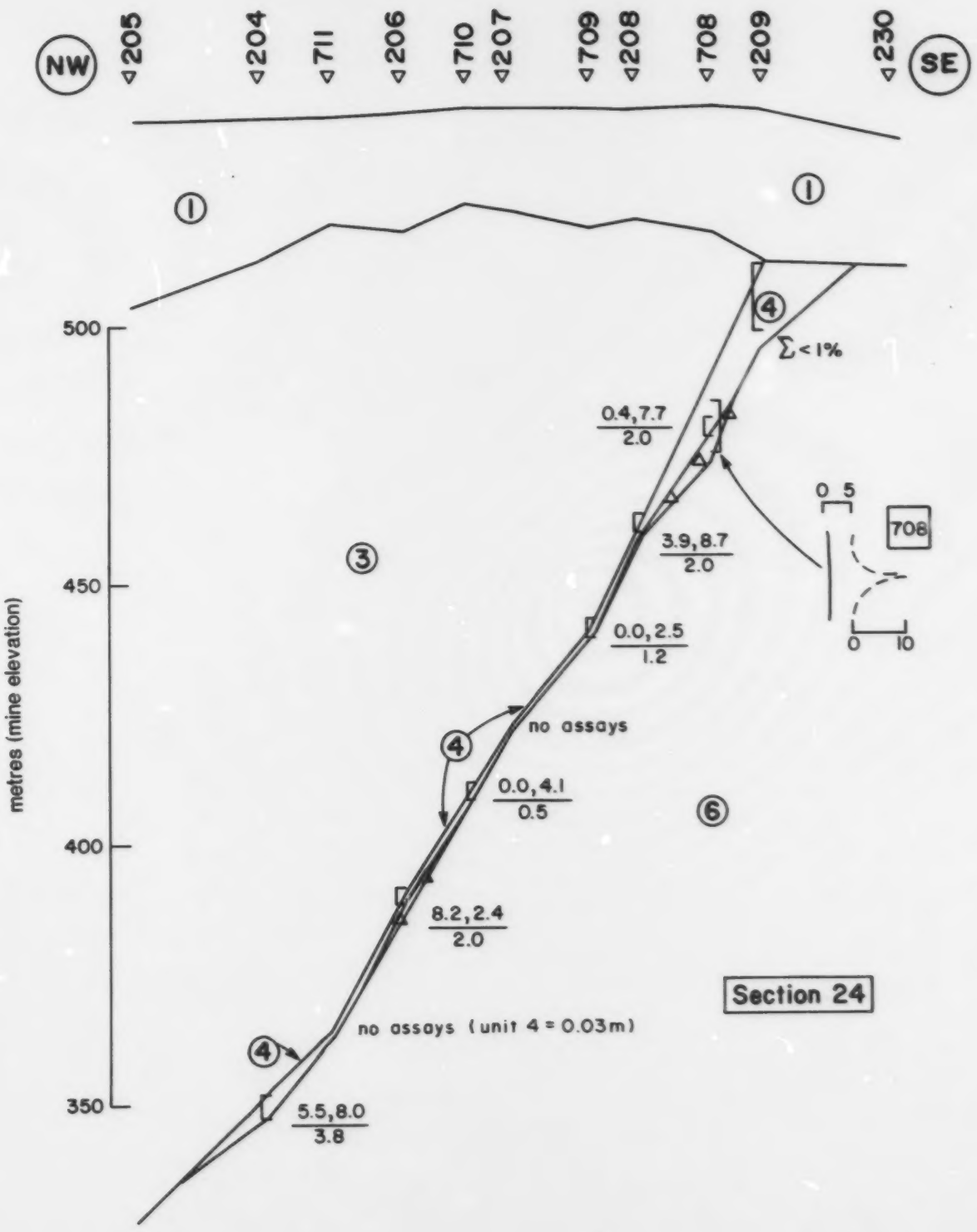
NW
205
204
711
206
710
207
709
208
708
209
230
SE
1
1
4
Σ<1%
0.4,7.7
2.0
0 5
708
3
3.9,8.7
2.0
0.0,2.5
1.2
0 10
500
450
400
350
metres (mine elevation)
4
no assays
0.0,4.1
0.5
6
8.2,2.4
2.0
Section 24
4
no assays (unit 4 = 0.03m)
5.5,8.0
3.8

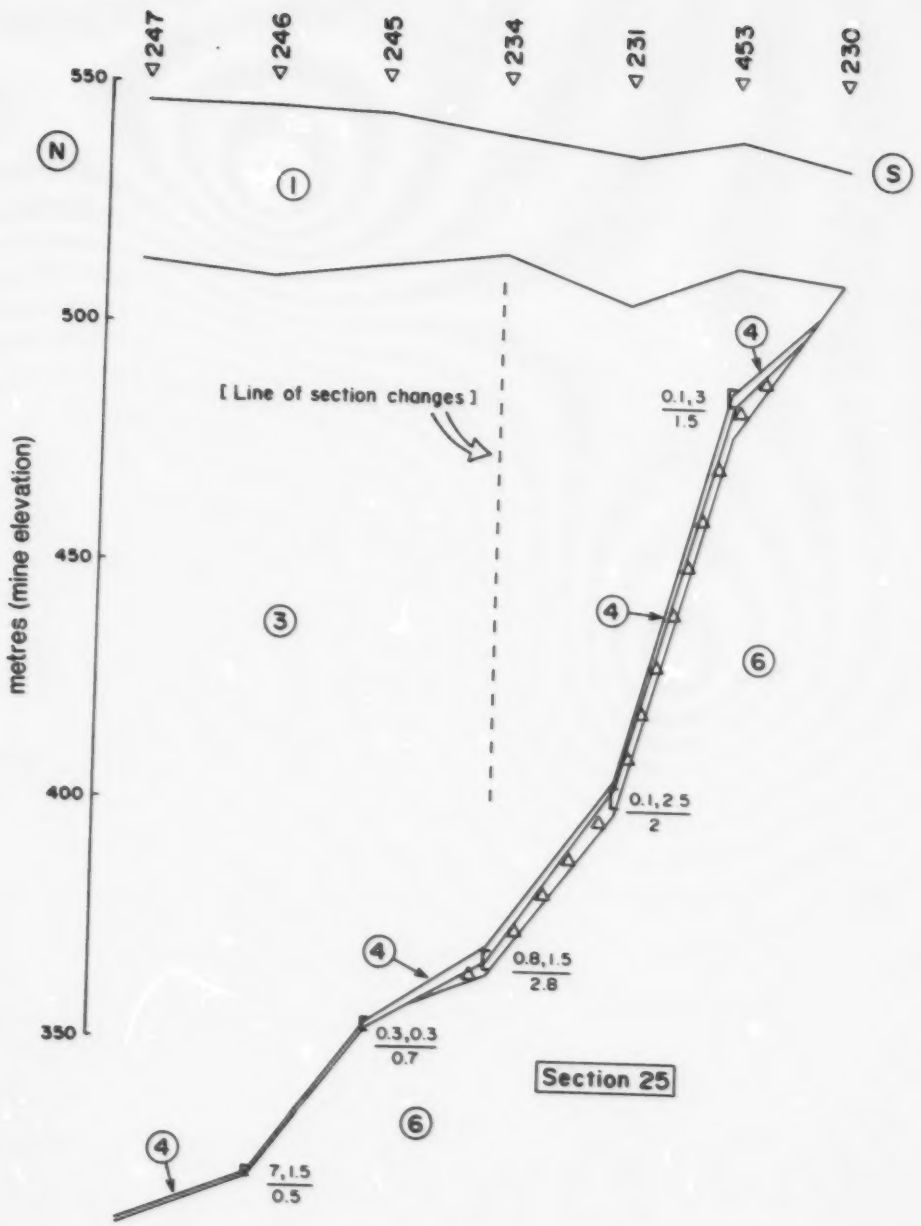
247
246
245
234
231
453
230
550
500
450
400
350
N
S
1
3
4
6
[Line of section changes]
metres (mine elevation)
0.1, 3
1.5
0.1, 2.5
2
0.8, 1.5
2.8
0.3, 0.3
0.7
7, 1.5
0.5
Section 25

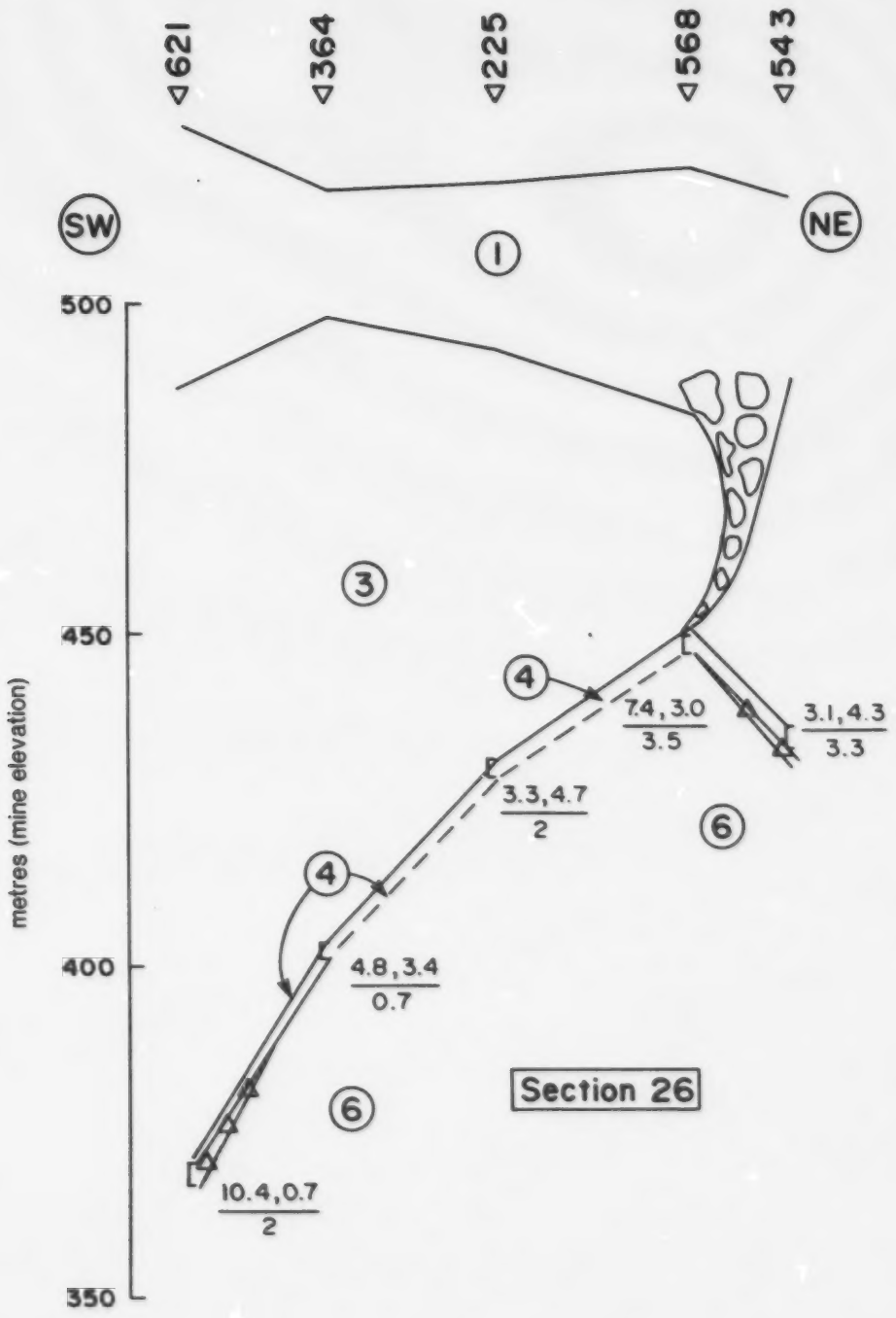
621
364
225
568
543
SW
NE
1
500
450
400
350
metres (mine elevation)
3
4
7.4, 3.0
3.5
3.1, 4.3
3.3
3.3, 4.7
2
6
4
4.8, 3.4
0.7
6
10.4, 0.7
2
Section 26

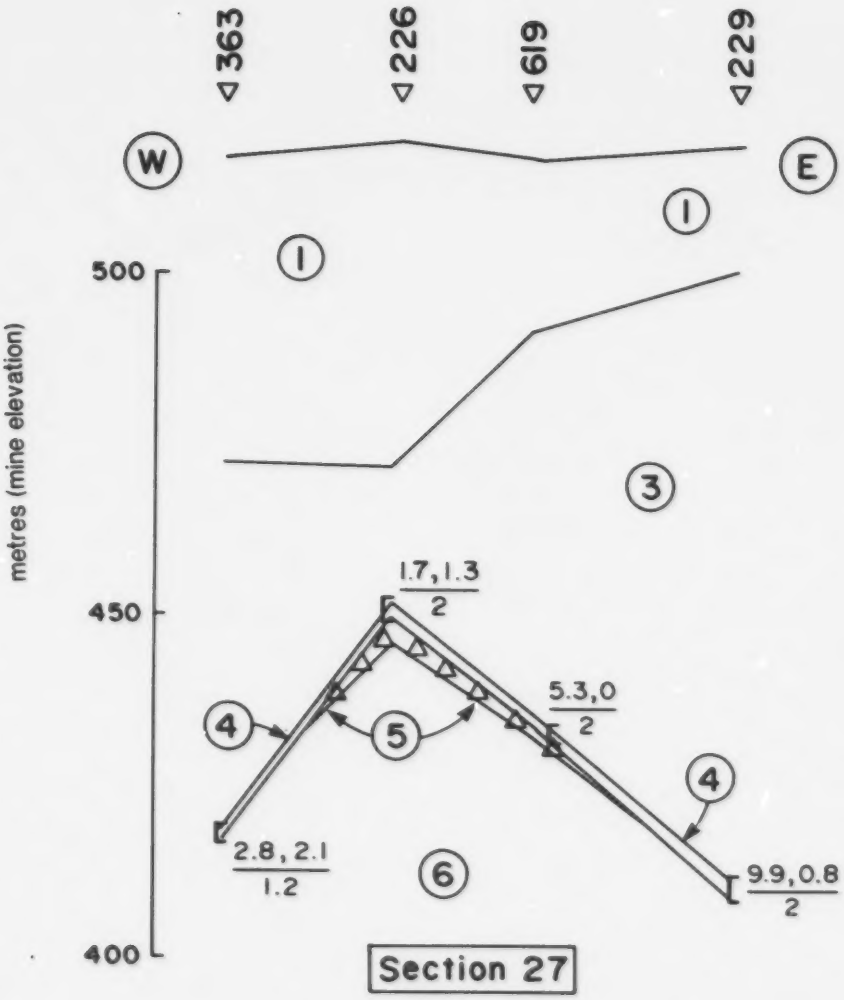
363
226
619
229
W
E
1
1
500
450
400
metres (mine elevation)
3
1.7, 1.3
2
4
5
5.3, 0
2
4
2.8, 2.1
1.2
6
9.9, 0.8
2

Section 27

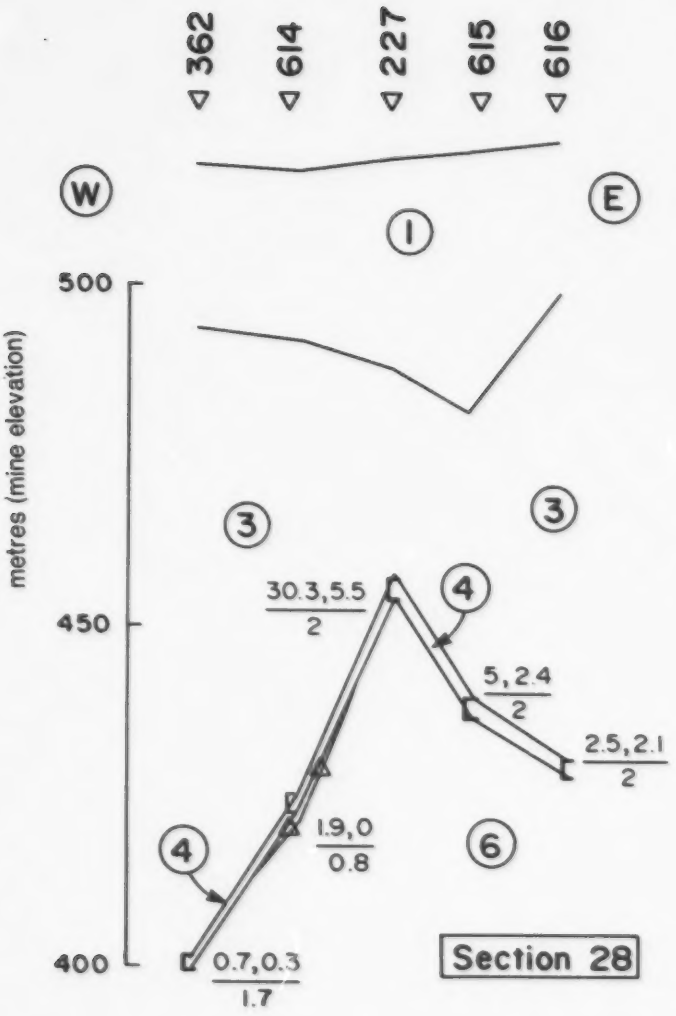
362
614
227
615
616
W
E
1
500
450
400
metres (mine elevation)
3
3
30.3,5.5
2
4
5,2.4
2
2.5,2.1
2
4
1.9,0
0.8
6
0.7,0.3
1.7
Section 28

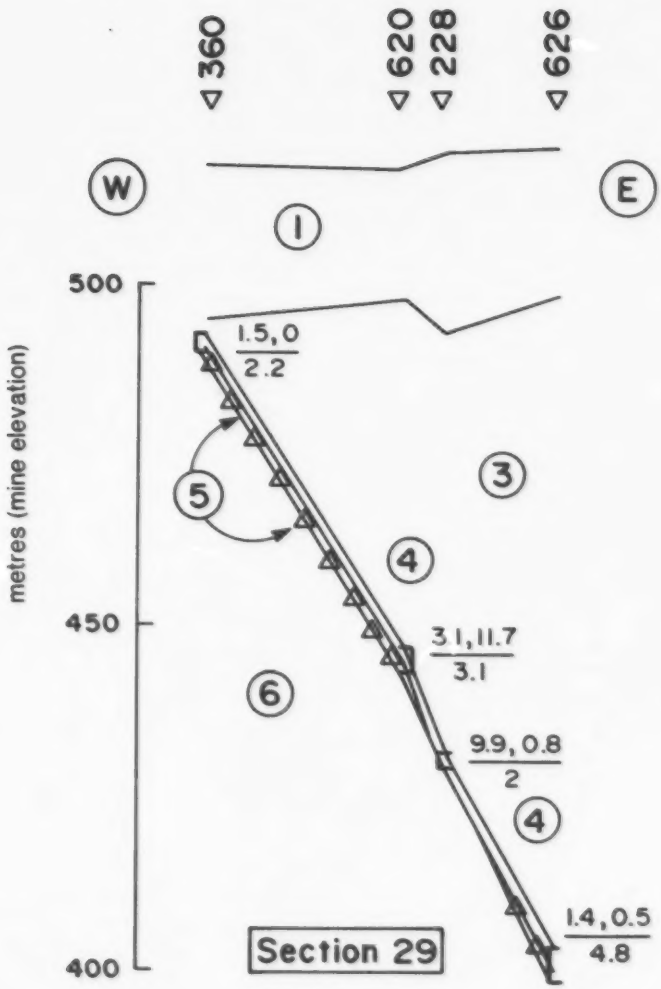
360
620
228
626
W
E
1
500
450
400
metres (mine elevation)
1.5, 0
2.2
5
3
4
31, 11.7
3.1
6
9.9, 0.8
2
4
1.4, 0.5
4.8
Section 29

SW
NE
272
158
219
211
212
213
125
214
215
24
216
550
500
450
meters (mine elevation)
Section A-A'
0.7,2.3 / 30.7
0.7,2.5 / 4.5
1.7,4.7 / 2
1.2,2.7 / 3.9
0.2,1.5 / 4
5.5,2.4 / 2
4.5,2.6 / 2
1.7,0 / 2
0.6,2.3 / 5.6
0.0,1.7 / 7.6

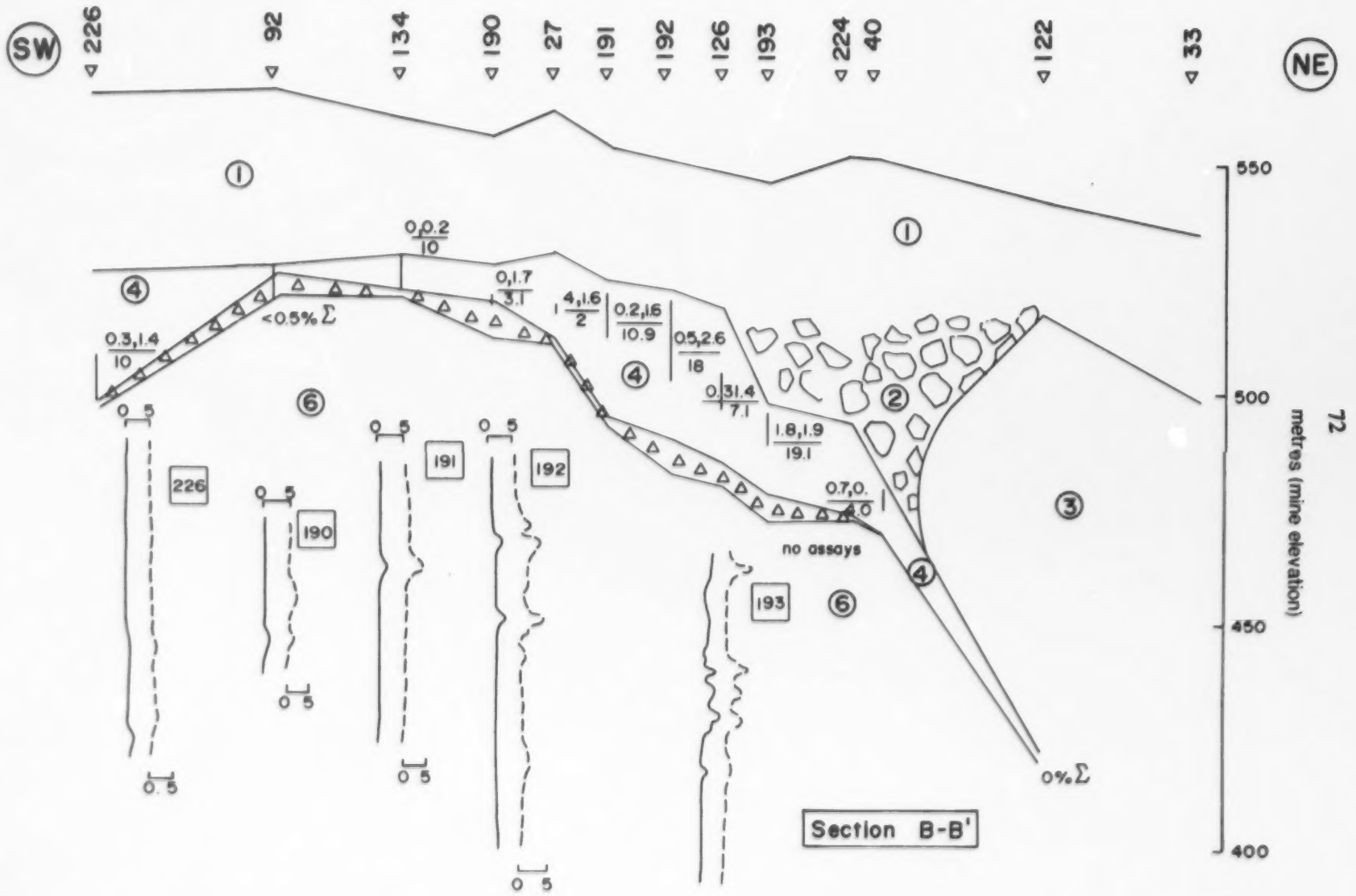
SW
NE
226
92
134
190
27
191
192
126
193
224
40
122
33
550
500
450
400
72
metres (mine elevation)
<0.5% Σ
0% Σ
no assays
226
190
191
192
193
Section B-B'

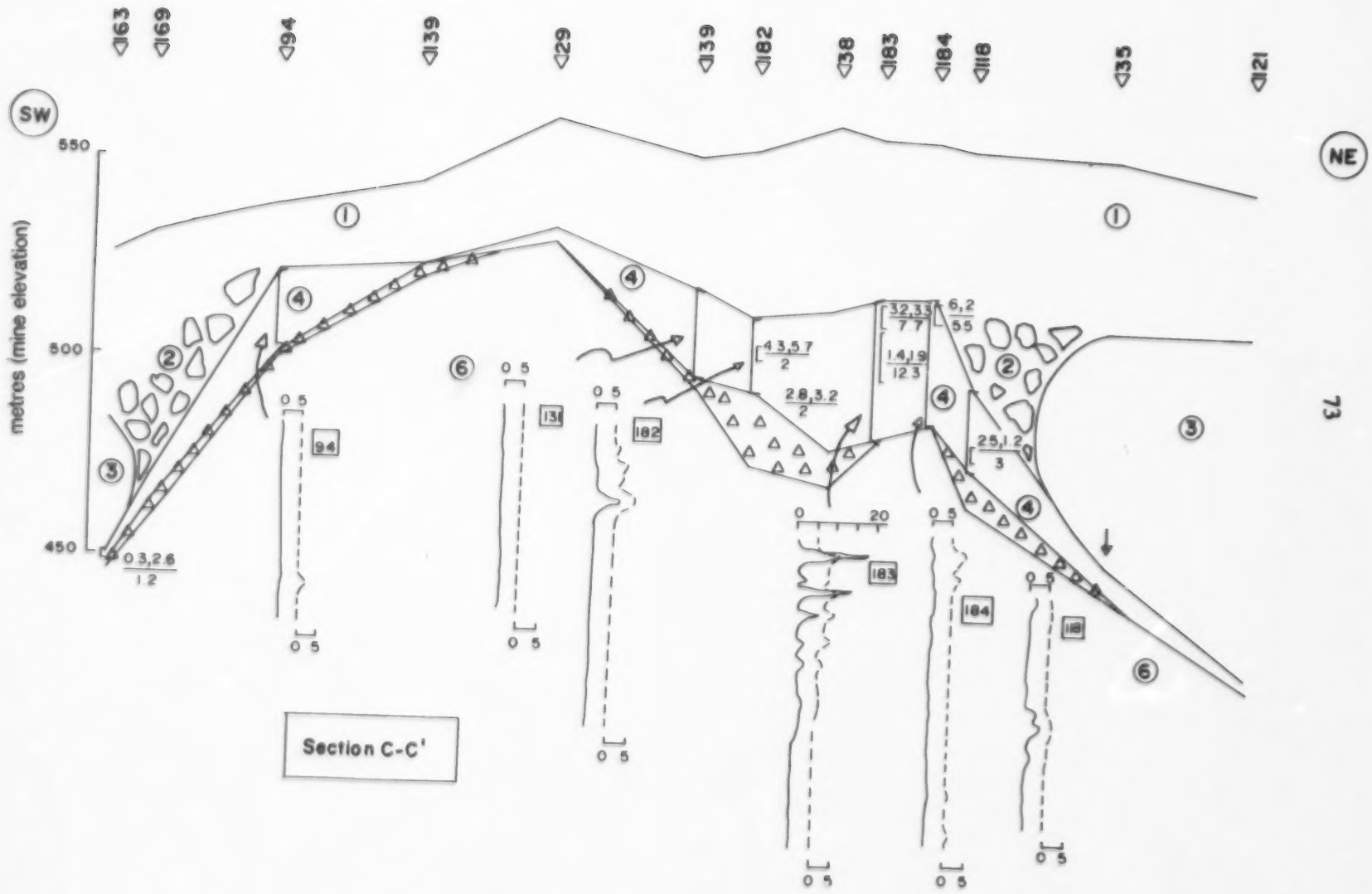
163
169
94
139
29
139
182
38
183
184
118
35
121
SW
NE
550
500
450
metres (mine elevation)
Section C-C'

SW
NE
274
159
205
21
206
207
129
208
209
210
25
25A
123
90
550
500
450
400
metres (mine elevation)
no assays
0.03/8
0.1.5/12
0.5
205
206
0.6.2.4/30
.4/2.5
11.47/2.4
2.8.3.1/2.3
11.01/1
8.6.01/3.2
<0.1% Σ
Section D-D'

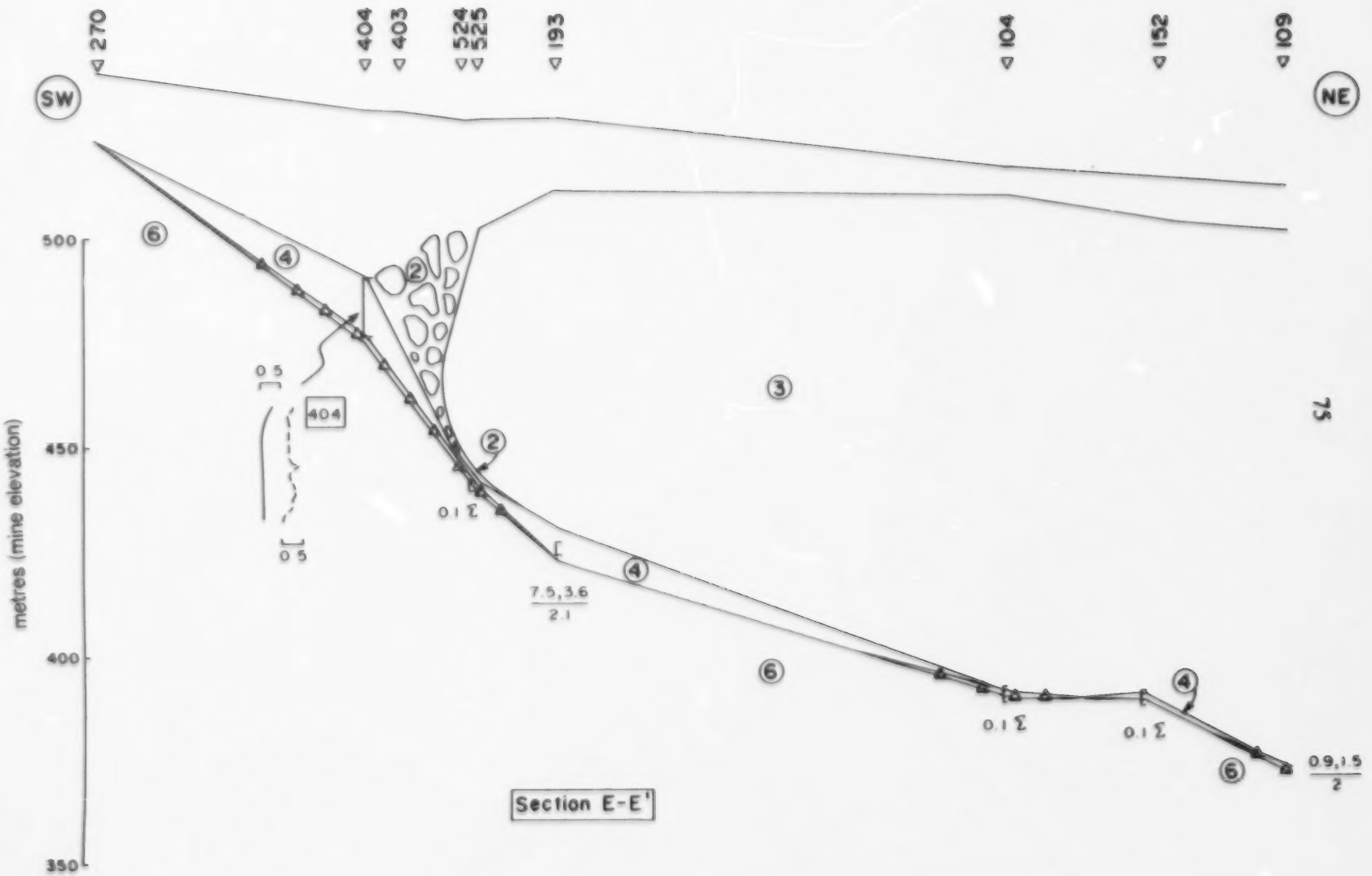
270
404
403
524
525
193
104
152
109
SW
NE
500
450
400
350
metres (mine elevation)
6
4
2
3
404
0.5
0.5
0.1 Σ
7.5, 3.6
2.1
0.1 Σ
0.1 Σ
0.9, 1.5
2
Section E-E'

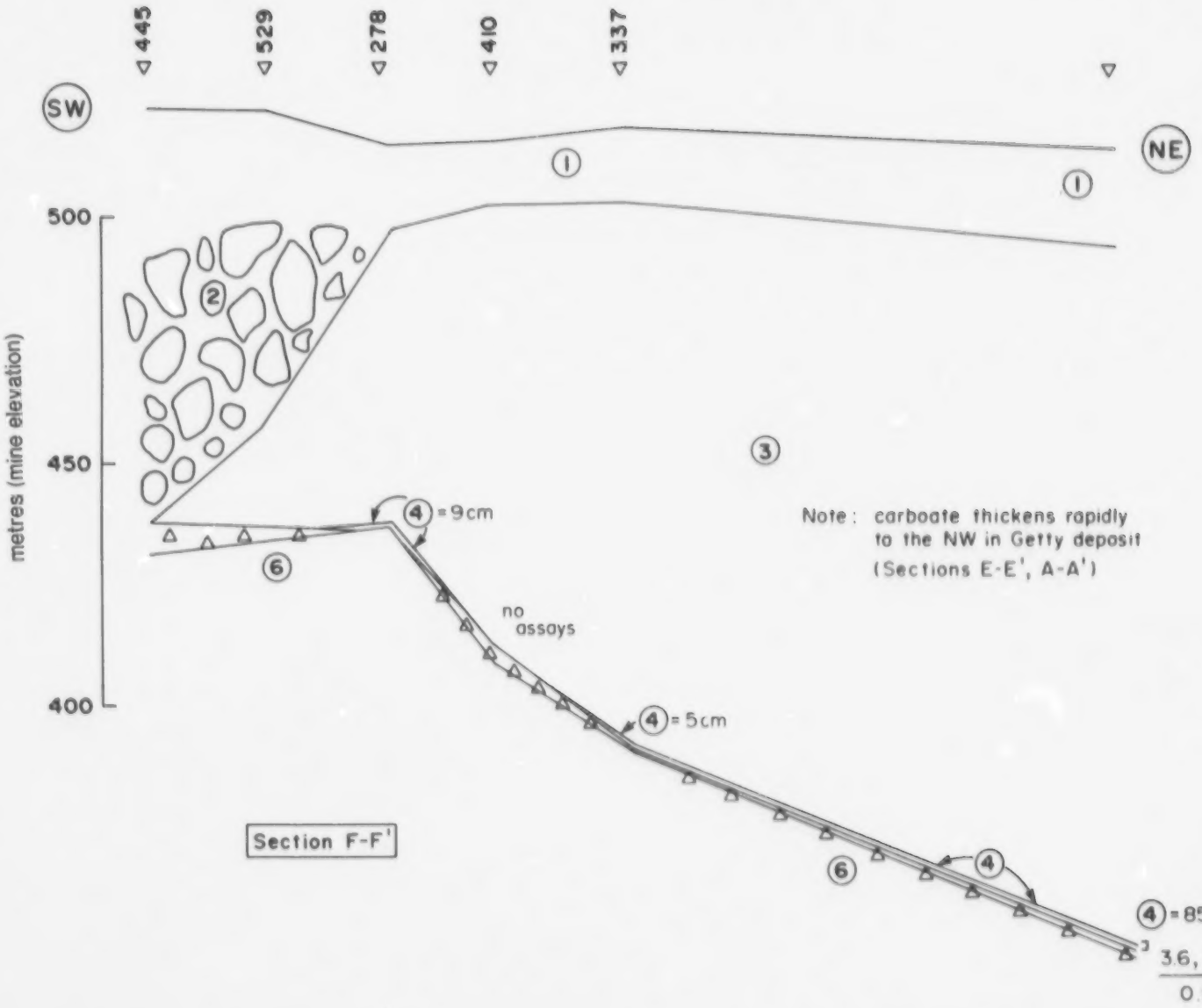
445
529
278
410
337
SW
NE
1
1
500
450
400
metres (mine elevation)
2
3
4 = 9cm
6
Note: carbonate thickens rapidly to the NW in Getty deposit (Sections E-E', A-A')
no assays
4 = 5cm
Section F-F'
6
4
4 = 85cm
3
3.6, 2.0
0.5

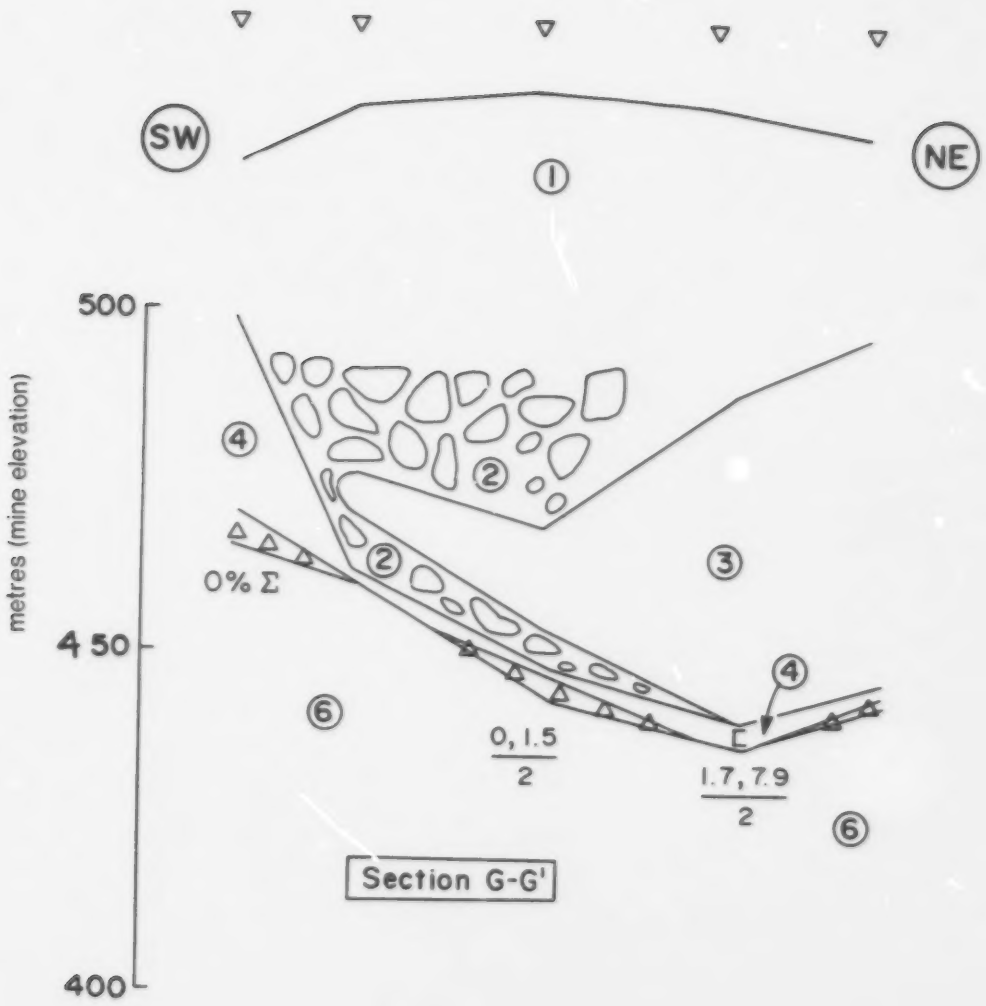
SW
NE
1
500
450
400
metres (mine elevation)
4
2
2
3
0% Σ
4
6
0, 1.5
2
1.7, 7.9
2
6
Section G-G'

Fig. 2.7. Longitudinal sections along the Main deposit and the Getty deposit showing the variation in reef thickness. Data interpreted from the vertical sections in Figure 2.6.

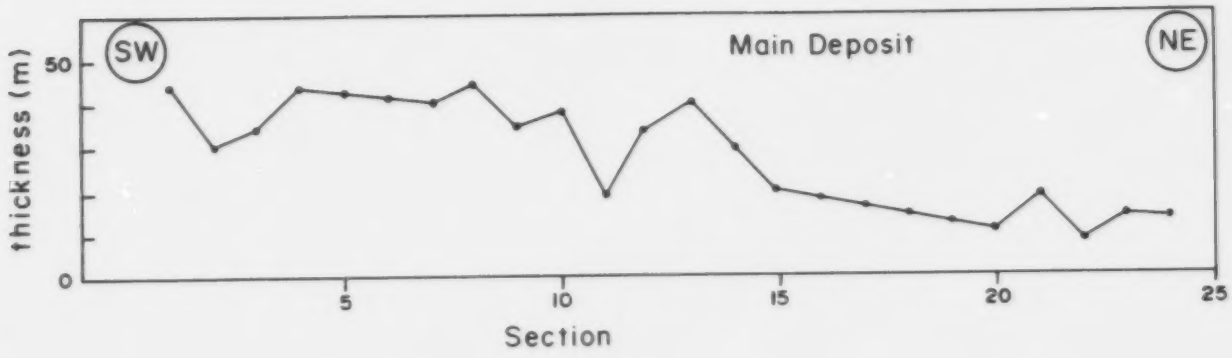

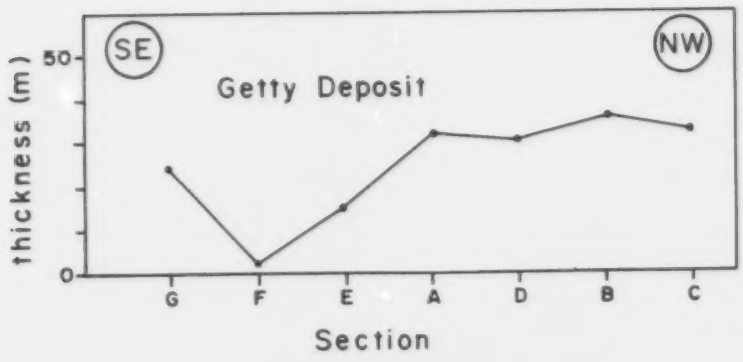

Fig. 2.8. Binary element diagrams for biotite in Meguma Group psammitic lithologies as determined from electron microprobe analyses.

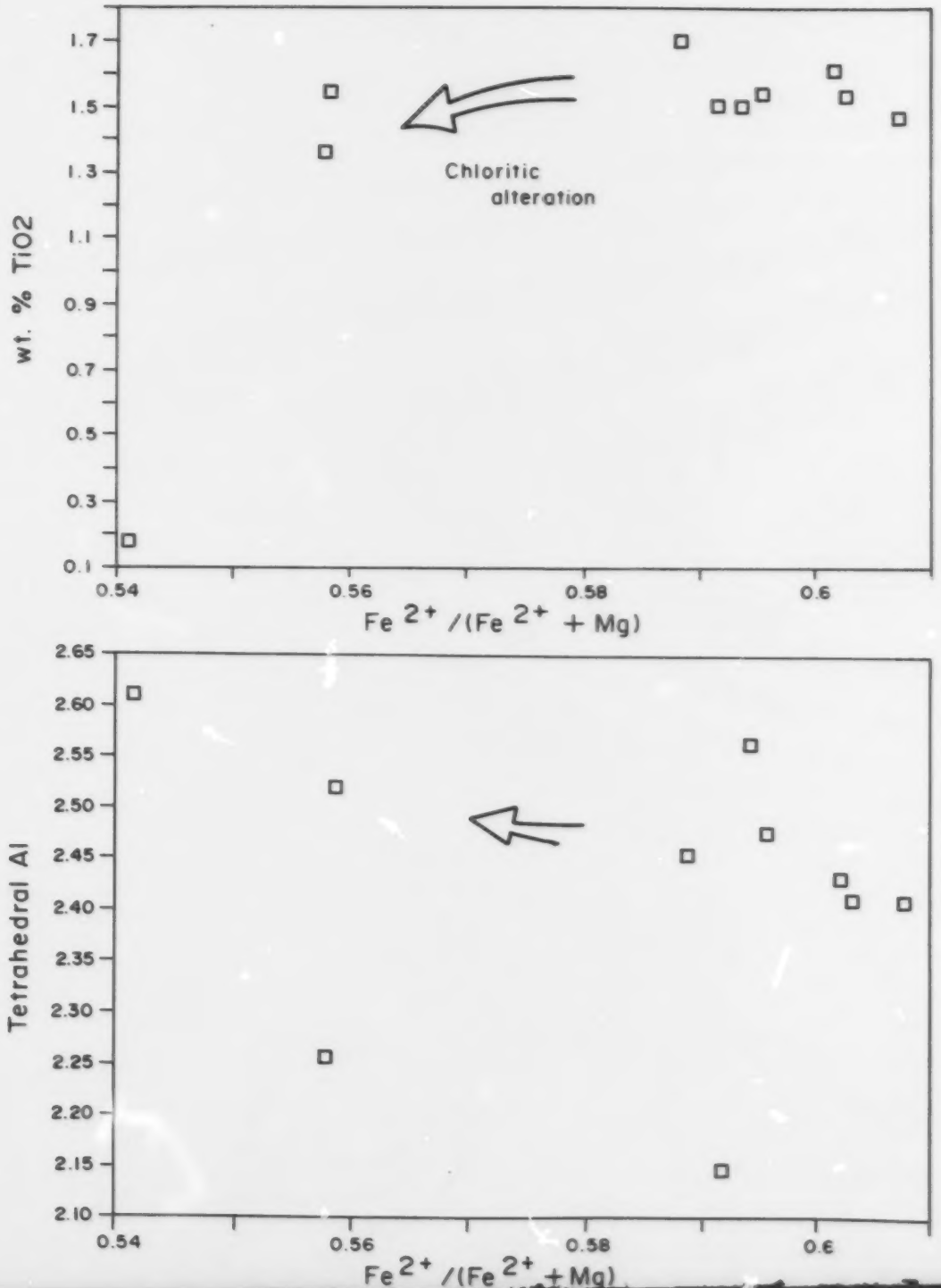

Fig. 2.9. Ternary element plot of ΣAl-Si-M^{2+} for biotite and muscovite (electron microprobe data) from Meguma Group psammitic lithologies. Abbreviations refer to annite (Ann), phologopite (Phl), Eastonite (East) and siderophyllite (Sid). Data defining the field for muscovites from Meguma gold deposits from Kontak and Smith (in prep.). M^{2+} refers to doubly-charged positive cations (Mg, Mn, Fe).

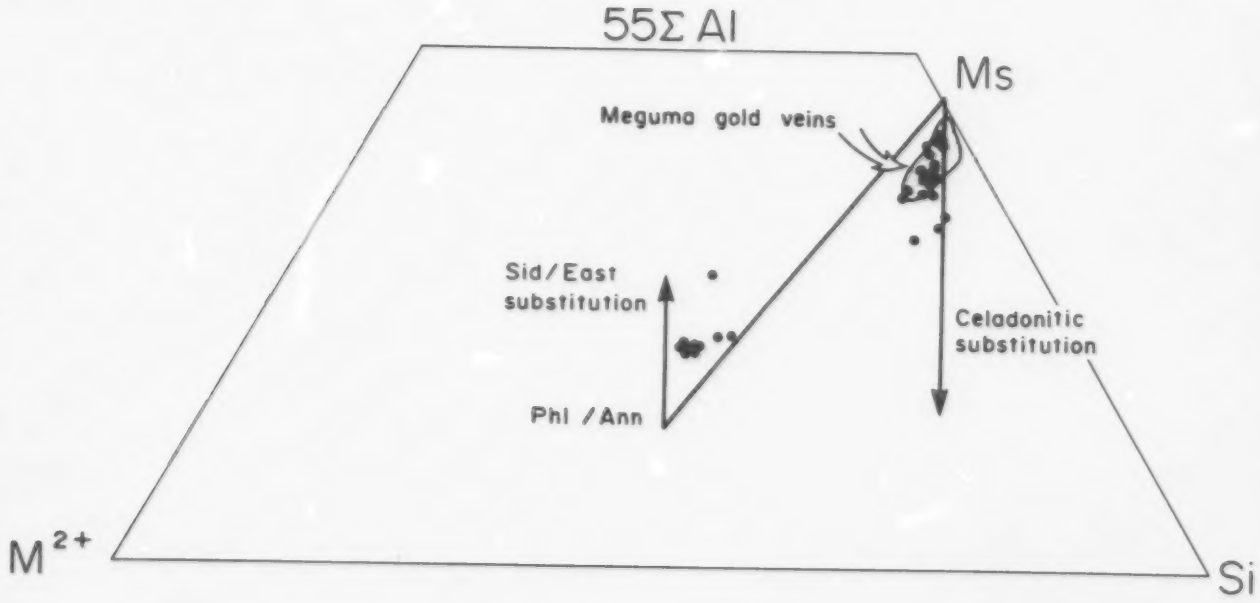

Fig. 2.10. Binary element diagrams for muscovite in Meguma Group psammitic lithologies as determined from electron microprobe analyses. Abbreviation for p.f.u. refers to per formula unit.

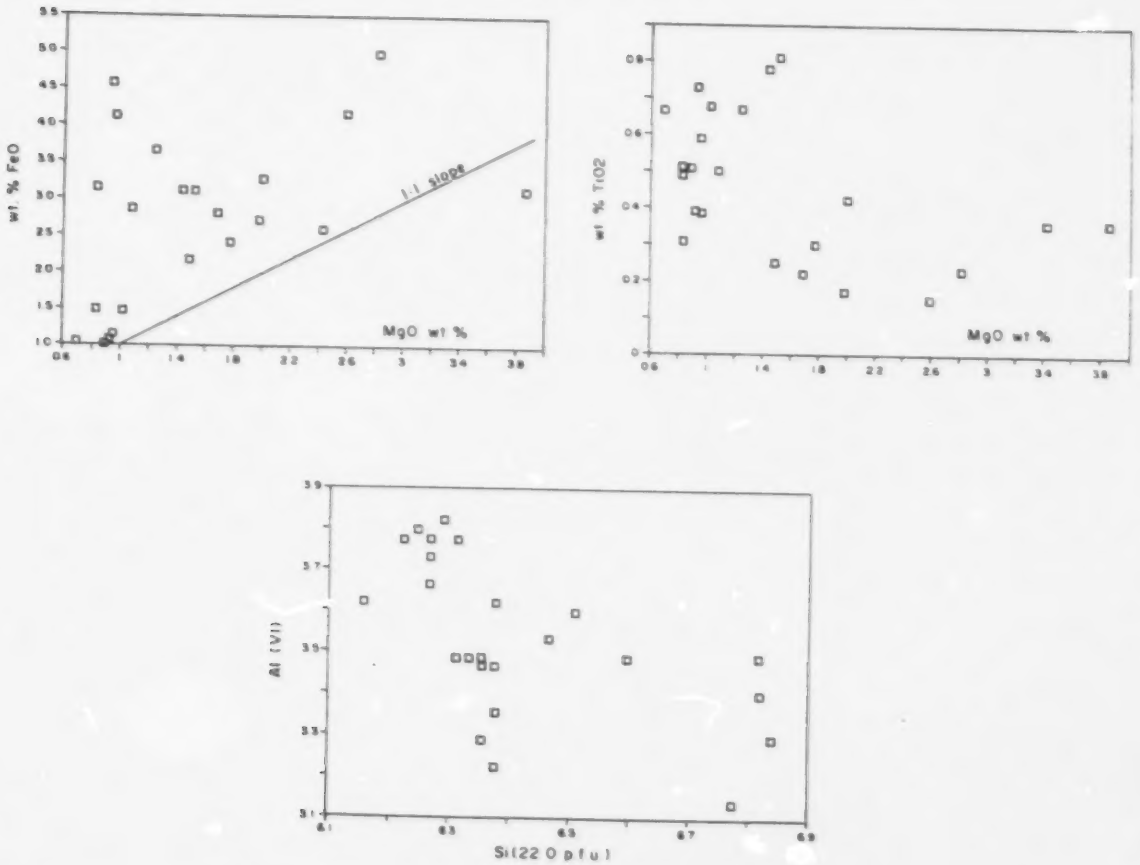

Fig. 2.11. Histogram of wt. % BaO determined in muscovite from a single sample of Meguma Group psammite.

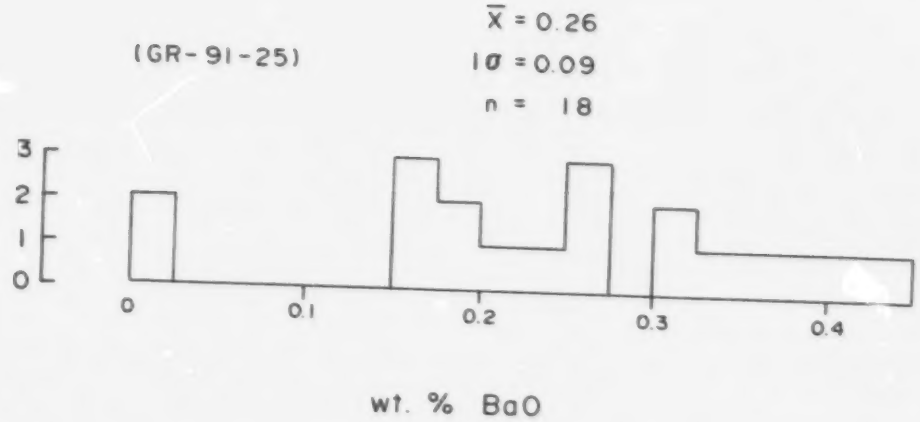

Fig. 2.12. Photos of the basal breccia unit. Except for (a) all photos are photomicrographs taken in plane polarized light and width of field of view is 2.6 mm. (a) Boulder (ca. 1 m) of Meguma Group psammite in matrix of dolostone (underground photo). (b) Two fragments of Meguma Group lithologies with contact modified by pressure solution phenomenon (i.e., note the deep embayment of one fragment into the other and the discordance of the fabrics in the two fragments). (c) Pelitic and psammitic fragments of Meguma Group lithologies with galena (black phase) and sphalerite (disseminations in the psammite and pelite, bordering galena) mineralization. Note that the pelitic fragments are corroded and rimmed by a fine grained red-brown phase. (d) Dark red-brown dolomite cement in breccia rock. Note the disseminated sphalerite in the psammite clast and the corroded outline of the clast. (e) Quartz grain rimmed by dolostone with paragenetically later sphalerite, galena and calcite. Morphology of the quartz probably reflects breakage along a conchoidal fracture during transport giving the curvilinear shape. (f) Clasts of Meguma Group lithologies cemented by dark red-brown dolomite and calcite cement which is then cross-cut by a veinlet of calcite. Note the disseminated sphalerite mineralization in the pelitic clasts and the corroded outline of the clasts. (g) Clast of Meguma Group containing disseminated sphalerite grains subparallel to cleavage. Also note the presence of coarse galena and finer grained sphalerite cement and paragenetically later calcite cement. (h) Several fragments of Meguma Group which have been variably corroded and cemented by dolomite, sphalerite, galena and finally calcite. Note that the fabrics in the clasts are discordant to each other.

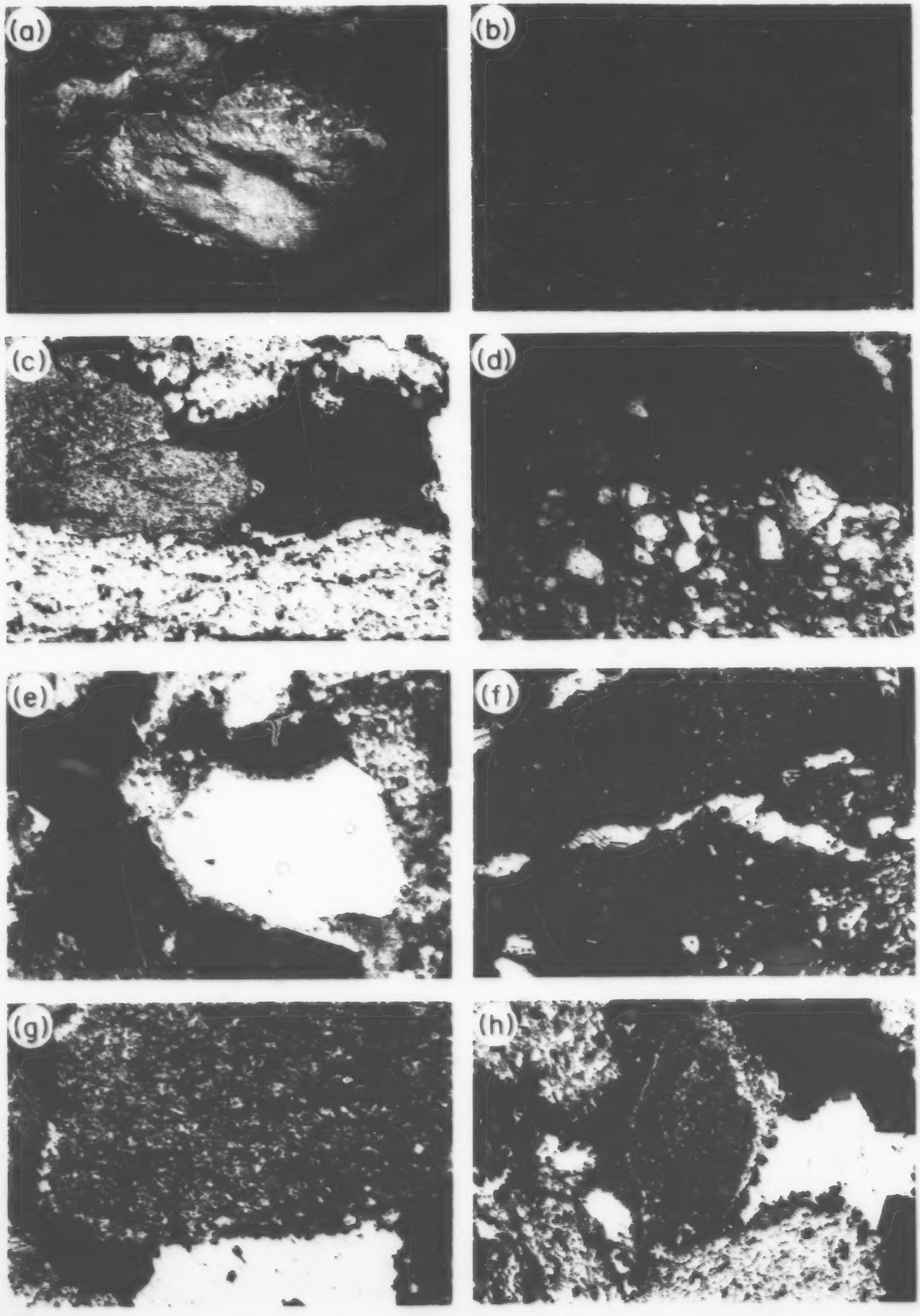
(a)
(b)
(c)
(d)
(e)
(f)
(g)
(h)

Fig. 2.13. Photos of carbonate lithologies of the Gays River bank; a and b are rock photos whereas d to h are photomicrographs (plane polarized light except for crossed Nicols in c; field of view is 1 cm in a, b, c and 2.6 mm in others). (a) Fine grained (i.e., aphanitic), beige colored dolostone with primary porosity partially infilled by fine grained dolomite cement and coarser, euhedral dog-tooth dolomite. (b) Cut slab of fine grained, beige colored dolostone with calcite cementing primary porosity and infilling subparallel fractures. Note the small galena euhedra in the calcite cement and traces of galena in the fractures with calcite. (c) Thin section of dolostone illustrating the abundance of primary porosity left in this carbonate sample. Note the presence of the granular dolomite cement and the coarse calcite cement (crossed Nicols). This sample is barren of mineralization. (d) Remnant coral structure illustrating the preservation of fine-scale features during the dolomitization of primary limestone. Note that calcite is cementing parts of the fossil (plane polarized light). (e) Fine grained detritus (quartz and feldspar grains) in dolostone. Note that the areas rich in debris are preferentially mineralized with galena and sphalerite (plane polarized light). (f) Fine grained dolostone with styolitic structure. Note the presence of quartz-feldspar grains along the styolite which may reflect concentration during pressure solution (plane polarized light). (g) Dolostone showing the presence of granular (recrystallized ?) dolomite that is frequently observed (crossed Nicols). (h) Dolostone showing development of new texture in areas cut by microfractures along which there is a distinct lightening of the red-brown dolostone, dissolution and cementation by calcite. Note that sphalerite mineralization also occurs along the microfractures (plane polarized light).

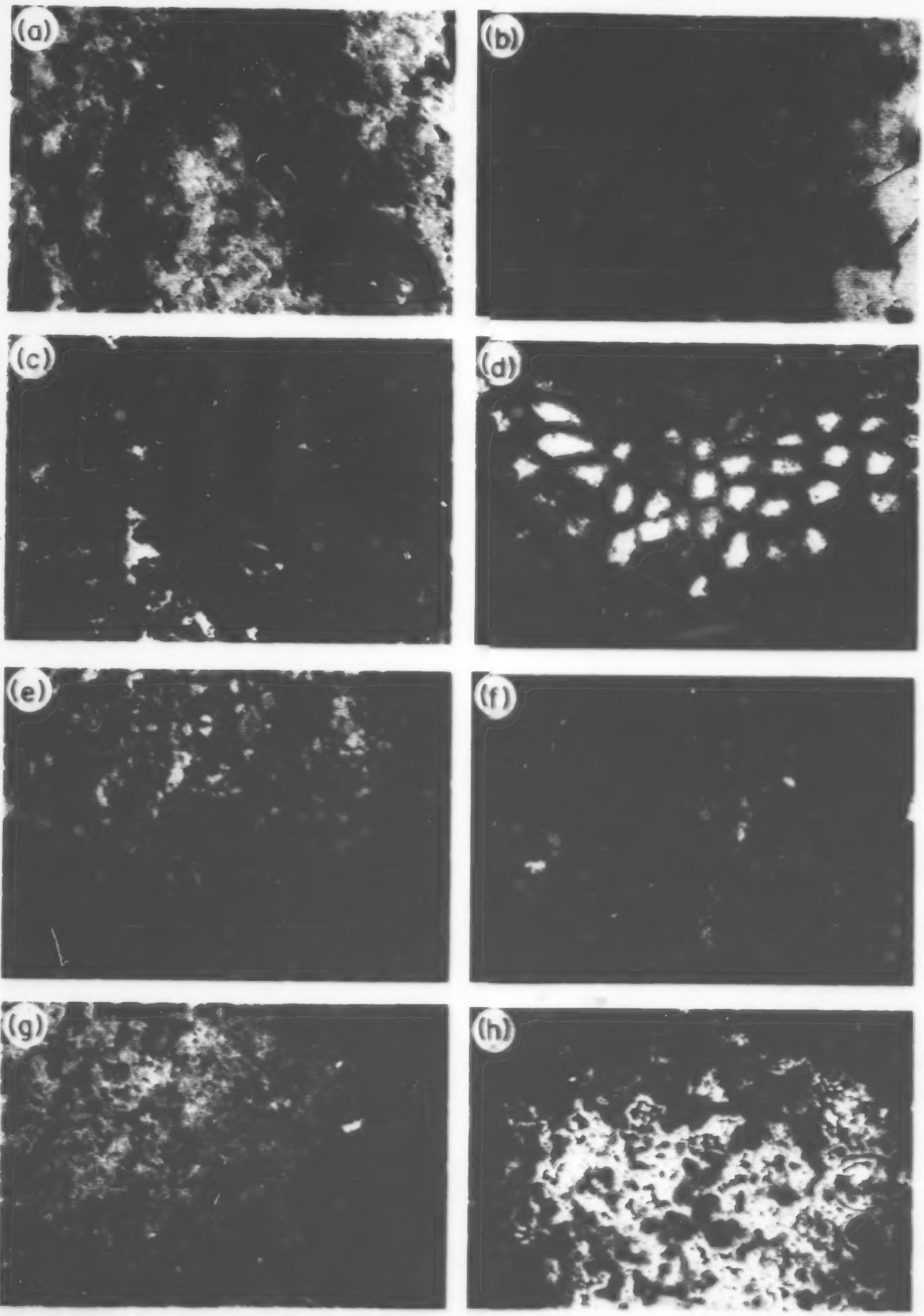
(a)
(b)
(c)
(d)
(e)
(f)
(g)
(h)

Fig. 2.14. Photomicrographs (except for a) of dolostone samples. (a) Primary porosity in dolostone partially cemented by fine grained dolomite which is then overgrown by coarser dolomite euhedra (1 cm wide). (b) Primary porosity with marine dolomite cement showing radial texture and later calcite cement which is partly inundated with fluid inclusions (crossed Nicols, width 5 mm). (c) Remnant fossil with primary porosity cemented by dolomite euhedra and later calcite. Note traces of fine grained, euhedral galena (plane polarized light, width 2.6 mm). (d) Fossil structures cemented by granular dolomite, euhedral sphalerite and late calcite (crossed Nicols, width 5 mm). (e) Fine grained dolosotne with quartz and feldspar debris. The rock is cut by fractures infilled by late calcite. Irregular black spots represent porosity (crossed Nicols, with 1 cm). (f) Dolostone with clacite cementing primary porostiy and also infilling subparallel fractures (crossed Nicols, width 1 cm). (g) Primary porosity in dolostone cemented by radial dolomite, coarse euhedral galena and later calcite (crossed Nicols, width 1 cm). (h) Primary porosity in dolostone cemented by fine grained, massive sphalerite (whitish material) and calcite (grey) (combined reflected and transmitteed light; width 1 cm).

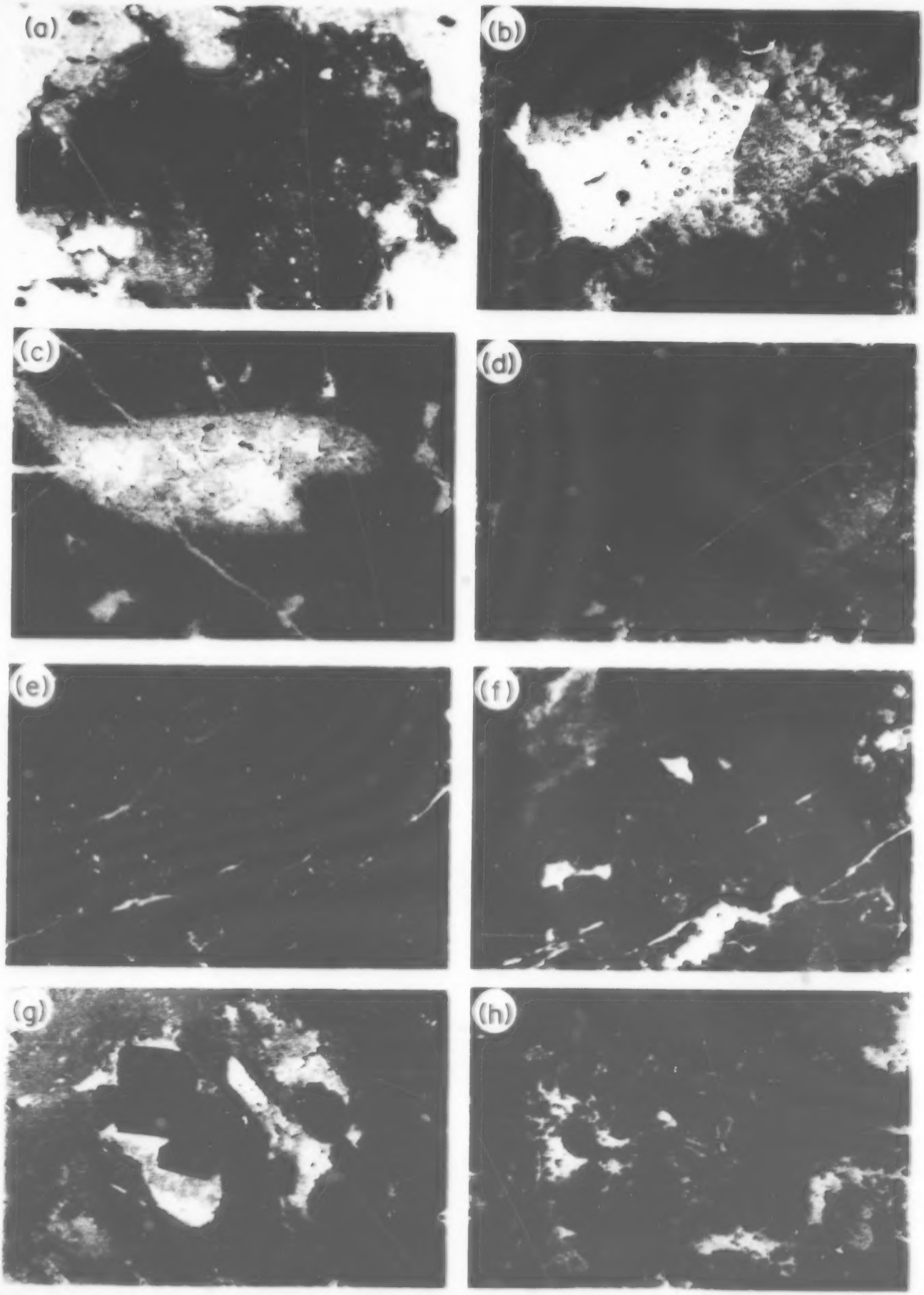
(a)
(b)
(c)
(d)
(e)
(f)
(g)
(h)

CHAPTER 3

MINERALIZATION AT GAYS RIVER

3.0 INTRODUCTION

In this chapter the nature of mineralization at the Gays River deposit is discussed from the micro- to the macroscale. Note that this discussion is restricted to the Gays River deposit and does not include the Getty Deposit area which will be included in a more comprehensive account of the area in a subsequent publication. The cross sections presented in Chapter 2 are used in conjuction with geochemical profiles of Pb and Zn to discuss the geometrical relationship of mineralization to the different lithologies. In addition, mineralization has been studied in terms of paragenesis, ore textures and zonation using geochemical profiles for the diamond drill holes, hand specimens and polished sections.

Work done at the deposit by Westminer Canada Ltd. over the past several years has redefined the nature of the ore zones, consequently the tonnage and ore grade at the deposit have been modified. The present resource outlined at Gays River is 2.4 million tonnes of 8.63 % Zn and 6.33 % Pb differs from the earlier resource estimate of 12 million tonnes of 7 % Pb+Zn by Esso Minerals. The differnce between the two companies in part reflects the different cut-off parameters used to calculate the ore zones.

3.1 DEFINITION OF ORE ZONES (ESSO VERSUS WESTMINER CANADA INTERPRETATION)

The present status of the ore zones at the Gays River deposit are shown in Figure 3.1 and the metal accumulation per level is summarized in Table 3.1 (from Westminer Canada). The ore

TABLE 3.1 Pre-mining insitu metal accumulations for Pb and Zn by level based on data from Westminer Canada Ltd.

MINING LEVEL	No. DDH USED	TONNAGE PB	ZN	PB/ZN (WT. %)
490	8	3391.5	4241.6	0.80
480	43	9884.9	12913.4	0.77
470	74	7547.1	17485.8	0.43
460	74	19853.3	43890.3	0.45
450	50	21015.6	41051.1	0.51
440	43	30714.0	36062.2	0.85
430	22	22606.5	22567.9	1.00
420	19	14820.5	13495.8	1.10
410	12	7325.9	7640.7	0.96
400	5	2016.5	2568.6	0.79
390	3	1644.0	1746.7	0.94
380	3	1777.9	852.8	2.08

zones have been obtained from using a data base of some 2000 surface and underground holes and using as a cut-off grade >7 % Zn equivalent (1% Pb = 0.8 % Zn) over 2 m. Using this criterion the ore zones were delineated and the tonnage figure calculated. This method diverges from that of the previous operator in that the latter used a cut-off of 2.4% combined metal (Pb+Zn) over 3 m which resulted in a larger tonnage but lower grade estimate of the resource. It should also be noted that whereas the high-grade, massive ore located against the trench was included in the ore reserve calulation (Esso Minerals), the mine development plan did not include this material because of the precipitous nature of the hanging wall in these areas. Esso Minerals mined approximately 550,000 tonnes of ore which average 3.3% combined metal (Akande, 1982). While this ore was above the cut-off for ore, it was significantly below the drill indicated grade and reserve estimate for the deposit (i.e., 7%) and probably reflected the fact that most of this development was done in the saddle part of the reef where the ore is lower grade and less continuous.

In contrast to the experience of Esso Minerals, the ore reserve figures and mine development done by Westminer Canada Ltd. was focused on the massive ore located against the trench. Westminer Canada Ltd.'s interpretation of the deposit is summarized in Figure 3.2 and, as is obvious, it is heavily biased towards the high-grade ore. This is similarly reflected in the mine production figures, summarized in Table 3.2, which indicate 131,359 tonnes ore mined with a grade of 3.35% Pb, 8.15% Zn.

The deposit geology of the Gays River area is portrayed schematically in Figure 3.2 (note, however, that this is quite realistic; see Figure 3.5) which indicates that the ore occurs as massive and disseminated types and that, most importantly, the massive ore is restricted to the dolostone-

TABLE 3.2 Summary of mine production from the Gays River deposit for different zones for the period September 1989 to May 1991 (data from Westminer Canada Ltd.).

ORE ZONE	PRODUCTION FISCAL 89/90 TONNES	Pb	Zn	PRODUCTION FISCAL 90/91 TONNES	Pb	Zn	TOTAL TONNES	Pb	Zn	PRODUCTION / RESERVE GRADE % of Pb	% of Zn
CAZU	20,340	6.40	8.56	17,686	4.08	7.96	38,026	5.32	8.28	94.8%	111.3%
CAZL				2,123	4.10	6.22	2,123	4.10	6.22	85.6%	77.1%
CCZ	8,590	4.86	5.58	21,885	4.01	9.66	30,475	4.25	8.51	111.5%	99.1%
CDZU				6,889	2.57	9.38	6,889	2.57	9.38	86.2%	126.1%
CGZU				4,794	3.38	5.83	4,794	3.38	5.83	114.6%	63.7%
WAZU	320	2.59	6.55	8,815	2.74	7.50	9,135	2.73	7.47	88.3%	72.2%
WBZU	6,155	4.85	10.63	21,889	5.47	14.27	28,044	5.33	13.47	72.3%	89.4%
WBZL				6,893	4.11	9.03	6,893	4.11	9.03	134.5%	129.9%
WCZU				9,204	2.19	7.49	9,204	2.19	7.49	89.4%	94.3%
WCZL				40	6.00	9.00	40	6.00	9.00	104.5%	189.5%
TOTAL RESERVE PRODUCTION	35,405	5.72	8.18	100,218	3.94	9.67	135,623	4.40	9.28	91.5%	97.2%
NON RESERVE PRODUCTION	22,945	1.03	2.80	31,141	1.46	3.27	54,086	1.28	3.07		
TOTAL PRODUCTION	58,350	3.88	6.06	131,359	3.35	8.15	189,709	3.51	7.51		

evaporite (or trench) contact. In addition, this schematic diagram indicates that the ore pinches out up dip towards the saddle part of the reef such that lower-grade material of Zn-rich nature dominates (halo to the higher-grade ore). Since the ore zones that were developed by Esso Minerals were within the upper part of the reef, these operators mined material that is not presently included in reseserve estimated of Westminer Canada Ltd. because of their higher-grade cut-off figure. Thus, the difference in the re figures between the two operators is predominantly a reflection of the different cut-off grades and to a lesser degree the interpretation of the deposit geology and geometry of the ore zone.

3.2 NATURE, EXTENT AND DESCRIPTION OF MINERALIZATION ON THE DEPOSIT SCALE

3.2.1 Generalizations Inferred From the Composite Vertival Sections

The geochemical profiles for Pb and Zn which accompany the vertical sections in Figure 2.6 have been used to examine the nature of the mineralization, the geometry of the ore zones, the relationship of the mineralization to different host rocks and element zonation in the deposit. The extent of the deposit area is approximately 4 km laterally and approximates the geometry of a corrugated sheet dipping gently towards the northwest (Fig. 3.1). The thickness of the ore intersections varies considerably with the narrowest obviously corresponding to the cut off of 2.0 m, whereas the thickest may exceed 10 metres on some levels (see below). A plot of the ore reserves per level versus cumulative frequency (Fig. 3.3) indicates that about 86% of the ore is located within 60 vertical metres between the 410 and 470 m working levels. This is reflected in the nature of the ore drawn schematically in Figure 3.2 which indicates that the mineralization

diminishes and then pinches out up dip.

Examination of the vertical sections in Figure 2.6 in further detail reveals the following important points with respect to the mineralization. Also see Table 3.3 for a summary of this information in terms of the appropriate sections and holes with examples of the intersections or geochemical profiles.

1. Mineralization is pretty much confined to the northwest side of the carbonate buildup despite the symmetrical nature of the geology. There is, however, a limited amount of mineralization in the Musquodoboit side of the reef as indicated in section 14 where grades of 3.7% Pb, 4.4% Zn/2.3 m (hole 536) and 0.9% Pb, 1.5% Zn/2 m (hole 535) are known. However, in section 13 the assays indicate only traces of Pb and Zn mineralization (<0.2 % Σ) or barren carbonate. Thus, despite a favourable environment in terms of the apparent geology there is very little mineralization relative to that observed on the other side of the carbonate bank.

2. Several generalizations can be made with respect to the mineralization in the saddle part of the reef: (i) the further one goes across the reef towards the southwest the more the grade diminishes compared to the fore reef area (sections 8, 12, 19, 21); (ii) there is generally a sudden reduction in the grade right at the hinge area of the reef where one goes from the fore reef proper to the saddle part of the reef (section 13); (iii) many sections of the saddle have intersections that are either very low grade or altogether barren (See table 3.3); (iv) where mineralization is present in the saddle, the Zn:Pb ratio >> 1, but there are exceptions to this (section 2 holes 50, 61; section 6 hole 163); and (v) mineralization in the saddle can occur at any stratigraphic level from near the contact with the Meguma Group basement or basal breccia (type 6 in Table 3.3) to the top of the reef as presently preserved (type 5 in Table 3.3). The mineralization is highly erratic

Table 3.3. Summary of Important Features of Mineralization in the Vertical Sections in Figure 2.6.

Feature	Sections/drillhole	Comments
1. Mineralization in the SE part of the reef complex (i.e., Musquodoboit Basin)	Sec. 15, holes 532, 533, 534 Sec. 14, holes 535, 536, 537	<0.2% Σ over 1-2 m grades to 5% Pb, 6% Zn over 1.2 m in hole 536; 2% Pb, 2% Zn over 0.6 m in hole 535
2. Mineralization in the saddle part of the reef.	Sections indicating barren or low grade nature: 1, 3, 4, 5, 7, 9, 11, 12, 19, 21	Sec. 1 = 0-2% Σ over 10-30 m Sec. 3 = 0.3% Σ over 35 m Sec. 4 = back part barren (<0.5% Σ over 16 m) Sec. 7 = hole 733 (30-35 m <0.2% Σ) Sec. 9 = low Pb in holes 672, 671, 676 Sec. 11 = back part barren Sec. 12 = barren to very low grade with only Zn assaying Sec. 21 = back part of the saddle only
	Sections indicating erratic nature of mineralization: 2, 6, 7, 12, 13	Sec. 2 = hole 50 (5.5, 1.7/2 m); hole 61 (11.3, 1.8/2.1 m) Sec. 6 = hole 163 (8.4, 1.2/3.4 m) Sec. 7 = hole 189 (0, 4.3/4 m) Sec. 12 = hole 539 (0, 3.2/3 m), 447 (8.2, 2/2.4 m)
3. Mineralization in the basal breccia	Sections indicating good mineralization: 4, 8, 9, 12, 13, 19, 20, 23, 25, 26	Sec. 4 = holes 12, 839 Sec. 8 = hole 555 Sec. 9 = hole 671 (bottom part) Sec. 12 = 542 (2, 11/0.9 m), 540, 499 Sec. 13 = holes 429, 655 (6.2, 2.7/4 m) Sec. 19 = hole 351 (1.4, 1.5/2.2 m) Sec. 20 = holes 93, 99 (14.3, 3.7/2 m), 91, 110, 115 Sec. 23 = hole 423 Sec. 25 = hole 231 Sec. 26 = hole 621 (10.4, 0.7/2 m)

4. Mineralization along the evaporite-dolostone contact	Sections giving the best example of this mineralization: 4, 7, 8, 9, 10, 11, 12, 13, 15, 17, 19, 20, 21, 22, 23, 24	Sec. 4 = holes 12 (12, 3.3/4.6 m), 839 (6.7, 4.0/2.7 m), 154 (2.8, 6.6/3 m) Sec. 7 = holes 185 (3.3, 10.2/2 m), 732 (4, 4.2/2 m) Sec. 8 = holes 555/8.5, 5.5/2 m) 549 (3.7, 4.6/2.2 m) Sec. 9 = holes 827 (3.9, 6.5/2 m), 828 (6.2, 14.7/3.2 m), 704 (10.8, 37/4 m) Sec. 10 = hole 473 (3.2, 6.8/2 m) Sec. 11 = holes 821 (6.5, 3.4/2 m), 367 (5.5, 6.2/6.9 m) Sec. 12 = holes 543 (4.3, 2.9/3.1 m), 542 (0.2, 9.5/2 m), 541 (6, 17.8/7.9 m) Sec. 13 = holes 429 (4.5, 7.2/2.6 m), 655 (6.2, 2.7/4.2 m) Sec. 15 = hole 99 (11.5, 3.5/3 m) Sec. 17 = holes 429 (4.5, 7.2/3.2 m), 427 (3.6, 5.1/2.2) Sec. 19 = holes 352 (0.2, 8.6/2 m), 678 (4, 2.1/4.7 m) Sec. 20 = holes 99 (14.3, 3.7/2 m), 110 (10.2, 19/4.2 m), 88 (0.2, 7.6/2 m) Sec. 21 = holes 117 (12.9, 6.8/2 m), 131 (4.7, 3.2/2 m) Sec. 22 = holes 450 (15.7, 1.5/2 m), 154 (9, 5.2/2 m), 712 (7.2, 11.9/2.1 m), 153 (4.6, 7.6/2 m) Sec. 23 = holes 423 (5.8, 9.1/5.6 m), 715 (1.5, 32.1/3.3 m), 716 (9.6, 13.9/3 m), 420 (0.3, 10.2/3.1 m) Sec. 24 = holes 204 (5.5, 8.0/3.8 m), 206 (8.2, 2.4/2 m), 208 (3.9, 8.7/2 m)
5. Mineralization within carbonate between the evaporite and basement contacts (i.e., carbonate hanging wall and footwall to ore)	Section 2	holes 50 (5.5, 1.7/2 m), 71 (4.5, 3.1/2 m)
	Section 3	hole 82 (1.2, 2.2/4.2 m)
	Section 4	hole 112 (11, 4.1/3.6 m)
	Section 6	hole 163 (8.4, 1.2/3.4 m)

6. Mineralization near base of carbonate (saddle part) at basement contact	Section 4	hole 216 (7, 1.6/0.6 m)
	Section 3	hole 85 (0.1, 2.6/4 m)
	Section 7	hole 189 (0, 4.3/4 m)
	Section 12	hole 447 (8.2, 2/2.4 m)
	Section 16	hole 287 (6.1, 19.4/2 m)
	Section 20	holes 88 (0.2, 7.6/2 m), 115
	Section 21	holes 131 (11, 19.7/4.7 m), 133 (8.8, 5.4/4.4 m)
	Section 24	hole 708 (0.4, 7.7/2 m)

both in terms of grade and thickness (Table 3.3).

3. Mineralization in the basal breccia is highly irregular and as a consequence this type of mineralization is not typically included in the ore reserve calculations (J. Campbell, pers. commun., 1991). Some good intersections are noted (Table 3.3), perhaps the most impressive being in sections 12 [e.g., hole 542 (2% Pb, 11% Zn/0.9 m)] and 20 [holes 99 (14.3% Pb, 3.7% Zn/2 m).

4. The evaporite-dolostone contact mineralization is the most consistent and high-grade of all the different styles of mineralization. Many sections exhibit high-grade intersections with grade-metre values of 20-50, with rare exceptions to 150-200. The best intersections occur between section 4 and 24 (grades are summarized in Table 3.3) and the degree of mineralization diminshes rapidly to the northeast (section 25) and southwest (sections 1 to 3).

5. In some sections the grade can change rapidly either up or down dip and the thickness of the mineralized interval is also susceptible to rapid variation. This is well illustrated for example in section 24.

A plan map for part of the underground workings of the deposit (Fig. 3.4) illustrate many of the features summarized above based on the drill hole data. The established stratigraphy is well illustrated on the plan map, but note that the massive and disseminated ores pinch and swell along strike. In particular note that in the eastern end of the drift the massive ore bifurcates. This reflects the fact that at this point on the plan map the mapping was done at an elevation 4 m higher up in a different stope and thus there is a change in the dip and strike of the trench:ore contact that is refleced in the map.

3.2.2 Detailed Examination of Some Composite Vertical Sections

Several sections are particularly useful in displaying features of the ore zone and these are described in some detail below. Section 13 is through the central part of the deposit and the complexity of the section is a reflection of the promontory or paleotopographic high of Meguma basement. Thus, the reef is bounded on both sides by small basins infilled at one time with evaporitic material. The distribution of Pb and Zn in this section indicates that in the central part of the reef (holes 466, 465, 464) there is good Zn mineralization with only trace Pb mineralization. This contrasts with the barren nature of the reef in holes 264 and 263 and suggests that this relatively better mineralized part of the reef is somehow related to its extension into the basin.

Section 12 represents one of the best mineralized sections examined in the deposit and in Figure 3.5 a detailed compilation of geochemical profiles is superimposed on the vertical extent of the carbonate rocks. Important features of this diagram include: (1) the specific occurrence of the massive, high-grade ore at the trench:carbonate contact; (2) the pinching out of the ore up section past the hinge zone (holes 256, 447, 257); (3) extension of the mineralization into the basal breccia and Meguma Group lithologies. However, note that this section is unique in that no where else has ore-grade mineralization been observed in the deposit extending from the trech:carbonate contact to the basal breccia unit (J. Campbell, personal communication, 1992); (4) harmonious and disharmonious nature of Pb and Zn in the geochemical profiles (e.g., hole 542 versus hole 540); and (5) enrichment of the metals with respect to the evaporite/trench-carbonate contact and carbonate-basement contact; and (5) metal zonation with the Pb:Zn ratio decreasing up dip towards the saddle part of the reef.

3.2.3 Evidence for Elemental Zonation in the Deposit

The geochemical profiles in the cross sections permit an evaluation of the zonation of Pb and Zn within the deposit area. There is observed a crude zonation such that Zn is enriched in the upper part of the deposit and Pb is the lower part (e.g., section 12 in Fig. 3.5). However, because galena is paragenetically later than sphalerite (see below), some of the trends are somewhat irregular and this explains the disharmonious behaviour of the two elements. The different paragenetic associations also account for why Pb mineralization well in excess of or to the exclusion of Zn mineralization may occur in the upper part of the carbonate. However, the best documentation of the elemental zonation is presented in Figure 3.6, a composite, longitudinal section through the central part of the deposit showing isopleths for the Pb:Zn ratio. Superimposed on this diagram is the outline of the ore zone which also indicates the thickness of the mineralized zone. Although it is obvious that there is a a general enrichment of Zn in the upper part of the deposit, the 50:50 contour is quite irregular with numerous highs and lows relative to a datum (e.g., 450 m level). This feature is highlighted, for example, at the 950E point where the countour punctures a Zn-rich area and at the 900E point where a Pb-rich zone overlies another zone of Zn enrichment. These features again suggest that Pb is paragenetically later than the Zn and, therefore, cross cuts the earlier Zn mineralization giving rise to the irregular contouring of the Pb:Zn ratio. Finally, this diagram also indicates the restricted nature of the ore zone to a vertical interval of 20-80 metres.

3.3 MACROSCOPIC AND MICROSCOPIC FEATURES OF THE MINERALIZATION

3.3.1 Macroscopic Features and Types of Ore

The mineralization at Gays River has been subdivided into three types based on hand specimen observations, these being massive, net-textured and disseminated. The distribution of these three types of mineralization has already been alluded to in the previous discussion.

The massive ore is composed of sphalerite and galena (Fig. 3.7a, b, c), although vestiges of remnant dolostone may be seen in thin section (Fig. 3.7e). Massive sphalerite is aphanitic in texture, beige to yellowish in colour and breaks with a conchoidal fracture pattern (Fig. 3.7a, b), but rarely coarser, crystalline-type, reddish-orange sphalerite may occur. Galena in the massive ore is considerably coarser than the sphalerite with an average grain size of 3-5 mm and the ore is characterized by a distinct vuggy texture and may contain later, clear calcite. The vuggy texture is in keeping with the fact that galena is about 80% denser than sphalerite and that while most of the massive ore formed by constant volume replacement of the dolostone (and possibly earlier sphalerite ?), some of the replacement must have been constant mass to generate the porous texture. Where the two minerals coexist, the galena always appears to post- date the sphalerite (Fig. 3.7b) and sometimes there is a distinct coarsening (recrystallization ?) of the sphalerite near the galena.

The massive ore almost always found at the contact between the dolostone and either the trench sediments or the evaporites (Figs. 3.8 and 3.9). The only exception to this occurs at the top of ore zones where the massive ore rolls into the carbonate unit and pinches out (Fig. 3.8). This phenomenon has been observed in numerous exposures underground during mining (J. Campbell, personal communication, 1992). In Figure 3.9, underground photos of the massive ore, several features are important to note: (1) the massive ore is located at the contact with the trech and there is no structural complexity at this location such as shearing or brecciation (cf. Akande

and Zentilli, 1984); (2) remnant bedding inherited from the carbonate is easily distinguished in the massive ore; and (3) galena mineralization cross cuts the massive sphalerite as subvertical veinlets, stringers or shoots.

The term net-textured is introduced to describe the ore which forms the footwall to the massive-type ore (Figs. 3.7c, 3.8, 3.9). The term is adopted from the literature on Ni sulphide deposits where similar type textures have been described. This ore consists of richly mineralized dolostone which is cross cut by a continuous network of sphalerite and galena. The mineralization is a combination of replacement and pore filling (cementation) in this ore and, therefore, there is rapid variation in the grades and texture. The sphalerite is again aphanitic, beige and massive, but the coarser, crystalline type of reddish-brown sphalerite is more abundant. Galena is of similar texture as in the massive ore. Both the sphalerite and galena form an almost continious lattice work and the contact with the massive ore is knife sharp.

The term disseminated mineralization (used by Westminer Canada for the footwall ore to the massive ore) is adopted here to describe the occurrence of Pb and Zn mineralization which appears to infill primary porosity (Fig. 3.7d). This mineralization overgrows dolomite euhedra and may be intergrown with calcite (Fig. 2.14g, h); the sphalerite is rarely oberserved to be intergrown with fluorite and barite. The texture of the sphalerite is highly variable and varies from reddish-orange euhedra of <2-3 mm to aphanitic and beige coloured. The galena occurs as <5 mm-size euhedral grains.

In addition to the above observations with respect to the ore material, there occurs late-stage pyrite and marcasite in the deposit area. This material was only observed in specimens collected from the high-grade stock pile and consisted of coarse grained Fe sulphides growing

on fracture surfaces (i.e., open space infilling) in barren dolostone rock but frequently associated with thick (1 cm) layers of pyrobitumen. In addition, pyrite is observed as euhedra lining vugs in the massive ore, co-existing with oxides along fracture surfaces and as crystalline layers on dedelomitized limestone. Finally, oxidation of hypogene minerals is observed in the form of Zn and Pb oxides minerals near the trench-massive ore contact (Fig. 3.7a), Fe and Mn oxides are common, and traces of malachite and azurite occur.

3.3.2 Microscopic Features of the Ore

Microscopic examination of the ore material using high magnification binocular microscopy and reflected light microscopy provides a considerable amount of textural information not available in the hand specimen study and each mineral is described independently. Note, however, that mofidications may be made pending further work and examination of a larger suite of samples. In addition, some mineral phases remain to be identified and will be reported on at a later date.

Galena:

Galena occurs as nearly inclusion-free, anhedral to euhedral grains with rare deformation textures as manifested by curved cleavage traces. Textural varieties in addition to the abundant massive sulphide ore include cement (i.e., porosity infill), vein type, replacement/disseminated and associated with styolites. The vein type occurs along fractures in both dolostone and clasts of Meguma Group (Fig. 3.10g, h) and consists of fine grained anhedral galena or euhedral grains with or without calcite. The disseminated type occurs as fine grained euhedral grains peppered

throughout massive dolostone either alone (Fig. 3.10c) or spatially associated with calcite and/or sphalerite (Fig. 3.7f, g). The origin of this galena is sometimes difficult to deduce and may represent either cementation or replacement. The occurrence of galena as a cementation of primary porosity is very common and it may be as irregular or euhedral grains, the nature of the porosity controlling the shape of the grain. Where the galena infills small irregular pores it tends to be anhedral, but where it occurs in large (i.e., >5 mm) pores it tends to be euhedral. The cement variety either overgrows a substrate of dolomite euhedra (i.e., cement) or more rarely be in direct contact with the dolostone, in which case a period of corrosion of the dolomite crystals is implied. Although this galena is frequently intergrown with calcite, it may also appear to post date it. Where galena is associated with styolites it occurs as either anhedral or euhedral grains and appears to post-date styolite development.

The galena is generally inclusion free, but variable amounts of dolostone, sphalerite, chalcopyrite, pyrite and unidentified Fe-sulphide phase occur as inclusions. The dolostone represents vestiges of the precursor dolomite and is only observed in the massive ore. The Fe and Cu sulphide phases generally, but not exclusively, are found near the margins of the galena host.

Deformational textures within the galena are rare, being defined by the presence of curved traces of cleavage outlined by triangular-shaped pitted surfaces. Sometimes this textural variety can be related to the proximity of the host to styolitic features, but sometimes the texture is found in massive sulphide samples and are locally well developed.

Sphalerite:

Sphalerite occurs as either massive, fine grained (<10-20 μ grains) material or coarser grained (to 300-400 μ size), subhedral to euhedral grains; both textural types occur as a cement (i.e., infilling a variety of pore spaces; Fig. 3.7f, g). The massive sphalerite is pale in colour (yellow-brown) and may occur in isolation or associated with the coarser type of sphalerite. Vestiges of remnant dolostone occur within the massive sphalerite (Fig. 3.7e) and rarely textures are present that appear to have been inherited from the precursor dolostone (e.g., oolitic or pisolitic). There have been no cases observed where conversion of dolostone to massive sphalerite has resulted in preservation of fossiliferous material, either from macro- (i.e., drill core or underground) or micro-scale observations, although such textures occur in the lower grade, mineralized dolostone. Whether this is a function of sampling remains to be tested by additional work. Where massive sphalerite replaces dolostone, there is a distinct recrystallization of the dolostone to equigranular, euhedral dolomite and/or calcite grains that may be cored by micron-size sphalerite grains (Figs. 3.7h, 3.10e).

Sphalerite as coarse grains is restricted in occurrence to cementation of primary porosity, both within the dolostone and the basal breccia lithologies (see Figure 2.12). In these cases, it only partially infills the porosity as euhedral to subhedral, equant grains of yellow, reddish-orange or red color (Fig. 3.7d, f). The coarse sphalerite is almost always inclusion free with rare grains of chalcopyrite and pyrite occurring as micro-inclusions. This coarse grained sphalerite is commonly surrounded by a corona or halo of finer grained, micron-size sphalerite (Fig. 3.10a, b). In rare instances color zoned sphalerite has been observed with clear and yellow zones alternating; no detectable difference is composition was noted between these zones by electron microprobe analyses. The most common occurrence of this sphalerite is as overgrowths of

dolomite euhedra and it is post-dated by calcite spar (Fig. 3.7f). However, it may also overgrow galena, be intergrown with barite and calcite and be spatially associated with pyrobitumen-rich styolites.

Additional features of sphalerite mineralization include: (1) occurrence as concentrically arranged inclusions within calcite euhedra in massive dolomite or massive sphalerite (Fig. 3.10e); (2) fine grained material replacing dolomite cement in both the basal breccia and Meguma Group lithologies (in this case presumably replacing a carbonate-rich precursor matrix which does occur in some lithologies of the Meguma Group); and (3) it appears to post-date styolitic textures (Fig. 3.10f) and rarely cross cut clacite cement (Fig. 3.10d).

Chalcopyrite:

Chalcopyrite (Fig. 3.11a, f) is found in trace amounts in about 15-20% of the specimens examined and occurs: (1) along the margins of sphalerite or galena grains with galena being the more common host, (2) in calcite cement and (3) within the dolomitic matrix. Grains are subhedral to anhedral and inclusions of euhedral to anhedral pyrite and an unknown Fe-sulphide occur (Fig. 3.11a).

Pyrite:

Pyrite is a rare but persistent phase at Gays River occurring in about 75-80% of the specimens examined (Fig. 3.11a, b, c, e, g). It occurs in a variety of forms including: (1) vein or net textured; (2) framboidal (Fig. 3.11g; mostly, but not exclusively, in doiomitic matrix); (3) subhedral to euhedral grains (Fgi. 3.11a); (4) colloform textured; and (5) grains within

pyrobitumen-rich styolites (Fig. 3.11e). The most common form of the pyrite is as types 2, 3 and 5. The most common occurrence of pyrite inclusions is within or associated with galena and more rarely sphalerite and calcite spar. Textural evidence and the occurrence of the pyrite suggests that in at least some cases the framboidal material coarsens up to become subhedral to euhedral grains.

As mentioned above, a later stage of pyrite growth occurs as fracture infillings (<1 cm) where coarse (3-5 mm) euhedra are intergrown with calcite and often associated with thick (1 cm) layers of pyrobitumen. Presumably these are the late pyrites which gave the very low $\delta^{34}S$ signatures reported by Akande and Zentilli (1984).

Marcasite:

Marcasite was rarely observed in close association with pyrite when the latter occurred in the matrix. It is anhedral, massive and inclusion free. A later generation of marcasite is reported by Akande (1982) and, as with the late pyrite, is characterized by very low $\delta^{34}S$ values (Akande and Zentilli, 1984).

FeS phases:

An unidentified Fe-sulphide phase (Fig. 3.11d), possibly bravoite, occurs in trace amounts associated with pyrite as either inclusions within galena or the dolostone. It is euhedral to subhedral and is color zoned with orange-brown and brownish bands.

Styolites:

Styolites occur in most samples examined and can be found both within the barren dolostone (Fig. 2.13f) and variably mineralized samples (Figs. 2.13e, 3.10f, 3.11e). The styolites are defined by the presence of dark red-brown to black material and less commonly detritus of the Meguma Group. The styolites commonly have in close spatial association several ore phases (sphalerite, galena, pyrite), but these phases appear in most cases to post date the styolite formation. In one case a calcite-bearing veinlet cross cut a styolite and in another a coarse, reddish-brown sphalerite (4-5 mm) grain overgrew the pyrobitumen concentrated along the styolite. However, there is some, albeit very limited, indication that styolite formation was post ore. The most convincing evidence for this is found in a sample where deformed cleavage traces in galena are restricted to an area adjacent the styolite. Another example is represented by styolites bounding massive sphalerite mineralization with barren dolostone on either side of this material (i.e., dissolution of dolostone until the massive, insoluble sphalerite was reached). Much of the framboidal textured pyrite occurs within styloites (Fig. 3.11g) and lesser amounts of the subhedral- to anhedral-textured pyrite.

Fluorite:

Fluorite has only been observed in 3 specimens and in each case it occurred intimately associated with mineralized, sparry calcite. In one case it could be seen to overgrow galena euhedra which were attached to a substrate of euhedral dolomite cement, whereas in another it contained fine grained (5-50 μ), disseminated sphalerite grains. The fluorite is anhedral to subhedral in habit and a variety of colors (clear, green, purple). In all of the fluorite samples observed, fluid inclusions are abundant.

Barite:

Barite was observed in only two samples. In one case it was as massive, fine grained, red-brown material cementing mineralized (sphalerite, galena) dolostone that also had an earlier calcite cement. However, the barite also contains fine grained disseminated sphalerite so it to partially overlapped mineralization. In the second case, barite was intergrown with sparry calcite cement and appeared to be syn-sphalerite mineralization which also occurred as a cement.

Ag-bearing Phase:

The concentrates at the deposit run about 25-30 ppm Ag and this suggest the presence of a Ag-bearing phase unless the Ag is tied up in the crystal lattice of the galena. Considering that massive samples of galena have been analyzed (maximum 3.5 ppm; Table 4.1) and galena has been analyzed with the electron microprobelse (Ag not detected; Table 4.8), it is probable that a discrete Ag-bearing phase remains to be identified. Future work will address this problem.

Alteration Minerals:

Oxidation of the hypogene mineralization has resulted in the formation of secondary minerals, including the following phases: malachite, azurite, native sulphur (?) and a Pb carbonate or sulphate (remains to be identified). Little attention has been given to this aspect of the mineralization and more work is required.

Hydrocarbons:

In the present investigation the only observation made of hydrocarbons were restricted to

the occurrence of pyrobitumen along styolites and a single sample containing yellowish organic matter intergrown with fine grained sphalerite. However, the presence of this material indicates at least previous occurrence of mobile hydrocarbons. This material was examined by Gize (1984; in Gize and Barnes, 1987) and he reported than the material was not fluorescent and because of problems associated with polishing no reflectance measurements could be made. In addition, it is important to note that Akande (1982) and Akande and Zentilli (1984) have reported the presence of oil within fluid inclusions hosted by fluorite, but the timing of influx of this organic matter remains poorly constrained.

3.4 PARAGENESIS AND TIMING OF MINERALIZATION AT GAYS RIVER

A summary of the paragenesis at Gays River, as deduced from the examination of the host rock and ore minerals, is presented in Figure 3.12. This scheme is generally in accord with ones presented for the deposit by Akande (1982), Akande and Zentilli (1983, 1984) and Savard (1992). Predating the main stage of Pb-Zn mineralization was the dolomitization of the carbonate reef and pervasive cementation by dolomite euhedra, although this latter phenonmenon was not so complete as to reduce the porosity and permeability to nil. These early stages are firmly established from consistent petrographic observations made on all samples and many independent observers. There was probably some mineralization of pyrite predating the main sulphides which may have been part of either stage I or II, or even both stages. However, the bulk of the sulphide mineralization is considered to represent a single event designated stage III. Although there is some justification to subdivide this stage into sub-stages given that in many cases there is clear evidence for a relatively late-stage growth of galena compared to sphalerite (e.g., Fig.

3.7b), at present the two minerals are grouped together paragenetically. Thus, galena is shown to extended slightly past sphalerite whereas the other sulphides are considered to be limited in their paragenesis and are interpreted to be early, but the scarcity of these minerals provides poor constraints.

The gangue constituents (barite, fluorite, calcite) overlap in part the Pb-Zn mineralization and extend beyond the main sulphide stage. Since detailed studies of calcite (isotopes, cathodoluminescence) has shown several distinct generations (M. Savard, 1992; personal communication, 1992), this mineral has been designated as potentially having different generations (e.g., I, II, III, ...) and further work will be aimed at refining this.

Petrographic observations clearly indicate that styolite formation was pre- and post mineralization, although the preponderance appear to be early with respect to mineralization. Presumably, this phenomenon also continued during the mineralizing event. However, the absence of intense fracturing or deformation of the ore minerals or associated gangue is noted and this is interpreted to favour a post styolite timing of the mineralizing event. Although there is clearly evidence for very local deformation of galena in the form of curved cleavage traces (i.e., glide planes) and some polysynthetic twinning of sphalerite, these are not pervasive features. Thus, this interpretation contrasts with the observations of Akande and Zentilli (1984) who infer that deformation textures both in galena and sphalerite are quasi-pervasive features. Further evidence for a post-styloite/pressure solution timing for mineralization is found in Figure 3.10g and h where galena infills fractrures that are clearly related to pressure solution processess in the basal breccia unit.

The degree to which the Pb-Zn mineralization and calcite cementation overlap is difficult

to determine. There is clear petrographic evidence that sphalerite ± galena lined that pore space as cement prior to calcite precipitation. However, calcite is intergrown with these minerals and in some cases sphalerite is observed to infill fractures in calcite cement (Fig. 3.10d). Thus, while the bulk of Pb-Zn mineralization may have pre-dated the calcite cement, this mineralization continued for some time after, albeit to a lesser degree.

Attempts to date the mineralizing event include apatite and zircon fission track track (Arne et al., 1990; Ravenhurst et al., 1989) and conventional K-Ar (Ravenhurst et al., 1989) and $^{40}Ar/^{39}Ar$ (Ravenhurst, 1987) techniques. All of this work has provided only very broad limitations on the absolute timing of mineralization: (1) the $^{40}Ar/^{39}Ar$ profile for a detrital muscovite in the Meguma Group basement rocks indicates a thermal overprinting at <320 Ma; (2) zircon fission track ages range from 308 to 342 (± 21-37) Ma whereas apatite fission track ages range from 203 to 241 (± 10) Ma; and (3) K-Ar dating of mixed illite-muscovite material indicates apparent ages of 345-350 (± 10-15) Ma. Thus, at present there is no good absolute age constraint on the mineralizing event except for the time of depostion of the host-rock carbonate which is ca. 330 Ma (Visean).

The last stage of the paragenesis involves the oxidation of the ore body and generation of supergene minerals. Many of these phases remain to be identified properly and, therefore, they will be reported on at a later date.

Fig. 3.1. Plan map of the Gays River deposit showing the outline of the ore zones and 10 m level contours as delineated by diamond drilling. Note that the ore zones dip off towards the basin (i.e., northwest). Lines indicate the locations of vertical sections and line (A-B) indicates the longitudinal section that shows the metal zonation in the deposit (see Fig. 3.6). The grid shown is the Westminer Canada Ltd. mine grid for the deposit. Diagram modified after a map of Westminer Canada Ltd..

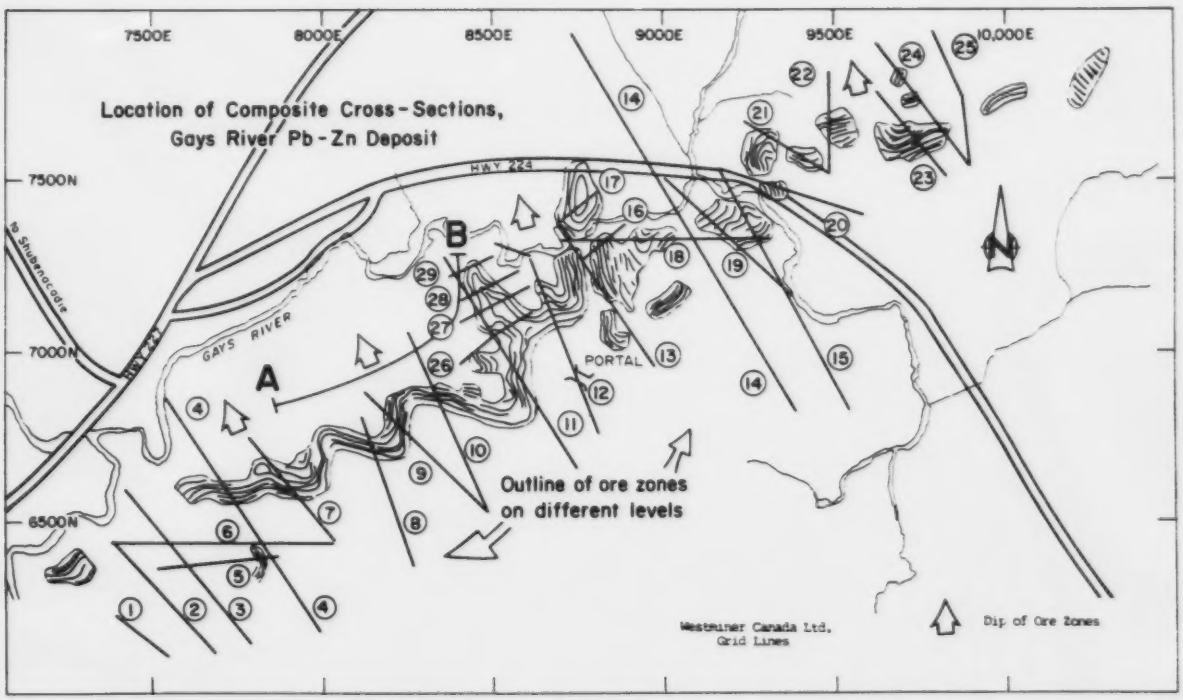

Fig. 3.2. Schematic section of the Gays River deposit (after J. Campbell, personal communication, 1992) showing the distribution of rock types and different ore types. Note that the use of the term disseminated ore in this diagram is different than the meaning inferred in the text by this writer.

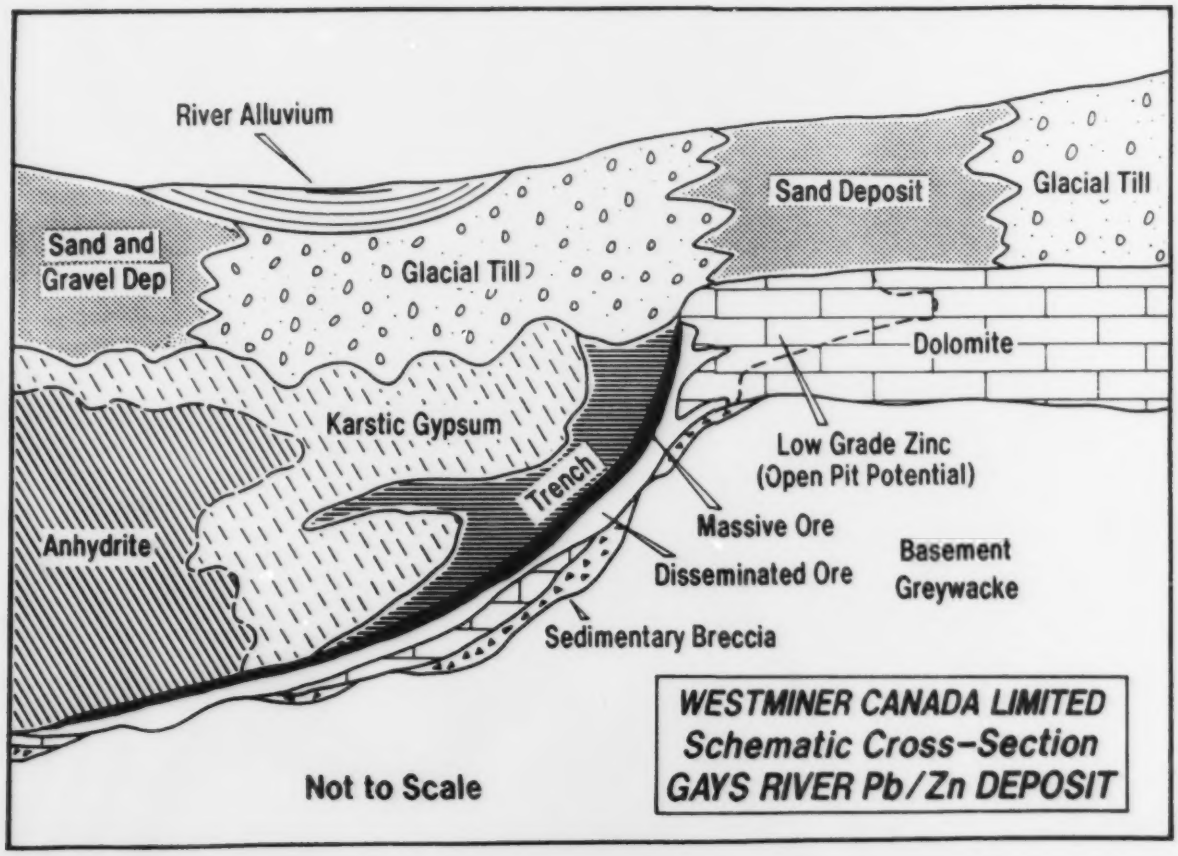

Fig. 3.3. Plot of cumulative % ore versus mine level for the Gays River deposit. Note that about 86 % of the ore is located between the 410 and 470 m levels (based on data from Westminer Canada Ltd.).

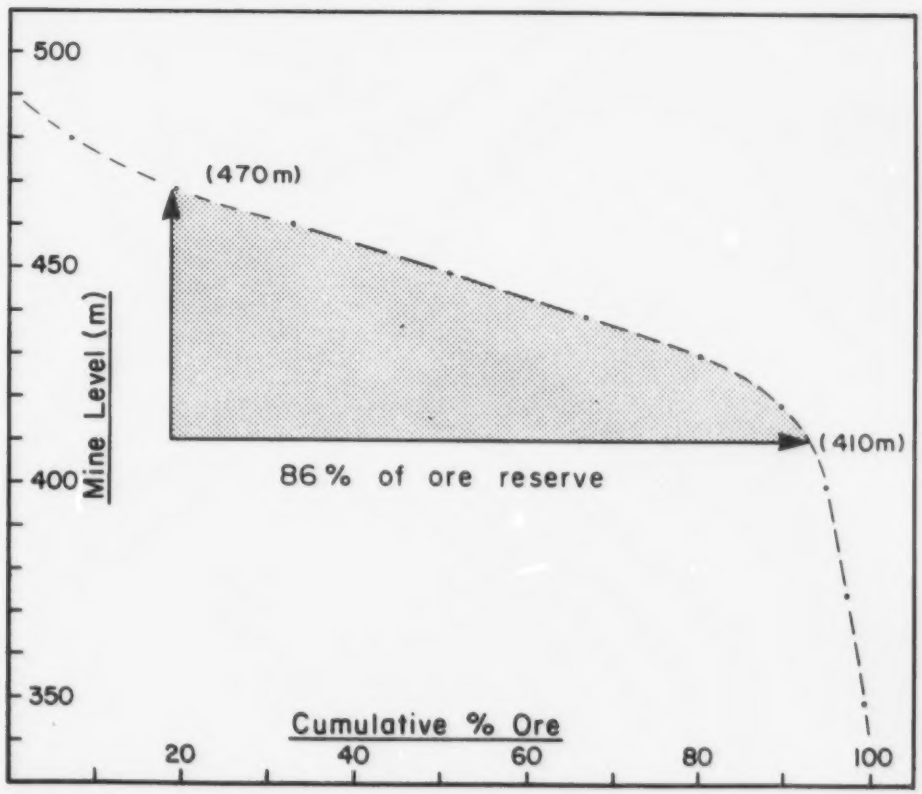

Fig. 3.4. Plan map of underground workings (460 and 464 levels) in the Gays River deposit illustrating the following features: (1) location of the massive ore at the dolostone-trench contact (paleo evaporite-dolostone contact). However, note that at the east end of the drift the massive ore lens bifurcates in part because of the change to the 464 level workings in the 82 sill; (2) the laterally continuous nature of the massive ore with pinch and swell features; and (3) location of the disseminated (net-textured in text) ore at the footwall of the massive ore and its highly variable thickness. The two diamond drill holes shown intersected ore up dip and and show the vertical variation of the geology and the grades of Pb and Zn mineralization. Note in particular that in hole U569 the massive ore has disappeared at this point, although it is present on both sides of the hole drilled, and that in U570 it is absent further up dip.

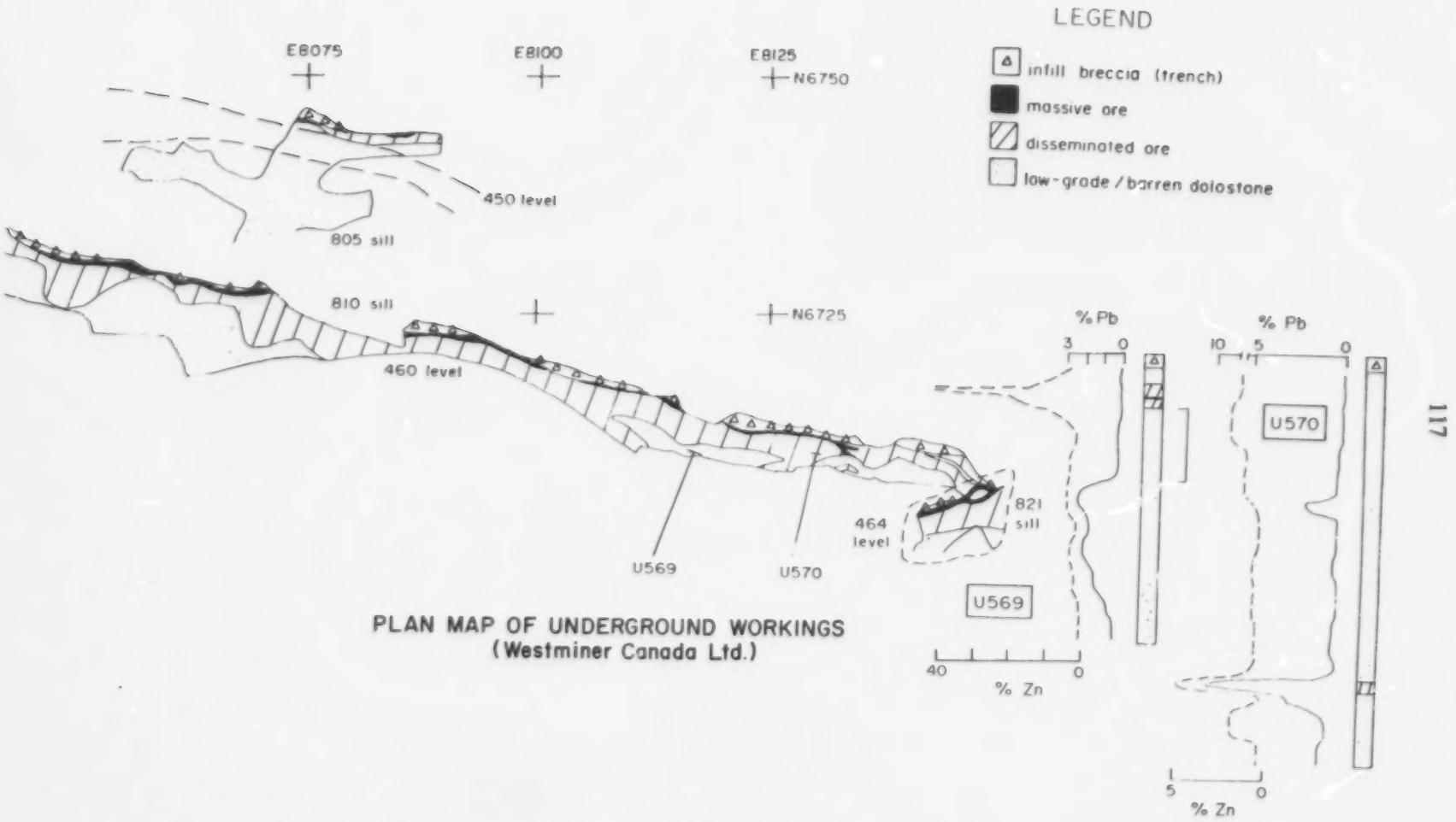

PLAN MAP OF UNDERGROUND WORKINGS
(Westminer Canada Ltd.)

Fig. 3.5. Section 12 (see Fig. 3.1) showing the outline of the carbonate unit and the geochemical profiles for Pb and Zn in the diamond drill holes. Note that for purposes of plotting the data the profiles have been plotted equidistant from each other (compare with cross section 12 in Figure 2.6). The significant features of this diagram are discussed in the text.

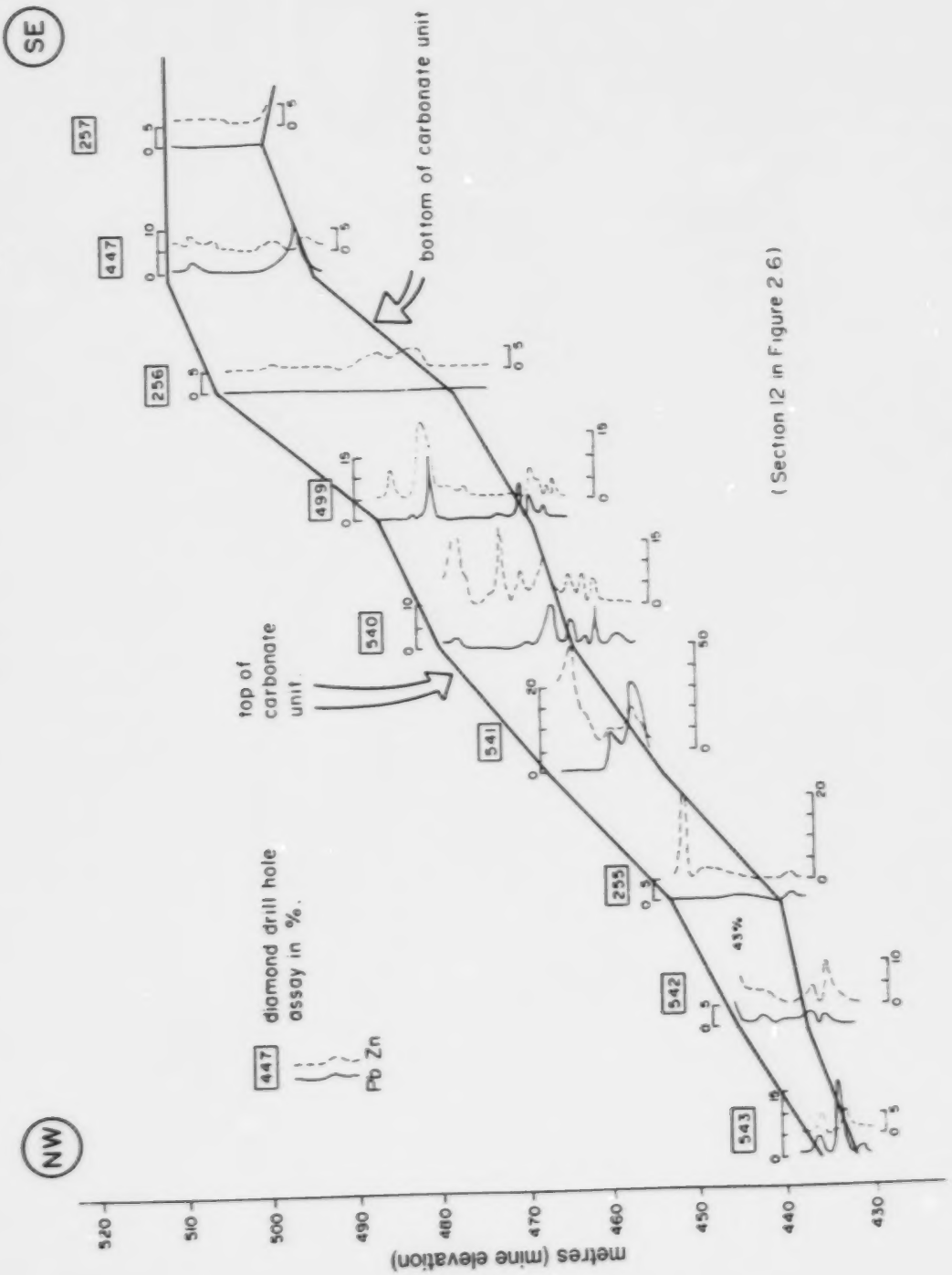

Fig. 3.6. Longitudinal profile along line A-B in Figure 3.1 showing the location of diamond drill holes in the section, the upper and lower boundaries of the ore zone (i.e., economic cut off of 7% Zn equivalent/2 metres) and the datum of 1:1 Pb:Zn. The diagram indicates that Pb is enriched over Zn in the lower part of the deposit and the converse is true for the upper part of the deposit.

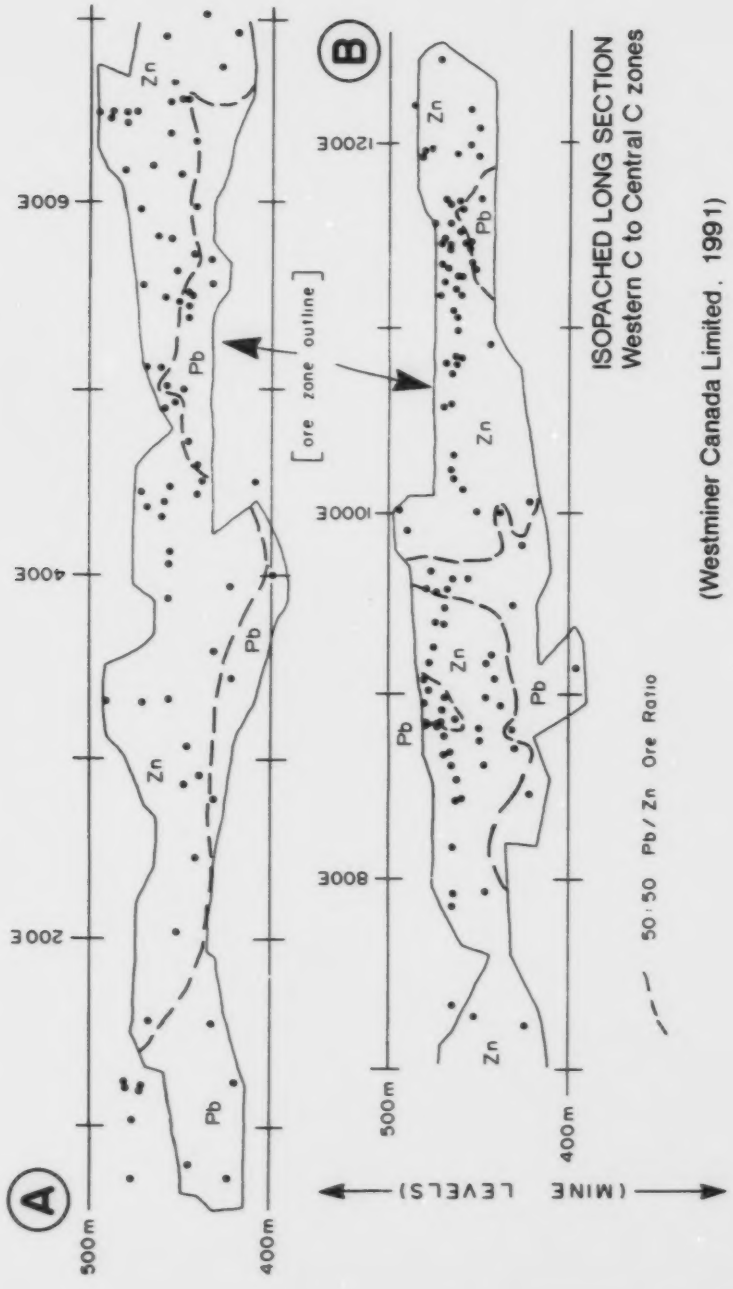

Fig. 3.7. Ore mineralogy of material at Gays River deposit. (a) Massive Zn-rich ore with typical aphanitic, massive texture and conchoidal fractures. (b) Massive Pb-Zn ore with galena occurring as veinlets cutting the sphalerite. Note the conchoidal fracture pattern in the massive sphalerite. (c) Underground photograph showing massive Zn-rich ore (white) and the net-textured disseminated ore in contact. Note the sharp contact between the massive ore and the net-textured ore. Width of photo 1.5 m. (d) Yellowish-red sphalerite euhedra cementing primary porosity in fine grained, beige dolostone. Width of photo 1 cm. (e) Photomicrograph (plane polarized transmitted light) of massive Zn-rich ore with remnant patches of corroded dolostone. Width of photo 1 cm. (f) Photomicrograph (plane polarized transmitted light) of mineralized dolostone showing sphalerite and calcite cements. Width of photo 2.6 mm. (g) Photomicrograph (combined transmitted and reflected light) of Zn($\pm$Pb)-rich ore showing the fine grained and crystalline types of sphalerite. Note the preservation of fossiliferous structures. Width of photo 1 cm. (h) Photomicrograph (plane polarized transmitted light) dolostone with sphalerite replacing dolostone and causing recrystallization and coarsening of the dolostone to dolomite euhedra. Width of photo 1.3 mm.

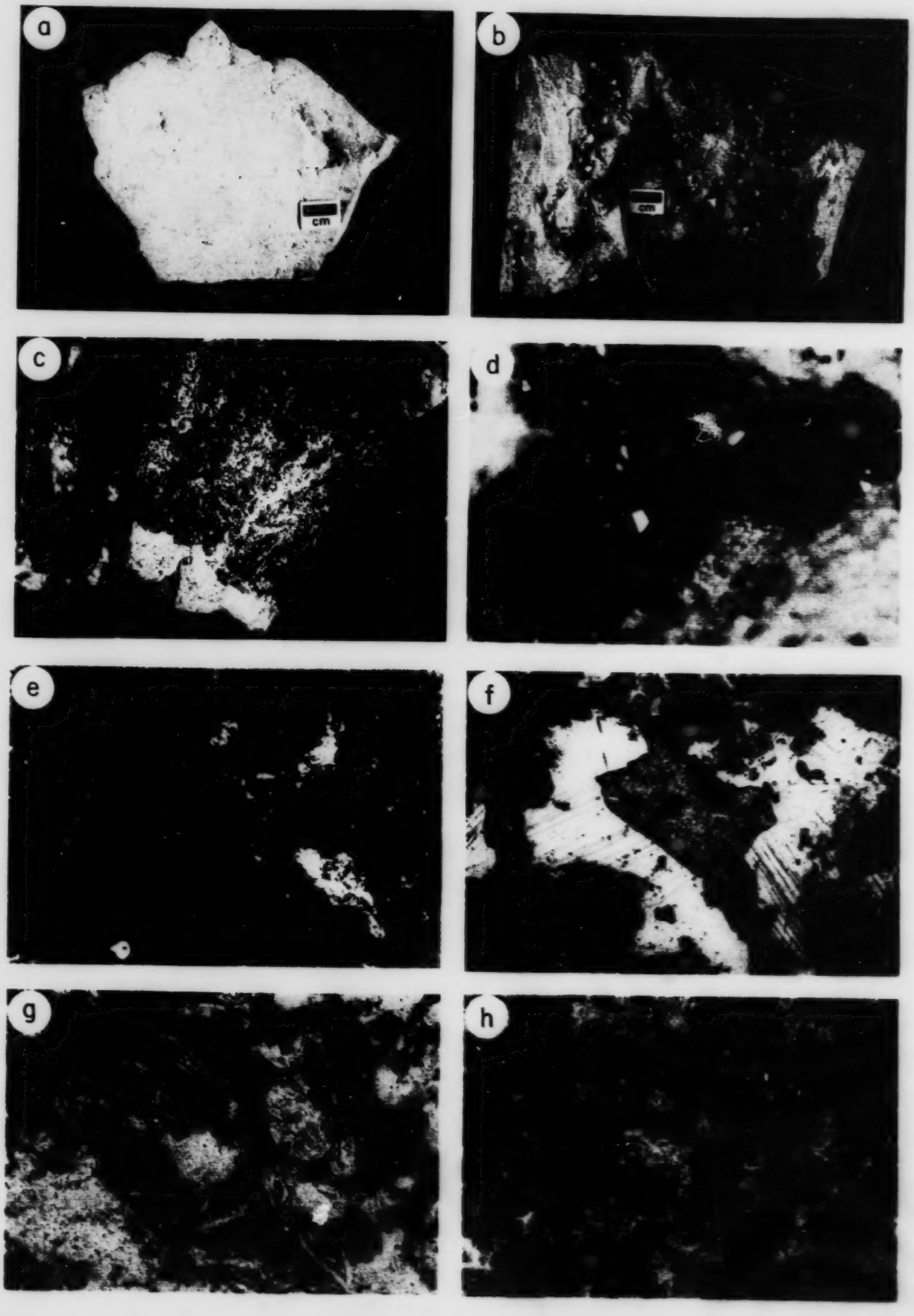
a
cm
b
cm
c
d
e
f
g
h

Fig. 3.8. Underground photo (Western A Zone, 841 stope) of mineralization at the Gays River deposit. Photo taken looking at the face of the stope where limy carbonate unit is surrounded by Zn-rich ore. At this point the massive ore is rolling into the carbonate as it pinched out near the top of an ore zone. Note the extent of the net-textured ore. Width of view about 1.5 m.

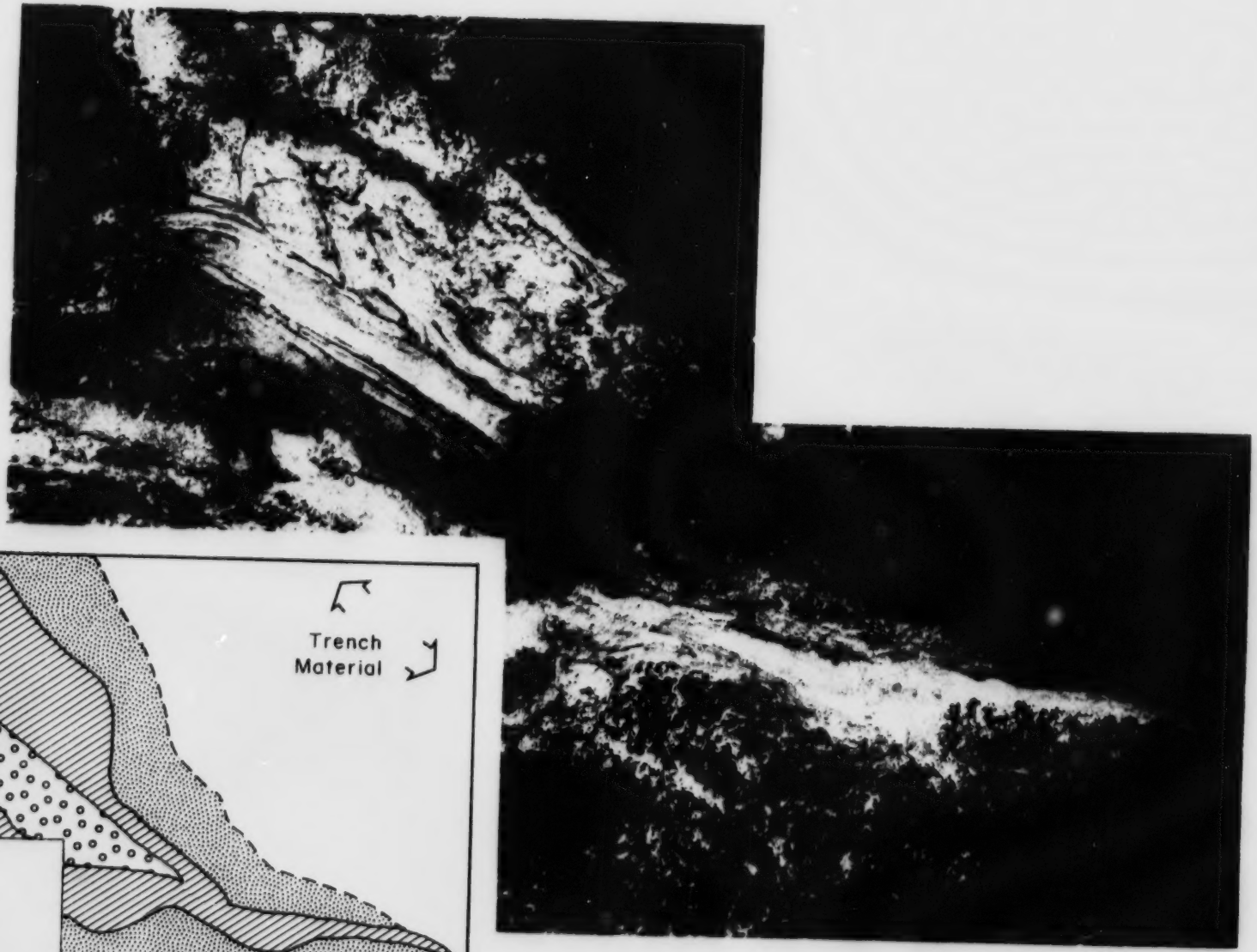
Trench
Material
vug
limestone
massive ore
net-textured ore

Fig. 3.9. Underground photos (855 stope, A Zone) of massive ore mineralization at Gays River deposit taken at the trench:massive ore contact. (a) Massive ore material (Zn-rich on right and Pb=Zn on left) near the trench (just off photo to the right). Note the remant bedding (fracture planes dipping from upper left to lower right). Width of photo about 2 m. (b) Close up of part of (a) showing the coarse galena cutting the earlier, fine grained sphalerite. Note the sub-vertical orientation of the galena-rich pods/veinlets. (c) Net-textured ore (Zn-rich) which occurs to the left of the photo in Figure 3.8c. Note the continuous nature of the fine grained, veing-like sphalerite mineralization. (d) Low-grade, Zn-rich mineralization in dolostone outside of the ore zone on this level. Note the erratic nature of the mineralization and the local, high-grade pod of sphalerite in the middle of the photo. Photo about 1 m wide.

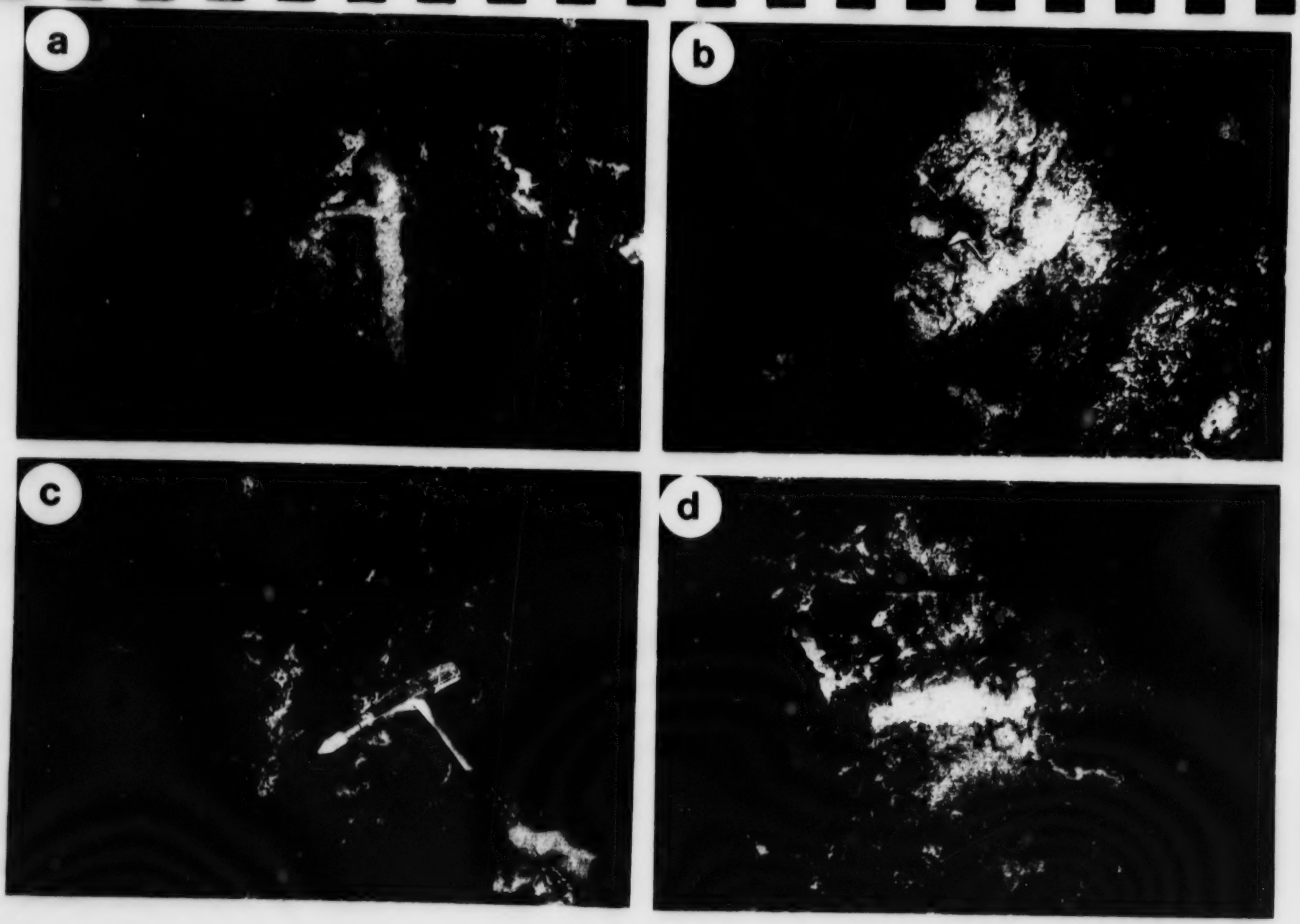
a
b
c
d

Fig. 3.10. Photomicrographs of Pb-Zn mineralization at Gays River deposit. (a, b) Reflected light photos of sphalerite mineralization as cement and replacement textures. In figure 5.10b the fine grained texture typical of the replacement mineralization is shown (average grain size 10-20μ). Width of photo 2.6 mm in (a) and 0.34 mm in (b). Note that the area outlined in black box in Figure 5.10a is enlarged in 5.10b. (c) Corroded pieces of dolostone surrounded by galena mineralization (plane polarized transmitted light). Width of photo 1 cm. (d) Calcite cement cross cut by fractures infilled with sphalerite (combined reflected and transmitted light). Width of photo 1 cm. (e) Calcite euhedra containing fine grained sphalerite in massive, fine grained sphalerite (combined reflected and transmitted light). Width of photo 6 mm. (f) Styolite in dolostone with sphalerite mineralization (crossed Nicols). Note that the crystalline sphalerite is not deformed despite being near the styolite. Width of photo 1 cm. (g) Basal breccia unit with Meguma Group clast being penetrated by a fragment of a similar nature (plane polarized transmitted light). Note the fractures that radiate outwards from the point of maximum penetration and the infilling of these by galena. Width of photo 6 mm. (h) Meguma Group clast with en echelon array of galena-infilled fractures. Note that in detail the fractures appear to be deformed (plane polarized transmitted light). Width of photo 1 cm.

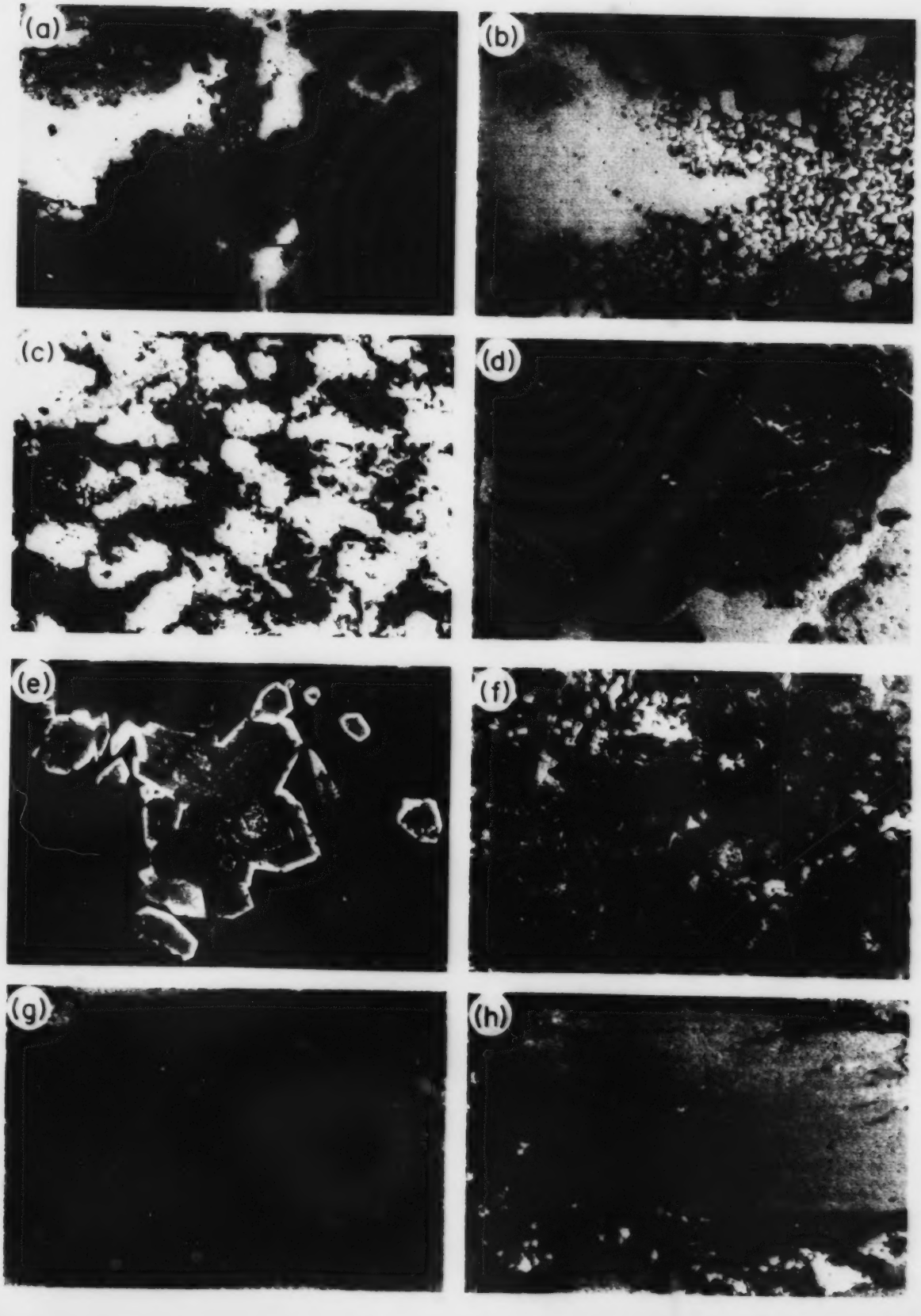
(a)
(b)
(c)
(d)
(e)
(f)
(g)
(h)

Fig. 3.11. Photomicrographs of Fe- and Cu-sulphide mineralization at Gays River deposit. All photos in reflected light. (a) Subhedral chalcopyrite with euhedral pyrite inclusions in calcite veinlet cutting coarse galena. Width of photo 0.3 mm. (b) Pyrite euhedra in dolostone matrix (black) with small anhedral grains of sphalerite (grey). Width of photo 0.34 mm. (c) Pyrite (py), sphalerite and galena (gal) along styolite in dolostone. Note the very fine grained pyrite in the dolostone. Width of photo 2.6 mm. (d) Unidentified FeS phase (?) of euhedral habit showing concentric zonation. This phase is intergrown with dolostone and anhedral grains of sphalerite (grey). The large grain in the centre is ca. 40 μ wide. (e) Styolite structure with pyrobitumen and pyrite concentrated. Note the euhedral shape of the pyrite. Width of photo 1.3 mm. (f) Anhedral chalcopyrite mineralization concentrated within pyrobitumen surrounded by galena. Width of photo 1 mm. (g) Pyrite framboids with concentric structure concentrated along pyrobitumen-rich styolite structure. Width of photo 150 μ.

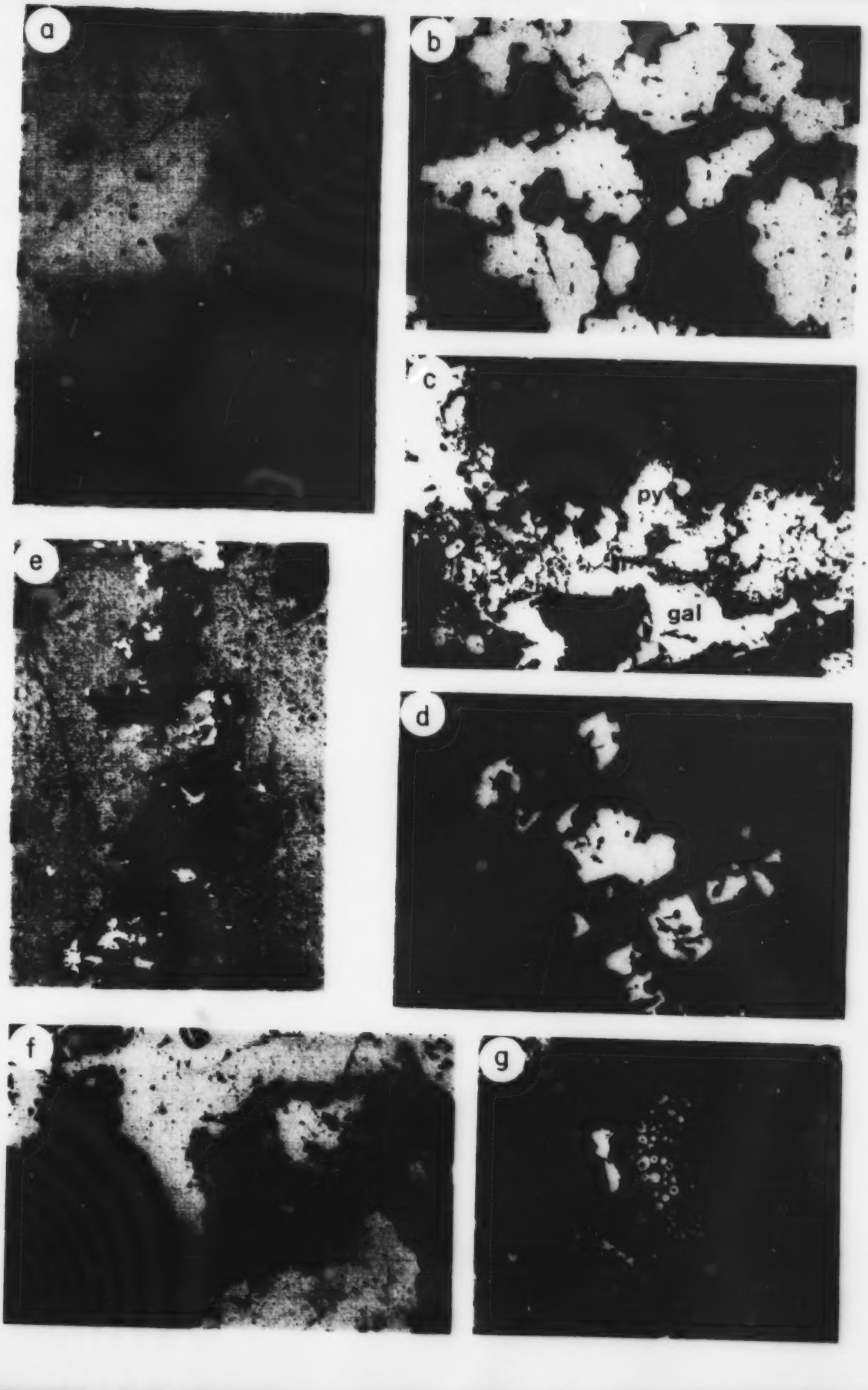
a
b
c
py
gal
d
e
f
g

Fig. 3.12. Parageneis of mineralization at Gays River deposit. See text for discussion of the relative timing of mineralization. Note that there is no Ag-bearing phase indicated in the parageneis at present because although such a phase is suspected to be present based on the ca. 30 ppm Ag in the concentrates, no mineral phase has yet been identified.

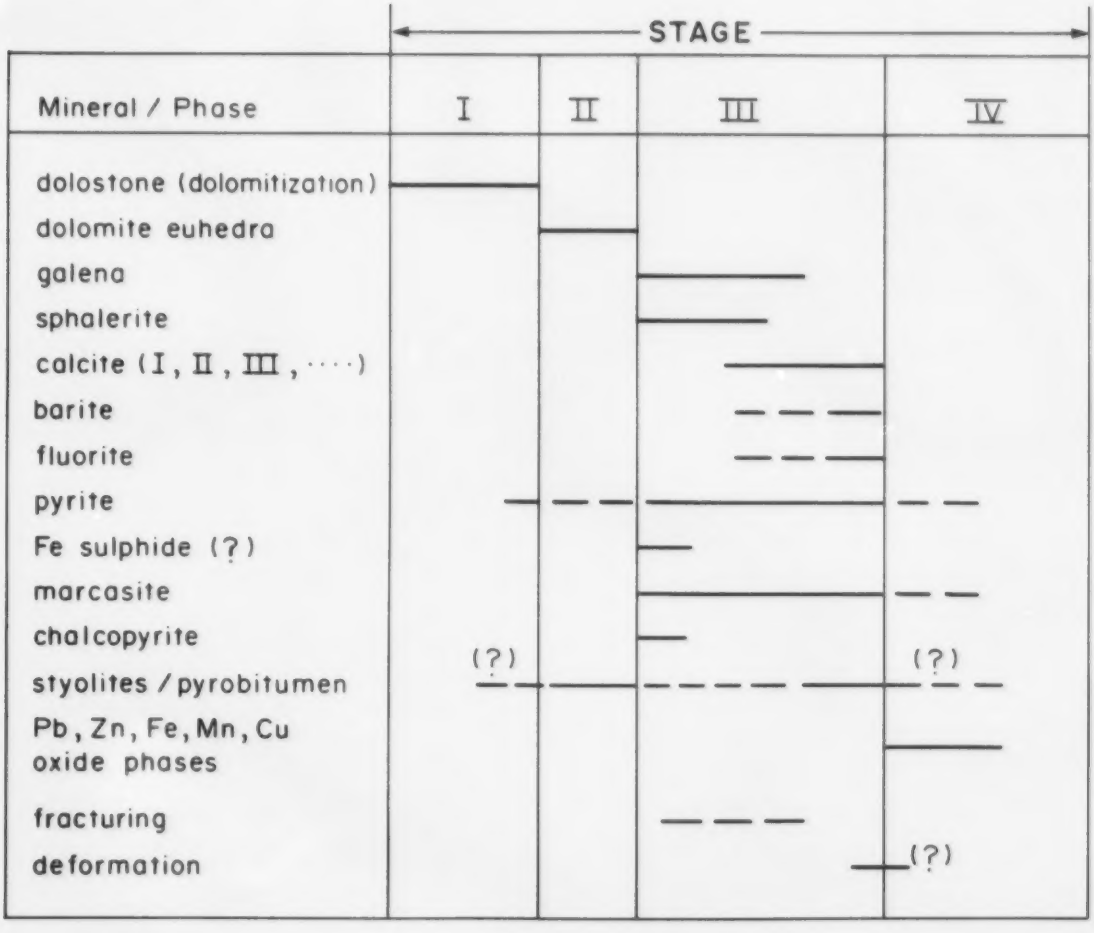

CHAPTER 4

GEOCHEMCIAL STUDIES

4.0 INTRODUCTION

Geochemical studies at the Gays River deposit include whole rock and mineral scale investigations and to date the following work has been completed: (1) multi-element analyses of high-grade ore material; (2) trace and rare-earth element (REE) analyses of both mineralized and barren whole rock material; (3) trace and REE element analyses of carbonates of different generations; and (4) electron microprobe analyses of carbonates sphalerite, galena and mineral phases in the Meguma Group clasts of the basal breccia (micas, feldspar). Additional work is in progress, specifically major and trace element analyses of whole rock material (i.e., variably mineralized dolostone), and these results will be reported elsewhere.

The purpose of the geochemical studies were: (1) to identify trace elements that could be used as path finders for application in regional geochemical exploration, (2) integrate the results of geochemistry to identify potential reservoirs for the fluids involved in the genesis of the ore deposit (i.e., REE in the calcites), (3) characterize the mineral phases in terms of their trace element signatures (e.g., Cd in sphalerite) since such features are potentially significant in terms of environments of formation, and (4) obtain information on the different styles of mineralization such as coarse- and fine grained sphalerite.

4.1 ANALYTICAL PROCEDURES

Whole rock samples of massive ore, disseminated ore and barren dolostone were crushed

to -200 mesh using the facilities at the Technical University of Nova Scotia (TUNS) and stored in plastic vials. Four representative samples of high-grade mineralization were subsequently anlayzed for a full suite of major and trace elements using standard wet chemical techniques to fully characterize the geochemical nature of the samples. In addition, 2 samples of massive ore, 6 samples of low-grade disseminated mineralization hosted by dolostone and 2 samples of apparently barren dolostone were anlayzed for trace (including REE) elements using the ICP-MS facilities at Memorial University, St. John's, Newfoundland. Full details of the analyses, including precision and accuracy, are given in Jenner et al. (1990) while Strong and Longerich (1985) discuss the general principles and operation of the instrument. The detection limits of this technique are low (ppm), and the the limit of detection is taken to be 3 standard deviations of the background determined on blank samples run with the unknowns. The detection limits and reagant blanks are generally about 10% of chondritic values (S. Jackson, personal communication, 1991). In Table 4.5 results of duplicate runs of both soiutions and samples (GR-91-32, 147, 60, 168, 172) indicate good agreement of the data.

Calcites of different generations were hand picked from comminuted samples (-20 to +65 mesh) of (1) high-grade ore, (2) low-grade disseminated mineralization, (3) barren dolostone and (4) late-stage calcite euhedra lining fractures. The calcite samples from types 2 and 3 are referred to as vug infill or sparry calcite and in type 2 are intimately intergrown with sphalerite $\pm$ galena. High quality separates were washed in deionized water, dried and crushed to -200 mesh prior to being analyzed using the ICP-MS facilities at Memorial University (see above).

Microanalyses of carbonates and silicates were obtained at the the Department of Earth Sciences, Dalhousie University, using a JEOL 733 Superprobe. An Energy Dispersive System

(EDS) was employed for all the analyses and the following operating conditions were employed: accelerating voltage of 15 kV, probe current of 5 nA and a beam diameter of 1-3 μ. Data reduction of raw counts was done using a ZAF software program.

4.2 ANALYTICAL RESULTS

4.2.1 Geochemistry of High-Grade Ore Samples

Results of analyses of the four high-grade ore samples are given in Table 4.1. As expected, the major element chemistry of the samples is dominated by Pb + Zn (59-75 wt.%), S (15-29 wt.%), CO_2 (4-7 wt.%), and Mg and Ca oxides (4-6 wt.%). The atomic ratio of Mg/Ca (Table 4.1) indicates that for three of the samples with values of about 0.55 the carbonate in the rock is dolomite (Mg/Ca atomic = 0.53 from microprobe analyses), whereas for the remaining sample the carbonate is dominantly calcite (Mg/Ca = 0.18).

The trace element contents of the mineralized samples (Table 4.1) indicate the following features: (1) Cd is elevated to >2600 ppm in Zn-rich samples (GR-91-B, D, F); (2) Ag contents are uniformly low at <3 ppm, even in the most Pb-rich (69 wt.%) sample. These low values contrast with the consistent level of 25-30 ppm Ag for the concentrates by both Esso Minerals Ltd. and Westminer Canada Ltd. (M. Cullen, personal communication, 1992). However, only four samples have been analyzed and it is possible that sufficient samples have been analyzed to give a representative value. This discrepancy is presently being investigated; (3) V, Co and Cu are consistently in the 1-35 ppm range and there is no apparent correlation with either the Pb- or Zn-rich nature of the samples; (4) Ge is consistently 1 ppm; and (5) Bi and Mn are <1 ppm. Semiquantitative spectrographic scans were done on the samples to ensure that elements present

TABLE 4.1 Chemical anlayses of massive ore samples, Gays River deposit.

	GR-91-B	GR-91-D	GR-91-E	GR-91-F
Al2O3 (%)	0.25	0.14	0.14	0.11
Fe (%)	0.23	0.24	0.20	0.21
Pb (%)	38.4	0.05	69.0	14.5
Zn (%)	28.5	60.9	6.24	45.5
CaO (%)	3.77	2.91	2.90	4.29
MgO (%)	0.77	1.77	1.79	2.73
CO2 (%)	4.32	4.99	3.85	7.06
S (%)	20.96	28.90	15.25	25.30
Ag (ppm)	0.5	0.2	3.5	1.6
Bi (ppm)	0.06	0.08	0.06	0.07
Cd (ppm)	1112	2618	267	2055
Co (ppm)	15	18	7	35
Cu (ppm)	11	2	30	12
Mo (ppm)	1	1	1	1
V (ppm)	3	3	5	8
Mn (ppm)	638	965	700	1520
Ge (ppm)	1.5	1.9	1.3	1.6
Hg (ppm)	0.08	0.03	0.02	0.01
Mg/Ca (atomic)	0.18	0.54	0.55	0.56

wt. %

Sample	<0.0001	.0001-.001	.001-.01	.01 -.1	.1 - 1	+1
GR-91-B	Be,Bi,Ag	Tl,Mo,Sn,V B,Ge,Ba,Ti	Cu,Co Ni	Mn,Al	Mg,Si,Fe Cd	Pb,Zn,Ca
GR-91-D	Be,Bi,Ag	Tl,Mo,Sn,V B,Ge,Cu,Ba Ni	Co	Si,Mn,Al Pb	Cd,Fe	Zn,Ca,Mg
GR-91-E	Be,Bi	Tl,Mo,Sn,V B,Ge,Ba,Ag Co	Cu,Ni	Si,Mn,Al Cd	Fe	Pb,Zn,Ca Mg
GR-91-F	Be,Bi	Tl,Mo,Sn,V B,Ge,Ba,Ag	Cu,Ni Co	Al	Si,Mn,Fe Cd	Pb,Zn,Ca Mg

in significant amounts (i.e., >10 ppm) were measured, but this work indicated no other elemental enrichments. A more detailed list of trace elements analyzed by ICP-MS is given in Table 4.2, and the results are comparable with the previous data discussed above with the following additional points noted: (1) Cu values are slightly higher by ICP-MS; and (2) low abundances are indicated for U, Th, Rb, Y, Ba and Sr.

REE data for the massive ore samples are given in Table 4.2 and chondrite-normalized patterns plotted in Figure 4.1. The samples have ΣREE between 9-38 ppm, they are LREE enriched and strongly fractionated with $(La/Lu)_N$ = 6-21, and have small negative Eu anomalies (Eu/Eu*=0.8-0.72).

4.2.2 Geochemistry of the Dolostone

The trace element data for both the mineralized (n=6) and unmineralized dolostone (n=2) are presented in Table 4.2 and the two data sets are compared in Table 4.3. In general, the dolostones are characterized by low abundances of most trace elements, the exceptions being Pb, Zn, Sr and Ba. Before comparing the mineralized and unmineralized data sets, however, it is noted that sample GR-91-125 is anomalous compared to the other unmineralized dolostone (GR-91-96) in terms of elevated contents of Li, Sc, V, Cr, Cu, Zr, Cs, Ba and Th. This elemental enrichment is interpreted to reflect the presence of Meguma Group detritus, specifically feldspar, mica (chlorite) and zircon in the dolostone.

Comparison of the chemical data for the two dolostone groups (Table 4.3) suggests that in general the samples have the same chemistry aside from the obvious relative enrichment of Pb and Zn in the mineralized set. There is slight relative enrichment of Li, Rb, Cr and V in the

TABLE 4.2. Whole Rock Geochemisty, Gays River.

Sample #	GR91-91	GR91-91	GR91-91	GR91-92	GR91-93	GR91-98	GR91-164	GR91-164	GR91-96	GR91-125
Lab. #	M1688	M1689	M1690	M1691	M1692	M1694	M1696	M1696*	M1693	M1695
Material	mass ore	mass ore	*dolostn	*dolostn	*dolostn	*dolostn	*dolostn	*dolostn	dolostn	dolostn
Li	2.4	0.48	10.9	16.3	13.9	5.1	10.2	9.5	3.9	74.1
Be	4.3	1.1	1.4	1.8	1.8	1.9	3.5	3.2	2	3.6
Sc	5.3	ND	4	5.2	4.4	3.8	4.6	4.1	3.4	9.9
V	2.3	1	10.6	11.3	11.1	1.6	12.2	12.4	2.3	79.7
Cr	1.3	ND	9.9	9.2	9.5	1.7	19.2	19.2	1.7	66.1
Cu	38.2	49.3	13.5	31.2	93.8	62.5	58.6	58.4	15.5	30.9
Zn			8181	23249	52611	22208	35537	34986	1259	241
Rb	1.77	0.48	10.44	14.1	15.3	0.77	16.3	16	1.1	99.8
Sr	11.5	8.44	126.5	154.6	125.6	110.4	66.8	47.6	96.3	103.5
Y	1.77	2.61	6.34	8.3	7.02	4.69	4.32	4.42	4.14	5.24
Zr	1.4	ND	8.7	13.4	12.5	0.9	15.9	14.2	3.3	90
Nb	0.2	0.1	1.4	1.7	1.8	0.1	1.8	1.8	0.2	12.9
Mo	0.1	0.2	0.5	0.4	0.5	0.7	0.7	0.8	0.4	1.4
Cs	0.5	0.1	0.5	0.7	0.7	0.1	0.7	0.7	0.1	6.3
Ba	1.8	1.1	48.2	63.1	62.9	8.3	49.9	19.9	38.6	469.5
Hf	ND	ND	0.4	0.3	0.3	ND	0.6	0.3	0.2	2.5
Ta	0.05	0.04	0.4	0.3	0.3	0.2	0.2	0.2	0.2	0.8
Tl	7.7	0.6	0.2	0.6	0.4	0.2	8.4	6.7	0.05	0.4
Pb		393	9421	29867	1463	60			138	110
Bi	2.82	ND	0.23	0.49	ND	ND	7.03	5.49	ND	ND
Th	0.09	0.04	1.1	1	1	0.12	1.2	1	0.2	7.3
U	0.36	0.25	1.6	2.5	2.4	3	1.4	1.3	2.4	3.8
La	1.26	6.4	4.15	7.95	3.06	3.4	2.01	1.86	3.03	2.63
Ce	3.62	16.62	10.28	20.06	8.35	8.68	5.29	5.02	7.95	6.79
Pr	0.47	1.95	1.09	2.06	0.95	0.82	0.63	0.6	0.78	0.84
Nd	1.8	7.49	4.41	7.74	4	3.39	2.53	2.56	3.3	3.62
Sm	0.37	1.76	1.12	1.62	1.04	0.73	0.65	0.64	0.89	0.87
Eu	0.11	0.4	0.3	0.4	0.24	0.17	0.15	0.14	0.18	0.19
Gd	0.48	1.64	1.33	1.99	1.29	1.01	0.71	0.66	0.98	1.02
Tb	0.06	0.19	0.21	0.28	0.19	0.14	0.13	0.12	0.13	0.14
Dy	0.34	1.01	1.16	1.58	1.25	0.71	0.8	0.75	0.8	1.08
Ho	0.1	0.14	0.24	0.31	0.27	0.17	0.17	0.16	0.16	0.22
Er	0.22	0.32	0.7	0.83	0.81	0.43	0.48	0.49	0.39	0.8
Tm	0.03	0.04	0.09	0.11	0.12	0.05	0.07	0.06	0.05	0.14
Yb	0.18	0.27	0.51	0.72	0.67	0.29	0.53	0.41	0.33	0.94
Lu	0.02	0.03	0.07	0.08	0.08	0.04	0.06	0.06	0.04	0.15
SUM REE	9.06	38.26	25.66	45.73	22.32	20.03	14.21	13.53	19.01	19.43
(LA)N	4.00	20.32	13.17	25.24	9.71	10.79	6.38	5.90	9.62	8.35
(LA/LU)N	6.46	21.88	6.08	10.19	3.92	8.72	3.44	3.18	7.77	1.80
EU/EU*	0.81	0.73	0.76	0.69	0.64	0.61	0.68	0.67	0.60	0.62

* mineralized sample

Table 4.3. Summary of Whole Rock Trace Element Geochemistry for Barrem and Mineralized Dolostones, Gays River.

Element	Mineralized Dolostone	Barren Dolostone	
	*(n=6)	GR-91-96	GR-91-125
Li	10.9 ± 3.5	3.9	74
Be	1-2	2	3.6
Sc	4.3 ± 0.4	3.4	9.9
V	9.8 ± 3.7	2.3	79
Cr	9.1 ± 3.5	1.7	66
Cu	52 ± 25	15	30
Zn	29461 ± 13828	1259	241
Rb	12.1 ± 5.4	1.1	99
Sr	104 ± 36	96	103
Y	5.8 ± 1.5	4.1	5.2
Zr	10.9 ± 4.9	3.3	90
Cs	< 1	0.1	6.3
Mo	< 1	0.4	1.4
Ba	42 ± 20	38.3	469
Pb	60 - > 30,000	138	110
Bi	< 1; 2 samples 5-7	ND	ND
Th	< 1	0.2	7.3
U	1-3	3	3.8

ND - not detected
* - average ± 1 σ for samples

mineralized set, and two of these samples also have elevated Bi and Tl. However, the limited data base prevents a more conclusive statement. The Zn and Pb values are elevated in the apparently unmineralized samples (i.e., no Pb or Zn sulphides observed in thin sections), possibly reflecting very fine grained mineralization, but more data is required before this interpretation can be considered more than tentative.

The REE data for the dolostones are given in Table 4.2 and the chondrite-normalized patterns are shown in Figure 4.1. As discussed above, there is reason to believe that sample GR-91-125 is probably contaminated by fine grained detritus of Meguma Group origin and this is further indicated by the elevated abundance and prominent inflection in the chondrite-normalized pattern for the HREE's (e.g., McLellan, 1989). Inflections such as that observed in GR-91-125 are normally attributed to zircon contamination (McLellan, 1989) and the high Zr content of the sample (90 ppm) confirms this. Thus, further interpretation of the REE data excludes the HREE of sample GR-91-125. The ΣREE in the barren dolostone sample GR-91-96 is 19 ppm, there is LREE enrichment and strong fractionation with $(La/Lu)_N$ = 7.7, and a prominent negative Eu anomaly with Eu/Eu* = 0.59-0.62. For the LREE portion of the chondritic plots, the two barren dolostone samples analyzed are remarkably similar.

The REE data for the mineralized dolostone samples (Table 4.2, Fig. 4.1) indicate the following features: (1) generally similar abundances (avg.=23.5 $\pm$ 10.7, n=6) and patterns compared to the barren dolostones; (2) LREE enrichment and strongly fractionated patterns with $(La/Lu)_N$ = 5.9 $\pm$ 2.7; and (3) uniform negative Eu anomalies with Eu/Eu* = 0.66 $\pm$ 0.04. Although there is a larger spread of the data than observed for the two unmineralized dolostone samples, the abundances, patterns and significant ratios (i.e., $(La/Lu)_N$, Eu/Eu*) are generally

similar.

4.2.3 Geochemistry of Carbonate Cement

Major element chemistry of a few selected samples of various carbonates was determined using the electron microprobe. A list of the analyses is given in Table 4.4 with photomicrographs of some of the material analyzed in Figure 4.2 and binary element plots of the chemistry in Figure 4.3. Chemically the data fall into three populations corresponding to the nature of the carbonates: (1) dolomite of either massive, equigranular texture (Fig. 4.2a, b, c) or equant euhedra (Figs. 4.2a, b), (2) calcite cement (Fig. 4.2a, b, c), and (3) anhedral calcite of secondary origin in Meguma Group wackes (Fig. 4.2d). In Figure 4.3a, b it is seen that three groupings are discriminated in terms of their Fe, Mn and Mg contents. The dolomites are characterized by elevated Mg contents (19-24 wt. % MgO) and the 1:1 substitution of Fe and Mn (0-4 wt. % MnO). There is no consistent chemical difference noted for the two texturally distinct dolomites based on the present data set, although the massive type is generally a dirty red-brown colour whereas the euhedral grains are clear. The sparry calcite cement has a much more limited range in terms of Mn (1.5-3 wt. %) compared to the dolomite and is enriched in both Fe and Mn relative to the secondary calcite in Meguma Group lithologies. The analyses reported here confirm the earlier findings of Akande (1982) who reported very similar results for carbonate chemistry.

Trace element data for different calcite types are reported in Table 4.5 and various chemical plots of the data are presented in Figure 4.4. The samples, listed in Table 4.6, have been subdivided into the following 5 types based upon their nature of occurrence: (1) intergrown

TABLE 4.4. Carbonate Geochemistry (EMPA Analyses), Gays River

No.	SPOT	FeO	MgO	MnO	CaO	TOTAL
GR-91-	22	0.62	0.51	2.3	57.86	61.29
13	23	0.84	0.64	2.51	57.94	61.93
dolostone	24	0.68	21.3	0.47	31.11	53.56
	27	0.7	0.71	2.59	58.55	62.55
	28	0.74	1.28	2.81	58.12	62.95
	29	1.15	11.23	1.52	42.96	56.86
	30	0.66	0.67	2.56	57.67	61.56
	31	0.58	1.12	1.52	54.8	58.02
	32	0.16	0.27	0.97	57.84	59.24
	35	0.37	0.34	1.94	58.67	61.32
	36	0.69	0.75	2.5	58.59	62.53
	37	0.39	1.19	2.01	57.75	61.34
	38	2.5	14.01	2.19	38.86	57.56
GR-91-	111	0.38	0.29	1.8	57.11	59.58
6	112	0.27	22.3	0.15	32.66	55.38
dolostone	113	0.46	20.45	0.21	32.38	53.5
	114	1.38	21.26	0.94	31.21	54.79
	115	1.51	20.08	1.51	32.62	55.72
	116	0.23	21.93	0.1	31.92	54.18
GR-91-	85	0.7	0.69	2.56	59.43	63.38
3	86	3.21	18.66	2.83	31.4	56.1
dolostone	87	2.3	17.11	2.22	28.87	50.5
	88	4.09	18.1	4.17	31.68	58.04
	89	3.04	19.67	2.98	31.51	57.2
	90	0.6	0.6	2.4	58.99	62.59
	91	0.6	0.6	2.5	58.52	62.22
	92	2.34	19.46	2.2	32.22	56.22
	93	3.47	19.28	3.27	31.91	57.93
	94	2.87	17.86	2.63	31.15	54.51
	95	2.51	19.24	2.32	29.53	53.6
	96	2.15	19.02	1.87	30.9	53.94
	97	3.43	18.72	3.56	32.12	57.83
	98	1.18	20.96	1.91	31.95	56
	100	0.68	0.58	2.27	58.79	62.32
	101	0.68	0.45	2.32	58.4	61.85
	102	0.48	0.21	2.53	59.82	63.04
	103	0.86	4.31	2.22	53.1	60.49
	104	0.41	0.12	1.67	53.67	55.87
	105	0.65	0.52	1.94	61.87	64.98
	106	4.33	18.01	4.46	31.8	58.6
	107	2.1	20.92	2	32.51	57.53
	108	0.33	23.31	0	32.84	56.48
	109	0.47	21.33	0.25	33.36	55.41
	110	0.64	0.77	2.32	58.85	62.58
GR-91-	64	0.22	0.24	1.34	58.08	59.88
10	65	0.23	0.09	0	59.9	60.22
Meguma	67	0	0.21	0.99	55.75	56.95
Group	70	0.26	0.31	0.88	58.19	59.64
	83	0.17	0.15	1.12	56.45	57.89

TABLE 4.5. Trace Element Geochemistry of Carbonate Cement, Gays River.

Sample #	GR91-22	GR91-32	GR91-32	GR91-48	GR91-48	GR91-39	GR91-82	GR91-6	GR91-34	R91-109
Material	B	B	B	B	B	O	F	Vb	Vb	Vb
Li	ND	0.76	ND	ND	ND	ND	ND	ND	0.22	0.63
Be	0.06	0.05	ND	ND	ND	ND	ND	1.61	5.77	2.52
Sc	1.59	2.3	2.63	1.76	2.45	ND	ND	ND	ND	ND
V	0.14	0.09	ND	ND	0.44	ND	0.28	ND	ND	ND
Cr	13.9	1.57	ND	2.31	4.39	1.68	ND	ND	ND	ND
Cu	3	4.29	3.83	4.19	3.09	5.35	8.18	5.57	3.14	4.24
Zn	16.06	318	328	56.57	27.24	215	87.2	141	39.7	55
Rb	0.098	0.11	ND	ND	ND	ND	ND	0.14	0.09	0.22
Sr	238	196	191	184	184	195	122	209	143	201
Y	66.4	102	98.7	73.8	57.3	18.8	8.48	34.49	50.63	110.9
Zr	ND	0.89	ND	ND	ND	ND	ND	0.48	0.94	0.28
Nb	0.01	0.02	ND	ND	ND	ND	ND	0.66	0.05	0.04
Mo	0.42	0.21	0.13	0.22	0.24	0.29	0.19	0.87	0.57	0.77
Cs	0.02	0.032	ND	ND	0.036	ND	ND	0.05	0.02	0.1
Ba	18.64	33.24	36	13	18.45	883	220	2.21	4.19	397
Hf	0.07	0.05	ND	ND	ND	ND	ND	ND	ND	ND
Ta	0.015	0.01	ND	ND	ND	ND	ND	0.72	0.06	0.04
Tl	0.044	0.26	0.42	ND	ND	0.19	ND	ND	ND	ND
Pb	61.13	660	668	79.8	72.5	525	8.87	21.45	14.68	5.62
Bi	0.33	ND	ND	ND	ND	ND	ND	ND	ND	ND
Th	0.082	0.052	ND	ND	ND	ND	0.12	0.12	0.07	0.29
U	0.021	0.04	0.051	ND	ND	ND	4.59	1.43	ND	ND
La	17.2	19.3	18.65	12.59	8.94	6.75	3.18	16.45	20.48	152.5
Ce	55.79	66.19	64.63	42.34	31.66	17.76	6.36	37.4	51.27	368.8
Pr	6.78	8.18	7.86	4.99	3.78	2.1	0.7	3.92	6.25	38.86
Nd	27.92	34.68	31.48	19.2	14.32	8.87	3.02	15.05	26.31	135.6
Sm	8.26	11.22	10.77	6.35	4.98	2.6	0.87	3.53	8.73	25.61
Eu	2.86	2.72	2.59	1.78	1.53	0.55	0.27	0.83	2.32	6.13
Gd	10.15	14.1	12.76	8.14	6.34	3.06	1.13	3.97	11.1	25.47
Tb	1.92	3.02	2.86	1.94	1.54	0.63	0.16	0.75	1.91	4.12
Dy	13.15	21.38	19.38	14.1	11.38	4.12	1.07	5.4	11.36	27.56
Ho	2.71	4.47	4.04	3.03	2.32	0.87	0.22	1.18	2.09	5.58
Er	7.51	12.5	11.04	8.36	6.5	2.42	0.59	3.49	5.42	16.12
Tm	0.99	1.69	1.5	1.1	0.85	0.32	0.079	0.48	0.63	2.38
Yb	4.49	9.78	8.78	6.24	4.8	1.9	0.39	3.12	3.66	14.99
Lu	0.59	1.15	1.06	0.63	0.52	0.24	0.07	0.37	0.43	1.89
SUM REE	160.32	210.38	197.4	130.79	99.46	52.19	18.109	95.94	151.96	825.61
(LA)N	54.603	61.270	59.206	39.968	28.381	21.429	10.095	52.22	65.02	484.13
(LA/LU)N	2.99	1.72	1.80	2.05	1.76	2.88	4.66	4.56	4.88	8.27
EU/EU*	0.90	0.63	0.64	0.72	0.79	0.56	0.79	0.68	0.73	0.74

O = ore F = fracture Vb = vug barren Vm = vug mineralize ed B = breccia

TABLE 4.5. Carbonate Cement Geochemistry, Continued.

Sample #	GR91-142	R91-146	R91-147	GR91-147	GR91-147	GR91-26	GR91-26	GR91-51	GR91-60	GR91-60
Material	Vb	Vb	Vb	Vb	Vb	Vm	Vm	Vm	Vm	Vm
Li	ND	0.42	ND	0.31	ND	0.4	ND	ND	ND	ND
Be	ND	8.93	2.83	5.52	3.92	2.4	0.039	ND	ND	ND
Sc	ND	2.88	ND	1.66	0.74	ND	0.44	2.45	ND	ND
V	ND	ND	ND	0.61	0.42	ND	0.203	ND	ND	ND
Cr	0.23	ND	ND	2	1.12	ND	1.74	ND	ND	ND
Cu	5.7	9.65	2.44	2.92	2.68	3.55	3.77	4.05	16.6	26.3
Zn	1073	5465	197	210	190	209	322	82.7	53.15	60.45
Rb	ND	0.17	0.03	ND	ND	0.19	0.15	ND	0.24	ND
Sr	172	122	103	100.3	103.2	136	215	178	2992	2646
Y	18.1	12.03	20.48	20.4	20.9	87.77	435	66.8	3.4	2.96
Zr	ND	6.44	1.04	2.28	1.04	0.16	1.97	ND	4.94	6.79
Nb	ND	0.11	0.13	0.19	0.03	0.06	0.01	0.05	0.077	0.04
Mo	0.18	0.45	0.36	0.4	0.4	0.83	0.58	0.3	0.13	ND
Cs	ND	0.01	0	ND	ND	0.08	0.05	ND	0.084	0.17
Ba	7.66	232	84	83.9	82.1	4.3	788	78.2	9768	
Hf	ND	ND	ND	0.29	ND	ND	0.46	ND	ND	ND
Ta	ND	0.03	0.45	0.4	ND	0.1	0.08	0.01	ND	ND
Tl	0.08	ND	ND	ND	ND	ND	0.11	ND	ND	ND
Pb	118	32.72	12.55	2.78	3.23	303	240	53.1	11.26	15.34
Bi	ND	ND	ND	ND	ND	ND	ND	ND	ND	ND
Th	0.64	1.15	1.16	1.29	1.21	0.11	0.11	ND	ND	0.113
U	0.68	8.1	2.7	2.68	2.77	0.01	0.1	ND	0.14	0.114
La	13.08	4.76	15.92	15.66	15.15	26.87	97.9	8.81	2.31	2.31
Ce	27.91	11.75	34.98	34.87	34.36	59.55	252	26.53	4.92	4.58
Pr	2.89	1.39	3.76	3.77	3.72	7.61	34.73	3.39	0.5	0.47
Nd	10.7	5.94	14.52	13.94	13.95	32.05	163.9	15.41	1.83	2.06
Sm	2.33	1.52	3.19	3.04	3.13	9.26	49.3	5.06	0.56	0.52
Eu	0.54	0.37	0.67	0.7	0.67	2.79	14.17	1.6	0.2	0.005
Gd	2.59	1.54	3.47	3.42	3.32	13.46	65.47	7.38	0.69	0.67
Tb	0.47	0.24	0.54	0.52	0.53	2.18	12.85	1.67	0.099	0.09
Dy	2.67	1.61	3.4	3.27	3.31	14.06	87.64	12.75	0.58	0.52
Ho	0.51	0.32	0.67	0.62	0.65	2.92	18.34	2.89	0.1	0.09
Er	1.34	0.85	1.71	1.64	1.71	7.4	53.12	8.97	0.25	0.26
Tm	0.17	0.1	0.2	0.2	0.19	0.85	7.08	1.39	0.038	0.03
Yb	0.93	0.5	1.18	1.07	1.1	4.11	40.95	8.58	0.21	0.16
Lu	0.1	0.08	0.15	0.13	0.14	0.45	4.58	1.01	0.03	0.018
SUM REE	66.23	30.97	84.36	82.85	81.93	183.56	902.03	105.44	12.317	11.783
(LA)N	41.524	15.11	50.54	49.71	48.10	85.30	310.794	27.968	7.333	7.333
(LA/LU)N	13.41	6.10	10.88	12.35	11.10	6.12	2.19	0.89	7.90	13.16
EU/EU*	0.63	0.75	0.62	0.67	0.64	0.77	0.72	0.76	0.93	0.02

TABLE 4.5. Carbonate Cement Geochemistry, Continued

Sample #	GR91-61	GR91-168	GR91-168	GR91-171	GR91-172	GR91-172	GR91-172
Material	Vm	Vm	Vm	Vm	Vm	Vm	Vm
Li	0.41	0.66	0.69	0.43	ND	0.62	0.56
Be	1.39	3.23	1.55	4.24	3.47	3.28	2.76
Sc	ND	1.23	3.6	2.52	ND	1.44	1.24
V	ND	0.72	ND	ND	ND	0.3	0.4
Cr	ND	3.62	ND	ND	ND	2.38	2
Cu	3.49	5.64	5.13	5.09	2.38	2.81	2.73
Zn	23.2	72.5	64.66	345	25.7	27.3	19
Rb	0.26	0.33	0.28	0.16	0.12	0.15	0.14
Sr	3868	272	240	196	228	229	224
Y	3.21	18.9	17.3	10.63	20.83	21.5	20.7
Zr	0.14	0.27	1.34	0.22	0.88	0.18	1.17
Nb	0.05	0.05	0.06	0.04	0.03	0.05	0.03
Mo	0.12	0.24	0.37	0.34	0.39	0.46	0.39
Cs	0.18	0.1	0.11	0.03	0.02	0.03	0.03
Ba	12763	10.5	10.47	40	30.3	30.2	34.4
Hf	ND	ND	ND	ND	ND	ND	0.22
Ta	0.07	ND	0.36	0.03	0.03	ND	ND
Tl	ND	ND	ND	ND	ND	ND	ND
Pb	5.65	16	16.81	2.71	9.13	10.2	10.2
Bi	ND	ND	ND	ND	ND	ND	ND
Th	0.03	0.11	0.35	0.09	0.08	0.08	0.07
U	0.08	0.63	0.67	0.02	ND	ND	ND
La	2.71	40.58	39.71	9.14	5.64	5.68	5.67
Ce	4.41	76.39	76.9	18.18	15.52	15.49	15.45
Pr	0.45	7.87	7.82	1.88	1.98	1.99	2.01
Nd	1.79	27.73	27.4	7.02	8.58	8.23	8.58
Sm	0.44	4.13	4.13	1.75	2.6	2.49	2.53
Eu	0.37	1.03	0.95	0.45	0.56	0.53	0.55
Gd	0.7	3.69	4.25	1.84	2.81	2.87	2.96
Tb	0.08	0.44	0.49	0.25	0.56	0.57	0.57
Dy	0.53	2.77	2.84	1.59	3.84	3.88	4.11
Ho	0.1	0.55	0.53	0.27	0.78	0.83	0.86
Er	0.26	1.54	1.52	0.63	2.48	2.48	2.5
Tm	0.03	0.2	0.21	0.07	0.29	0.32	0.34
Yb	0.26	1.18	1.14	0.38	1.75	1.78	1.87
Lu	0.02	0.15	0.14	0.04	0.19	0.2	0.21
SUM REE	12.15	168.25	168.03	43.49	47.58	47.34	48.21
(LA)N	8.60	128.83	126.06	29.02	17.90	18.03	18.00
(LA/LU)N	13.89	27.74	29.08	23.43	3.04	2.91	2.77
EU/EU*	2.06	0.81	0.70	0.77	0.64	0.61	0.62

TABLE 4.6 Calcite Samples Analyzed for Trace Element Chemistry.

Sample #	Type	Comments
GR-91-22	breccia	cal + gal intergrown; clear
GR-91-32	breccia	cal + gal ± sphal
GR-91-48	breccia	cal + gal + sphal; gal along edge of cal
GR-91-48A	breccia	cal + gal + sphal
GR-91-39	massive ore	cal intergrown with Pb ore
GR-91-82	late stage	clear cal euhedra coating fracture
GR-91-26	mineral. vug	cal + gal in network texture
GR-91-26A	mineral. vug	cal + gal infilling vug
GR-91-60	mineral. vug	cal + gal ± sphal ± py infilling vug
GR-91-61	mineral. vug	cal ± gal
GR-91-51	mineral. vug	cal ± gal; very clear cal
GR-91-168	mineral. vug	cal + gal; cloudy cal, irregular vug
GR-91-171	mineral. vug	cal + gal + sphal; clear cal
GR-91-172	mineral. vug	cal ± gal; clear cal
GR-91-6	barren vug	clear cal
GR-91-34	barren vug	cal in fossil. vug
GR-91-109	barren vug	cal in fossil. vug
GR-91-142	barren vug	clear cal
GR-91-146	barren vug	small clear cal partially infilling vug
GR-91-147	barren vug	infilling vug

abbreviations: cal = calcite, gal = galena, sphal = sphalerite

with massive ore (n=1), in this case a Pb-rich sample; (2) late-stage fracture coating of calcite euhdra (n=1); (3 and 4) sparry calcite either associated (n=8) or unassociated (n=6) with Pb-Zn mineralization. This also includes a sample of vein calcite (GR-91-26); and (5) calcite in the basal breccia (n=3).

The calcites are all characterized by low abundances of most of the trace elements, but enrichment is noted for Sr, Ba, Pb, Zn, Y and the REE. The extreme enrichment of some samples in Sr (to 4000 ppm) is probably related to microinclusions of barite (same samples have elevated Ba contents; see Table 4.5) as Akande and Zentilli (1984) report up to 4.2 wt. % Sr in barite. Comparison of the chemistry of the different calcite types is made by use of extended element plots in Figures 4.4a-f and the following points are noted: (1) the breccia calcites have the most uniform chemistry; (2) there is a relative enrichment of U in unmineralized sparry calcite and the single fracture coating calcite; (3) there may be considerable elemental variation within a single calcite type (e.g., Sr in mineralized sparry calcite); (4) there is a very uniform negative Eu anomaly of about 0.6-0.8 except for one sample of mineralized sparry calcite; and (5) the sparry calcites are generally more fractionated than other calcites (i.e., $(La/Lu)_N$ values higher). The binary element plots (Figs. 4.4g-i) indicate that in general there is not a very strong positive correlation between elements, although a weak correlation is suggested between U and Th. The Zn versus Pb plot (Fig. 4.4h) indicates that significant amounts of Pb and Zn mineralization, presumeably as microinclusions, occur in the calcite since the material analyzed was considered to be essentially free of sulphide grains. The Pb:Zn ratio indicates that, except for a single sample, Pb is favoured over Zn as an impurity which is consistent with petrographic observations that galena overlaps more the growth of sparry calcite.

The chondrite-normalized REE plots for the various calcite types are shown in Figure 4.5 and some of the data are also summarized in Figures 4.4d, e and f. The most notable feature of the data is the considerable variability given that the same mineral has been analyzed, albeit from different paragenetic stages, and that carbonate is unable to fractionate the REE (Graf, 1983). However, the common feature of the data is that except for one sample (GR-91-61) all the calcites have a negative Eu anomaly of about 0.6-0.9 (Fig. 4.4e). Examining the data more specifically, the following features are emphasized: (1) the breccia calcites have the same slightly fractionated chondritic pattern with $(La/Lu)_N = 2 \pm 0.4$, absolute abundance (159 ± 41 ppm) and positive Ce anomaly. It is perhaps important to further note that the Ce anomaly is unique to this type of calcite based on the present data set, while only three other calcite samples from the deposit have a similarly unfractionated pattern (GR-91-26A, 39, 51); (2) for the barren, sparry calcites the chondritic patterns are broadly similar with $(La/Lu)_N$ varying from 4 to 13, whereas there is a large range in the absolute abundance of the REE (30 to 825 ppm); (3) for the mineralized sparry calcite the greatest variation is observed for a group with a broad range in degree of fractionation with $(La/Lu)_N = 0.9$ to 29, $\Sigma REE = 12$ to 902 ppm and for one sample a positive Eu anomaly ($Eu/EU^* = 2.06$); (4) the calcite associated with the massive ore has a chondrite pattern broadly similar to that of the breccia calcite although relatively depleted; and (5) the late-stage calcite is similar to some of the mineralized sparry calcite (GR-91-60, 61) in terms of fractionation and abundance.

There are several calcite samples that come from the same drill hole and within a few metres of each other, thus these samples permit examination of variability on a local scale. For example, samples GR-91-142, 146 and 147, all barren calcite cements from within 4 metres of

each other, have similar chondrite-normalized REE patterns and only minor variations in ΣREE. Similarly, samples GR-91-60 and 61, mineralizaed calcite cements, have identical chondrite-nrormalized patterns although their Eu/Eu* values are different. However, samples GR-91-168, 171 and 172, representing mineralized calcite cements, come from within a few metres of each other and yet they have different degrees of fractionation, ΣREE and Eu/Eu*. Samples GR-91-26 and 26A, both mineralized calcite cements, have similar REE chondrite-normalized REE patterns and Eu/Eu*, but quite different ΣREE. Thus, there is considerable variability for the calcite cements regardless of proximity of samples.

4.2.4 Geochemistry of the Ore Minerals

Results of microanalysis of sphalerite are summarized in Table 4.7 and Figures 4.6 and 4.7. There is no consistent chemical difference between the fine grained sphalerite that occurs either in the massive ore or as disseminations within low-grade ore or sub-ore material. Similarly, the fine and coarse (i.e., mm-size euhedral grains) sphalerite have the same chemistry as summarized in the histograms for Fe, Ge and Cd (Fig. 4.6). In general, the sphalerite is Fe poor with <<1 mole% FeS and contains trace amounts of Ge (to 0.6 wt.%), Cd (to 0.6 wt. %) and As (to 0.3 wt. %). A series of binary element plots summarize all the chemical data (Fig. 4.7), but there appears to be very little to note concerning the data with cluster patterns apparent. This contrasts with the good interelement correlations (e.g., Cd versus Fe) found by More et al. (1991) for the chemistry of banded sphalerite from the North Penine Orefield in England. In addition to the results shown, trace amounts of Cu and Mn (to 0.2 and 0.1 wt. %, respectively) were noted in a few analyses of the Gays River material. These data confirm the earlier results

TABLE 4.7. Sphalerite Geochemistry (EMPA Analyses), Gays River.

No.	SPOT	ZN	CU	FE	AS	S	NI	GE	CD	TOTAL
GR-91-	1	67.23		0.27	0.19	32.6		0.38	0.24	100.91
117	2	66.92		0.21	0.13	32.82	0.17	0.46	0.25	100.96
	3	67.35			0.25	32.4		0.36		100.36
	4	67.92	0.19	0.17	0.21	32.53		0.24		101.26
	5	67.36		0.51	0.11	32.74		0.33	0.28	101.33
	6	65.94		0.57	0.17	32.62		0.29	0.39	99.98
	7	67.22		0.43	0.21	32.87		0.39	0.25	101.37
	8	66.36		0.47	0.1	32.58	0.11	0.43	0.18	100.23
	9	67.21		0.54		32.62		0.36	0.21	100.94
	10	64.17		0.51	0.15	32.07	0.13	0.39		97.42
	11	67.16		0.27	0.15	32.86		0.46	0.25	101.15
	12	67.73			0.36	32.35		0.41	0.19	101.04
	12A	67.07		0.23	0.18	32.7		0.28	0.24	100.7
	13	66.99			0.27	32.86		0.58		100.7
	14	67.5		0.36	0.16	32.91	0.1	0.34	0.19	101.56
	15	66.35		0.52	0.12	32.77			0.36	100.12
	16	67.82		0.62	0.2	32.79		0.43	0.39	102.25
	17	67.03		0.53	0.16	32.58		0.17	0.34	100.81
	18	67.17		0.51	0.16	32.78		0.33	0.21	101.16
	19	67.86		0.44	0.23	32.71		0.31	0.2	101.75
	20	67.33		0.43	0.23	32.79	0.16	0.2	0.17	101.31
	21	67.41		0.34	0.13	32.64		0.29		100.81
	22	66.63		0.28		32.63		0.18	0.21	99.93
	23	66.61		0.5	0.28	32.91		0.3	0.36	100.96
GR-91-	24	66.61		0.38	0.16	32.74	0.09	0.31		100.29
108	25	67.33		0.26	0.19	33.42	0.11	0.23	0.26	101.8
	26	66.11		0.29		32.59			0.21	99.2
	26A	64.86		0.8	0.19	32.54		0.21	0.25	98.85
	27	66.68		0.31	0.13	32.59			0.2	99.91
	28	66.04		0.25	0.17	32.77	0.1		0.26	99.59
	29	65.39		0.35	0.15	32.51		0.17	0.15	98.72
	30	67.39		0.14	0.3	32.63		0.36	0.23	101.05
	31	65.88		0.52	0.12	32.53		0.3	0.32	99.67
	32	66.54		0.69	0.25	32.68		0.31	0.38	100.85
GR-91-	33	66.45		0.55	0.16	32.86			0.39	100.41
54	34	66.22		0.31	0.15	33.2		0.27	0.49	100.64
	35	67.39		0.33	0.24	32.99		0.35	0.34	101.64
	36	66.82		0.48	0.18	32.54	0.1		0.53	100.65
	37	67.03		0.3	0.26	33.05	0.11	0.52	0.47	101.74
	39	66.72		0.33	0.19	32.95	0.13	0.29	0.46	101.07
	40	65.91		0.3	0.2	32.97		0.38	0.4	100.16
GR-91-	41	67.44		0.16	0.19	32.79		0.46	0.15	101.19
F	42	66.94		0.16	0.15	33.36		0.24	0.16	101.01

TABLE 4.7. Continued

No.	SPOT	ZN	CU	FE	AS	S	NI	GE	CD	TOTAL
	43	65.81		0.2	0.14	32.74	0.12	0.35		99.36
	44	66.82		0.22	0.16	32.57	0.11	0.2	0.15	100.23
	45	64.92		0.08	0.22	32.06		0.18		97.46
	46	67.31			0.22	32.83		0.37	0.48	101.21
GR-91-	47	65.37		0.19	0.19	32.78		0.34	0.13	99
6	49	65.39		0.46	0.14	33.18			0.32	99.49
	50	65.95			0.17	32.74		0.54	0.21	99.61
	51	64.83		0.56		33.1			0.2	98.69
	52	65.53		0.65	0.26	32.93		0.21	0.43	100.01
GR-91-	53	66.03		0.39	0.2	32.49		0.27	0.48	99.86
4	54	65.7		0.39	0.13	32.64		0.4	0.41	99.67
	55	65.3		0.39	0.18	32.52		0.18	0.48	99.05
	56	66.25		0.48	0.13	32.56				99.42
	57	66.32		0.26		32.5		0.23	0.24	99.55
	58	66.64			0.1	33.45		0.18	0.44	100.81
	59	65.18		0.17	0.13	32.29	0.15		0.28	98.2

of Akande (1982) who determined the Zn, Fe and S content of sphalerites with the electron microprobe and trace element contents (ppm) using wet chemical techniques [Cu (6-112), Cd, Co (14-62), Ni (<1-41), Ag (<2), Mn (350-3095), V (5-20), Sn (8-25)].

Analyses of galena are give in Table 4.8 for both massive and disseminated styles of mineralization. The analyses conform to nearly pure PbS with <0.1-0.3 wt.% combined impurities, mainly Ge, Mn, As and Zn. Of the impurities, Ge is the only element consistently detected in the galena at 0.1-0.2 wt.%.

Chemistry of the Fe and Cu sulphide phases have not yet been obtained and results will therefore be reported at a later data.

4.3 DISCUSSION

The geochemical data presented above permit some interpretation to be made with respect to the nature of the fluids responsible for the depostion of the ore minerals and the calcites. With respect to the ore, the most intriguing feature is the relative enrichment in Pb and Zn to the exclusion of most other elements, particularly Ag, in this deposit. Whereas there frequently occurs additional, and sometimes significant, amounts of other elements in the MVT deposits (Cu, F, Ba, Co, V), the Gays River deposit is characterized by the relative purity of the ore. As noted above, the only significant enrichment in the whole rocks is noted for Cd (to 2600 ppm), whereas sphalerite contains up to 0.5 wt.% Ge and Cd (electron microprobe analyses).

The analyses of the whole rocks for REE contents indicates that the massive ore is characterized by both a similar chondritic pattern and absolute enrichment as the dolostone, both barren and mineralized. This strongly suggests that the massive ore inherited the REE signature

TABLE 4.8. Geochemistry of Galena (EMPA Analyses), Gays River.

No.	SPOT	GRAIN	ZN	AS	S	MN	GE	PB	TOTAL
GR-91-	1	1	0.44		13.7		0.09	85.75	99.98
164	2	2		0.08	13.21		0.11	86.25	99.65
dolostone	3	3			13.57		0.17	86.17	99.91
	4	4		0.07	13.55			85.4	99.02
	5	5			13.34		0.21	86.05	99.6
	6	6			13.95		0.2	86.62	100.77
	7	7			13.38	0.17		86.25	99.8
	8	8			13.41		0.09	86.79	100.29
	9	9			13.32		0.16	85.92	99.4
	10	9		0.97	12.31	0.15	1.07	80.64	95.14
	11	9	0.27	0.11	13.5	0.21		86.75	100.84
	12	9		0.07	13.34	0.09		86.32	99.82
	13	9			13.77			86.74	100.51
GR-91-	14	1		0.2	13.22		0.18	86.36	99.96
84A	15	1			13.48		0.12	86.18	99.78
dolostone	16	2			13.51		0.21	86.78	100.5
	17	2		0.12	13.22		0.22	86.58	100.14
	18	2	0.35		13.63		0.18	86.38	100.54
	19	3		0.13	13.44		0.13	86.97	100.67
	20	3		0.11	13.25		0.16	86.97	100.49
	21	3		0.14	13.41		0.16	86.04	99.75
GR-91-	22	1			13.47		0.11	86.15	99.73
F	23	1		0.08	13.57			85.33	98.98
massive	24	1		0.1	13.48	0.12	0.21	86.64	100.55
ore	25	2			13.28			85.61	98.89
	26	3		0.11	13.34		0.13	86.22	99.8
	27	4			13.37			86.87	100.24
	28	5			13.37		0.16	85.96	99.49
	49	6		0.45	12.91		0.29	86.49	100.14
	50	7		0.11	13.63		0.23	86.28	100.25
	51	8			13.36		0.13	86.31	99.8
GR-91	29	1			13.62		0.19	86.09	99.9
54	30	1			13.24	0.1	0.1	86.03	99.47
dolostone	31	2			13.5		0.27	85.49	99.26
	33	2		0.13	13.46			85.65	99.24
	34	3			13.41			85.64	99.05
GR-91-	36	1		0.11	13.32	0.11	0.13	85.9	99.57
32	37	1			13.22		0.14	85.48	98.84
breccia	38	2		0.1	13.31		0.23	85.59	99.23
	39	3			13.07		0.13	85.49	98.69
GR-91-	40	1			13.33		0.1	85.22	98.65
26A	41	2	0.3	0.1	13.25		0.12	85.79	99.56
dolostone	42	3			13.23		0.25	86.35	99.83
	43	3			13.07		0.11	86.43	99.61
	44	4			13.53		0.11	86.5	100.14
GR-91-	45	1			13.13		0.17	86.7	100
26B	46	2			13.49		0.16	85.62	99.27
massive	47	3		0.12	13.27		0.18	86.24	99.81
ore	48	4			13.65			86.64	100.29
GR-91-	52	1			13.39		0.18	86.17	99.74
4	53	1			13.99		0.22	86.63	100.84
massive	54	2			13.48			85.68	99.16
ore	55	2		0.15	13.44		0.2	86.17	99.96
GR-91-	56	1		0.1	13.24			86.04	99.38
G	57	1			13.35		0.22	85.76	99.33
massive	58	2			13.31	0.09		84.54	97.94
ore	59	2			13.59		0.12	85.91	99.62
	60	2			13.53			86.71	100.24

of the dolostone rock during constant volume replacement.

Mineral chemistry of the different types of carbonate within the deposit (i.e., different host rock, mode of occurrence) indicates that the major element chemistry is strongly dependent on the type of occurrence. For example, in terms of Fe and Mn three populations are easily discriminated (Fig. 4.3) corresponding to dolostone, vug infill calcite and breccia-hosted calcite. Thus, local environments were important in controlling the chemistry with respect to these elements. However, in terms of some trace elements analyzed there may be considerable variation even within a population or single mode of occurrence. These variations, while attributable to microinclusions as contaminants (e.g., barite), must reflect some variations in either the physio-chemical conditions of formation or the source reservoirs for the fluids.

A detailed study of the REE chemistry of the calcites indicates a similar scenario as noted for the trace elements. For example, for a single population such as ore-stage calcite cement there is considerable variation in terms of the absolute abundance of the REE's and their chondritic patterns. In contrast, the several samples analyzed from breccia-type mineralization (i.e., hosted by basal breccia) indicate similar patterns and abundances. The REE's are particularly informative about source reservoirs because calcites are incapable of fractionating these elements and, therefore, are frequently used as tracers in MVT type deposits (e.g., Graf, 1983, 1984; Grant and Bliss, 1983). In the case of the Gays River deposit the following points are therefore noted: (1) the range in both abundance and patterns indicates different reservoirs for the REE's; (2) the prominent Ce anonmaly in calcites from the breccia ore suggest inheritance of this pattern from a distinctly different reservoir than indicated from the other calcite samples. Rocks having a positive Ce anomaly are rare, the best example being Mn nodules (Fleet, 1983).

Thus, for the breccia-hosted calcites a unique reservoir or set of conditions is required to account for their REE patterns; and (3) the negative Eu anomaly in most of the calcites indicates that in general oxidizing conditions prevailed within the deposit environment. In addition, comparison of the REE paterns with those of the immediate country rocks indicates that simple inheritance from the local wall rocks (psammites, carbonates) cannot adequately explain the observed patterns.

In order to interpret the calcite REE data more fully a variogram plot adopted from Moller et al. (1979) is shown in Figure 4.8. This diagram was designed to discriminate between the REE patterns of carbonates which originate from different processess (i.e., assimilation, fractionation, remobilization) and is based on the principle that the LREE and HREE are partitioned differently into CO2-bearing fluids (i.e., the transporting complex of the REE's). For example, there is a clear trend in the data showing that Yb/La increases with Yb/Ca and parallels the trend established for fractionation dominant processes, thus excluding either assimilation or remobilization as being the dominant processes. Thus, the REE data suggest that a local reservoir for the REE's via remobilization is unlikely to explain the calcite chemistry. Instead, an exotic source of either single or mutiple reservoirs is required. Once the fluid is in the ore environment precipitation of calcite occurs such that there is a constant trend established with respect to the Yb/Ca versus Yb/La plot.

Fig. 4.1. Chondrite-normalized REE plots for whole rock samples of dolostone (barren and mineralized) and massive ore samples from Gays River.

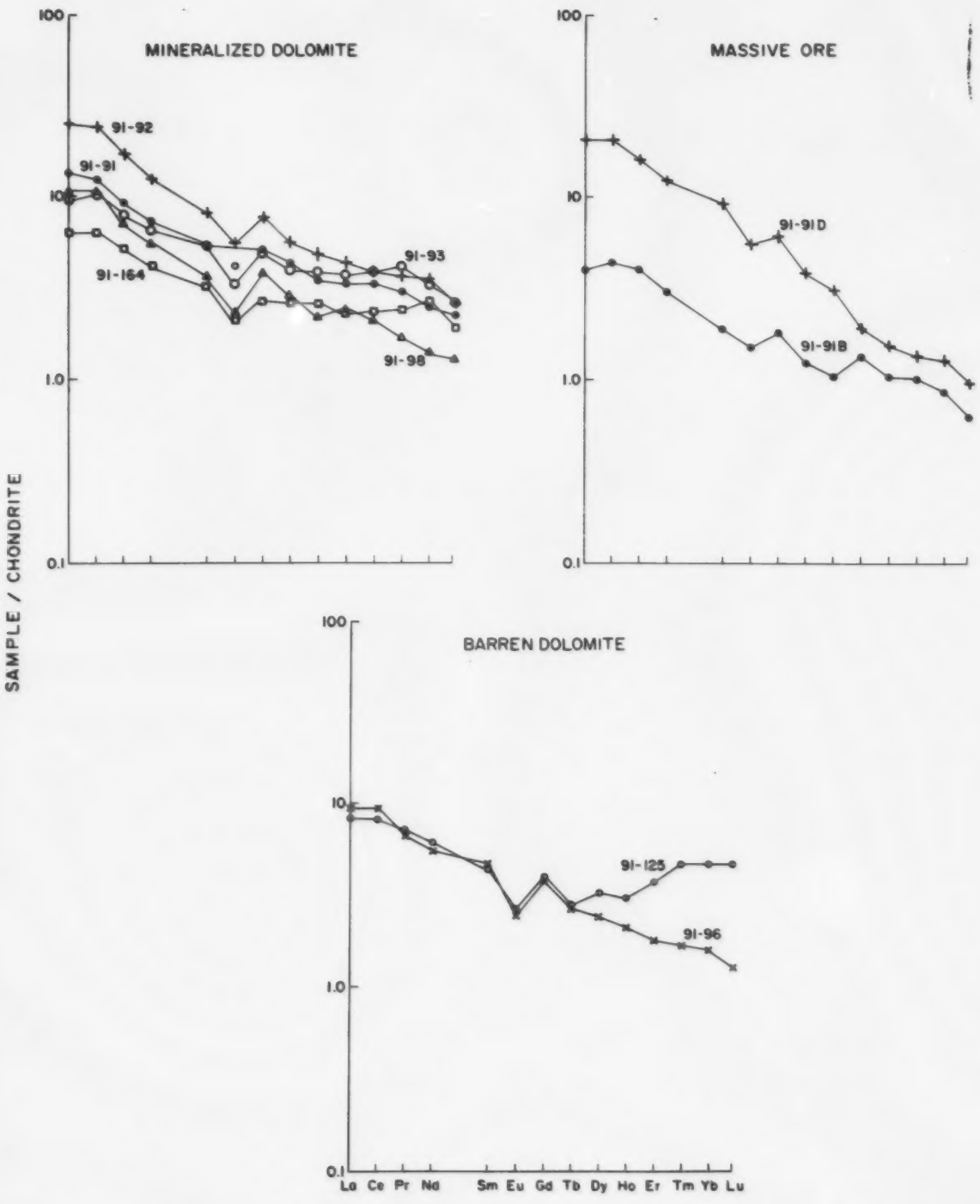

Fig. 4.2. Photomicrographs (plane polarized transmitted light except Fig. 4.2d which is crossed Nicols; field of view is 2.6 mm in all photos) indicating the location of electron microprobe spot analyses of carbonate minerals (see Table 4.4 for list of data). (a, b) Sample GR-91-3 showing red-brown dolostone with pore space infilled with clear, euhedral dolomite and coarse, sparry calcite. Note the lighter color of the dolostone as one approaches the calcite cement (lower right of b and the abundant fluid inlcusions in a). A few sphalertie euhedra are present in (b). (c) Sample GR-91-6 showing calcite veinlet bordered by dolomite euhedra and cemented by coarse calcite. Note the light color of the dolostone host. (d) Sample of Meguma Group psammite (GR-91-10) with disseminated calcite (crossed Nicols). Note that points 68 and 69 are muscovite analyses and point 71 a biotite analysis.

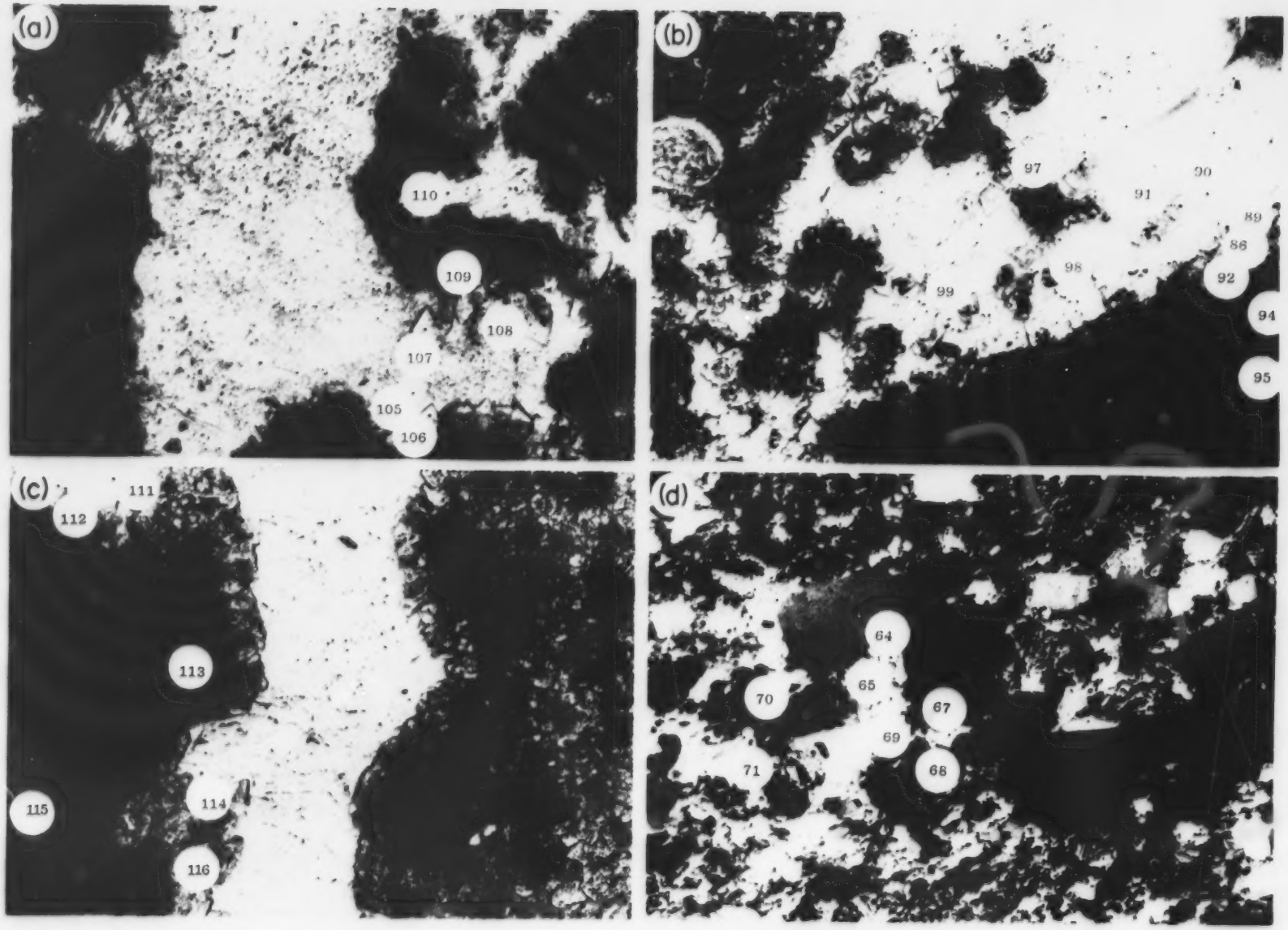
(a)
110
109
108
107
105
106
(b)
97
90
91
89
86
98
92
99
94
95
(c)
111
112
113
115
114
116
(d)
64
65
70
67
69
71
68

Fig. 4.3. Binary element plots (wt. % in all cases) of electron microprobe data for carbonates from different host rocks at Gays River. (a) FeO versus MnO showing dolomite corresponds to a 1:1 exchange mechanism. (b) MnO versus MgO. (c) CaO versus MgO. (d) FeO versus MgO. Note that in Figures 4.3c and 4.3d the fields for vug calcite and Meguma Group-hosted calcite overlap.

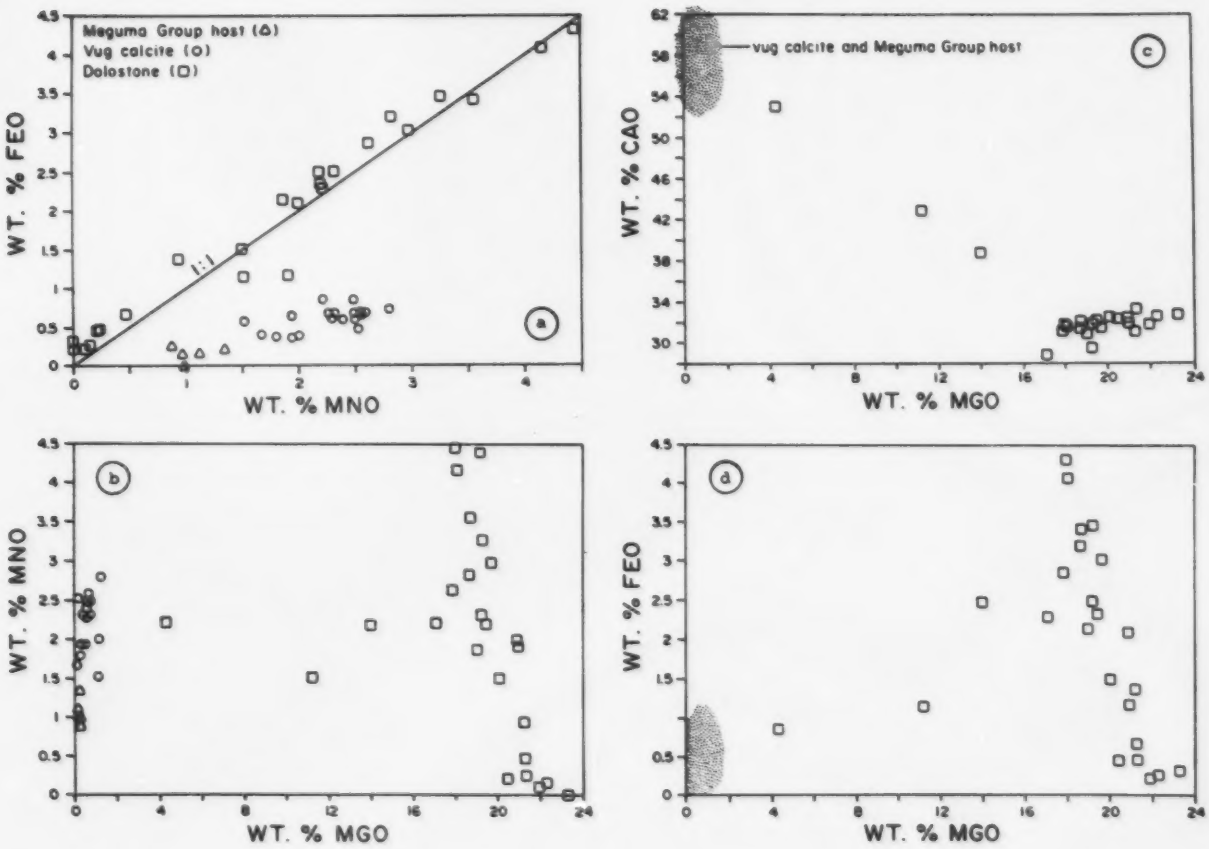

Fig. 4.4. Single element and binary element diagrams summarizing the trace element data (in ppm) for calcite cements from Gays River.

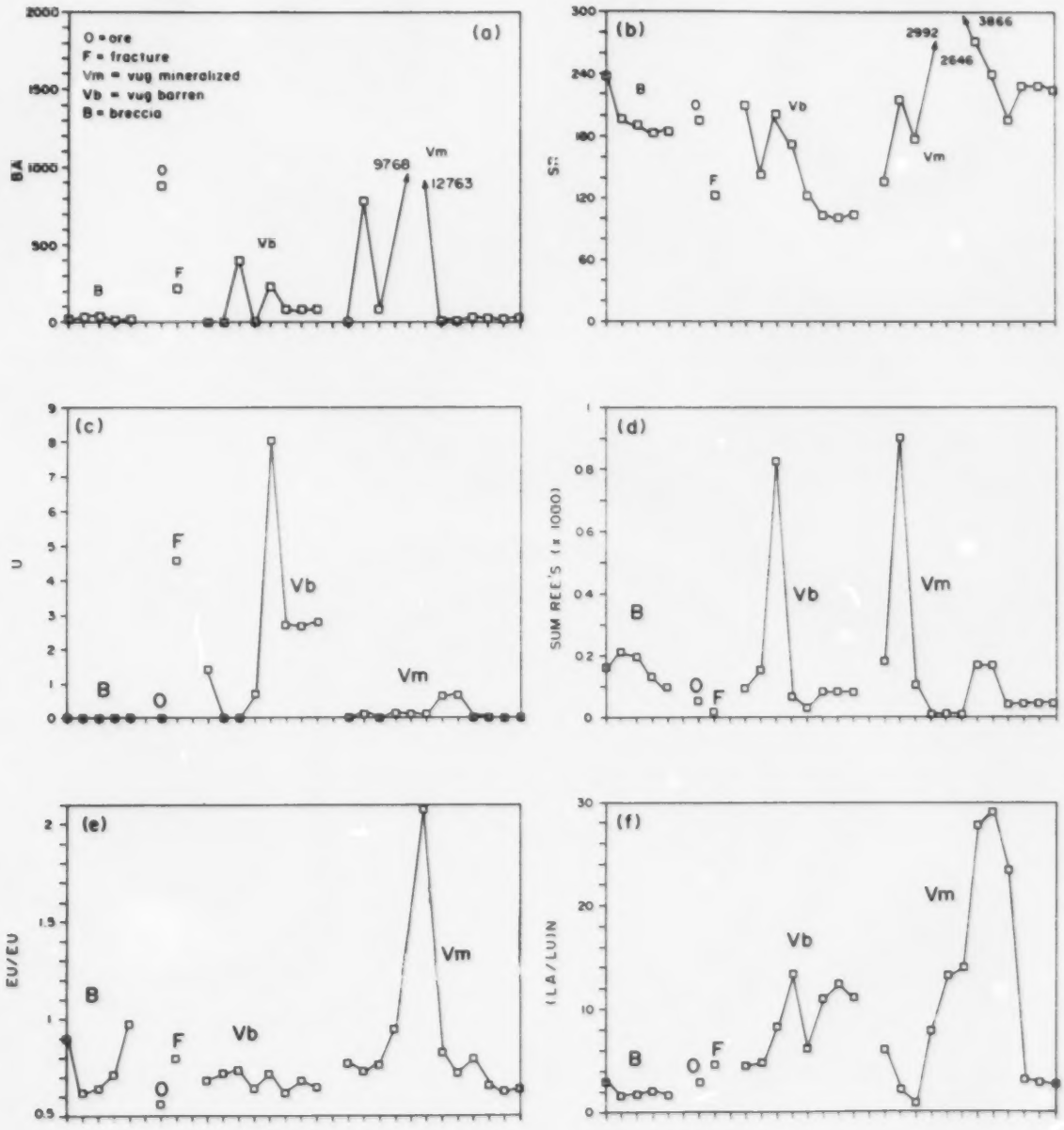

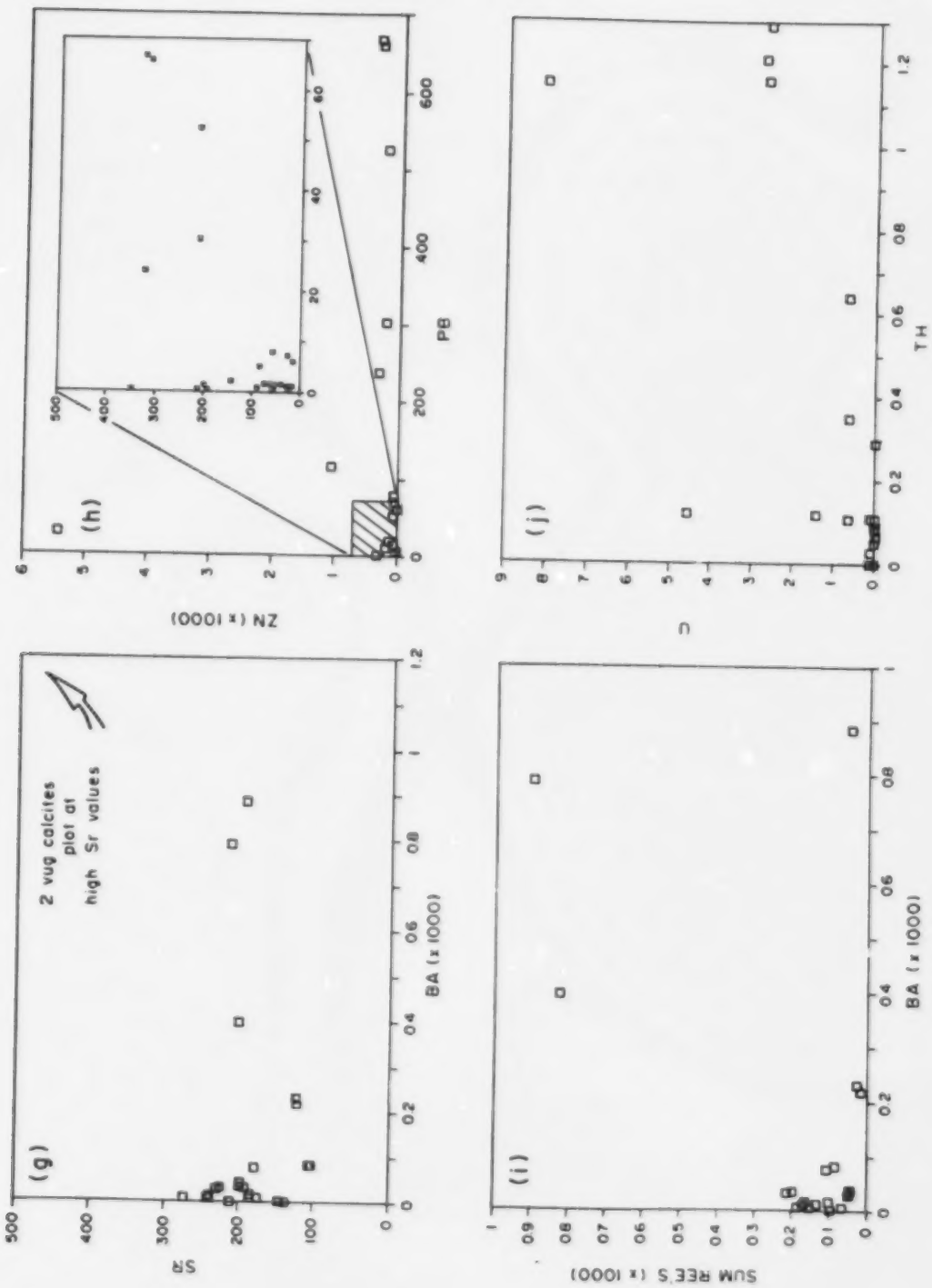
(g)
2 vug calcites plot at high Sr values
SR
BA (x 1000)
(h)
ZN (x 1000)
PB
(i)
SUM REES (x 1000)
BA (x 1000)
(j)
U
TH

Fig. 4.5. Chondrite-normalized REE plots for calcites of different paragenesis at Gays River. Note the large diversity in the degree of fractionation, ΣREE and Eu anomalies. Note that the following samples are averages of several analyses: GR-91-60 (n=2), GR-91-172 (n=3), GR-91-147 (n=3).

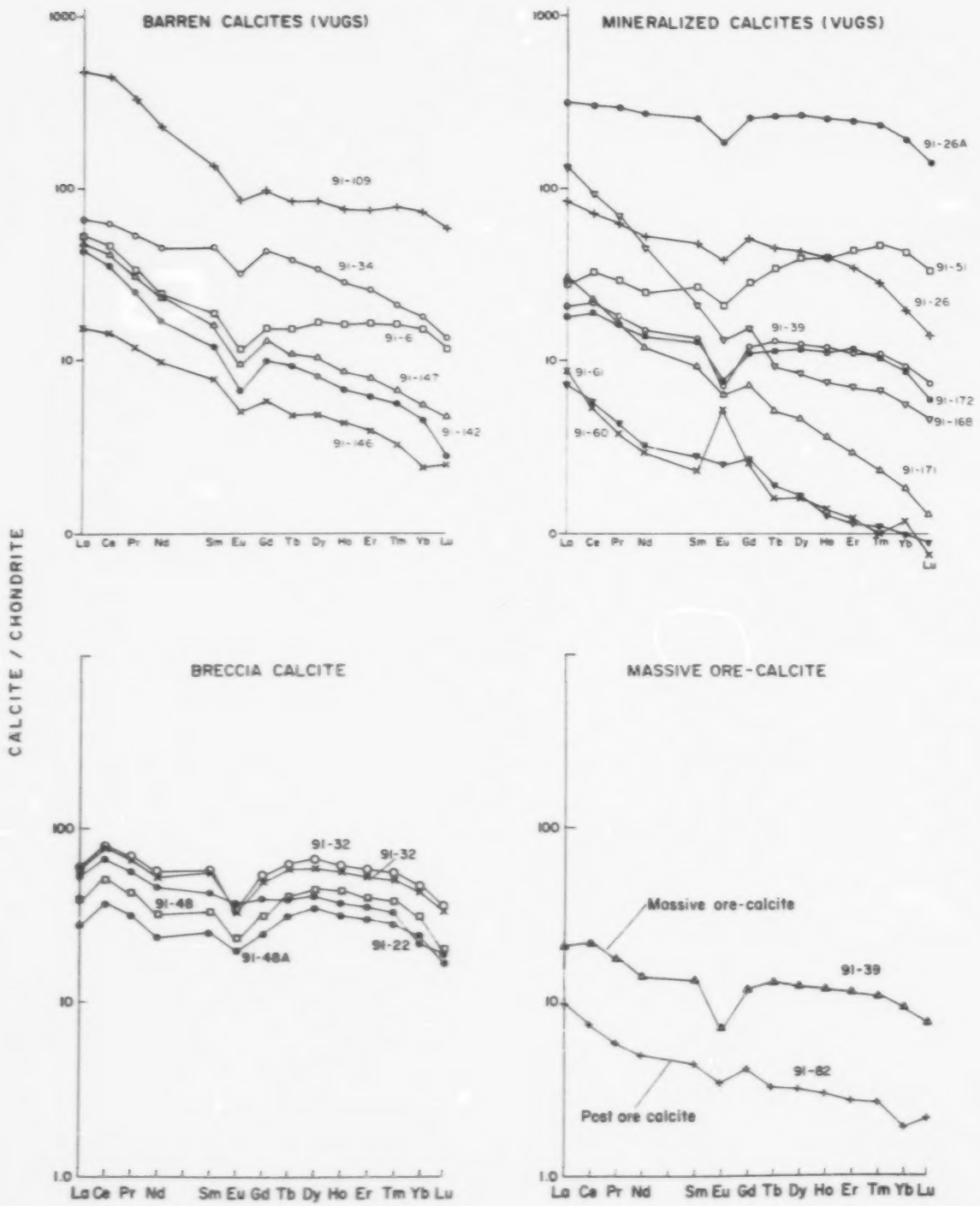

Fig. 4.6. Histogram plots of electron microprobe data (Fe, Cd, Ge in wt. %) for sphalerite in massive and disseminated ore from Gays River. The detection limit for the electron microprobe is indicated and the range of results reported by Akande (1982) as determined from wet chemical analyses of sphalerite separates.

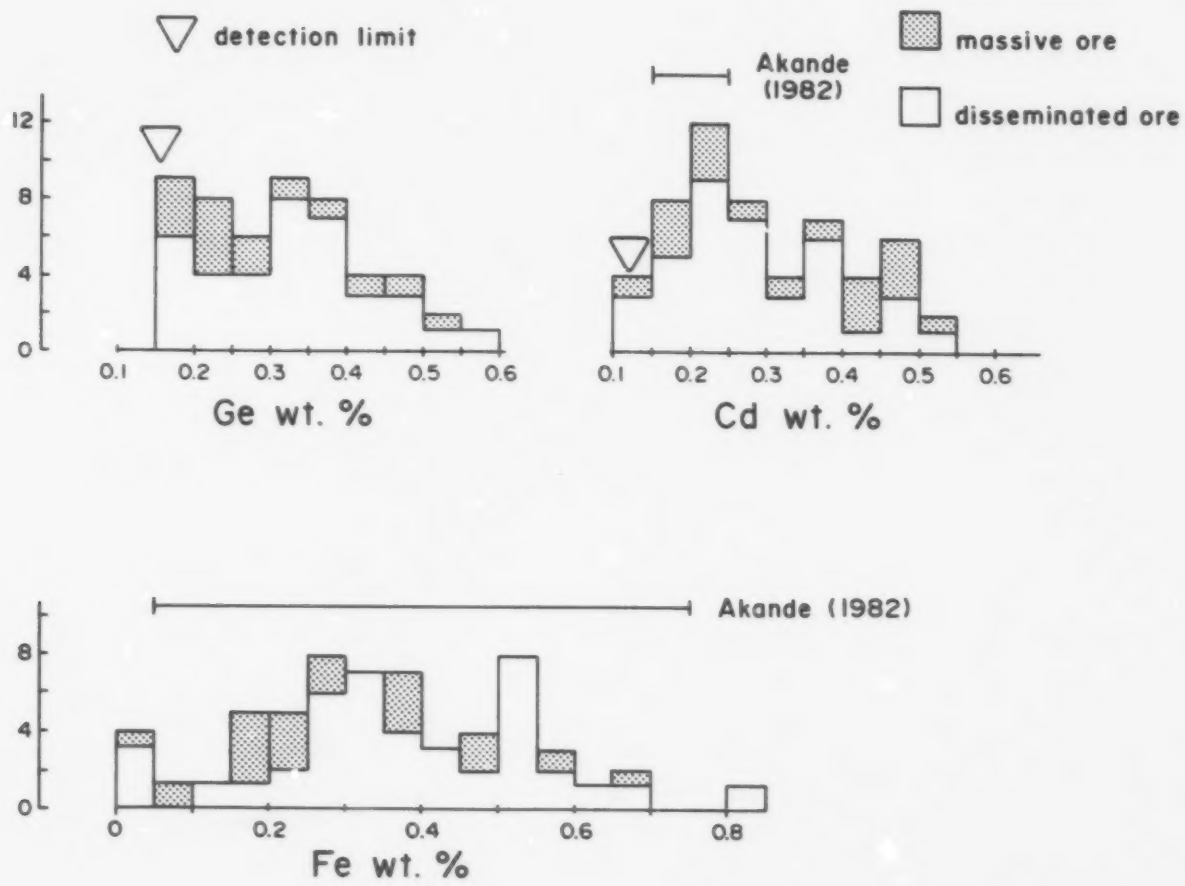

Fig. 4.7. Binary element diagrams for sphalerite (electron microprobe data) in massive and disseminated ore from Gays River.

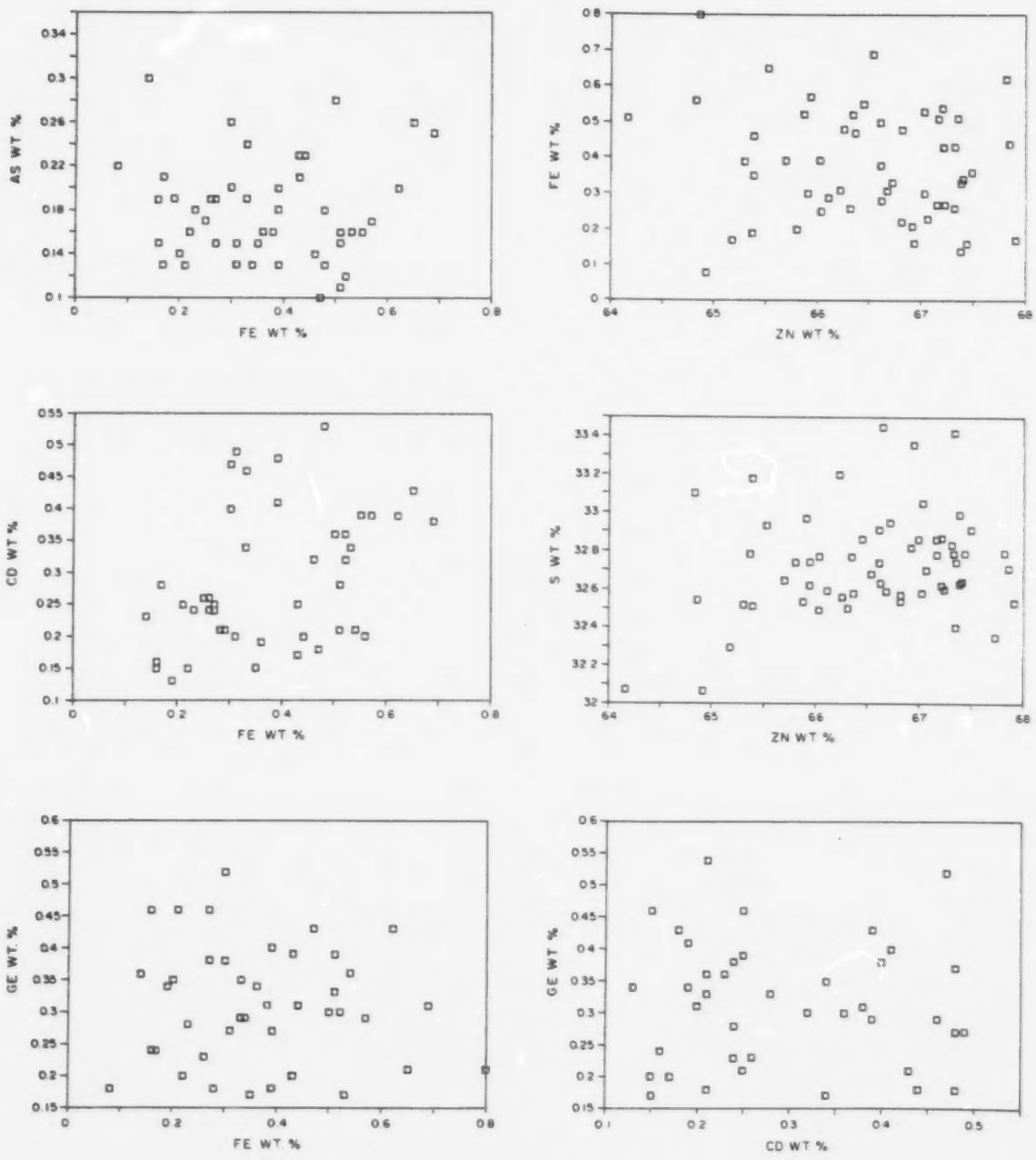

Fig. 4.8. Variogram plot (after Möller et al., 1979) showing the variation of Yb/Ca versus Yb/La for calcite from Gays River (note that the bottom diagram is an enlargement of the top one). Inset in the top diagram shows the distribution that would result if the REE were concentrated due to the various mechanisms indicated. Data for Gays River calcites suggest that the most important process was fractionation (i.e., precipitation of calcite from the fluid).

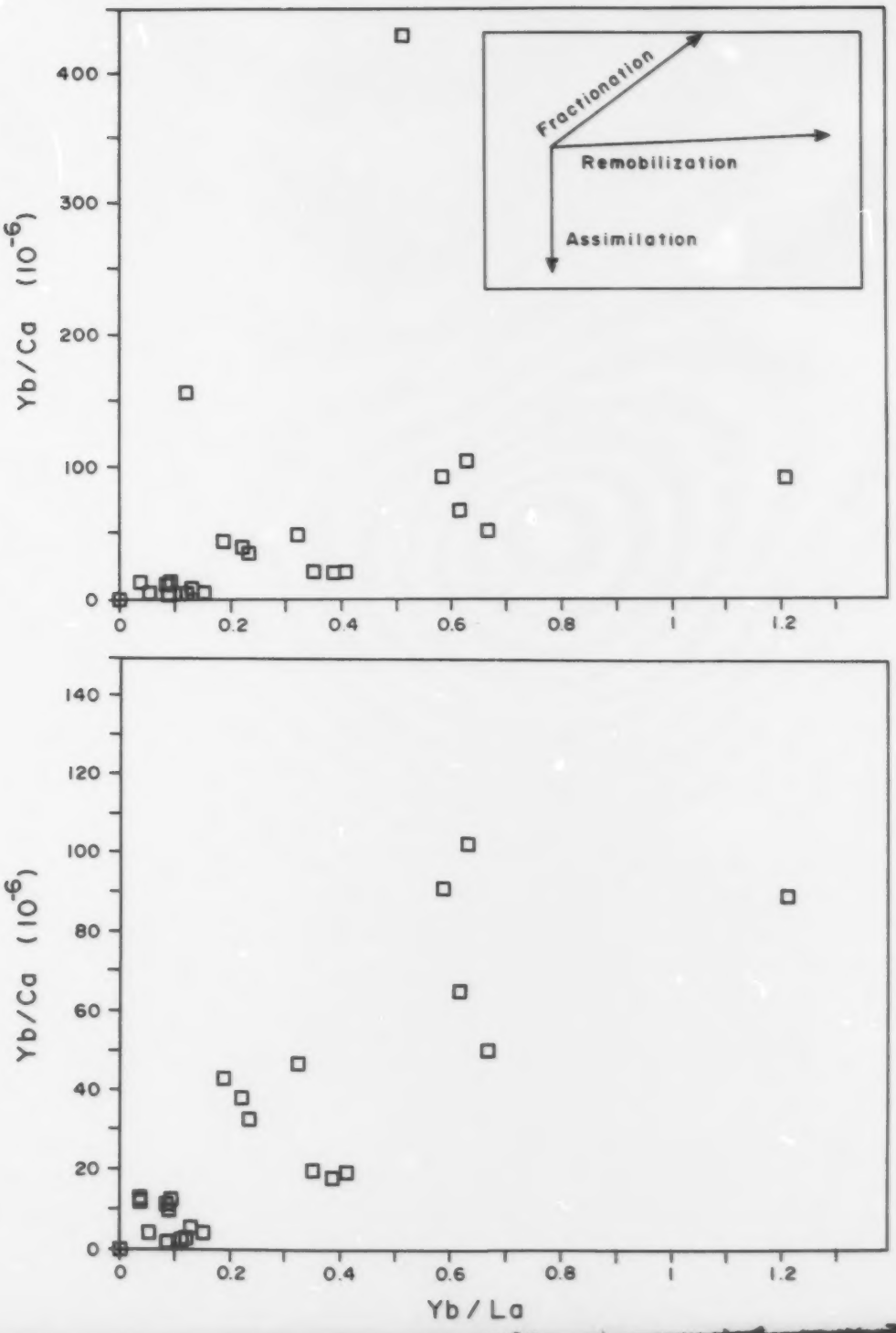

CHAPTER 5

FLUID INCLUSION STUDIES

5.0 INTRODUCTION

Fluid inclusions provide the only direct information on the physio-chemical conditions of the fluids attending mineralization at Gays River. Previous work on fluid inclusions at the deposit area has been reported by Akande (1982; also in Akande and Zentilli, 1983, 1984) and Ravenhurst et al. (1989). Neither of these studies was exhaustive, however, they provided a sound basis from which this study was able to progress from. This initial work indicated that both high temperatures (i.e., >200°C) and salinities (>20 wt. % equivalent NaCl) characterize the early stage fluid responsible for Pb-Zn mineralization with an incursion of cooler fluids, but still of high salinity, during the later, barren stages (i.e., calcite, fluorite, barite stage). The high temperatures noted by the above authors for the Gays River deposit contrast with the generally lower temperatures reported for MVT deposits (e.g., Anderson, 1982; Roedder, 1968, 1984; Sangster and Carriere, 1991). However, the high temperatures for Gays River are not unique as similarly high temperatures have been noted at the Gayna River (156-231°C; Carriere and Sangster, 1992) and Nanisivik (165-210°C; Arne et al., 1991) MVT deposits. The purpose of this fluid inclusion study was, therefore, to: (1) resolve the nature of the apparently high-termperature mineralizing fluids and fit them into the context of the mineral deposit; (2) determine the full extent of the fluid history including pre-, syn- and post-mineralizing fluids; (3) and compare the fluid inclusion data to the fluids related to dolomitization of the carbonate rocks (Savard, 1992).

5.1 FLUID INCLUSION PETROGRAPHY

In this section the nature of the fluid inclusions as observed at room temperature (i.e., 20-25°C) and viewed with a petrographic microscope are described. For details concerning the classification, recognition and general feautures of fluid inclusions the reader is referred to the authoritative text of Roedder (1984). Material examined for fluid inclusions included sphalerite, calcite, fluorite and detrital quartz (in Meguma Group clasts in the basal breccia).

5.1.1 Sphalerite

The sphalerite at Gays River is not a good host for fluid inclusions, as noted by Akande (1982), and it is an onerous task trying to get suitable material. Three morphological types of sphalerite were examined as potential host material for fluid inclusions. (1) Vug-infill or cementation sphalerite which occurs as small (<1-2 mm) euhedra lining cavity walls. This type of sphalerite is generally lost during sample preparation due to vibration from the saw blade combined with the delicate nature of the crystals. However, where suitable sections were successfully prepared for fluid inclusion study, the material was generally barren of inclusions. (2) The massive Zn-rich ore examined is barren of fluid inclusions even though numerous samples were prepared and examined specifically for inclusions. This includes areas in the ore where there was coarsening of the sphalerite (mm size). (3) Sphalerite infilling irregurlar-shaped vugs or occurring as vein-like material (Fig. 5.1a, b) is the best host for fluid inclusions. This material contrasts with type 1 above in that it is generally not euhedral, but occurs as anhedral, massive material of yellow to reddish-orange colour. Unforturately this material was difficult to cut into suitable fluid inclusion chips since it would dislodge due to vibrations during sawing.

Consequently, whole-rock material was comminuted (-35 to +60 mesh) and sphalerite grains hand picked and subsequently mounted in cold epoxy and ground down. The slides produced contained 50-100 sphalerite grains and about 20-50% of the grains contained fluid inclusions (Figs. 5.1, 5.2). The following description of the fluid inclusions refers specifically to the type 3 occurrence.

The fluid inclusions cannot be related to any growth feature in the sphalerite (Figs. 5.1, 5.2) and, therefore, they are cautiously treated as being of secondary origin although it is quite possible that they are pseudosecondary. Inclusions range in size from <5μ to >50μ, with 10-15μ size inclusions the best to work with due to darkening of the smaller inclusions. Inclusions occur as clusters (e.g., Fig. 5.1b), single isolated inclusions (rare), along healed fracture planes (e.g., Fig. 5.1h) and along grain boundaries. In some cases inclusions forming a single generation appear to radiate outwards from a central point (Fig. 5.1b); the reason for this remains unknown, but may represent an advanced stage of necking (Roeder, 1984) or possibly a decrepitate feature (?). In many instances there are several generations of fluid inclusions present within single grains (Figs. 5.1, 5.2) and the inclusions may exhibit markedly different shapes and sizes, either within the same sample (Figs. 5.1c, d, 5.3) or between different samples. The variations noted for the fluid inclusions, that is with respect to size and shape, probably reflect variable amounts of re-equilibration with respect to ambient conditions at the time of formation. It is rare, although not impossible, to find isolated inclusions of equant shape which lack any associated complications. Although these may be classified as primary inclusions using the criteria of Roedder (1984), such inclusions are relegated to a secondary origin here (cf. Bodnar et al., 1985).

The types of inclusions present in sphalerite include:

1. simple two phase: these may have variable L/V ratios (Fig. 5.3), which are reflected in the range obtained for T_H (see below), but most often a constant ratio is found for inclusions of single populations (Figs. 5.1d, 5.2b). Where a large departure is observed for one or more inclusions compared to the population or cluster, necking is the likely mechanism responsible for this. Where necking is common in the inclusions, and this has the effect of changing the original volume of the inclusions and potentially the L/V ratio, it is sometimes possible to join the two separated or necked-down partners. However, such is not always the case and it is possible that some monophase inclusions (see below) may be attributed to such an origin.

Frequently the two phase inclusions appear dark (i.e., V-rich) because of the refraction of light towards the host sphalerite and away from the inclusion; in such cases it is impossible to work with the inclusions and get reliable thermometric data.

The two phase inclusions are generally elongate (Figs. 5.1c, d) to equant or ovoid (Figs. 5.2b, e), but they may have a variety of other shapes (Figs. 5.3) which presumably reflect post-formation complications. Their size can vary considerably from <5μ to 100-200μ, but 5-15μ is more normal.

2. three phase (L-V-S) incluions: in one sample a solid phase (daughter mineral) was observed in a group of inclusions lying along a healed fracture plane. These inclusions are of equant shape and have similar sizes (5-10μ). The inclusions all have the same L/V ratio and similar size solid inclusion. The shape and strongly birefringent nature might suggest carbonate as the mineral phase within the inclusion. Although not observed, Akande (1982) reported halite daughter minerals in sphalerite. It should also be noted that several inclusions nucleated halite upon freezing to -100°C.

3. monophase inclusions: inclusions containing a single phase (either L or V) may be common in some cases, and these inclusions tend to be large, of irregular shape and occur on healed fracture planes. However, these inclusions may also form as a result of necking and thus it is possible to find monophase inclusions present together with two-phase types with constant L/V ratios. The incluions forming from necking are 5-20μ size and generally of equant to tear-drop shape, but the irregular-shaped inclusions may be 50-100μ in size.

5.1.2 Calcite

Calcite is either inundated with multiple populations of fluid inclusions (Figs. 5.4a, 5.5a) or essentially barren of inclusions. Where the inclusions occur, they frequently represent several different types based on their morphology and other features such as L:V ratio (Figs. 4d, e, f, 5.5c). In contrast to sphalerite, fluid inclusions in calcite are observed, albeit rarely, as being confined to growth zones of the host crystal (Figs. 5.5a, b, d, e) which permit classification of the inclusions as primary. However, such features are rare and most inclusions must be considered as secondary. In many instances inclusions occur along healed fractures planes (Figs. 5.5c, f, g, h) and these inclusions are generally characterized by very uniform L:V ratios and smaller size.

As stated above, when fluid inclusions are present they are abundant (Fig. 5.4), but unfortunately it is not possible to isolate separate populations or determine the chronology of their generation. Fluid inclusions range in size from <5μ to >100μ, although most are 5-15μ size. The inclusions occur as clusters, single isolated inclusions (rare), along healed fracture planes and along grain boundaries. Most often areas inundated with inclusions occur near calcite-dolostone

or euhedral dolomite contacts, as opposed to the central parts of the sparry calcite. As observed in the sphalerite samples, there is considerable local variation with respect to size and shape of inclusions which may reflect variable amounts of re-equilibration. Also, as with sphalerite, it is rare to find isolated, equant-shaped inclusions with an absence of complicating circumstances (i.e., multiple generations of inclusions occur).

The types of inclusions present in calcite include:

1. simple two phase: these inclusions are highly variable with respect to their shapes, sizes and L/V ratio and may occur as: (i) large (50-100μ), irregular-shaped inclusions either along healed fracture planes or as isolated groups; (ii) clusters of 5-15μ size, equant- to elliptical-shaped inclusions; (iii) rare isolated inclusions (primary ?); and (iv) small (<3-4μ) inclusions of low temperature (based on L/V ratios) outlining healed fracture planes (Fig. 5.5c, f, g, h). As with sphalerite, necking of the inclusions is a common phenomenon and has the effect of changing the original volume of the inclusions and potentially the L/V ratio. Although it is sometimes possible to join the two separated or necked-down partners, such is not always the case and it is possible that some monophase inclusions (see below) may have originated from such a process.

2. three phase (L-V-Halite) inclusions: these inclusions are not common and occur both in areas inundated with incluions and as secondary inclusions along planar arrays. Where observed only a few inclusions of this type occur coexisting with two phase inclusions, probably reflecting either (1) metastablility of the two phase inclusions or (2) that they are close to, but not sufficiently saturated with repsect to halite to cause precipitation of this phase.

3. three phase (L-V-CO2) inclusions: in a single sample (GR-91-111), CO_2 bearing incluions (n=3) were observed coexisting (?) with large, regular-shaped aqueous inclusions and large,

irregular-shaped decrepitates. The CO_2 inclusions, 30-50μ size, consisted of three phases at 25°C and the CO_2 phase (V+L) composed about 5-20 volume % of the inclusion.

4. decrepitate clusters: these represent areas of large, highly irregular-shaped inclusions of quite variable L/V ratio that are surrounded by areas of smaller inclusions with similar proportions of L:V. They are interpreted from petrographic observations to represent decrepitated inclusions.

5. monophase inclusions: these inclusions may be either L or V dominant. Where L-dominant they occur: (1) along healed fracture planes as large to small inclusions, or (2) as randomly oriented, regular-shaped inclusions forming part of a variable cluster of inclusions (i.e., coexisting with L-V types). The V-dominant types may occur: (1) with equant-shaped two-phase inclusions of a single population where the V-rich ones are generally of different shape and size; (2) within areas of variably-shaped two-phase inclusions; (3) as irregularly-shaped, large inclusions along healed fracture planes, at grain boundaries or junctions or forming part of decrepitates; and (4) as the bulbous end of a necked inclusion. The type 1 occurrence is probably related to necking, whereas occurrence 2 and 3 are more questionable.

5.1.3 Fluorite

A single sample of fluorite-bearing dolostone obtained in this study was suitable for fluid inclusion analyses, although fluorite containing fluid inclusions was also observed during petrographic study of polished thin sections. In all the samples of fluorite observed fluid inclusions are present in abundance. The inclusions (Fig. 5.6) are consistent in terms of their shapes and sizes: (1) of equant shape and sometimes even negative-shaped inclusions are present; (2) 5-50 μ size with most 5-15 μ; and (3) randomly oriented throughout the host and/or

concentrated along healed fracture planes.

The types of inclusions present include: (1) L+V: these are the most common by far; (2) L+V+Halite: only a few of these inclusions have been observed and the inclusions are consistently of large size (>15-20 μ). Akande (1982) also noted halite in fluid inclusions hosted by fluorite; (3) monophase L or V: these are of variable size and occur along healed fracture planes coexisting with type 1 inclusions; and (4) L+V+Solid: in this case the solid is fine grained (i.e., 1-3 μ) sphalerite crystals (Fig. 5.6). Since there is abundant fine grained sphalerite in the fluorite hosting this inclusion the sphalerite crystals are considered to be an accidental inclusion rather than a true daughter phase. In addition to the phases noted here, Akande (1982) also noted the presence of petroleum within fluid inclusions hosted by fluorite.

5.1.4 Quartz Grains in Meguma Group Clasts

Quartz grains in psammitic clasts of Meguma Group lithologies within the basal breccia unit are frequently inundated with fluid inclusions. The inclusions generally occur where the quartz-bearing sedimentary fragments are found near calcite veinlets cutting the breccia rock. Where fluid inclusions occur, they are generally very abundant and occur along healed fracture planes that traverse the quartz grains from rim to rim, hence a secondary origin.

The inclusions are of the following types: (1) two phase L+V; (2) V-rich (>90% by volume); and (3) three phase L+V+Halite (?). The inclusions are generally negative-shaped and vary from <3μ to 20-30μ size, but irregular-shaped inclusions also occur.

5.2 THERMOMETRIC DATA

Thermometric measurements were made on 100-150μ thick waffers of material using a FLUID Inc. adapted U.S.G.S. gas-flow heating/freezing stage. The temperatures of homogenization are considered accurate to within ±1°C and the freezing temperatures are considered accurate to ±0.2°C.

In the present study, heating measurements were made first because of potential problems related to strectching within calcite and fluorite when freezing runs were made due to the volume increase in H_2O upon freezing. In addition, heating of samples was done such that all areas of interest in a given chip were monitored continuously as the temperature was increased as opposed to heating one area to its T_H and then another area in the same chip. This technique was employed such that problems related to over heating and stretching of inclusions in calcite and fluorite would be avoided. However, it is noted that reheating of some inclusions in calcite produced identical T_H values even after heating 50-70°C above the original T_H.

5.2.1 Heating Data

Preliminary results of heating runs are portrayed as histogram plots in Figures 5.9-5.16. In many cases the size of the vapor phase combined with the nature of the fluid inclusion prevented observation of final homogenization even using cycling techniques and in these cases the minimum T_H value is indicated by an arrow in the histogram plots.

Sphalerite Data:

Homogenization data for heating experiments on five sphalerite-bearing samples are summarized in Figure 5.7. The 128 T_H measurements made thus far collectively range from 90-

>210°C. However, examining the data for individual samples indicates that there is a more limited spread of data such that for sample GR-91-170 T_H is limited between 145-170°C and for GR-91-171 T_H is between 125-175°C. However, it is also noted that for individual grains within single samples [e.g., GR-91-108 (Fig. 5.8B)] there is a much more limited range in T_H values suggesting that the fluid inclusions record entrapment of distinctly different fluids over a period of either fluctuating or wanning temperature. Also of interest is that samples GR-91-170 and GR-91-171 were collected from a 1.5 m interval of the same drill hole; note that they record broadly similar T_H values. Finally, a single temperature for halite dissolution has been obtained (163°C, sample GR-91-117) and several inclusions decrepitated in range 185-205°C.

Calcite Data:

The total data set of T_H values for fluid inclusions in sparry calcite are summarized in Figure 5.9. It is important to note several things with respect to this diagram: (1) the peak at ca. 130°C actually contains about n=80 measurements if all the data were plotted rather than summarized by the hatchered boxes. However, this would bias the data becasue T_H is easier to get for these inclusions but they are not necessarily more abundant than other inclusions; (2) there appears to be a continuum of T_H recording a range of temperatures from >250°C to 70°C. This range is far greater than reported by Akande (1982) or Ravenhurst et al. (1987, 1989); (3) the dissolution temperature for halite (n=2) of 155°C is similar to the single measurement made for halite in sphalerite (above). For these halite-bearing inclusions, T_H of the vapor was about 150°C; (4) the upper limit to the range of decrepitation temperatures is similar to that for fluid inclusions hosted by sphalerite; and (5) there is no relationship between the size of inclusion and

their T_H values. In addition, T_H values for inclusions were measured in a single heating run as opposed to reheating different parts of the same sample, therefore, stretching of the inclusions is not considered to be reflected in the plot of T_H data.

The large spread of the T_H for calcite warrants more detailed examination of the data, thus, for some samples the data have been subdivided into the individual chips and areas examined. In Figure 5.10 the data for different areas in a single chip from sample GR-91-111 is shown and it can be seen that for the individual areas examined there is a restricted range for T_H compared to the histogram plot for the full data set in Figure 5.11. Furthermore, as the sketch in Figure 5.10 illustrates, there can also be a large range of T_H within individual areas suggesting possible sub-domains. These sub-domains, labelled 1, 2, 3 in Figure 5.11, are reflected by the peaks in the histogram plot for the entire data set for this sample (Fig. 5.11).

In Fiugre 5.12 the data for sample GR-91-156 is also summarized for individual areas within different calcite chips. This sample is well mineralized with sphalerite intimately intergrown with calcite. Again there is a limited range for T_H for individual areas compared to the data set as a whole. Finally, the T_H data for sample GR-91-80 and the accompanying sketches of the inclusions ((Fig. 5.13) indicate that for this sample there is a very uniform and low temperature range for the fluid inclusions. This data is unique among the many samples studied to date in terms of this very restricted range in T_H.

In two samples examined to date, data was obtained for both calcite and sphalerite and these results are compared in Figure 5.8. Although there is not a great deal of data for the calcite, especially given the large variation in T_H that can be expected for this mineral (see above), there is nevertheless a good correlation for sphalerite and calcite.

Fluorite Data:

Homogenization data have only been obtained for a single sample of fluorite and the results are summarized in 5.14 with the data for individual areas shown in Figure 5.15. The sample of fluorite is intergrown with calcite and the results of T_H for this mineral are also shown in Figure 5.15 for comparative purposes. Data were collected from 5 areas within the fluorite and collectively there is a spread from 145 to >250°C (Fig. 5.14), with individual areas showing both a restricted (areas 1, 2) or broad (areas 3, 4, 5) range. There is clearly a concentration of the data in the 150-200°C range with only 20% of the data giving higher values of T_H. The spatially associated calcite shows a broader range (70 to >250°C) which incorporates the spread in the fluorite data (Fig. 5.15).

Meguma Group Quartz Data:

Quartz grains in the Meguma Group clasts (i.e., wackes) contain abundant fluid inclusions which do not contain carbonic species (CO_2, CH_4) in sufficient quantity to be detected using routine fluid inclusion procedures. Homogenization data for a single sample of this material in the basal breccia is shown in Figure 5.16; although both calcite and sphalerite in this sample contain fluid inclusions, the T_H have not yet been determined. The data for the five different areas indicate a total spread for T_H from 180 to 320°C, but a more restricted range (i.e., 30-60°C) is indicated for specific areas.

Comparison to Previous Homogenization Data:

Compared to the previous work of Akande (1982) and Ravenhurst et al. (1989), the following points are noted with respect to the homogenization data:

1. the new data define a much broader range for sphalerite compared to the 205-218°C and ca. 158°C reported by Akande and Ravenhurst et al., respectively.

2. the calcite data reported here contrast markedly with the ore-stage (172 $\pm$ 3°C, 163-176°C) and post-ore stage (142 $\pm$ 3°C, none reported) calcite data of Akande and Ravenhurst et al., respectively. Most remarkable are the narrow ranges reported by these respective authors when one considers the diversity of inclusions that have been observed in single samples. The reason for the large discrepancy between this previous work and the present study remains unresolved.

3. as with calcite, the fluorite data reported here contrast with the restricted range reported by Akande (143 $\pm$ 3°) and Ravenhurst et al. (138-165°C). While the results of Ravenhurst et al. overlap the lower temperature range reported here, the data of Akande is lower than the lowest T_H values recored in the present study.

5.2.2 Freezing Data

Only a limited amount of freezing data have been obtained thus far and this is summarized in Figure 5.17. Since the results are generally similar for sphalerite and calcite, the data are discussed together. The eutectic (T_E) or first melt temperatures range from -75 to -52°C and there is clearly a broader range for the sphalerite data compared to calcite which is quite restricted. Similarly, the last melting temperatures for sphalerite are depressed to lower temperatures and cover a broader range than for calcite, the former being -20 to -40°C whereas calcite is near -20 to -25°C.

The freezing data indicate that the first and last melting temperatures are too depressed to be accounted for by a simple binary solution of NaCl-H_2O (i.e., eutectic -20.8°C, Crawford, 1981), instead additional dissolved salts such as $CaCl_2$ (eutectic of -52°C for system $CaCl_2$-NaCl-H_2O, Crawford, 1981) are probably present. However, since many of the T_E measurements in inclusions hosted by sphalerite are well below the eutectic in the $CaCl_2$-NaCl-H_2O system, other salts which may depress the eutectic temperature must also be present. Similarly depressed T_E have been been reported by Williams-Jones et al. (1992) for fluid inclusions associated with Ba-Pb-Zn mineralization hosted by dolomitized sediments in the eastern townships of Quebec. These authors appealed to $MgCl_2$ and $BaCl_2$ as possible solutes causing the depression of eutectic temperatures. An additional solution may be carbonic species (Burruss, 1981) given the presence of pyrobitumen in the dolostones at Gays River and presence of petroleum in some fluid inclusions (Akande, 1982).

The freezing data reported here are consistent with the few measurements reported by Akande (1982) and Ravenhurst et al. (1989). Both authors noted the high salinities of the fluids and Ravenhurst et al. also noted the very depressed T_E values.

The salinities of the fluids have been estimated using two approaches. In the first case the composition of the fluid inclusions can be estimated using the technique of Williams-Jones and Samson (1990) in which the dissolution T of halite and T_m(ice) data are combined in the ternary system H_2O-NaCl-$CaCl_2$. The three inclusions for which data are presently available indicate an average composition for the fluid of 14 wt.% $CaCl_2$ and 19 wt.% NaCl. For the remaining inclusions, the fluid chemistry is estimated using the last melting temperature of ice and calculating the solute component as equivalent wt. % NaCl (Crawford, 1981). For the calcite

data the composition is approximately 23-25 wt. % equiv. NaCl, whereas for sphalerite the data indicate salinities of 23-35 wt. % equiv. NaCl. If we assume that the fluids are predominantly mixtures of NaCl-$CaCl_2$-H_2O, then we can use the final melting temperature of ice to estimate the ratio of NaCl to $CaCl_2$ (X_{CaCl2}) in the fluids. These estimates of X_{CaCl2} range from 0 for fluids with last melting of ice near -20.8°C to 0.9 for those inclusions with last melting temperatures near -40°C.

The observation that some material persisted upon heating to above 0°C (+8 to +11.5°C) suggests the presence of clathrates in the inclusions. These clathrates could be either carbonic in nature or calcium chloride species. More specific determinations of the fluids are required before it is possible to be sure what clathrate species may be present.

In addition to the above information, the following observations are also noted with respect to the freezing runs made: (1) many of the inclusions would not freeze upon cooling (to -100°C), even when held at low temperatures for 10-15 minutes. However, repeated attempts at freezing the inclusions sometimes proved successful; (2) in a few inclusions a solid phase appeared during cooling (metastable halite perhaps ?); and (3) during heating up of the inclusions most of the melting occurred within a very narrow temperature interval commencing within a few degrees of the final melting temperature.

5.3 DISCUSSION OF THE FLUID INCLUSION DATA

Despite the accumulation of considerable data on fluid inclusions hosted by calcite and sphalerite, and to a limited extent on fluorite, the physio-chemical evolution of the fluid remains undefined. There is no obvious relationship between the host mineral phase and temperature, as

was suggested on a more limited data set by Akande and Zentilli (1984), and calcite and sphalerite appear to give the same range for T_H. The presence of distinct temperatures for some groups of inclusions in both minerals suggests that real changes in temperatures (i.e., fluctuations) have been detected, but of what significance this may be remains unknown. If the T_H recorded for sphalerite represent temperatures close to mineral formation, then mineralization extended over a wide range (100°C) but the fluid remained constant in terms of its chemistry which can be approximated by the $NaCl-CaCl_2-H_2O$ system with variable X_{CaCl2}.

There remain outstanding problems with the fluid inclusion data and petrographic observations, including: (1) the origin of vapor-rich inclusions; (2) the possibility of localized fluid unmixing (i.e., fluorite sample); (3) the large range in T_H within calcite of variable paragenesis; (4) the presence of CO_2-bearing inclusions, albeit of very minor extent, given the low temperature and pressure of formation of the mineral deposit; and (5) the origin of the high temperatures recorded in calcite, fluorite and to a certain extent sphalerite. Further work is in progress to address these problems.

Fig. 5.1. Photomicrographs (plane polarized light) of fluid inclusions in sphalerite chips. (a) Sphalerite cement in dolostone with a cluster of fluid inclusions showing a radial texture which is illustrated in the enlarged photo in photo 5.1b. Width of photo 1.3 mm. (b). Group of inclusions showing radial distribution that may represent necking of a single large inclusion. The constant L:V ratio suggests that the necking must have occurred prior to phase separation. Width of photo 0.34 mm. (c) Sphalerite chip showing variety of fluid inclusions in close spatial association; inclusions are considered to be of secondary origin. Width of photo 0.67 mm. (d) Area in photo 5.1c enlarged showing array of fluid inclusions of similar nature; note the constant L:V ratios. Largest inclusion about 40 μ. (e) Sphalerite chip illustrating color zonation (primary growth banding) and different arrays of fluid inclusions. Width of photo 1.3 mm. (f) Sphalerite chip with numerous arrays of fluid inclusions. Width of photo 1.3 mm. (g) Sphalerite chip with large (30-40 μ) fluid inclusions of equant to irregular shape. These inclusions have a range in their L:V ratios and do not represent a single generation of inclusions. Width of photo 1.3 mm. (h) Sphalerite chip with numerous arrays of fluid inclusions which cross cut the color bands in the sphalerite (primary growth zones). Width of photo 1.3 mm.

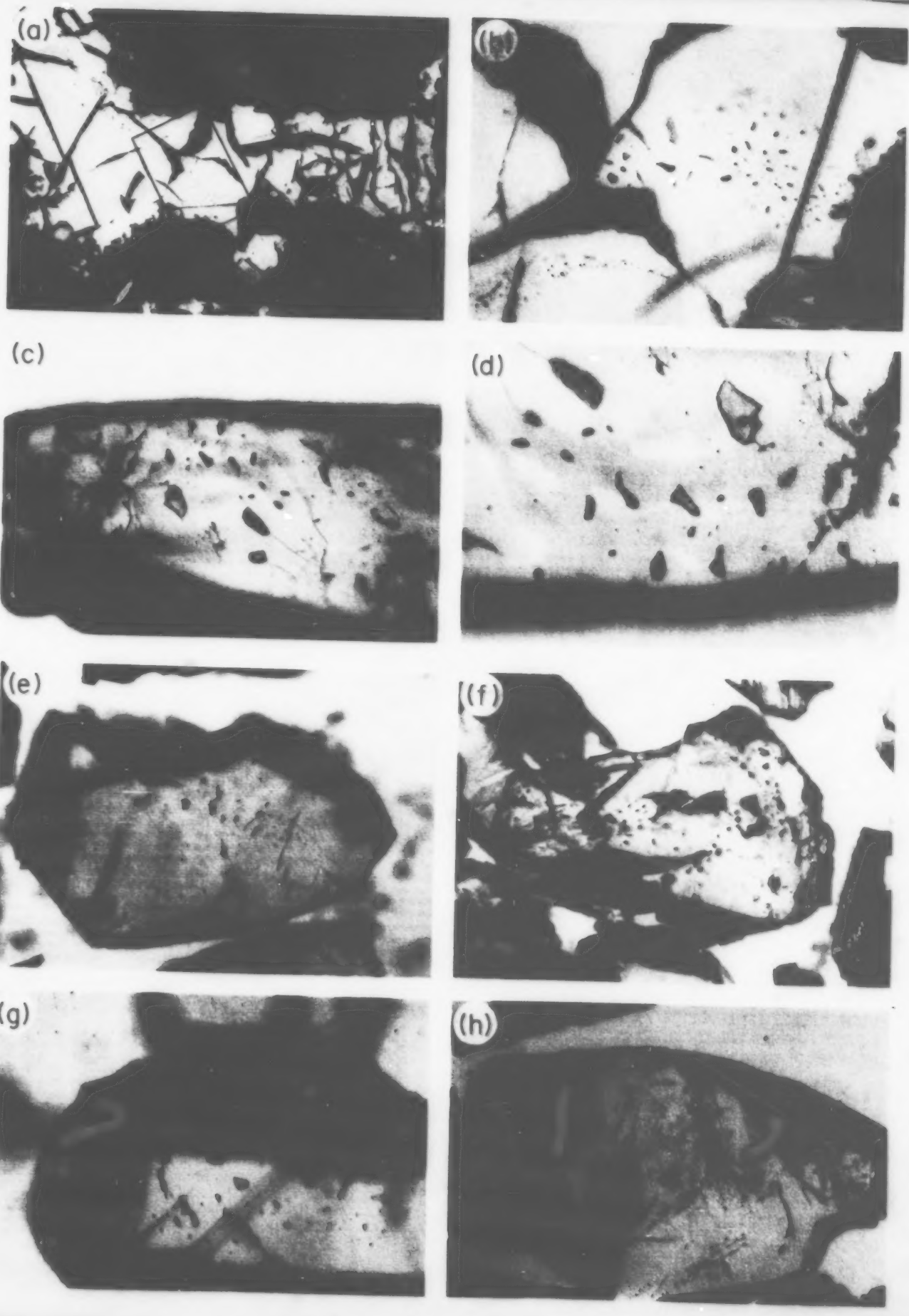
(a)
(b)
(c)
(d)
(e)
(f)
(g)
(h)

Fig. 5.2. Photomicrographs (plane polarized light) of fluid inclusions in sphalerite chips. (a) Sphalerite grain with euhedral termination cementing primary pore space in dolostone and overgrowing earlier dolomite cement. The sphalerite contains planar array of fluid inclusions that may be of pseudosecondary origin. Width of photo long dimension 1.3 mm. (c) Area in photo 5.2a enlarged showing a cluster of equant, negative-shaped inclusions with constant L:V ratio in sphalerite chip. Width of photo 0.34 mm. (c) Sphalerite chip showing fluid inclusion with a variety of shapes. Width of photo 0.67 mm. (d) Sphalerite grain with large isolated inclusions (20-30 μ) and healed fracture planes with smaller inclusions. Width of photo long dimension 0.67 mm. (e) Enlargement of area in photo 5.2d showing the range in inclusion size and occurrence (large inclusion about 40 μ).

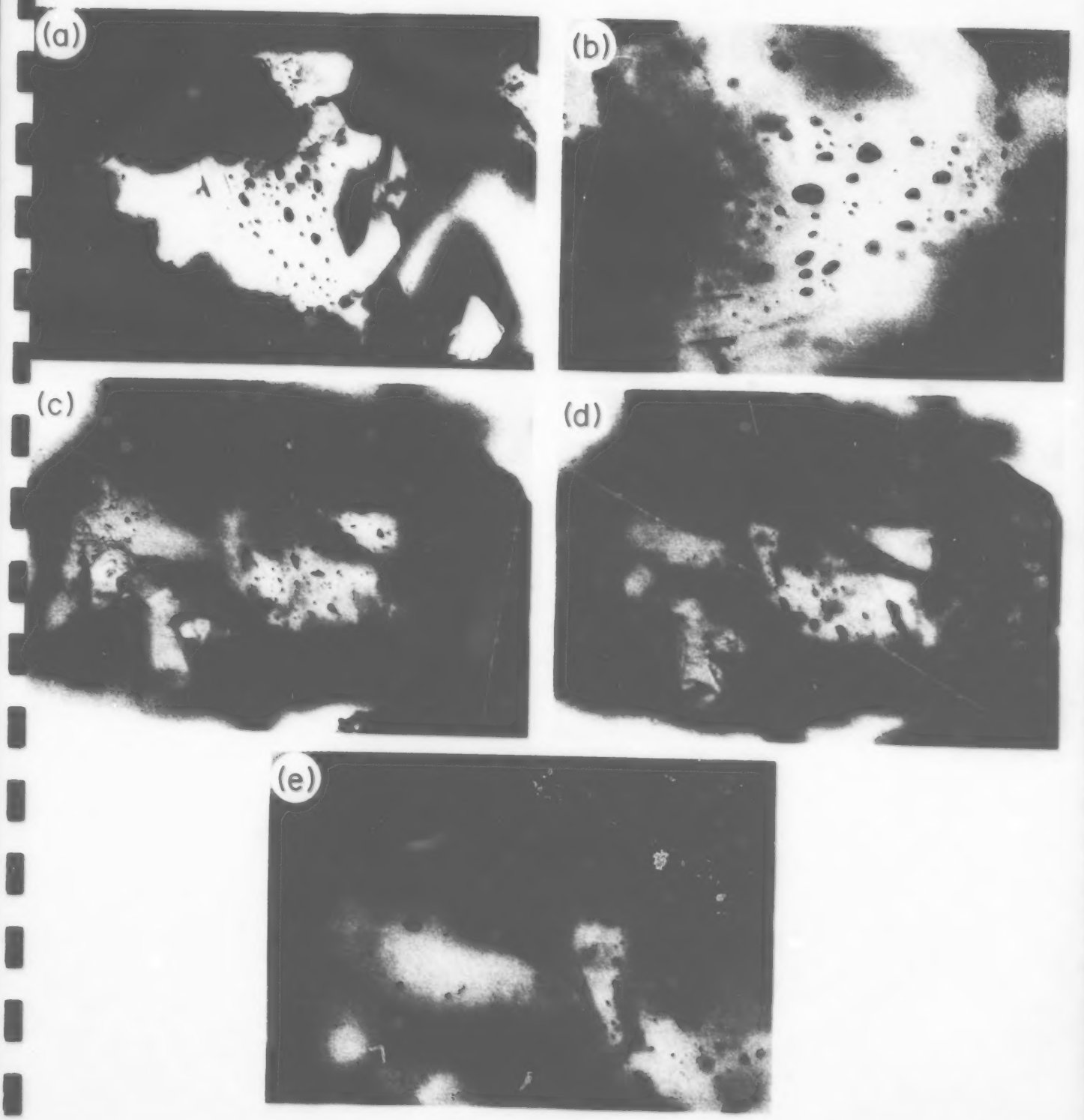
(a)
(b)
(c)
(d)
(e)

Fig. 5.3. Sketches of fluid inclusions in sphalerite illustrating the variable L:V ratios within groups of inclusions and the different shapes.

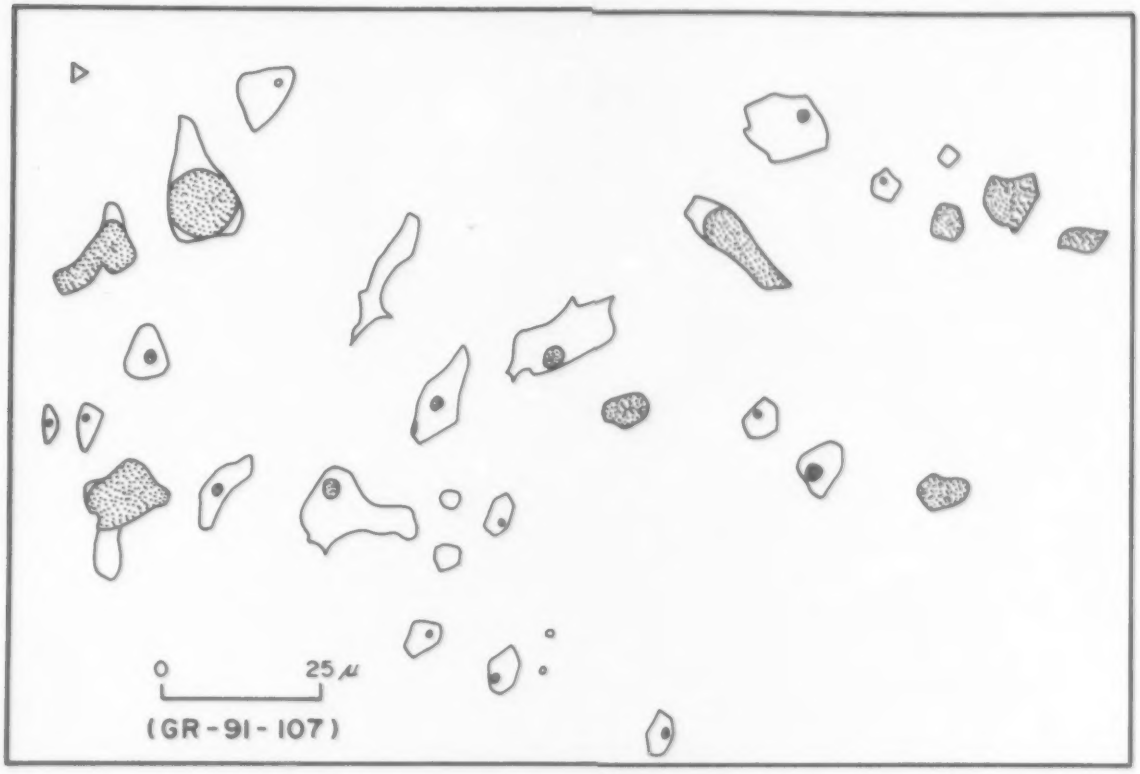

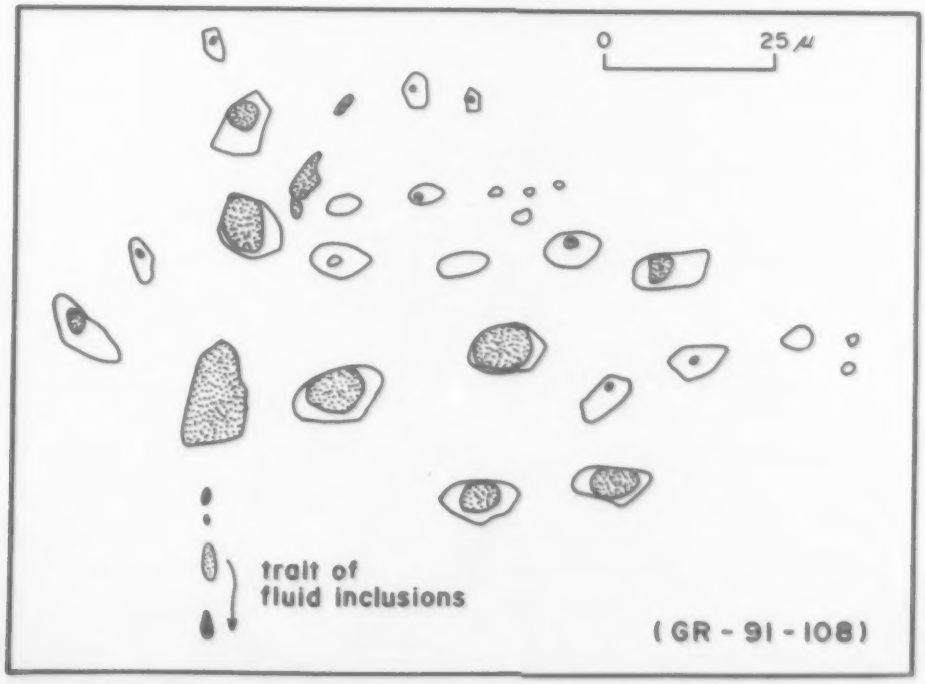

Fig. 5.4. Photomicrographs (plane polarized light) of fluid inclusions in calcite cements. (a) Calcite cement post-dating sphalerite and dolomite cements (lower part of photo) in dolostone. Note that the fluid inclusions occur in clusters and have no relationship with any crystallographic orientation of the calcite. Area outlined in black box enlarged in photo 5.4b. Width of photo 2.6 mm. (b) Enlargement of part of photo 5.4a showing the abundance of fluid inclusions and, in some cases, their obvious planar arrangement. Note the large range in size and shape of the inclusions. Width of photo 1.3 mm. (c) Calcite cement inundated with fluid inclusions. Area outlined in black box enlarged in photo 5.4d. Width of photo 0.67 mm. (d) Enlargement of photo 5.4c showing the large variety of inclusions with respect to shape and L:V ratios (see arrows). Note that some contain halite as a daughter mineral. Width of photo 0.34 mm. (e, f) Same sample as in photo 5.4d showing the range of fluid inclusion types (see arrows). Width of photo 0.34 mm.

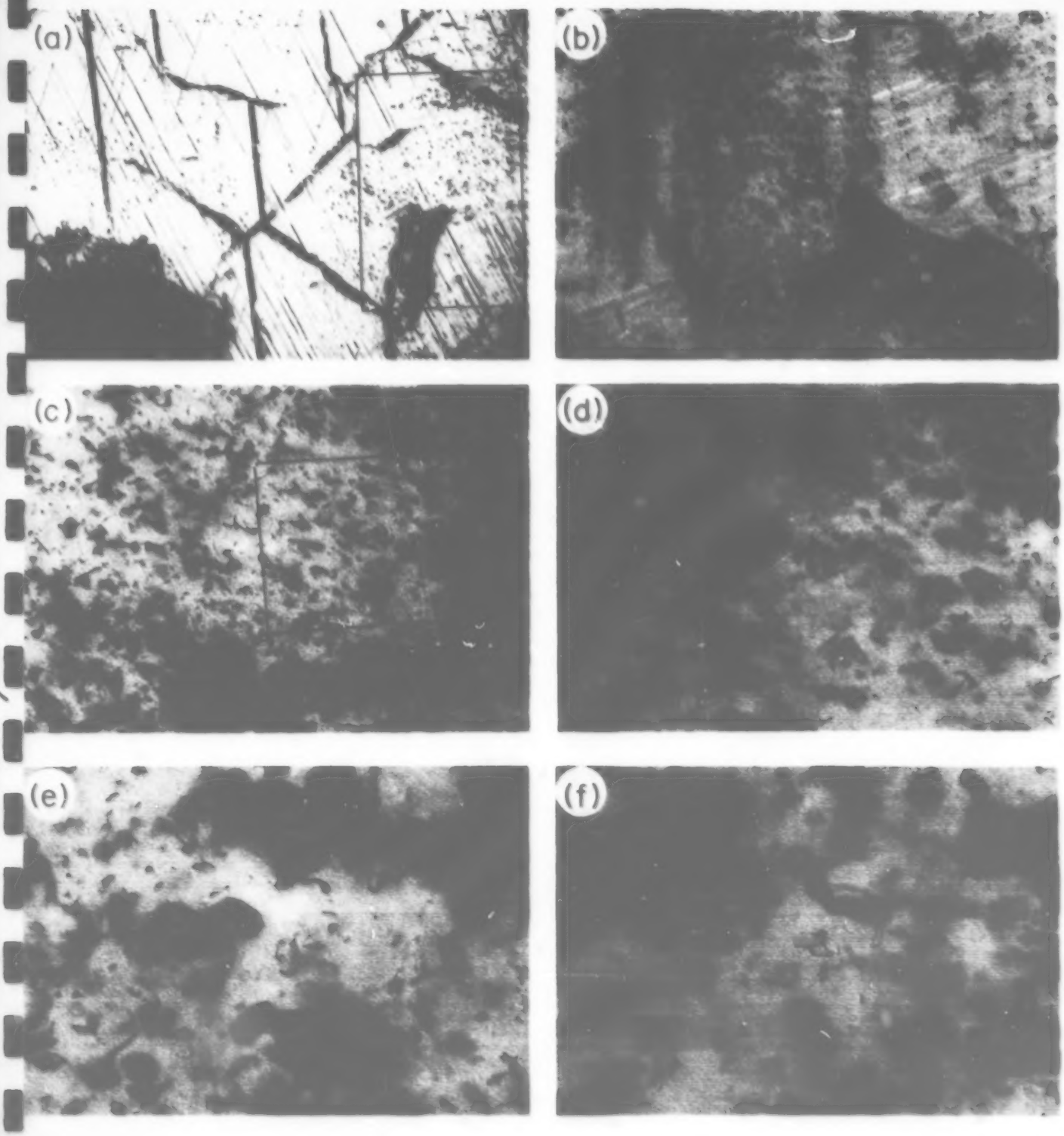
(a)
(b)
(c)
(d)
(e)
(f)

Fig. 5.5. Photomicrographs (plane polarized light) of fluid inclusions in calcite cements. (a) Calcite cement with fluid-inclusion rich area overgrown with clear calcite. These inclusion would be considered to be of primary and pseudosecondary origin. Area outlined in black box enlarged in photo 5.5b. Width of photo 1.3mm. (b) Enlargement of photo 5.5a showing that a variety of inclusion types coexist therefore suggesting a pseudosecondary origin for at least some of the inclusions. Width of photo 0.34 mm. (c) Arrays of secondary inclusions in calcite concentrated along a healed fracture plane. Note the constant L:V ratios for the inclusions and their square to rectangular shapes that reflect control by cleavage planes in the host mineral. Width of photo 0.34 mm. (d) Calcite cement with zonally arranged fluid inclusion-rich areas plus unidentified material outlining growth zones in the calcite. Note that the calcite post-dates sphalerite and dolomite cements. Width of phot 2.6 mm (e) Enlargement of part of central part of previous photo. Width of photo 1.3 mm. (f, g, h) Secondary fluid inclusions in calcite that are characterized by their samll size, constant L:V ratios and additional complexities (e.g., photo 5.5g). Width of photos 0.34 mm in (f) and 0.67 mm in (g, h).

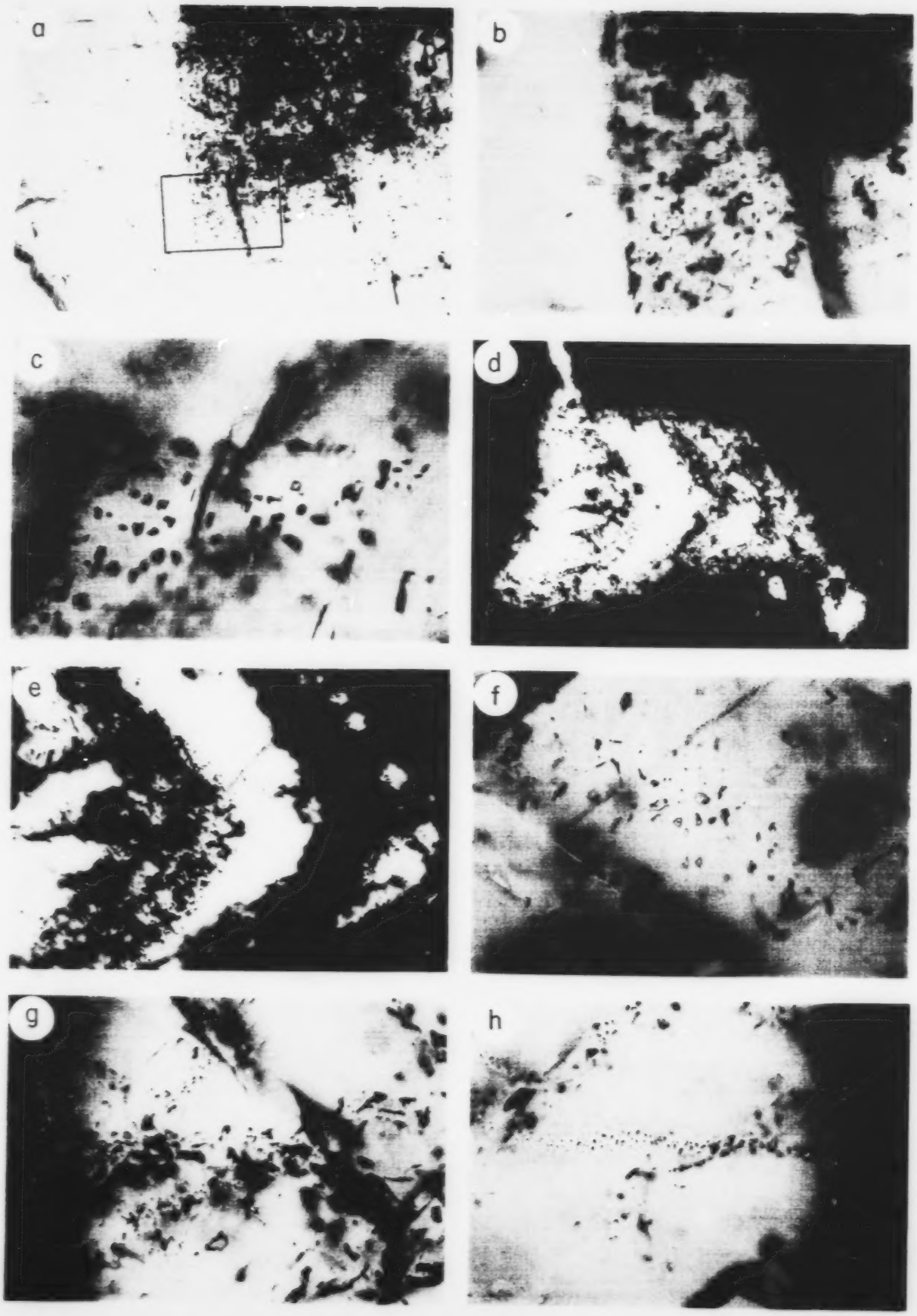
a
b
c
d
e
f
g
h

Fig. 5.6. Sketch of fluid inclusions occurring within fluorite cement associated with calcite, galena and sphalerite. (a) Vapor- and liquid-rich fluid inclusions coexisting along the same fracture planes. (b) Same as in previous sketch but also showing the occurrence of halite-bearing inclusion and trapped sphalerite grains in a fluid inclusion.

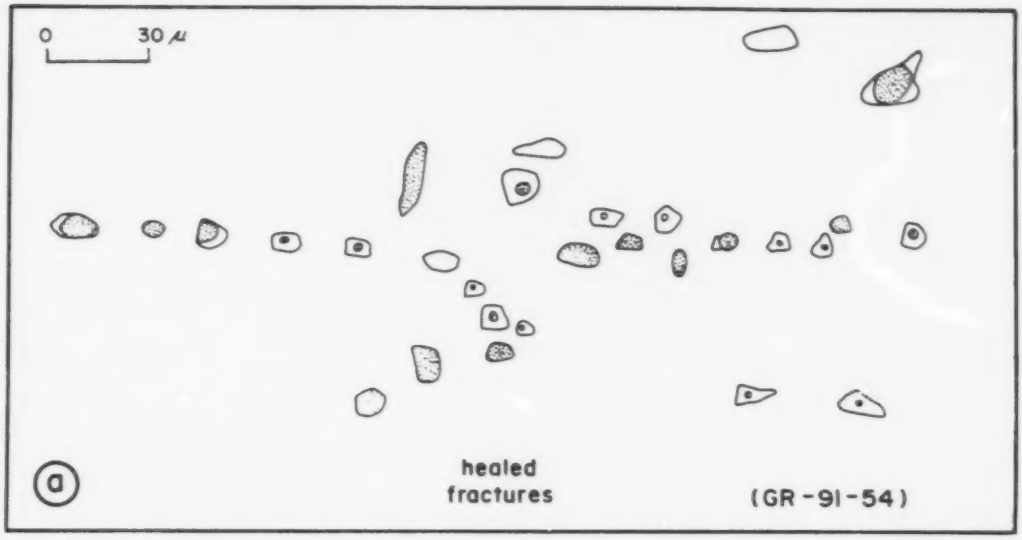

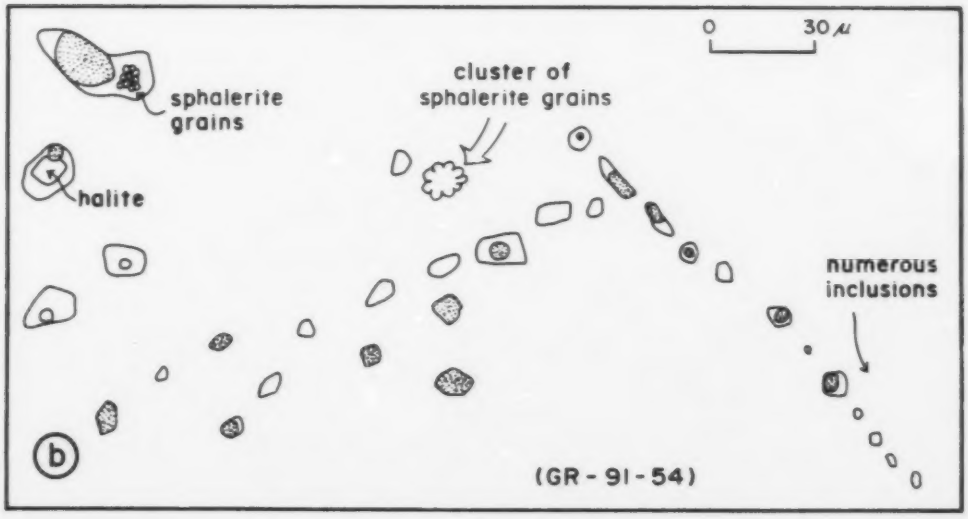

Fig. 5.7. Histogram plots for homogenization temperatures (T_H) in sphalerite from five different samples (n=128). Symbols are for: (□) halite dissolution; (>) T_H greater than that indicated; (D) decrepitation temperature.

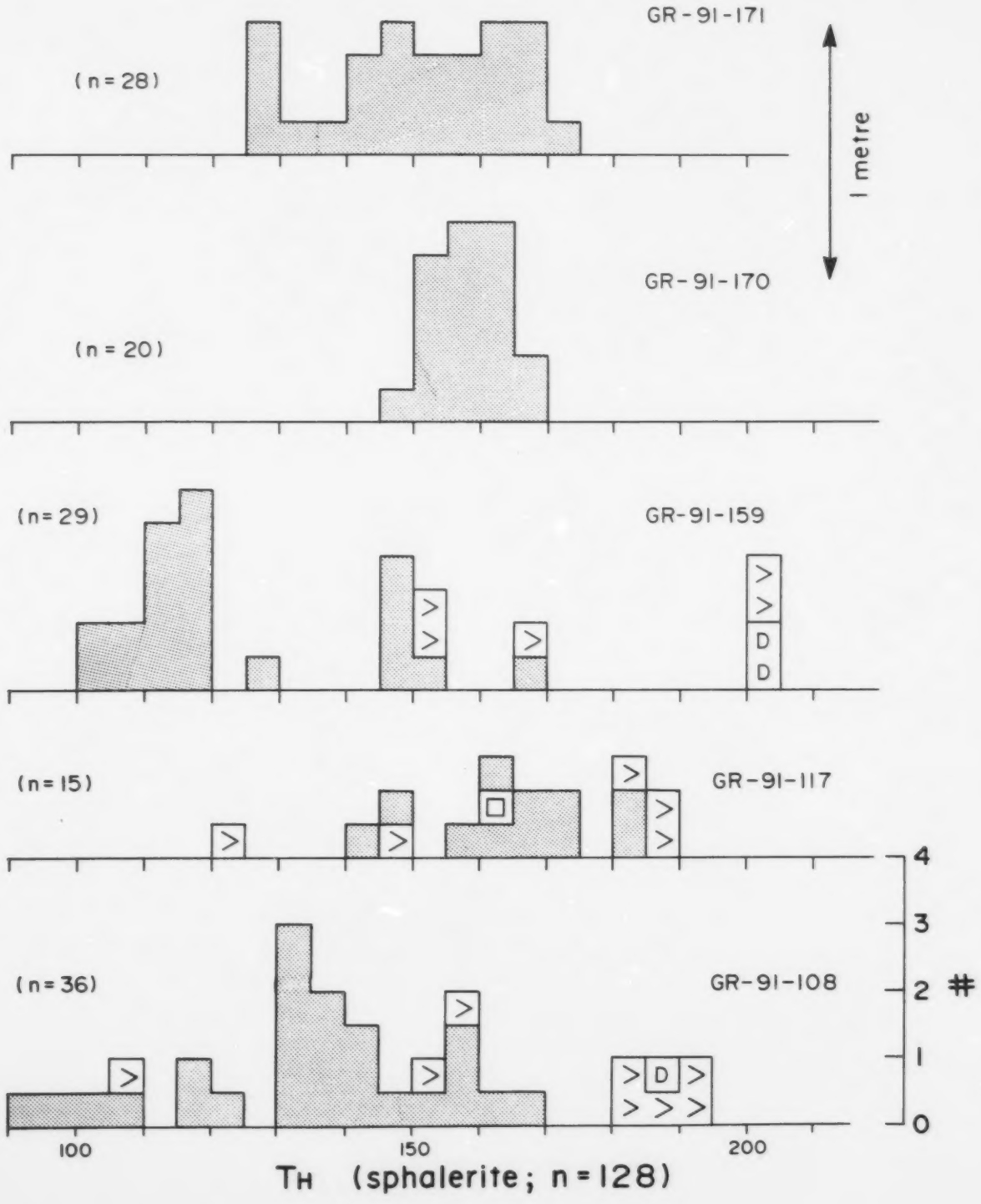

Fig. 5.8. Histogram plots for homogenization temperatures (T_H) in sphalerite and calcite from the same sample. In (b) the data have been separated for the different grains studied in order to compare the T_H results. Note the good comparison for the T_H data from sphalerite and calcite. Symbols as in Figure 5.7.

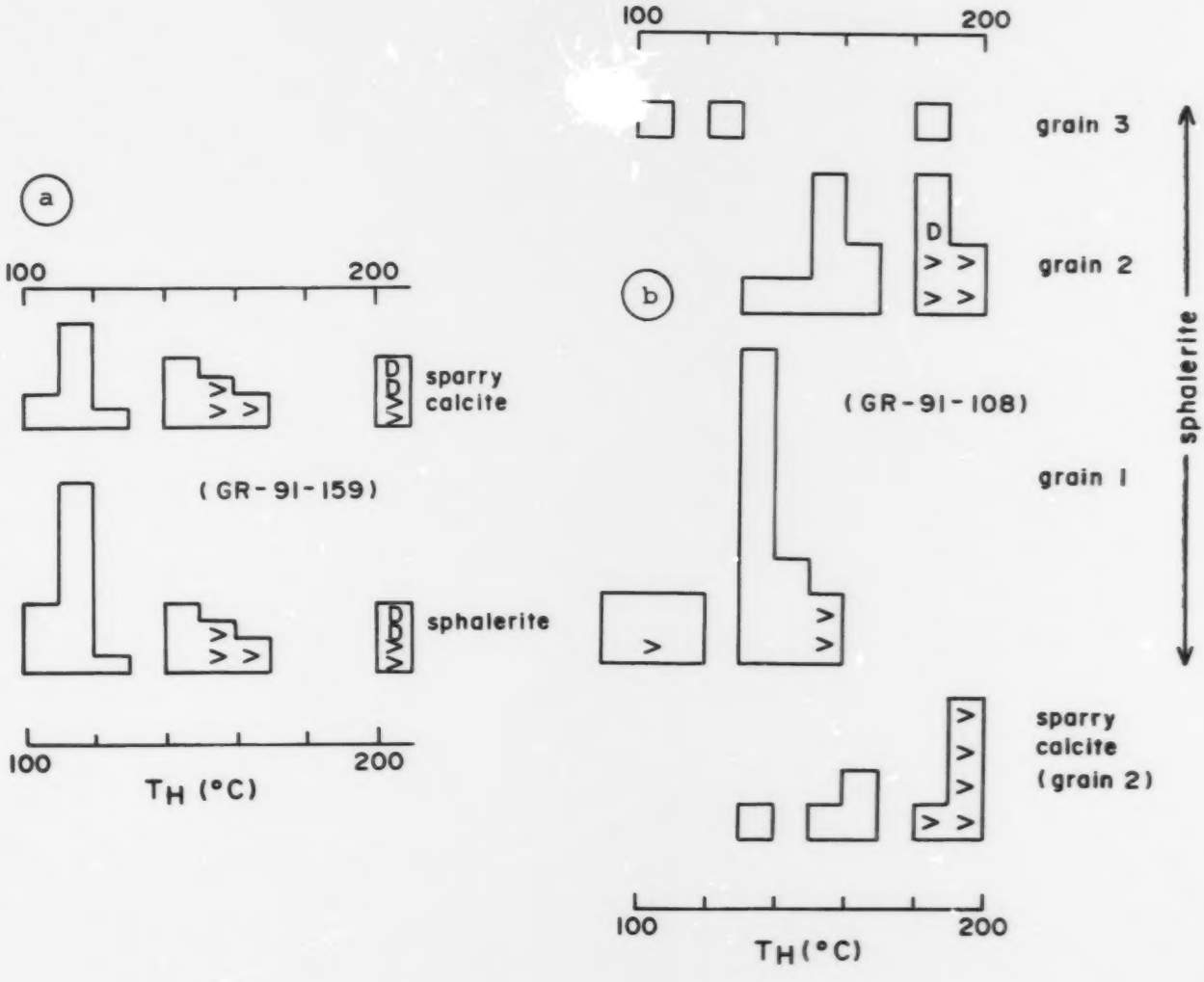

Fig. 5.9. Histogram plot of homogenization temperatures (T_H) for all the samples of calcite cement studied.

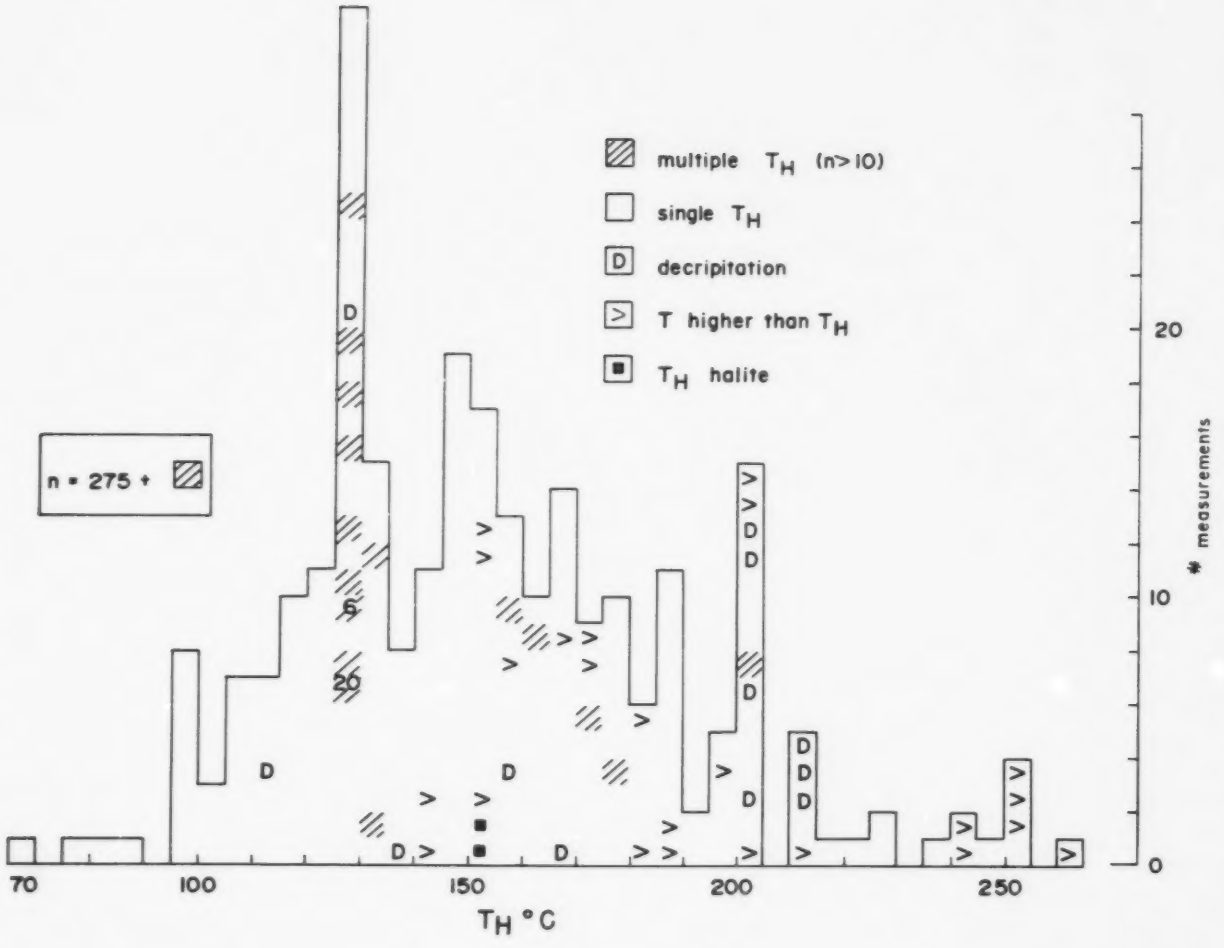

Fig. 5.10. Histogram plot of homogenization temperatures (T_H) for different calcite cements in the same sample (chip samples referred to by numbers). D refers to decrepitated inclusions.

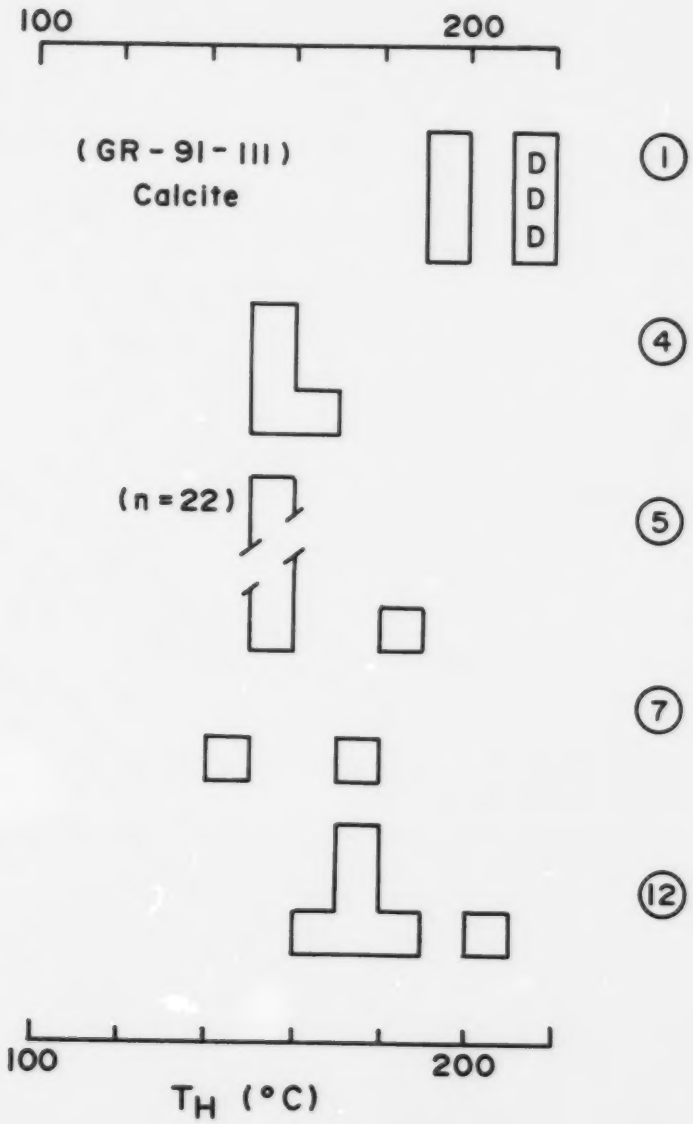

Fig. 5.11. Sketch of dolostone sample containing galena and sphalerite mineralization and calcite cement with results of homogenization temperatures (T_H) determined for fluid inclusions in the calcite. Inset diagram shows histogram plot of the all the T_H data for this sample. Outlined in the sketch are areas designated 1, 2, 3 which may be subdomains for different popluations of inclusions based on their T_H values and these are also indicated in the histogram plot (1, 2, 3).

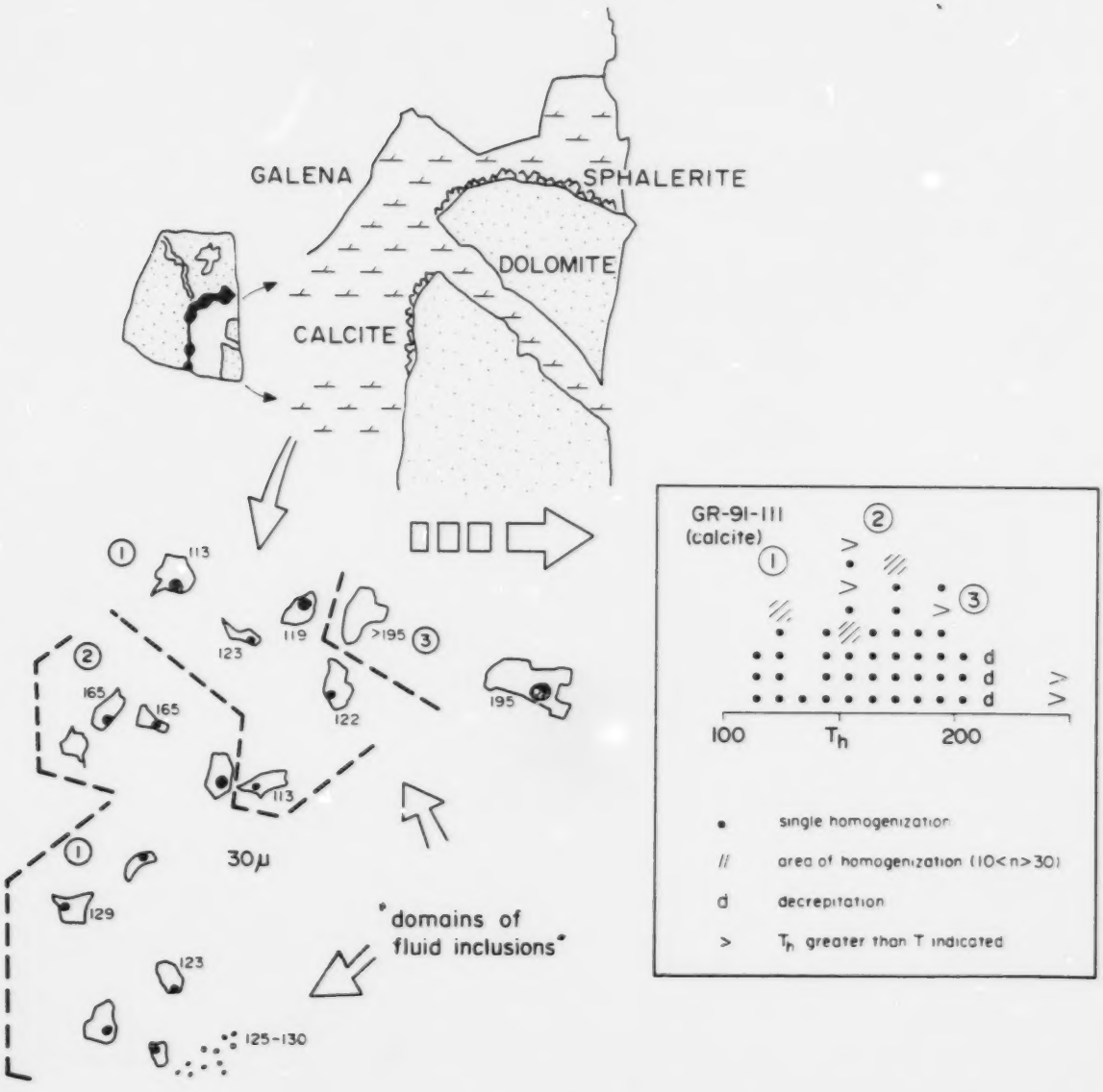

Fig. 5.12. Histogram plots of homogenization temperatures (T_H) for sample GR-91-156 calcite showing the data for separate areas in three different chips. Note the restricted range of T_H for the individual areas compared to the range for all the data. (>) indicates T_H greater than indicated.

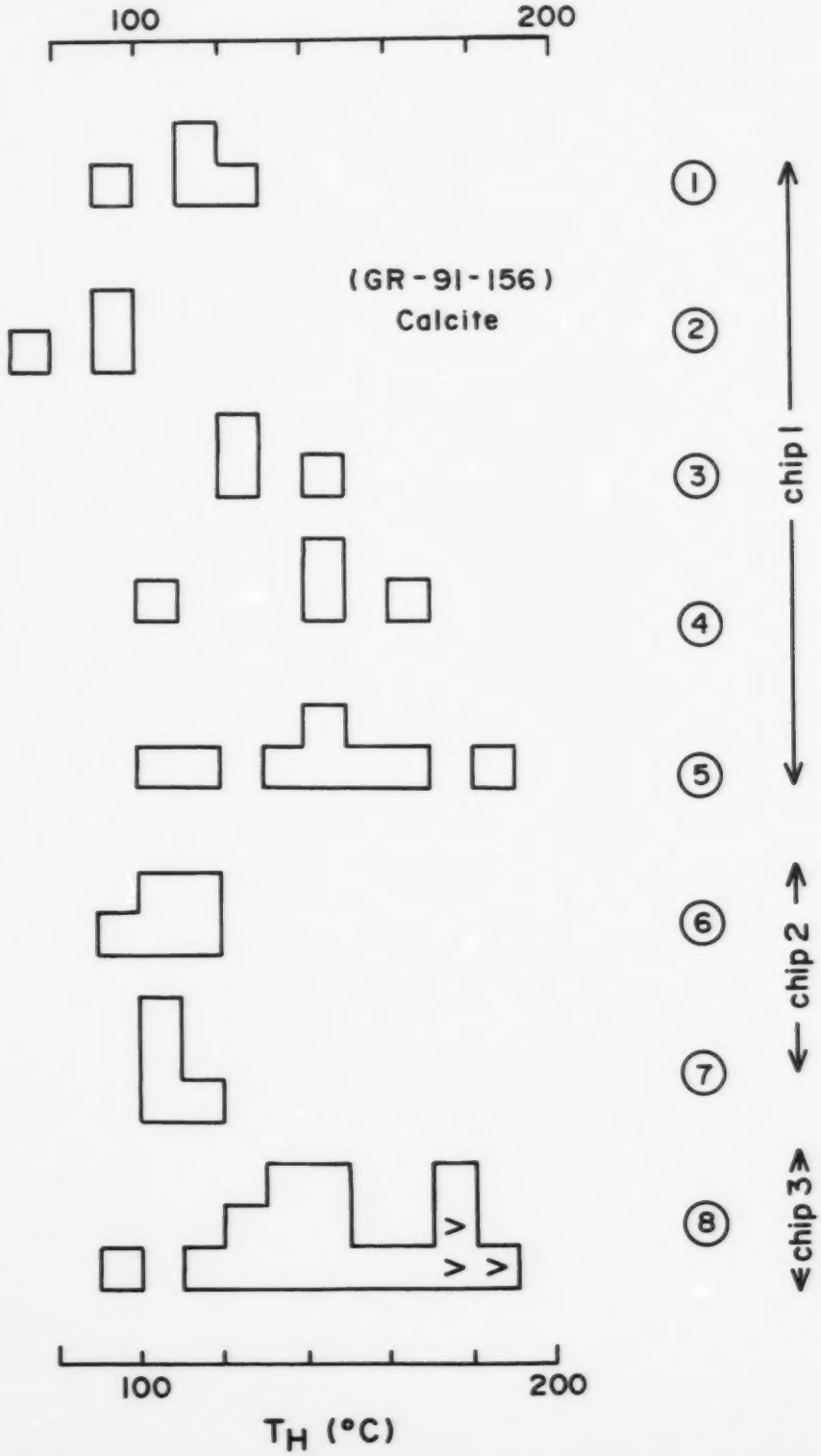

Fig. 5.13. Sketch of fluid inclusions with homogenization temperatures (T_H) for calcite cement associated with galena mineralization. Inset is histogram plot of T_H data for this sample and note the very restricted range in T_H for this sample compared to the data in Figure 5.9.

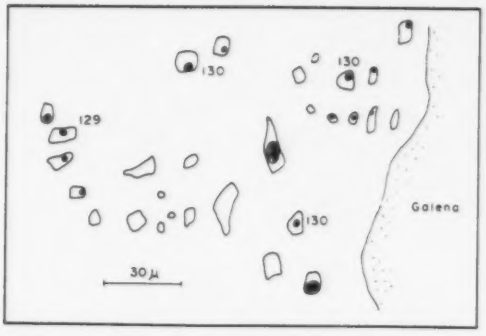

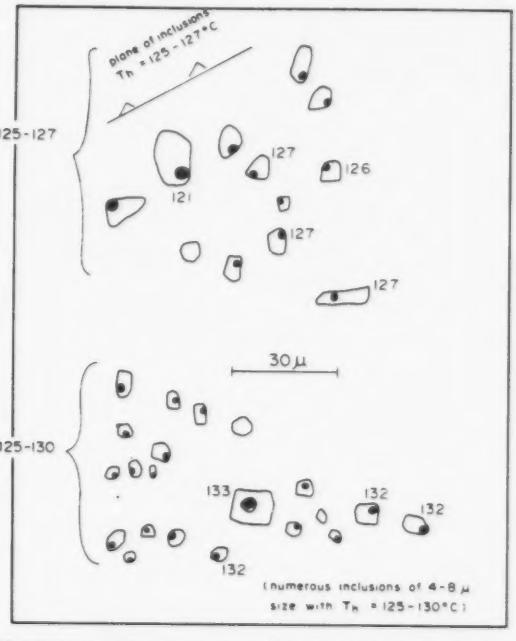

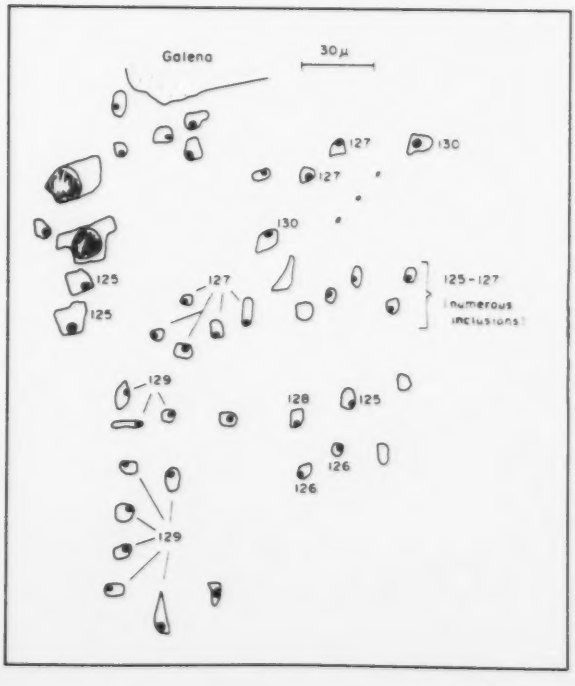

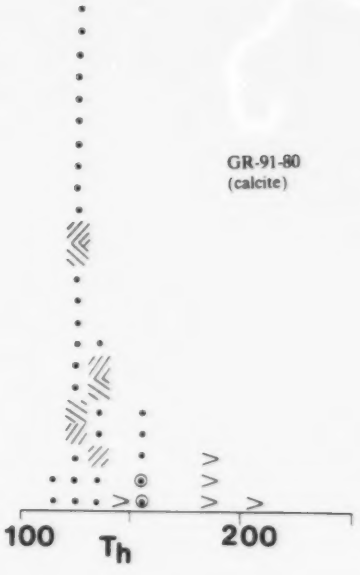

- • single homogenization
- // area of homogenization (10<n>30)
- d decrepitation
- > T_h greater than T indicated
- ⊙ disappearance of halite daughter mineral

Fig. 5.14. Histogram plot of homogenization temperatures (T_H) for a single sample containing fluorite.

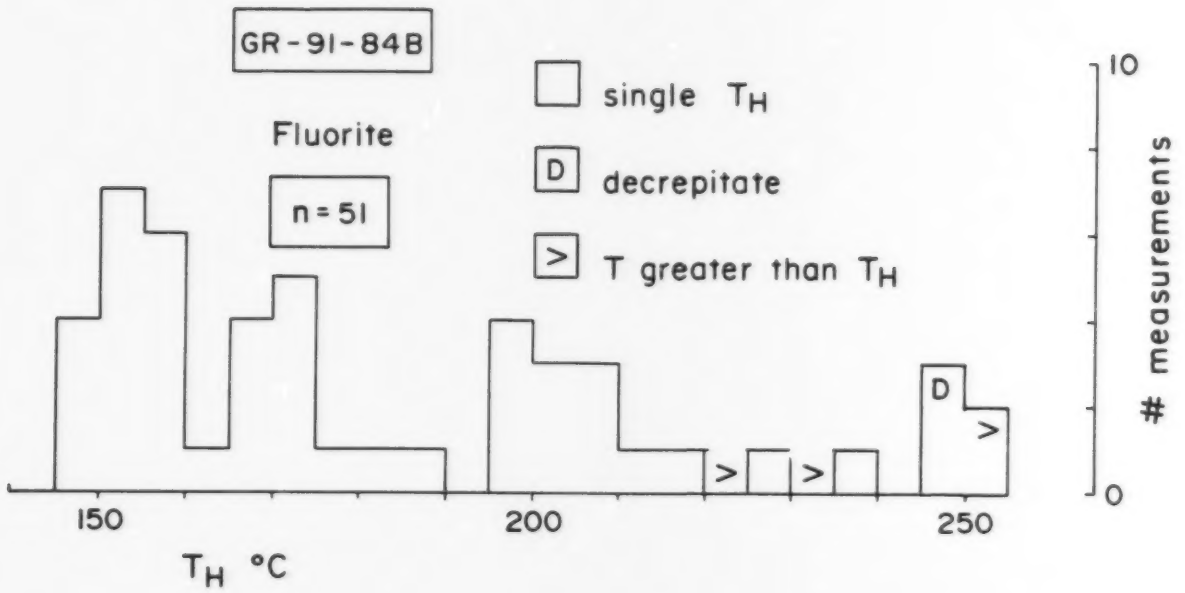

Fig. 5.15. Sketch of sample GR-91-84B that contains calcite and fluorite cements with the results of homogenization temperature (T_H) determinations.

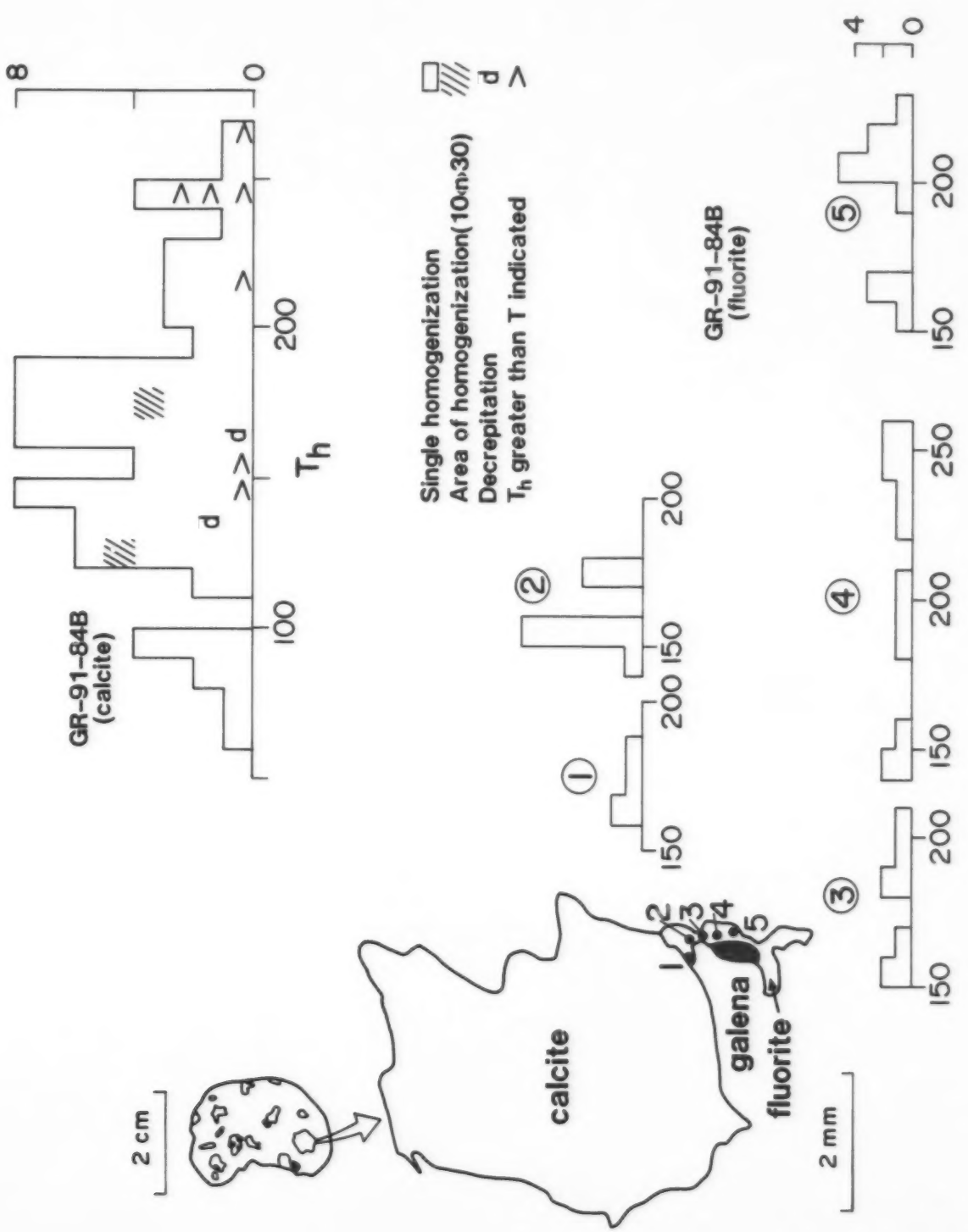

Fig. 5.16. Histogram plots of homogenization temperatures (T_H) for different areas in two chips of basal breccia material. The fluid inclusions are hosted by quartz grains in fragments of Meguma Group psammites.

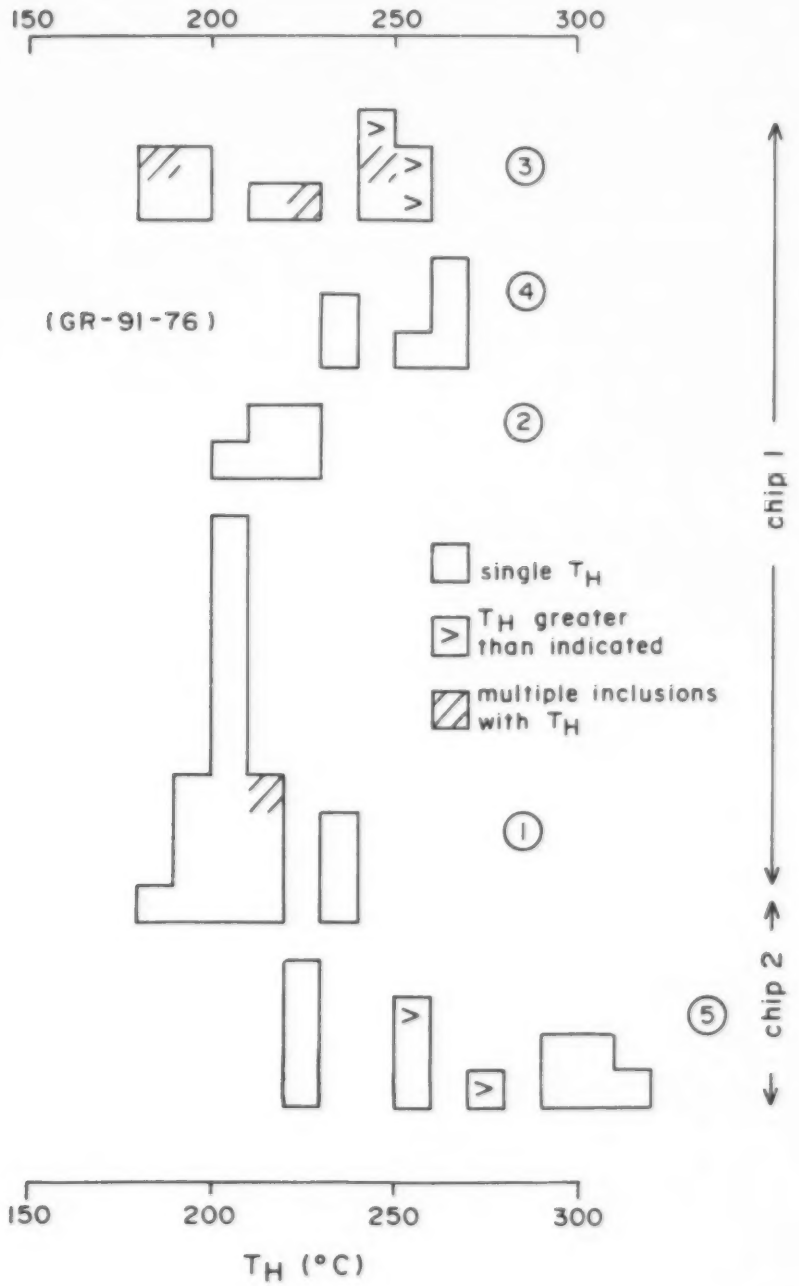

Fig. 5.17. Histogram plots of first melting (T_E; eutectic temperature) and last melting (T_m ice) temperatures for fluid inclusions hosted by sphalerite and calcite.

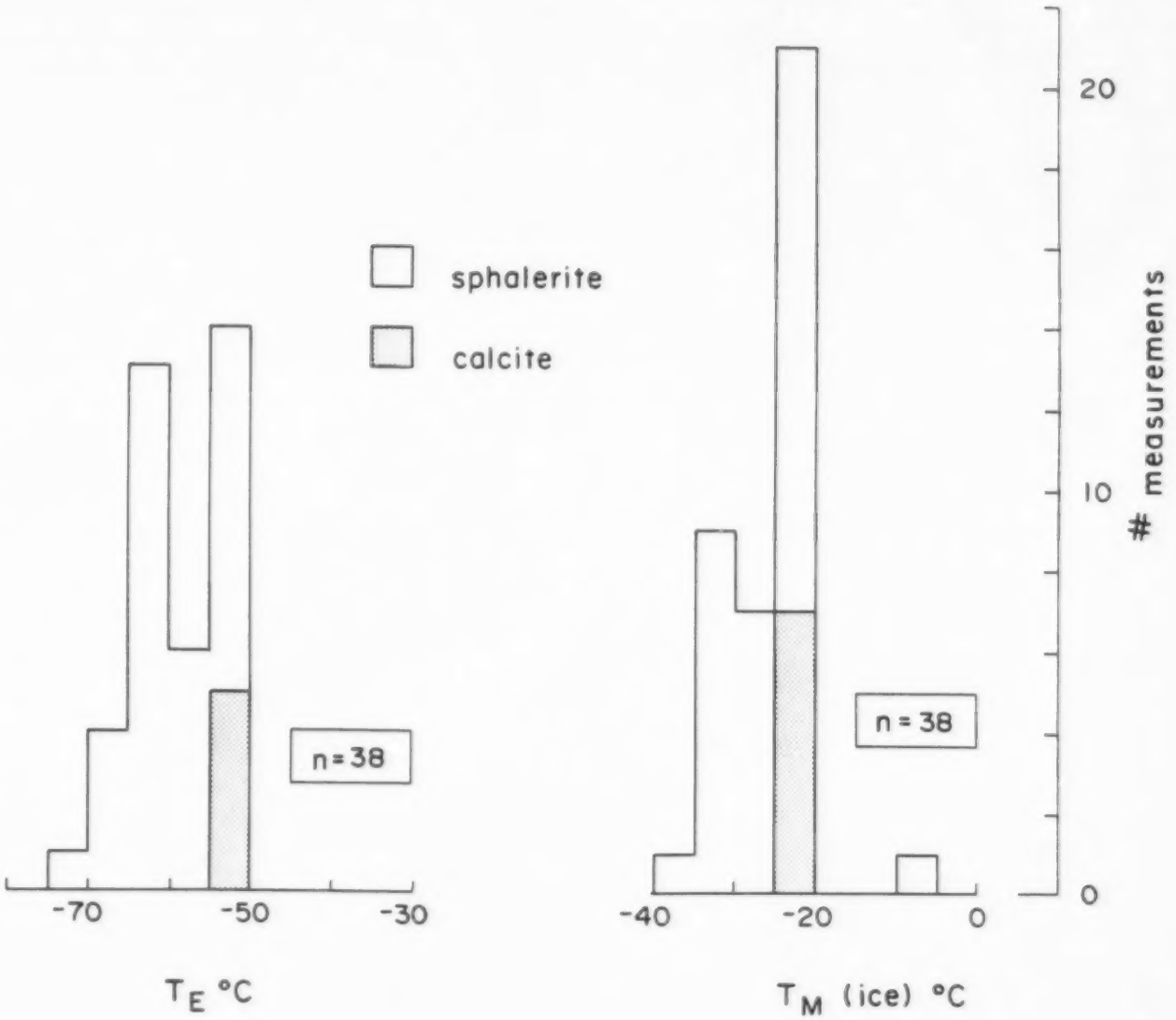

CHAPTER 6

ISOTOPIC STUDIES

6.0 INTRODUCTION

Previous isotopic work done at Gays River includes analyses for S, C, O, Pb and Sr as summarized in Akande (1982), Akande and Zentilli (1983, 1984) and Ravenhurst et al. (1986, 1987, 198º). The salient aspects of these studies are reviewed in the context of the present investigation. New analyses done as part of this study include S isotopic analyses of the massive ore and breccia-hosted ore for comparison to the earlier work of Akande (1982). Work in progress includes additional C, O and Sr isotopic analyses of the carbonates analyzed for trace elements (discussed in Chapter 4) and this data will be reported on elsewhere.

6.1 SULPHUR ISOTOPIC ANALYSES

Sulphur isotopic analyses provide direct information on the source(s) of S present at Gays River and also provide indirect information on the nature and origin of the Pb-Zn mineralization. However, since the S and Pb-Zn may not have the same source reservoirs, as is commonly the case for MVT deposits (e.g., Anderson, 1982), the S isotopic data are limited in terms of their direct bearing on mineralization.

6.1.1 Previous Sulphur Isotopic Analyses

Previous S isotopic analyses done at Gays River include the exhaustive study of Akande (1982) which included all sulphide phases in the paragenesis and also the sulphate minerals. The

data have been summarized and presented by Akande and Zentilli (1983, 1984) and Ravenhurst et al. (1987).

Akande's data is summarized in Figure 6.1a and the following points are noted: (1) sulphate minerals have very similar $\delta^{34}S$ signatures with gypsum = 14.6 (n=5), anhydrite = 14.0 (n=5) and barite = 14.1 (n=2); (2) ore-stage sulphides are similar in their $\delta^{34}S$ signatures with massive "vein" sphalerite = 10.3 $\pm$ 0.9 (n=11), disseminated "stratiform" sphalerite = 11.9 $\pm$ 1.9 (n=4), massive "vein"galena = 10.9 $\pm$ 0.8 (n=9), disseminated "stratiform" galena = 10.7 $\pm$ 0.7 (n=7), and a single chalcopyrite = 10.4; (3) pre-ore marcasite (n=3) has $\delta^{34}S$=11.7; and (4) post-ore marcasite and pyrite have very depleted $\delta^{34}S$ values with ranges of -9.7 to -42.9 (n=5) and -45.2 to -46.0, respectively. Akande and Zentilli (1984) interpreted these data to indicate that: (1) a marine source, that being Mississippian seawater which has an average $\delta^{34}S$ value of 14‰ (Thode and Monster, 1965), is the likely reservoir for the S in the sulphate minerals; (2) a common, uniform source of suphur for the main-stage suphide minerals with uniform physical and chemical conditions prevailing during their precipitation (e.g., Ohmoto and Rye, 1979); and (3) that the post-ore sulphides reflect low temperature precipitation with biogeneic reduction of suphur from a sulphate-rich solution. Ravenhurst et al. (1987), using the isotopic data for the main-stage sulphides, calculated that for a temperature of 200°C (inferred from fluid inclusion data, see Ravenhurst et al., 1987), the $\delta^{34}S_{fluid}$, assuming the sulphur species present in the ore fluid was H_2S, would have been 12-15‰ using the sphalerite and galena data, respectively. Thus, the marine sulphate of the Windsor Group, as represented by the evaporites, was interpreted as a likely source of the sulphur present within the deposit area.

6.1.2 New Sulphur Isotopic Analyses

In the present study, nine sulphide-bearing samples from massive ore and breccia ore have been analyzed for their sulphur isotopic composition. Material was anlayzed at the Department of Physics, McMaster University, Hamilton, Ontario. Samples of hand-picked sulphide separates were ground to -200 mesh and then thoroughly mixed with copper oxide in a ratio dependent on the composition of the mineral phase. The mixture was then oxidized in a furnace at 1200°C and the SO_2 produced was subsequently purified on the extraction line and analyzed using a 6-inch-radius magnetic sector mass spectrometer. The analyses are considered accurate to $\pm$0.2‰ and several pyrite duplicates run over the course of several years at this laboratory indicate precision is consistently $\pm$ 0.1 to 0.2‰.

A list of the samples analyzed, their type of mineralization and the results are provided in Table 6.1 and Figure 6.1b. Galena and sphalerite from the massive ore average 11.8‰ and 13.0‰, respectively, which compare with values of 10.9 and 10.3, respectively, reported by Akande and Zentilli (1984). The difference between the sphalerite $\delta^{34}S$ values is more than can be attributed to experimental error and is considered, therefore, to perhaps reflect real differences which may reflect sampling bias. The two samples anlayzed in the present study with coexisting sphalerite-galena have $\Delta_{sph\text{-}gal}$ = 1.6 and 1.2 which would translate into paleotemperatures (using equations in Ohmoto and Rye, 1979) of approximately 400 $\pm$ 45°C and 500 $\pm$ 45°C, respectively. These temperatures are clearly too high for the environment of formation and suggest disequilibrium as has been discussed already based on the petrographic obervations (see Chapter 3).

The three galena samples from the basal breccia have $\delta^{34}S$ values of 10.8, 7.9 and 10.7

TABLE 6.1 Samples Analyzed for Sulphur Isotopes, Gays River.

Sample	Mineral	$\delta^{34}S$ (‰)	Comments
GR-91-B	gal sphal	11.6, 11.1 13.1	coarse gal cutting f gr, massive sphal
GR-91-C	sphal	13.5	massive f gr sphal
GR-91-1	gal	10.8	f-coarse gal in cal in basal breccia
GR-91-5	gal	12.4	massive coarse gal
GR-91-19	sphal	12.5	massive f gr sphal
GR-91-22	gal	7.9	coarse gal in cal in basal breccia
GR-91-32	gal	10.7	coarse gal in cal in basal breccia
GR-91-39	gal	11.7	massive, coarse gal cutting f gr massive sphal
GR-91-56	gal sphal	11.8 13.0	coarse massive gal and f gr massive sphal

Abbreviations: gal = galena, sphal = sphalerite, f gr = fine grained, cal = calcite.
which are slightly lower than the lowest values for galena from the massive ore. Insufficient samples have been analyzed at present to infer the significance of this difference and additional sampling is warranted to resolve this discrepancy.

6.2 CARBON AND OXYGEN ISOTOPIC DATA

Previous analyses of C and O have been presented in Akande (1982), with the data subsequently discussed in Akande and Zentilli (1983, 1984), and more recently by Ravenhurst et al. (1987; data also in Ravenhurst, 1987). The data (Figs. 6.2 and 6.3) indicate that the Gays River dolomite has a C and O isotopic signature similar to host rock carbonate from regional sampling of the basal Windor Group carbonate, but both of these fields are slightly depleted with respect to both C and O isotopic signatures of Windsor limestone as determined by analyzing seven Mississippian brachiopod shells. The reason for the shift in the dolomite samples to slightly depleted C and O values may reflect either a single process or a combination of processes, including post depositional diagenetic alteration or exchange with hydrothermal fluids. While Akande (1982) favoured the latter process, the work of Ravenhurst et al. (1987) indicates that this depletion is of regional extent and, therefore, it might be more consistent with a process reflecting evolution of the basin (i.e., diagenetic).

Akande (1982) also examined the potential affect of mineralization on modifying the isotopic signature of the dolomite host rock. A detailed traverse across a massive ore-host rock contact (Fig. 6.8 of Akande, 1982) indicated no systematic change in either C or O isotopic signatures.

In Figure 6.2, C and O isotopic data for mineralized and unmineralized calcite are plotted and compared to the fields for dolomitic host rock. The following features are indicated: (1) mineralized calcite has similar $\delta^{13}C$ values but depleted $\delta^{18}O$ values compared to the dolomite; and (2) unmineralized calcite shows a progression with respect to $\delta^{13}C$ from values similar to the dolomite to values that are relatively depleted.

In order to summarize all the isotopic data for calcite, Ravenhurst et al. (1987) normalized the results to the average ore-stage calcite defined within the mine; the resulting plot is shown in Fiugre 6.3. In this latter figure it is quite obvious that there is a relative enrichment of ^{18}O in calcite outside the limits of the ore deposit. Alternatively, the data indicate that samples from outside the deposit area are in isotopic equilibrium with the dolomite compared with samples from within the mine area that are relatively depleted in ^{18}O.

In general, the C and O isotopic data indicate that in the initial stages of the mineralizing event the calcite precipitated was in isotopic equilibrium with respect to the wall rock carbonate in terms of C but not O. While isotopic equilbrium was attained with O in the later stages of mineralization, C was also being contributed from an additional reservoir, the depleted nature of the isotopic signature suggestive of oxidation of organic carbon.

6.3 STRONTIUM ISOTOPES

As part of a regional study of Pb-Zn-Ba mineralization study of the Shubenacidie basin, Ravenhurst et al. (1986, 1989) analyzed Sr-rich, Rb-poor phases such as carbonate, sulphate and flourite for their $^{87}Sr/^{86}Sr$ values. In such phases the measured Sr isotopic value is considered a good approximation of the initial ratio of the fluid from which the mineral phase was in equilibrium. For the Gays River deposit mineralized calcite from veins and vugs is characterized by highly radiogenic Sr isotopic values up to 0.712 which compare to <0.7085 for the host dolomite, 0.709 for the evaporitic anhydrite and ca. 0.708 for Mississippian sea water (Burke et al., 1982). A similar trend, that being a radiogenic signature for the ore-stage minerals, was also documented by Ravenhurst et al. for other mineralized districts in the Shubenacadie basin.

6.4 LEAD ISOTOPES

Ravenhurst (1987) and Ravenhurst et al. (1989) present seven Pb isotopic analyses for galena from Gays River, including two samples first reported by Zentilli et al. (1980) and also quoted in Akande (1982). Unfortunately, the raw data are only provided for the two samples discussed by Akande (1982), and no detailed descriptions of the samples are provided for any of the samples. However, the data provide some interesting points to consider: (1) the galenas are characterized by nonradiogenic compositions, espcially for this ore deposit type (Doe and Zartman, 1979), and have model ages of ca. 450 Ma depending on the model curve used (e.g., Stacey and Kramers, 1975); (2) the data define a steep slope in the $^{207}Pb/^{204}Pb$ versus $^{206}Pb/^{204}Pb$ plot, although the maximum variation in $^{207}Pb/^{204}Pb$ is only 15.59 to 16.2, thus the data generally reflect homogeneous isotopic compositons for the galena; and (3) the data are comparable to other mineralized Pb-Zn-Ba districts within the Windsor basin of southern Nova Scotia. In addition, a complete analysis (U, Th, Pb) of a single sample of Horton Group siltstone indicates that at ca. 300 Ma the Pb isotopic composition of galena from Gays River was similar to that of the siltstone sample selected. The significance of this is realized when one considers that the source of the detritus for this rock was exposed Meguma Group basement and the South Mountain Batholith.

Fig. 6.1. Sulphur isotope data for Gays River deposit. (a) Summary of the previous work of Akande (1982) and Akande and Zentillie (1983, 1984). Results of new data from this study also shown. (b) New sulphur isotopic analyses done as part of the present study.

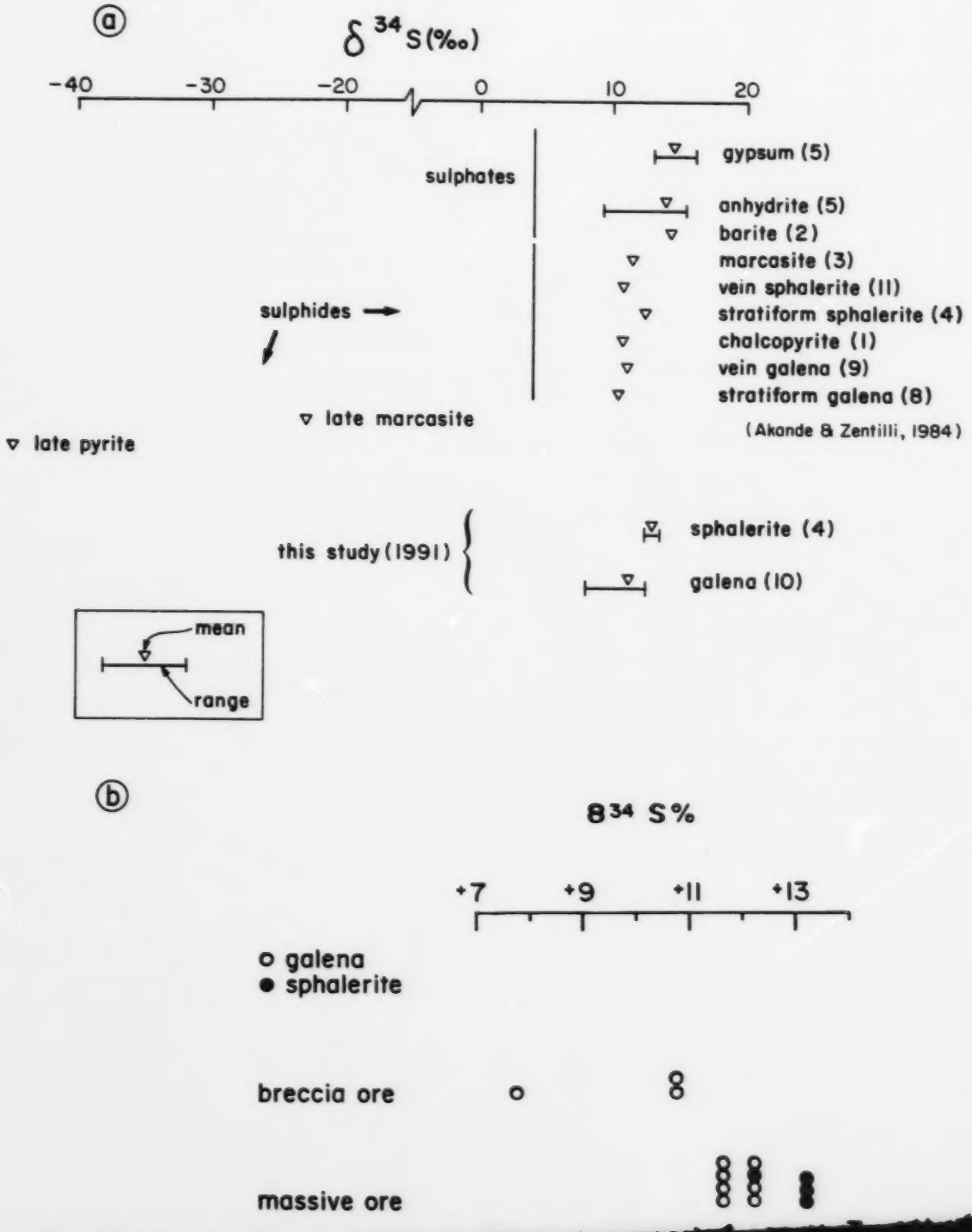

Fig. 6.2. Carbon and oxygen isotope data for carbonates from Gays River deposit as compiled by Ravenhurst et al. (1987). Symbols refer to mineralized (■) and unmineralized (□) calcite cement, postore calcite (X) and average for Carboniferous limestone (star, C.L.). Outlined fields are from Akande (1982).

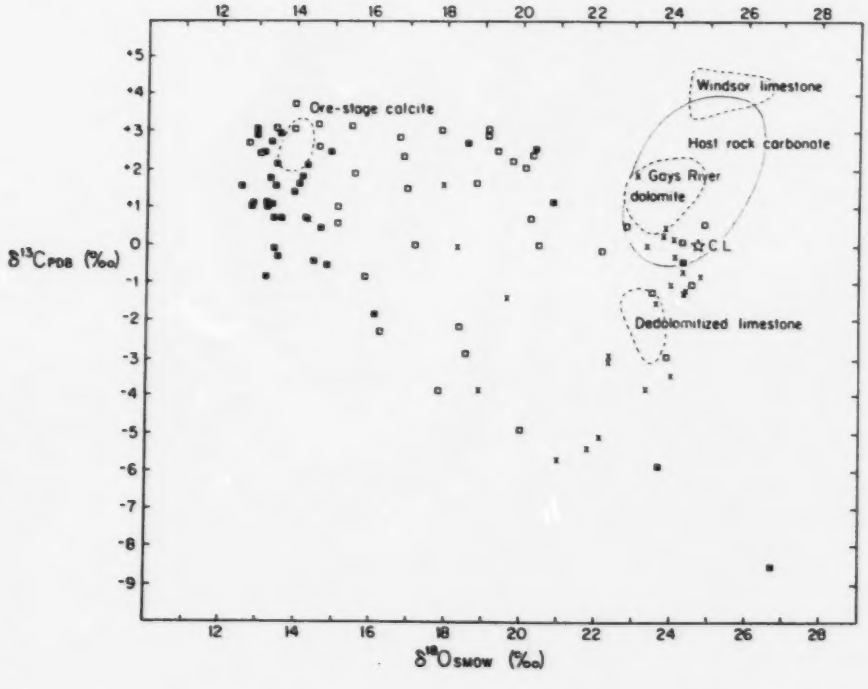

Fig. 6.3. Spatial distribution of mineralized and unmineralized calcite at the Gays River deposit area with the oxygen isotopic signature ($\delta^{18}O$) of the calcite normalized to the value for ore-stage calcite (from Ravenhurst et al., 1987).

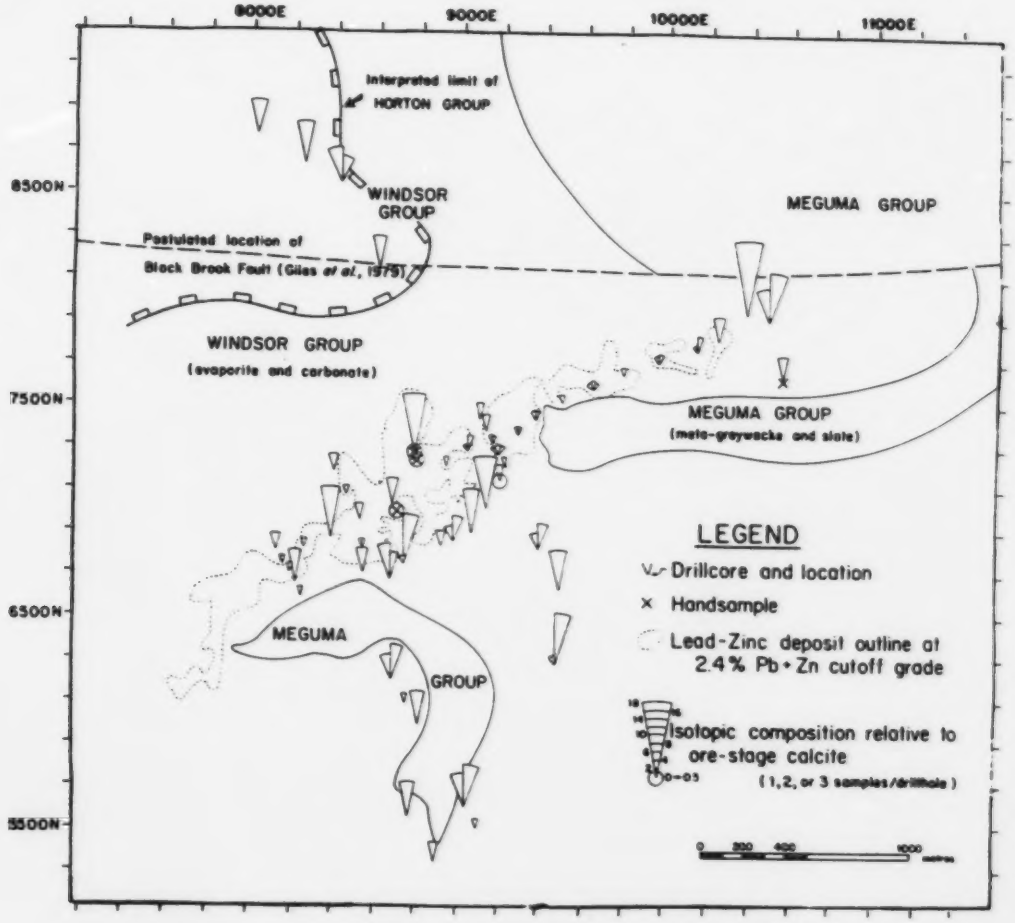

CHAPTER 7

GENERAL DISCUSSION OF THE GAYS RIVER DEPOSIT IN LIGHT OF RECENT GEOLOGICAL, GEOCHEMICAL AND FLUID INCLUSION STUDIES

7.0 INTRODUCTION

The previous chapters have outlined the status of work conducted to date at the Gays River Zn-Pb deposit which bears on the nature and origin of the mineralization. As the research into this deposit is continuing, it would be premature to draw definitive conclusions at this point. Instead, the salient aspects of the features documented above are summarized and the direction of future work outlined.

7.1 SUMMARY OF PRESENT INVESTIGATION

The results of the present study are summarized below.

1. The outline of the ore body was discussed in Chapter 3 where it was shown to reflect the paleotopography of the Meguma Group basement rocks and the basement structures. These features controlled the location of the Gays River buildup which presently is the control on the location of the ore zones. The deposit has a limited vertical dimension of 60-70 metres (i.e., ~85-90% ore) with a lateral extent of some 4 km; its overall geometry reflects a corrugated sheet trending NE-SW and dipping to the NW.

2. Detailed cross-sections of the deposit indicate that most of the ore is localized to the leg of the reef, more specifically to the evaporite-carbonate contact. Mineralization is found in the saddle part of the reef, but it is of lower grade and where high-grade pockets occur there is a lack

of continuity. There is an overall elemental zonation in the deposit such that the Pb:Zn ratio increases down dip towards the Shubenacadie basin.

3. The ore is divided into three types: (1) massive, (2) net-textured and (3) disseminated. The first two constitute the ore zones and are primarily localized to the leg of the reef, while the third type can occur throughout the buildup. While the net-textured and disseminated ore exploit primary pore space, the massive ore and to a lesser extent the net-textured ore represent constant volume replacement of the dolostone precursor.

4. The mineralization consists almost exclusively of Pb and Zn with only trace amounts of other elements (F, Ba, Cu, Ag, Cd, Ge). The ore minerals are Fe-poor sphalerite and Ag-poor galena. The massive ore consists almost exclusively of fine grained (<50-100 μ), buff colored sphalerite and massive, medium to coarse (1-4 mm) grained euhedral to subhedral galena. Sphalerite occurring as a cement can be subhedral, up to 2-3 mm and is yellow to reddish-orange color.

5. Paragenetically sphalerite is early with galena generally post-dating it. However, both minerals post-date the occurrence of dolomite euhedra which cement primary porosity. Sparry calcite cement overlaps some of the Pb-Zn mineralization and is, therefore, syn- to post-ore stage; the same can be said of the trace amounts of fluorite and barite.

6. Geochemical studies are consistent with a replacement origin for the massive ore as the REE chemistry for this material suggests inheritance from unmineralized dolomite. The REE patterns for a variety of calcite cements indicate multiple reservoirs for the REE's. Trace element analyses of sphalerite indicate similar chemistry (i.e., low Fe, Ge, Cd) for both the fine- and coarse-textured material. New S isotope analyses agree with previous work and in addition indicate a slight depletion in $\delta^{34}S$ for breccia-hosted mineralization compared to carbonate-hosted

mineralization.

7. An extensive fluid inclusion study confirms the high temperatures previously reported for the mineralization, but the restricted range in temperatures reported by earlier workers did not hold up in the present study. There is a broad range in T_H recorded for calcite, sphalerite and fluorite from <100°C to >250°C, although most of the data fall between 120-200°C. However, in many cases there is a limited spread of data in individual areas suggesting that in some instances sampling of a single, homogeneous fluid is represented. The implications of the high temperatures and complexities (see Chapter 5) are not yet understood. Freezing data indicate the fluids are of high salinity (23-35 wt.% equivalent NaCl) with variable X_{CaCl2} estimated at 0.0 to 0.9. However, the presence of halite daughter minerals in a few inclusions permitted more precise determinations of the fluid to be made (14 wt. % $CaCl_2$, 19 wt. % NaCl, 67 wt. % H_2O) which approximate well the less precise estimates. The low eutectic temperatures suggest additional solute components in the fluid (e.g., Mg and Ba chlorides) and the possible presence of carbonic species is noted.

While many of the features of the deposit are somewhat similar to MVT deposits in general (Anderson, 1982), there are features that are unique to Gays River. The deposit is clearly of replacement origin (i.e., bulk of ore) and exploitation of primary porosity was an important part of the mineralizing process. Structural preparation did not include karsting or brecciation, but a basal breccia unit (sedimentary conglomerate) is present and locally is well mineralized. While isotopic data (Sr, S, C, O, Pb) indicate that several source reservoirs were involved, the ultimate origin of the fluids and the base metals themselves remain speculative. Further comments on this subject are reserved for later after additional work has been completed.

7.2 FUTURE WORK PLANNED

Additional work planned for the Gays River deposit is summarized below.

1. Further fluid inclusion work on samples from the saddle and leg of the reef to contrast possible differences in temperature. More work is required on freezing of samples to determine possible variation of the fluid chemistry through time. To aid in this work more sophisticated techniques will be employed to determined the presence and abundance of gaseous species in the fluid.

2. The sparry calcite cements will be studied with cathodoluminescence (CL) and this work integrated with the fluid inclusion work, isotope analyses (Sr, C, O), laser ablation ICP-MS and electron microprobe analyses to further examine the later stages of the mineralizing system. More specifically, to see what the nature and origin is of the late fluid at the deposit.

3. An attempt will be made to date the mineralization using the Rb/Sr technique. This method has been shown recently to be successful in dating MVT mineralization of the Tennessee district (Nakai et al., 1990).

4. Lithogeochemistry of mineralized and barren dolostone in the deposit area will be completed to test for broad-scale zonation of elements in addition to Pb and Zn and to see what metal associations are present. This work is presently in progress but results are not yet available.

5. Petrographic study of samples from a larger area within the deposit. Most of the samples collected were from the central part of the deposit and additional sampling will be done to get a more representative suite from the deposit.

6. Further sulphur isotopic analyses are planned to examine in more detail the reason for the difference in $\delta^{34}S$ of sulphides in the basal breccia ore compared to the ore hosted by the carbonate.

7. Incorporation of material from the Getty deposit to the west of the Gays River deposit area.

8 A synthesis of the data in the light of other MVT mineralization with a broad comparison of the salient features. Included in this will be a more regional scale interpretation of the deposit in the geological evolution of the Carboniferous basins of southern Nova Scotia.

ACKNOWLEDGEMENTS

Funding for this project was provided through the Canada-Nova Scotia Cooperation Agreement on Mineral Development (1990-1992). Work at the Gays River deposit was supported by Westminer Canada Ltd. and in particular the cooperation of geologists Joe Campbell and Bruce Hudgins is sincerely acknowledged. Discussions with Drs. M. Savard and D. Sangster, Geological Survey of Canada, regarding various aspects of carbonate diagenesis and MVT mineralization, respectively, have been very beneficial in the present study. Discussions with J. Campbell, B. Hudgins and M. Cullen, of Westminer Canada Ltd., concerning the geology of the Gays River deposit have proved invaluable and preparation of this report would not have been possible without their input and geological expertise. In addition, M. Cullen and J. Campbell are acknowledged for having read an earlier draft of the manuscript which lead to some important modifications of certain aspects of the geology. Analytical work was done most capably by Mr. C. Coyle of the Technical University of Nova Scotia (Halifax) and Dr. S. Jackson of Memorial University (St. John's, Newfoundland), while Mr. B McKay of Dalhousie University (Halifax) provided assistance with the electron microprobe analyses. Preparation of figures was capably done by the drafting section of the Nova Scotia Department of Natural Resources. Finally, discussions with colleagues at the Mineral Resources Division, Nova Scotia Department of Natural Resources, on many aspects of this and related topics provided stimulus and insight into geological aspects of the Gays River deposit.

REFERENCES

Anderson, G.M. (1982): Ore deposit models - 6. Mississippi Valley-Type lead-zinc deposits. Geoscience Canada, v. 9, No.2, 108-117.

Akande, S.O. (1982): Genesis of the lead and zinc mineralization at Gays River, Nova Scotia, Canada: A geologic, fluid inclusion and stable isotopic study. Ph.D. thesis, Dalhousie University, Halifax, Nova Scotia.

Akande, S.O. and Zentilli, M. (1983): Genesis of the lead-zinc mineralization at Gays River, Nova Scotia, Canada. In Proceedings of an International Conference on Mississippi Valley-Type Lead-Zinc Deposits (W. Pratt, editor). University of Missouri-Rolla Press, 546-557.

Akande, S.O. and Zentilli, M. (1984): Geologic, fluid inclusion and stable isotope studies of the Gays River lead-zinc deposit, Nova Scotia, Canada. Economic Geology, v. 79, 1187-1211.

Arne, D.C., Curtis, L.W. and Kissin, S.A. (1991): Internal zonation in a carbonate-hosted Zn-Pb-Ag deposit, Nanisivik, Baffin Island, Canada. Economic Geology, v. 86, 699-717.

Arne, D.C., Duddy, I.R. and Sangster, D.F. (1990): Thermochronological constraints on ore formation at the Gays River Pb-Zn deposit, Nova Scotia, Canada, from apatite fission track analysis. Canadian Journal of Earth Sciences, v. 27, 1013-1022.

Belt, E.S. (1968): Carboniferous continental sedimentation, Atlantic Provinces, Canada. In Late Paleozoic and Mesozoic Continental Sedimentation, Northeastern North America (G. de V. Klein, editor). Geological Society of America, Special Paper 106, 127-176.

Bodnar, R.J., Reynolds, T.J. and Kuehn, C.A. (1985): Fluid inclusion systematics in epithermal systems. In Geology and Geochemistry of Epithermal Systems (B.R. Berger and P.M. Bethke, editors). Reviews in Economic Geology, v. 2, 73-98.

Boehner, R.C., Giles, P.S., Murray, D.A. and Ryan, R.J. (1989): Carbonate buildups of the Gays River Formation, Lower Carboniferous Windsor Group, Nova Scotia. In Reefs, Canada and Adjacent Areas (edited by H.H.J. Geldsetzer, N.P. James and G.E. Tebbutt). Canadian Society of Petroleum Geologists, Memoir 13, 609-621.

Bradley, D.C. (1982): Subsidence in Late Paleozoic basins in the northern Appalachians. Tectonics, v. 1, 107-123.

Burke, W.H, Denison, R.E., Heatherington, E.A., Koepick, R.B., Nelson, H.F. and Otto, J.B. (1982): Variation of seawater $^{87}Sr/^{86}Sr$ throughout Phanerozoic time: Geology, v. 10, 516-519.

Burruss, R.C. (1981): Analysis of phase equilibria in C-O-H-S fluid inclusions. In Short Course

in Fluid Inclusions (L.S. Hollister and M.L. Crawford, editors). Mineralogical Association of Canada Short Course Handbook, v. 6, 39-74.

Carriere, J.J. and Sangster, D.F. (1992): Preliminary studies of fluid inclusions of sphalerite, quartz and dolomite from Gayna River MVT deposit, Northwest Territories. In Current Research, Part A; Geological Survey of Canada, Paper 92-1A, 47-53.

Crawford, M.L. (1981): Phase equilibria in aqueous fluid inclusions. In Short Course in Fluid Inclusions (L.S. Hollister and M.L. Crawford, editors). Mineralogical Association of Canada Short Course Handbook, v. 6, 75-100.

Davies, E.H., Akande, S.O. and Zentilli, M. (1984): Early Cretaceous deposits in the Gays River lead-zinc mine, Nova Scotia, Canada. In Current Research, Part A, Geological Survey of Canada, Paper 84-1A, 353-358.

Doe, B.R. and Zartman, R.E. (1979): Plumbotectonic, the Phanerozoic. In Geochemistry of Hydrothermal Ore Deposits (H.L. Barnes, editor). 2nd edition, New York, Wiley, 22-70.

Dunham, R.J. (1962): Classification of carbonate rocks according to depositional texture. American Association of Petroleum Geologists, Memoir 1, 108-122.

Fleet, A.J. (1983): Aqueous and sedimentary geochemistry of the rare earth elements. In Rare Earth Element Geochemistry (P. Henderson, editor), Elsevier Science Publishers, Amsterdam, The Netherlands, 343-374.

Fralick, P.W. and Schenk, P.E. (1981): Molasse deposition and basin evolution in a wrench tectonic setting: the Late Paleozoic, eastern Cumberland Basin, Maritime Canada. In Sedimentation and Tectonics in Alluvial Basins (A. Miall, editor). Geological Association of Canada, Special Paper 23, 77-97.

Geldsetzer, H.H.J. (1978): The Windsor Group in Atlantic Canada - an update. In Report of Activities, Geological Survey of Canada, Paper 78-1C, 43-48.

Giles, P.S. (1981): Major transgressive-regressive cycles in middle to later Visean rocks of Nova Scotia. Nova Scotia Department of Mines and Energy, Paper 81-2.

Giles, P.S. and Boehner, R.C. (1982): Geological map of the Shubenacadie and Musquodoboit Basins, central Nova Scotia. Nova Scotia Department of Mines and Energy, Map 82-4, scale 1:50 000.

Giles, P.S., Boehner, R.C. and Ryan, R.J. (1979): Carbonate banks of the Gays River Formation in central Nova Scotia. Nova Scotia Department of Mines, Paper 79-6.

Gize, A.P. (1984): The organic geochemistry of three Mississippi Valley-Type ore deposits.

Ph.D. thesis, the Pennsylvania University.

Gize, A.P. and Barnes, H.L. (1987): The organic geochemistry of two Mississippi Valley-Type lead-zinc deposits. Economic Geology, v. 82, 457-470.

Graf, J.L., Jr. (1983): Rare earth elements in carbonate rocks and minerals from the Viburnum Trend, southeast Missouri. In Proceedings of an International Conference on Mississippi Valley-Type Lead-Zinc Deposits (W. Pratt, editor). University of Missouri-Rolla Press, 131-139.

Graf, J.L., Jr. (1984): Effects of Mississippi Valley-type mineralization on REE patterns of carbonate rocks and minerals, Viburnum Trend, southeast Missouri. Journal of Geology, v. 92, 307-324.

Grant, N.K. and Bliss, M.C. (1983): Strontium isotope and rare earth element variations in non-sulphide minerals from the Elmwood-Gordonsville mines, central Tennessee. In Proceedings of an International Conference on Mississippi Valley-Type Lead-Zinc Deposits (W. Pratt, editor). University of Missouri-Rolla Press, 206-210.

Ham, L.J. and Kontak, D.J. (1988): A textural and chemical study of white mica in the South Mountain Batholith, Nova Scotia: primary versus secondary origin. Maritime Sediments and Atlantic Geology, v. 24, 111-121.

Hancock, B.J. (1982): Depositional environment of a carbonate section exposed in the Gays River decline - A Carboniferous build up in mainland Nova Scotia. B.Sc. thesis, Dalhousie University, Halifax, Nova Scotia.

Hartling, A.A. (1977): Paleoenvironment of a small portion of the Gays River carbonate complex, Nova Scotia. B.Sc. thesis, Dalhousie University, Halifax, Nova Scotia.

Hatt, B.L. (1978): An interpretation of the carbonate geology exposed in the decline at Gays River, Nova Scotia. M.Sc. thesis, Dalhousie University, Halifax, Nova Scotia.

Hatt, B.L. and Schenk, P.E. (1977): Sedimentology of a Lower Carboniferous carbonate complex, Gays River, Nova Scotia. Geological Association of Canada, Program with Abstracts, v. p. 23.

Howie, R.D. and Barss, M.S. (1975): Upper Paleozoic rocks of the Atlantic Provinces, Gulf St. Lawrence and adjacent continental shelf. In Offshore Geology of Eastern Canada. Geological Survey of Canada, Paper 74-30, 35-50.

Jenner, G.A., Longerich, H.P., Jackson, S.E. and Fryer, B.J. (1990): ICP-MS - a powerful tool for high precision trace element analyses in earth sciences; evidence from analysis of selected USGS reference samples. Chemical Geology, v. 83, 133-148.

Keppie, J.D. (1982): The Minas Geofracture. In Major Structural Zones and Faults of the

Northern Appalachians (P. St. Julien and J. Beland, editors). Geological Association of Canada, Special Paper 24, 263-280.

Keppie, J.D. and Dallmeyer, R.D. (1987): Dating transcurrent terrane accretion: an example from the Meguma and Avalon composite terranes in the northern Appalachians. Tectonics, v. 6, 831-847.

Keppie, J.D. and Muecke, G. (1979): Metamorphic map of Nova Scotia, scale 1:1 000 000. Nova Scotia Department of Mines and Energy.

Kontak, D.J. and Smith, P.K. (1988): Meguma gold studies IV: Chemistry of vein mineralogy. In Mines Minerals Branch, Report of Activities 1987 (D.R. MacDonald and Y. Brown, editors). Nova Scotia Department of Mines and Energy, Report 88-1, 85-100.

Kontak, D.J. and Smith, P.K. (in prep.): Geological study of a metaturbidite-hosted lode gold deposit: the Beaver Dam deposit, Nova Scotia. I. Geological setting and vein mineralogy. Canadian Mineralogist.

Kontak, D.J., Kerrich, R. and Strong, D.F. (1991): The role of fluids in the late-stage evolution of the South Mountain Batholith, Nova Scotia: further geochemical and oxygen isotopic studies. Atlantic Geology, v. 27, 29-47.

MacEachern, S.B. and Hannon, P. (1974): The Gays River discovery - a Mississippi Valley type lead-zinc deposit in Nova Scotia. Canadian Mining and Metallurgy Bulletin, v. 67, No. 750, 61-66.

MacLeod, J.L. (1975a): Diagenesis and sulphide mineralization at Gays River, Nova Scotia. B.Sc. thesis, Dalhousie University, Halifax, Nova Scotia.

MacLeod, J.L. (1975b): Diagenesis and sulphide mineralization of a section of Lower Carboniferous carbonates at Gays River, Nova Scotia - a progress report. Geological Society of America, Abstracts with Program, v. 7, 812.

MacLeod, J.L. (1984): Diagenesis and its effect on base metal mineralization within a Mississippian carbonate complex, Gays River, Nova Scotia, Canada. In. Ninth International Congress on Carboniferous Stratigraphy and Geology, Compte Rendu, v. 3, 193-204.

McLellan, S.M. (1989): Rare earth elements in sedimentary rocks: influence of provenance and sedimentary processes. In Geochemistry and Mineralogy of Rare Earth Elements (B.R. Lipin and G.A. McKay, editors). Review in Mineralogy, v. 21, 169-200.

Möller, P., Morteani, G., Hoefs, and Parekh, P.P. (1979): The origin of the ore-bearing solution in the Pb-Zn veins of the western Harz, Germany, as deduced from rare-earth element and isotope distributions. Chemical Geology, v. 26, 197-215.

More, A.P., Vaughan, D.J. and Ashworth, J.R. (1991): Banded sphalerite from the North Penine orefield. Mineralogical Magazine, v. 55, 409-416.

Muecke, G.K., Elias, P. and Reynolds, P.H. (1988): Hercynian/Alleghanian overprinting of an Acadian Terrane: $^{40}Ar/^{39}Ar$ studies in the Meguma Zone, Nova Scotia, Canada. Chemical Geology, v. 73, 153-167.

Nakai, S., Halliday, A.N., Kesler, S.E. and Hones, H.D. (1990): Rb-Sr dating of sphalerites from Tennessee and the genesis of Mississippi Valley type ore deposits. Nature, v. 346, 354-357.

Ohmoto, H. and Rye, R.O. (1979): Isotopes of sulfur and carbon. In Geochemistry of Hydrothermal Ore Deposits (H.L. Barnes, editor), New York, Wiley Interscience, 509-567.

Osborne, W.T. (1977): Carbonate petrography and stratigraphy of holes 96, 100, 106, Gays River, Nova Scotia: Implications for depositional environment. B.Sc. thesis, Dalhousie University, Nova Scotia.

Ravenhurst, C.E. (1987): An isotopically and thermochronologically constrained model for lead-zinc and barium mineralization related to Carboniferous basin evolution in Nova Scotia, Canada. Ph.D. thesis, Dalhousie University, Halifax, Nova Scotia.

Ravenhurst, C.E., Reynolds, P.H. and Zentilli, M. (1986): Strontium isotopic studies of rock and mineral samples in the Shubenacadie Basin, Nova Scotia. In Current Research, Part B; Geological Survey of Canada, Paper 86-1B, 547-555.

Ravenhurst, C.E., Reynolds, P.H., Zentilli, M. and Akande, S.O. (1987): Isotopic constraints on the genesis of Zn-Pb mineralization at Gays River, Nova Scotia, Canada. Economic Geology, v. 82, 1294-1308.

Ravenhurst, C.E., Reynolds, P.H., Zentilli, M., Krueger, H.W. and Blenkinsop, J. (1989): Formation of Carboniferous Pb-Zn and barite mineralization from basin-derived fluids, Nova Scotia, Canada. Economic Geology, v. 84, 1471-1488.

Ravenhurst, C.E. and Zentilli, M. (1989): A model for the evolution of hot (>200°C) overpressured brines under an evaporite seal; The Fundy/Magdalen Carboniferous Basin of Atlantic Canada and its associated Pb-Zn-Ba deposits. Canadian Society of Petroleum Geologists Memoir 12, 335-349.

Reynolds, P.H. and Muecke, G.K. (1978): Age studies on slates - applicability of the $^{40}Ar/^{39}Ar$ stepwise outgassing method. Earth Planetary Science Letters, v. 40, 111-118.

Roedder, E. (1968): Temperature, salinity and origin of the ore-forming fluids at Pine Point, Northwest Territories, Canada, from fluid inclusions studies. Economic Geology, v. 63, 439-450.

Roedder, E. (1984) Fluid Inclusions. Reviews in Mineralogy, v. 12, 644 p.

Roy, J.L. and Robertson, W.A. (1968): Evidence for diagenetic remnant magnetization in the Maringouin Formation. Canadian journal of Earth Sciences, v. 5, 275-285.

Ryan, R.J. (1978): The paleontology and paleoecology of the Gays River Formation in Nova Scotia. M.Sc. thesis, Acadia University, Wolfville, Nova Scotia.

Sangster, D.F. and Carriere, J.J. (1991): Preliminary studies of fluid inclusions in sphalerite from the Robb Lake Mississippi Valley-type deposit, British Columbia. In Current Research, Part E; Geological Survey of Canada, Paper 91-1E, 25-32.

Savard, M. (1992): Diagenèse pré- et post-minéralisation: implications pour le dépôt de Gays River, N.É. In Current Research, Part E; Geological Survey of Canada, Paper 92-1E, 1-10.

Schenk, P.E. and Hatt, B.L. (1984): Depositional environment of the Gays River reef, Nova Scotia, Canada. In Ninth International Congress on Carboniferous Stratigraphy and Geology, Compte Rendu, v. 3, 117-130.

Sheridan, R.E. and Drake, C.L. (1968): Seaward extension of the Canadian Appalachians. Canadian Journal of Earth Sciences, v. 5, 337-374.

Stacey, J.S. and Kramers, J.D. (1975): Approximation of terrestial lead isotopic evolution of two stage model. Earth and Planetary Science Letters, v. 26, 207-221.

Strong, D.F. and Longerich, H.P. (1985): The inductively coupled plasma/mass spectrometer (ICP/MS). Geoscience Canada, v. 12(2), 72-75.

Thode, H.G. and Monster, J. (1965): Sulfur isotope geochemistry of petroleum, evaporite and ancient seas. American Association of Petroleum Geologists, Memoir 4, 367-377.

Webb, C.A. (1969): Paleozoic wrench faults in the Canadian Appalachians. American Association of Petroleum Geologists Memoir 12, 754-786.

Williams-Jones, A. and Samson, I.M. (1990): Theoretical estimation of halite solubility in the system NaCl-$CaCl_2$-H_2O: Applications to fluid inclusions. Canadian Mineralogist, v. 28, 299-304.

Williams-Jones, A., Schrijver, K., Doig, R. and Sangster, D.F. (1992): A model for epigenetic Ba-Pb-Zn mineralization in the Appalachian Thrust Belt, Quebec: evidence from fluid inclusions and isotopes. Economic Geology, v. 87, 154-174.

Zentilli, M., Doe, B.R. and Delevaux, M.H. (1980): Isotopic composition of lead in some Nova Scotia galenas: metallogenic implications. Geological Association of Canada-Mineralogical Association of Canada, Program with Abstracts, v. 5, p. 89.